N79-15607

USE OF REWARD-PENALTY STRUCTURES IN HUMAN EXPERIMENTATION

Anthony C. Stein, R. Wade Allen, and Stephen H. Schwartz

Systems Technology, Inc.
Hawthorne, California

SUMMARY

This paper reviews the use of motivational techniques in human performance research and presents an example study employing a reward-penalty structure to simulate the motivations inherent in a real-world situation. The influence of motivation on human performance has been an issue since the beginning of behavioral science. Most often, motivation is controlled through procedures designed to minimize its influence as an uncontrolled variable. Driver behavior in a decision-making driving scenario was studied.

The task involved control of an instrumented car on a cooperative test course. Subjects were penalized monetarily for tickets and accidents and rewarded for saving driving time. Two groups were assigned different ticket penalties. The group with the highest penalties tended to drive more conservatively. However, the average total payoff to each group was the same, as the conservative drivers traded off slower driving times with lower ticket penalties.

INTRODUCTION

Reward-penalty structures have existed since the beginning of experimentation, and the effects of such structures have evolved into a separate area of research. As early as 1922, A. M. Johanson observed the effects of rewards and penalties on reaction times. These classic results (cited in Ref. 1) are shown in Fig. 1. Researchers have examined the motivational aspects (Refs. 2-6), looked at rewards' distracting effects (Refs. 7-10), and looked at the positive effects of rewards (Refs 11 and 12). What does this experimentation mean, and how can the researcher of today utilize the efforts of others?

Subject motivation is a primary concern in any experiment. "We want the subject motivated to come back for 12 experimental sessions;" or "we want the subject motivated to respond as quickly as possible;" or "we want the subject motivated to respond in a manner consistent with his or her normal behavior." Rewards and penalties play an important part in this motivation.

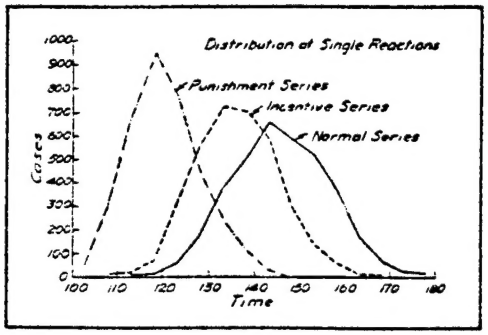

Figure 1. Change in the Distribution of Reaction Time Under the Influence of Incentives. Auditory stimulus. In the "incentive series" O was informed of his last RT; in the "punishment series" he received a shock in the finger when the reaction was at all slow. Each curve shows the distribution of 3600 single reactions obtained from three Os whose times were nearly the same. (Adapted from Ref. 1)

To assess reward-penalty structures with regard to their consequences, and to develop a structure for a given experiment, requires a basic knowledge of the literature, terminology, and present methodologies. This paper is a review of the present body of knowledge with an emphasis on reward-penalty design consequences for human performance research.

PREVIOUS RESEARCH

Definitions

The distinction between intrinsic and extrinsic motivation should be an important consideration when designing a reward-penalty structure. If a person chooses to work a series of complex mathematical problems because of personal enjoyment, then the "perceived locus of causality" (Ref. 6) is internal, and the task is intrinsically motivating. If, however, the person chooses to work the problems to gain an external reward, and the "perceived locus of causality" is external, then the task is extrinsically motivating (Refs. 3, 4, 6, 13-15).

Deci (Refs. 2 and 3), Deci, Benware, and Landy (Ref. 4), and Edwards (Ref. 16), all point out that reward-penalty structures can be designed to be either extrinsically motivating or neutral. If the experimenter chooses to have the structure of neutral influence on the subject, and at the same

time achieve high subject motivation, it becomes necessary to use a task that has been, or can be, shown to be intrinsically interesting to the subject population. If the choice is to have a structure that makes the reward or penalty contingent on performance, or in some other way extrinsically motivating, then the choice of experimental task is of secondary consideration. It has been shown by Lepper and others (Refs. 3, 4, 13, and 14) that subjects performing tasks of high intrinsic motivation, receiving extrinsic rewards, perceive the locus of causality to be external, and show low intrinsic motivation.

Purpose of Rewards and Penalties

As pointed out by Edwards (Ref. 16), rewards and penalties can serve three purposes: 1) motivators, 2) information givers, and 3) instructions. If the subject is rewarded only for participation in an experiment, then the reward serves as a motivator; the subject will perceive the locus of causality as internal, and the experimental task will be intrinsically motivating. If the reward-penalty structure is changed, and task performance is rewarded the reward or penalty will serve as information, in addition to any motivating influence it has. If the experimental task is solving complex mathematical problems, and the subject is paid hourly for experimental participation, then task performance is unrelated to the reward, and the reward's purpose is that of a motivator. If the reward is increased as a function of problem completion time, or number of problems solved, the reward takes on the additional quality of an information giver. In this case it is important to note that correct response is not required.

If correct response is required for a reward increase, or incorrect response is punished, the reward also serves as an instruction. In this case the reward not only provides motivation and information, it now tells the subject the relative desirability of a specific response. Withholding the reward until the completion of the experiment does not alter its motivational or instructional qualities. Because the reward is performance related, withholding payment (or information about the reward "earned") only eliminates the informational feedback quality.

Form of Rewards and Penalties

Rewards and penalties can take many forms, and the type of reward or penalty chosen by the experimenter should be an important part of the reward-penalty design. The overall effect of the reward or penalty needs to be assessed prior to its introduction in the experiment. For example, Deci (Ref. 2) found that monetary rewards caused a decrease in intrinsic motivation, while rewards by use of verbal reinforcement caused an increase. McCloskey (Ref. 17), in her work with staff turnover rates, found that psychological rewards such as recognition, help from peers, and educational opportunities were more important in keeping an employee than salary or job

benefits; and that money alone would not keep an employee. Viesti (Ref. 18) found that on an insightful learning task pay made no difference in performance.

One of the most commonly used rewards is money. Many researchers have examined the advantages and pitfalls of this reward form, and their findings can be of great assistance in developing a reward-penalty structure.

Money seems to provide the best balance between response and error rate. Daniels, et al.(Ref. 11), found that response speed remained constant, but a drastic reduction in error rate was observed when real instead of imaginary money was used. Slovic, Lichtenstein, and Edwards (Ref. 19) found that subjects employed simpler decision strategies in an imaginary incentive design than with real payoffs. Also Slovic (Ref. 20) found that when subjects made hypothetical choices, they maximized gain and discounted losses; however, when their choices had real consequences, the subjects were considerably more cautious.

The researcher should be cautioned by the work of Greenberg (Ref. 21) and Leventhal and Whiteside (Ref. 22), however. They have shown that monetary reward can be used to motivate performance, but that overreward is frequently employed. In some cases the overrewarding tendency was so strong that higher rewards were given to lower performing workers. Furthermore, Spence (Refs. 8 and 9), Miller and Estes (Ref. 10), and McGraw and McCullers (Ref. 7) point out that increased rewards may draw attention from the experimental task.

EXPERIMENTAL STUDY

The above research findings clearly show the need for appropriate reward-penalty designs, both in form and magnitude. The following examples, part of a study on alcohol-driver interaction, show how this information can be used to create a reward-penalty structure.

In a study concerning the effects of alcohol on drivers' decision making behavior, two separate experiments were conducted. The first was run in our fixed-base driving simulator (Ref. 23) and the second in an instrumented vehicle designed for the National Highway Traffic Safety Administration (Ref. 24).

In both experiments the subject was required to complete a driving scenario in both sober and intoxicated states. The following is a brief discussion of the requirements, design, and effects of variations in a motivational reward-penalty structure.

Reward-Penalty Structure

Driving in the real world is motivated by a variety of counteracting incentives. Drivers wish to minimize trip time but avoid tickets and accidents. Driving behavior is influenced by these motivations, particularly in risk-taking/decision-making tasks. In order to encourage real-world-like behavior we must attempt to simulate the real-world incentives. The problem with simulating typical driving incentives is that they include some difficult-to-quantify variables, such as the subjective value of time gained by driving faster and the subjective fear of low probability events such as auto crashes. Negative reinforcement with electric shock is a classical experimental technique and might serve to simulate the pain of an accident, but this technique is difficult to quantify and recent subject welfare guidelines make it unattractive. In a recent aircraft landing experiment involving pilot decision making (Ref. 25), the experimenters went so far as to inform their pilot subjects that they would be eliminated from the experiment in the event they crashed in order to make them as averse to crashes as they would be in real life. However, this approach would be logically awkward in this study because we would lose selected and trained subjects and, furthermore, the majority of driving accidents do not involve fatalities.

The traditional method of quantifying incentives for experimental control is to relate them to some well-defined variable with interval properties by measuring indifference curves (Refs. 26 and 27). The most well-defined, widely studied, and widely used norm is money, primarily because of its interval properties and interchangeability. Money has some limitations; for example, the decision-making behavior has been shown to be confounded by the subject's financial status. However, this can be experimentally controlled by controlling the knowledge of results (Ref. 28). In general, the additional experimental effort required to scale other disincentives (e.g., shock, loud noises, etc.) has led to widespread use of money for rewards and punishments in decision-making experiments.

In both experiments the reward-penalty structures had multiple requirements. A major concern was that the subject complete the driving scenario in a normal manner, with a reasonable motivation for timely progress and a desire to avoid tickets and accidents; that is, we wanted the subject to drive as if the driving situation were being experienced in the real world. A second requirement was that the subjects return for participation in six full-day experimental sessions. Finally, we chose to alter the penalty structure in the experiment to determine the behavioral effects of increased ticket penalty on the driver.

With the exception of ticket penalties, the reward-penalty structure for both experiments was the same. In order to provide a basic motivation to remain in the study, the subjects were paid an hourly wage. This payment was received by the subject irrespective of performance. To facilitate completion of the driving scenario, and to encourage normal driving behavior, we used an additional reward-penalty structure scaled to real world occurrences.

Rewards consisted of $10.00 for completing the driving scenario, and $2.00 for every minute of total elapsed driving time under 20 minutes. Assuming a real world situation of leaving a bar intoxicated, this rewarded the subject for making it home and for driving with the flow of traffic, thus avoiding detection.

In both experiments, crashes (i.e., hitting an obstacle or adjacent car, or running off the roadway) were penalized $2.00.

Tickets were given for running a red light or for speeding. Again to simulate a real world driving experience, the traffic police were present only 30% of the time. In experiment 1 (the simulation), tickets were either $1.00 or $2.00, depending on the group to which the subject was assigned. In experiment 2 (full-scale), tickets were either $1.00 or $4.00.

Subjects received immediate feedback if they crashed (buzzer), or received a ticket (siren and red lights), but total rewards and penalties were withheld until the completion of the experimental day. Again this simulates the real world, because the cost of a ticket or crash is rarely known when the incident occurs.

RESULTS AND DISCUSSION

To determine the suitability of our reward-penalty structure to the experiment, two criteria can be used. First, did all the subjects complete the experiments? In both experiment 1 and experiment 2 the answer was yes, indicating that we were able to keep the subjects sufficiently motivated to return. Second, to correlate our results with real world driving statistics, we compared our simulator and field test results with epidemiological data of over 7000 alcohol related traffic accidents. As evidenced in Fig. 2, the simulator results and the field results compare favorably with the actual accident data, thus indicating drivers motivated to take comparable risks.

Finally, in our investigation of the behavioral effects of a change in penalty structure, we found in experiment 1 no significant difference between the $1.00 ticket group and the $2.00 ticket group. Experiment 2, however, did show a significant difference between the $1.00 ticket group and the $4.00 ticket group.

In Fig. 3 we see that the high penalty group in the field study had on the average of one-third less tickets, with speeding tickets showing a greater sensitivity than signal light tickets. These results are statistically significant as shown in Table 1. Driving time differences between the two penalty groups were marginally significant (Table 1) and consistent with the ticket results, e.g, larger time and fewer tickets. Payoff was <u>not</u> significantly different between the penalty groups, however (Table 1), which indicates a compensatory tradeoff between driving time and ticket rate.

TABLE 1. ANALYSIS OF VARIANCE SUMMARY FOR OVERALL SCENARIO PERFORMANCE IN THE FIELD VALIDATION STUDY

SOURCE	ERROR TERM[a]	DEGREES OF FREEDOM	F RATIOS					
			PAYOFF	DRIVING TIME	ACCI-DENTS	SIGNAL TICKETS	SPEEDING TICKETS	ROUTE ERRORS
Day	DS(P)	1	19.33***	2.92	12.71**	2.09	13.96**	1.50
Penalty	S(P)	1	2.37	4.20†	1.92	10.80**	5.47*	1.33
Trial	TS(P)	2	10.44**	3.27	13.56**	4.78*	3.71*	1.41
DP	DS(P)	1	0.33	0.42	1.08	0.52	2.67	1.50
DT	DTS(P)	2	13.71***	1.0	11.55**	2.46	4.10*	1.26
PT	TS(P)	2	0.59	2.02	0.40	1.13	0.53	1.33
DPT	DTS(P)	2	1.40	1.65	1.27	2.08	0.90	1.49

Level of Significance: †$p < 0.10$; *$p < 0.05$; **$p < 0.01$; ***$p < 0.001$.

[a]Error term degrees of freedom: S(P) - 12, DS(P) - 12, TS(P) - 24, DTS(P) - 24.

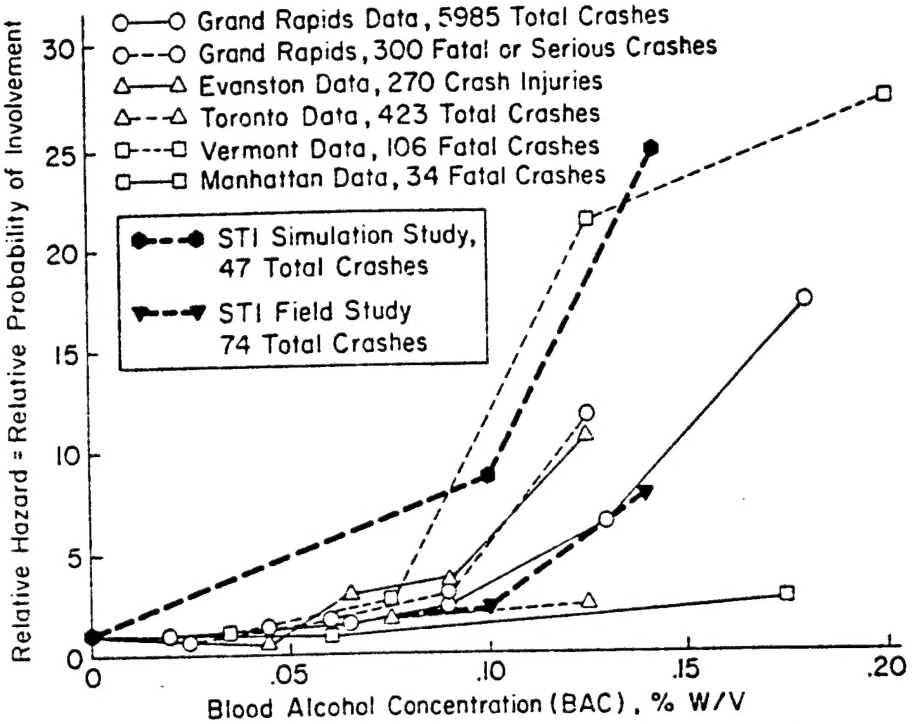

Figure 2. Relative Probability of Crash Involvement as a Function of BAC Where 1.0 = Relative Probability at Zero Alcohol (Adapted from Ref. 29)

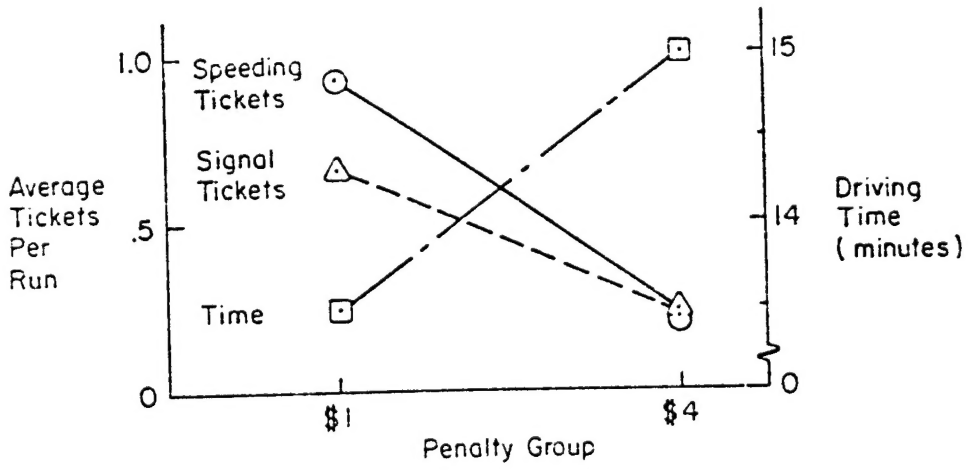

Figure 3. Penalty Effect on Ticket Rate and Total Time to Complete the Driving Scenario

Some insight into the ticket reduction with increased penalty can be gained from the signal light risk acceptance plot shown in Fig. 4 (Ref. 30). Here we see that the high penalty group perceived higher risks in signal failures (i.e., running the red light) and was willing to go less often. The combined effect was much more conservative behavior for the high penalty group, leading to better driving performance. The P(G) and SP(F/G) differences in Fig. 4 were statistically significant, but the SP_c difference was not. No group differences were observed for accident data in the experiment, and because of the magnitude of the ticket and P(G) group differences it is assumed that these are true penalty effects and not just between-group differences.

CONCLUDING REMARKS

The following conclusions were drawn with respect to the reward-penalty structure in our experiments:

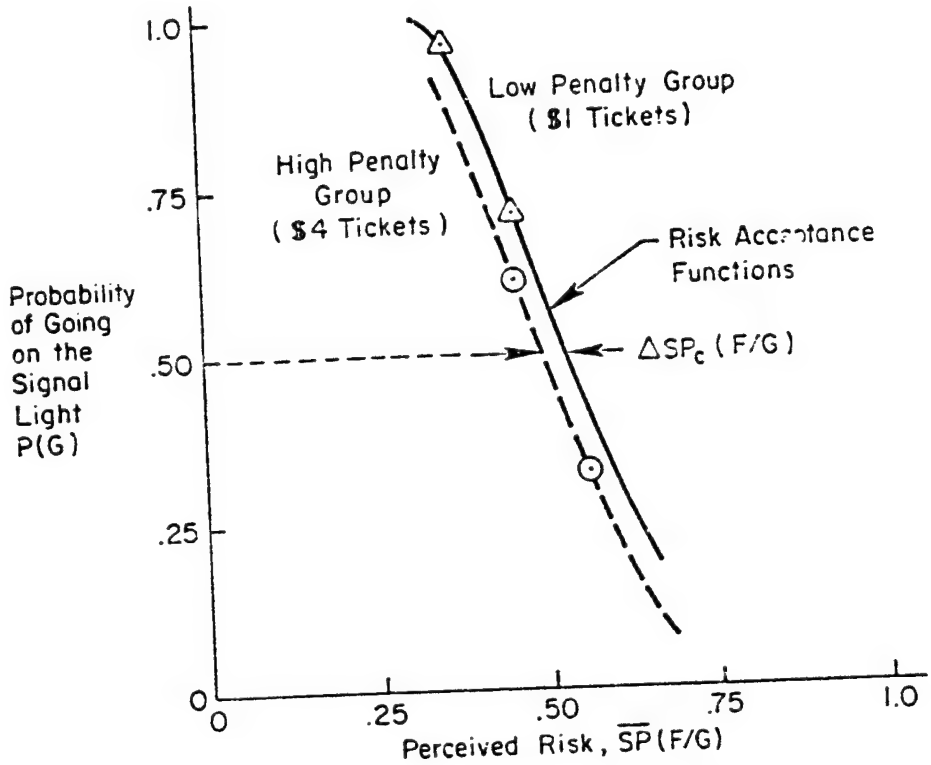

Figure 4. Mean Subjective Probability of Failure to Make It Through the Light If It Were Attempted

* Driving is not intrinsically motivating to the majority of the population, and in experimental tasks is even less so. Real-world Motivation incentives such as accidents, tickets, and desire to safe time, are extrinsic.

* Rewards and penalties must be tangible. Imaginary rewards and/or verbal reinforcement are not sufficient.

* Rewards and penalties should serve as general motivation, but not direct feedback in the driving scenario.

* Between runs in an experimental session, overall performance payoffs should be withheld in order to avoid feedback or reinforcement which might modify behavior on subsequent runs.

* Our results show that employing a specifically designed monetary reward-penalty structure provides sufficient extrinsic motivation to duplicate a "real world" driving situation.

These results on reward/penalty effects on driver risk taking might be extrapolated to real-world driving behavior. Perhaps drivers would drive more conservatively with increased and more evenly applied penalties for traffic violations.

REFERENCES

1. Woodworth, R. S.; and Schlosberg, H.: Experimental Psychology. Holt, Rinehart and Winston, 1964, p. 28.

2. Deci, Edward L.: Effects of Externally Mediated Rewards on Intrinsic Motivation. J. Personality and Soc. Psych., vol. 18, no. 1, 1979, pp. 105-115.

3. Deci, Edward L.: Work. Who Does Not Like It, and Why. Psych. Today, vol. 6, no. 3, Aug. 1972, pp. 57-58.

4. Deci, Edward L.; Benware, Carl; and Landy, David: The Attribution of Motivation as a Function of Output and Rewards. J. Personality, vol. 42, no. 4, 1974, pp. 652-667.

5. Lepper, Mark R.; and Greene, David: Turning Play Into Work: Effects of Adult Surveillance and Extrinsic Rewards on Children's Intrinsic Motivation. J. Personality and Soc. Psych., vol. 31, no. 3, pp. 479-486.

6. Heidler, F.: The Psychology of Interpersonal Relations. Wiley, 1958.

7. McGraw, Kenneth O.; and McCullers, John C.: The Distracting Effect of Material Rewards: An Alternative Explanation for the Superior Performance of Reward Groups in Probability Learning. J. Experimental Child Psych., 1974, pp. 149-158.

8. Spence, Janet T.: The Distracting Effects of Material Reinforcers in the Discrimination Learning of Lower- and Middle-Class Children. Child Development, vol. 41, 1970, pp. 103-111.

9. Spence, Janet T.: Do Material Rewards Enhance the Performance of Lower Class Children. Child Development, vol. 42, no. 5, 1971, pp. 1461-1470.

10. Miller, L. B.; and Estes, B. W.: Monetary Reward and Motivation in Discrimination Learning. J. Experimental Psych., vol. 61, 1969, pp. 501-504.

11. Daniels, E. B.; Kobas, G. B.; and Drury, C. G.: Monetary and Non-Monetary Incentives in Motor Performance. Ergonomics, vol. 19, no. 1, 1976, pp. 61-68.

12. Estes, W. K.: Reinforcement in Human Behavior. Am. Scientist, vol. 60, no. 6, Nov.-Dec. 1972, pp. 723-729.

13. Bem, D. J.: Self Perception Theory. Vol 6 of Advances in Experimental Social Psychology, L. Berkowitz, ed., Academic Press, 1972.

14. Lepper, Mark R.; and Greene, David: Turning Play Into Work: Effects of Adult Surveillance and Extrinsic Rewards on Children's Intrinsic Motivation. J. Personality and Soc. Psych., vol. 31, no. 3, 1975, pp. 479-486.

15. Strickland, L. H.: Surveillance and Trust. J. Personality, vol. 26, 1958, pp. 200-215.

16. Edwards, Ward: Cost and Payoffs Are Instructions. Psych. Review, vol. 68, no. 4, 1961, pp. 275-284.

17. McCloskey, Joanne: Influence of Rewards and Incentives on Staff Nurse Turnover Rate. Nursing Research, vol. 23, no. 3, May-June 1974, pp. 239-247.

18. Viesti, Carl R., Jr.: Effective Monetary Rewards on an Insight Learning Task. Psychonomics Sci., vol. 23, no. 3, 1971, pp. 181-184.

19. Slovic, P.; Lichtenstein, S.; and Edwards, W.: Boredom-Induced Changes in Preferences Among Bets. Am. J. Psych. vol. 78, 1965, pp. 208-217.

20. Slovic, Paul: Differential Effects of Real Vs. Hypothetical Payoffs on Choices Among Gambles. J. Exp. Psych., vol. 80, 1969, pp. 434-437.

21. Greenberg, Jerald: Equity and the Use of Over Reward to Motivate Performance. J. Personality and Soc. Psych., vol. 34, no. 2, 1976, pp. 179-190.

22. Leventhal, Gerald S., and Harold D. Whiteside. Equity and the Use of Reward to Elicit High Performance. J. Personality and Soc. Psych., vol. 25, no. 1, 1973, pp. 75-83.

23. Allen, R. Wade; Hogge, Jeffrey R.; and Schwartz, Stephen S.: An Interactive Driving Simulator for Driver Control and Decision-Making Research. Proceedings of the Eleventh Annual Conference on Manual Control, NASA TM X-62,464, May 1975, pp. 396-407.

24. McRuer, Duane T.; Peters, Richard A.; Ringland, R. F.; Allen, R. Wade; et al.: Driver Performance Measurement and Analysis System (DPMAS). Task I: Requirements and Plans for Prototype Equipment. DOT HS-801 234, Oct. 1974.

25. Curry, R. E.; Lauber, J. K.; and Billings, C. E.: Experiments in Pilot Decision-Making During Simulated Low Visibility Approaches. Proceedings of the Eleventh Annual Conference on Manual Control. NASA TM X-62,464, May 1975, pp. 19-23.

26. Raiffa, Howard: Decision Analysis: Introductory Lectures on Choices Under Uncertainty. Addison Wesley, Reading, Mass., 1968.

27. Fischer, Gregory W.: Multi-Dimensional Value Assessment for Decision Making. University of Michigan, Dept. of Psych., Rept. 037230-2-T, June 1972.

28. Rapoport, Amnon; and Wallsten, Thomas S.: Individual Decision Behavior. Ann. Review of Psych., vol. 23, 1972, pp. 131-176.

29. Hurst, P. M. Epidemiological Aspects of Alcohol in Driver Crashes and Citations. Chap. 6 of Alcohol, Drugs and Driving. DOT HS-801 096, Mar. 1974. pp. 151-171.

30. Schwartz, Stephen H.; and Allen, R. Wade: A Decision Model Applied to Alcohol Effects on Driver Signal Light Behavior. Presented at the 14th Annual Conference on Manual Control, published in this volume.

C-4 N79-15608

THE INFLUENCE OF VEHICLE AERODYNAMIC AND CONTROL RESPONSE CHARACTERISTICS ON DRIVER-VEHICLE PERFORMANCE

by

Alexander A. Alexandridis
Brian S. Repa
Engineering Mechanics Department
General Motors Research Laboratories
Warren, Michigan 48090

Walter W. Wierwille
Virginia Polytechnic Institute and State University
Blacksburg, Virginia 24061

SUMMARY

The effects of changes in understeer, control sensitivity, and location of the lateral aerodynamic center of pressure (c.p.) of a typical passenger car on the driver's opinion and on the performance of the driver-vehicle system were studied in the moving-base driving simulator at Virginia Polytechnic Institute and State University. Twelve subjects with no prior experience on the simulator and no special driving skills performed regulation tasks in the presence of both random and step wind gusts.

INTRODUCTION

The performance of the driver-vehicle system in the presence of cross-wind disturbances is influenced by the location of the lateral aerodynamic center of pressure (c.p.) of the vehicle.

The extent to which changes in c.p. location are discernible and/or objectionable to ordinary drivers has up to this time been unknown. Most of the previous studies on wind gust disturbance regulation tasks have concentrated on a single c.p. location with the c.p. most frequently placed at the front wheels (references 1-5). Also, although the influence of changes in design parameters, such as understeer and control sensitivity, have been studied previously (references 3, 4), the interaction of these parameters with the location of the c.p. in a closed-loop task is unknown.

The present study examines the influence of various combinations of understeer, control sensitivity, and c.p. location on the performance of twelve ordinary drivers in the presence of wind gust disturbances.

The Virginia Polytechnic Institute and State University (VPI&SU) moving-base driving simulator was chosen for the tests because of the control it offers over the parameters of interest and because of the success of previous research performed with the facility (reference 1). The following sections

describe the simulation facility, the experimental design and procedure employed, the performance measures utilized, and the results obtained.

THE VPI&SU DRIVING SIMULATOR

This experimental facility provides the subject with an on-line, computer-generated, television-type display of the roadway in coordination with the motion cues of yaw and roll, as well as lateral and longitudinal translation. In addition, four channels of sound along with vibration are provided for the enhancement of the simulation realism.

Three separate inputs were provided to the vehicle model used for the simulation; namely, steering wheel displacement, accelerator/brake displacement, and aerodynamic force (wind gust). The model consisted of a set of transfer functions relating the three inputs to the vehicle motion components.

References 1, 6, and 7 contain a detailed description of the driving simulator and related equipment; figure 1 shows the simulator motion platform.

DEFINITIONS AND EXPERIMENTAL PROCEDURE

Definitions

The three experimental variables are defined briefly as follows:

1. C.p. location, x_a : The distance between the front-wheel axis and the point of action of the lateral aerodynamic force F_a (see figure 2).

This variable is expressed as a percentage of the vehicle wheelbase (x_a = 0.0% corresponds to a c.p. location at the front wheels).

2. Understeer, K : The numerical difference between the sideslip angles developed at the front and rear wheels during a 1-g lateral acceleration.

Understeer is conventionally measured in deg/g. A more detailed description of this concept is given in reference 8. Figure 2 shows the paths that vehicles with understeer (K > 0), neutral steer (K = 0), and oversteer (K < 0) would follow under the influence of an external side force acting at the center of gravity.

3. Control sensitivity, C.S. : The steady-state lateral acceleration (in g's) developed by a vehicle following a steering wheel displacement of 1.75 rad (100.0 deg).

Experimental Design

A mixed between-subjects and within-subjects factorial design was used, containing two levels of understeer (K = 3.0, 5.0 deg/g), two levels of control sensitivity (C.S. = 0.8, 1.2 g/100 deg), and three c.p. locations (x_a = 0%, 19%, 37% of wheelbase) for a total of twelve vehicle configurations. Six male and six female college students without any previous simulator experience were used as subjects. Three male and three female subjects were randomly assigned to each of the two understeer conditions (understeer was a between-subjects variable). The other two variables were factorially complete and equally likely for all subjects. The subjects were given a 1.5 min period of practice following which they were required to maintain a constant speed of 97 km/h (60 mph) while keeping their normal lane position in the presence of random wind disturbances. Data were collected for a period of 2.0 min. Following the random wind disturbances, a series of step gusts were presented for an additional 2.0 min period. At the end of each run, the subjects rated the disturbances they encountered, taking into account the vehicle path deviations and the amount of steering activity needed to maintain course.

Data Collection

The time histories of the vehicle lateral position and yaw heading deviations, as well as the driver's steering wheel inputs were recorded on an F.M. tape recorder. The objective measures of performance were the root-mean-square (rms) values of these time histories, together with the peak lane overshoots during the step gusts.

RESULTS

Subjective Ratings

Figure 3 shows that the subjective ratings improve as the c.p. moves rearward. The other two variables had no significant effect on the ratings.

Random Disturbance Performance

Significant differences in lane-keeping performance occurred as a result of changes in C.S. and x_a . There is a strong indication of an

effect on lateral position deviation due to an interaction between understeer and c.p. location and a significant effect from this interaction on yaw deviations.

Figure 4 shows that increases in both C.S. and x_a result in decreases in lateral position deviations. The nature of the interaction between K and x_a that approached significance in shown in figure 5. The higher value of understeer has a beneficial effect on lateral position deviations only when the c.p. is located close to the front wheels. Figures 6 and 7 show similar effects for yaw angle deviations.

Steering wheel deviations were significantly affected by all three vehicle parameters. Furthermore, there were significant effects due to interactions between c.p. location and understeer and between c.p. location and control sensitivity.

Figure 8 shows that increases in K, C.S., and x_a all have a similar effect; namely, to decrease steering deviations. Figure 9 reveals that increases in both K and C.S. result in greater decreases in steering deviations the closer the center of pressure is to the front wheels.

Step Disturbance Performance

The peak lane position overshoot was measured from the actual vehicle position prior to the gust onset and not from the center of the lane.

Figure 10 shows that increases in x_a and in C.S. reduce peak lane position overshoot. The effects of understeer were accentuated as the c.p. location moved forward, with the lower level of understeer resulting in the largest lane position overshoot.

DISCUSSION

The subjective and objective measures used in the present study indicate that c.p. location is an extremely important parameter for wind gust regulation performance. Scores on the 0-10 Rating Scale, maximum lane deviations following a step wind gust, and steering wheel deviations during presentation of the random wind gust were all highly significantly affected by changes in c.p. location. Actual lane position deviations during the random wind gust task were only slightly less sensitive to changes in c.p. location than these other measures.

In spite of its great importance, however, c.p. location is difficult to control in practice (reference 9). For this reason, other means for improving disturbance responses of the closed-loop driver-vehicle system were explored; namely, through changes in understeer and control sensitivity. Both parameters were found to have a significant effect on wind gust regula-

tion performance, although subjective opinion data failed to detect this effect. Increased levels of understeer (K = 5.0 deg/g vs 3.0 deg/g) and control sensitivity (C.S. = 1.2 g/100 deg vs 0.8 g/100 deg) both had a beneficial effect on measures of path control and driver steering wheel deviations. These beneficial effects were accentuated where they were needed the most; namely, at forward c.p. locations.

CONCLUSIONS

The following conclusions were reached:

- Driver opinion ratings were significantly influenced by c.p. location only, with rearward locations rated the most favorable.
- Lane-keeping accuracy mproved as the c.p. moved rearward and as control sensitivity increased.
- For the forward c.p. locations, lane-keeping performance improved with increased understeer.
- Steering wheel activity required for control was reduced by increased understeer and control sensitivity and by rearward movement of the c.p., with the effects of understeer and control sensitivity accentuated at forward c.p. locations.

Overall, the location of the aerodynamic center of pressure was the predominant vehicle characteristic with an influence that could only partially be offset by changes in understeer and control sensitivity.

REFERENCES

1. Repa, B. S.; and Wierwille, W. W.: Driver Performance in Controlling a Driving Simulator with Varying Vehicle Response Characteristics. SAE Paper No. 760779, 1976.

2. Repa, B. S.; Zucker, R. S.; and Wierwille, W. W.: The Application of Integral Performance Criteria to the Analysis of Discrete Maneuvers in a Driving Simulator. Proc. Thirteenth Annual Conference on Manual Control, 1977.

3. Repa, B. S.; Alexandridis, A. A.; Howell, L. J.; and Wierwille, W. W.: Study of Vehicle Steering and Response Characteristics in Simulated and Actual Driving. SAE Paper No. 780011, 1977.

4. McRuer, D. T.; and Klein, R. H.: Automobile Controllability -- Driver/Vehicle Response for Steering Control. Systems Technology, Inc., Vol. I, Summary Report, Contract No. DOT-HS-359-3-762, 1975.

5. Crossman, E.; and Szostak, H.: Man-Machine Models for Car Steering. Fourth NASA-University Conference on Manual Control, NASA SP-214, 1968.

6. Wierwille, W. W.: A Part-Task Driving Simulator for Teaching and Research. Computers in Education for ASEE Transactions, December 1973.

7. Wierwille, W. W.: Driving Simulator Design for Realistic Handling. Proc. Third International Conference on Vehicle System Dynamics. Swets and Zeitlinger, B. V., Amsterdam, 1975.

8. Bundorf, R. T.; and Leffert, R. L.: The Cornering Compliance Concept for Description of Vehicle Directional Control Properties. SAE Paper No. 760713, 1976.

9. Bundorf, R. T.; Pollock, D. E.; and Hardin, M. C.: Vehicle Handling Response to Aerodynamic Inputs. SAE Paper No. 716B, 1963.

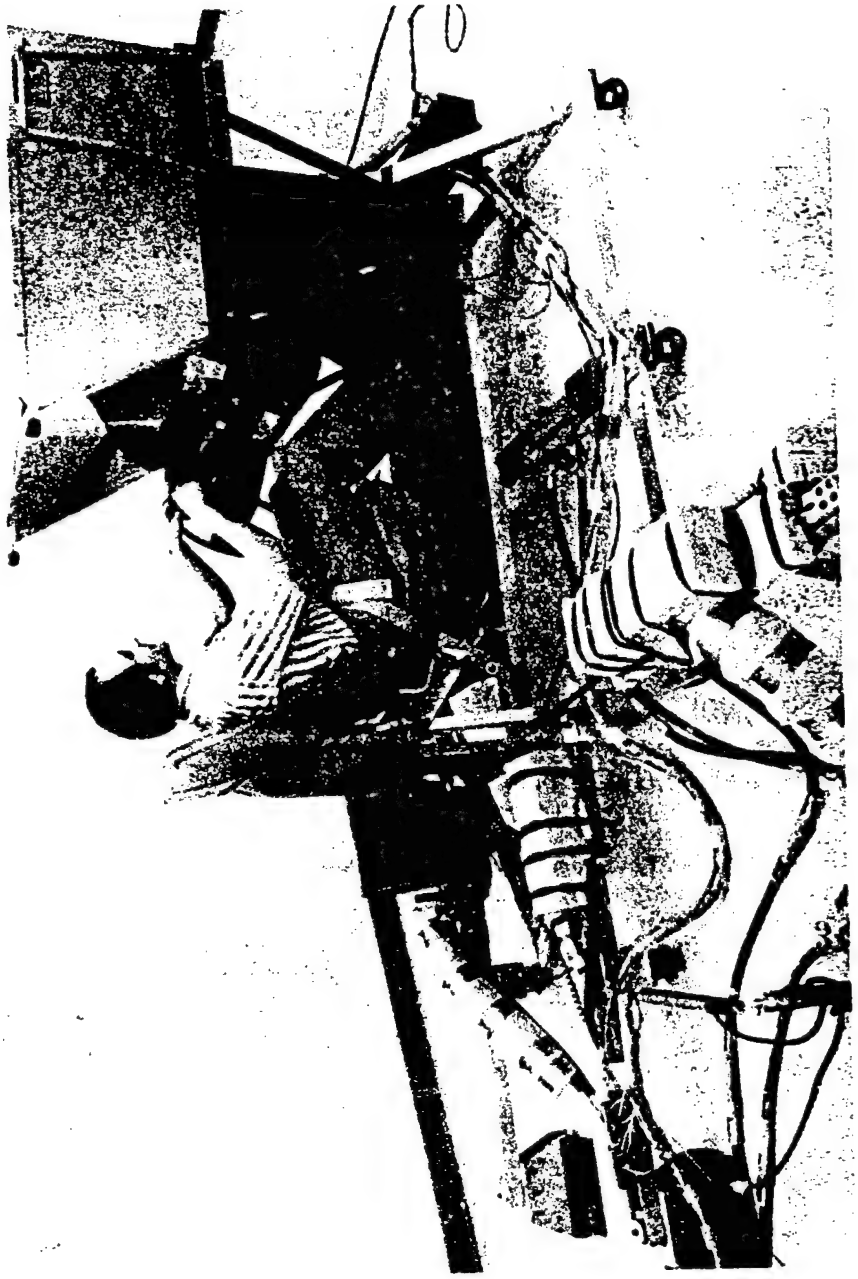

FIG. 1 DRIVING SIMULATOR MOTION PLATFORM

C. P. LOCATION

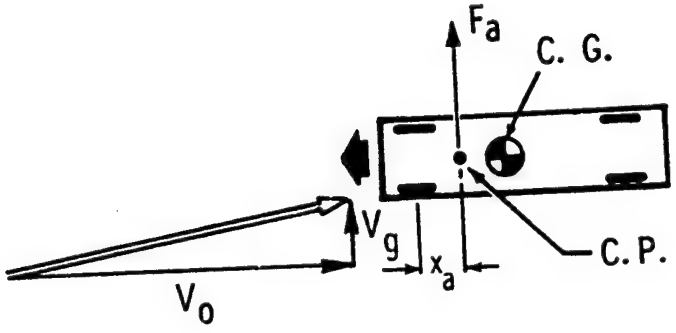

UNDERSTEER

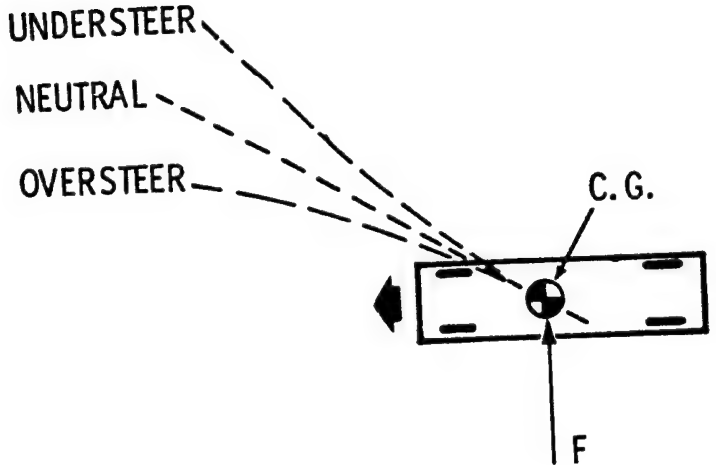

FIG. 2 DEFINITIONS

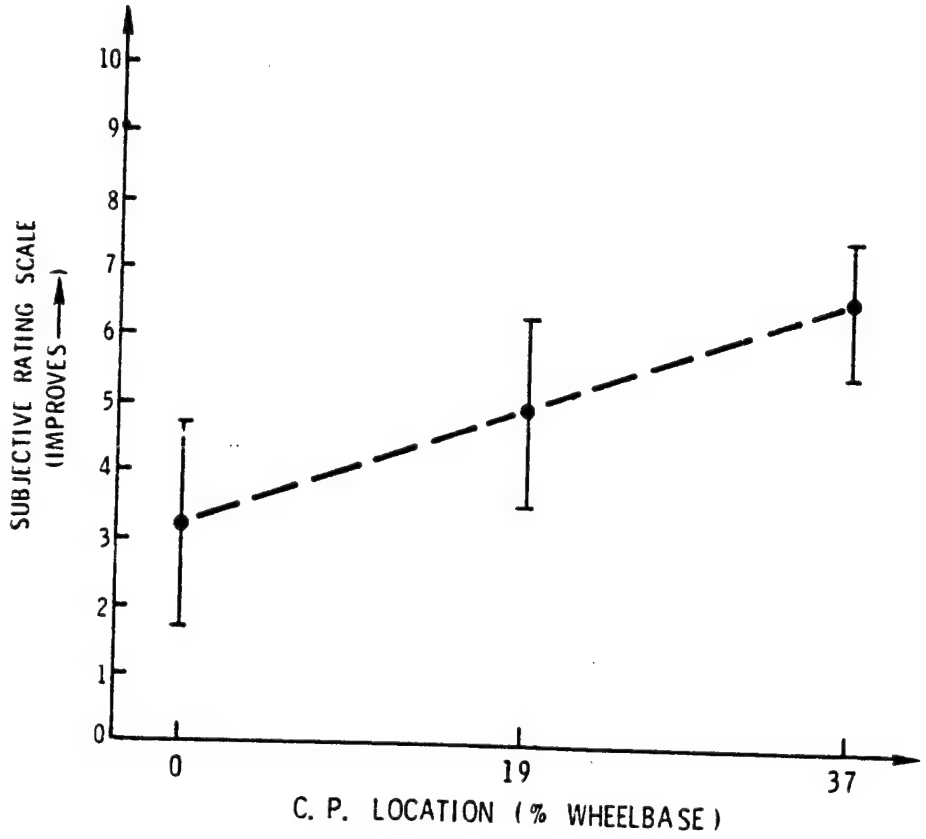

FIG. 3 DEPENDENCE OF SUBJECTIVE RATINGS OF VEHICLE CONFIGURATIONS ON C.P. LOCATION

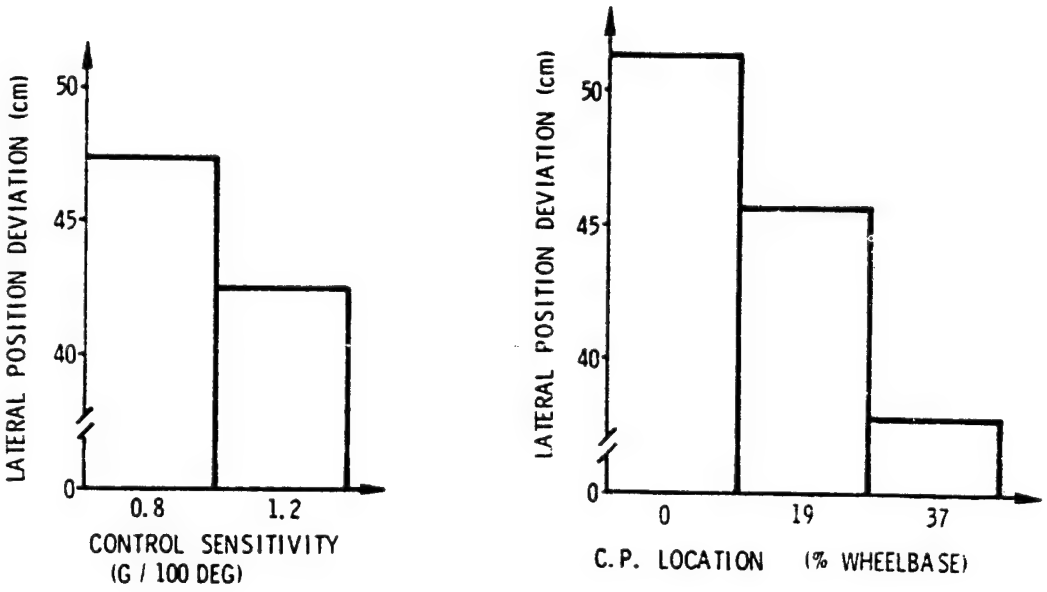

FIG. 4 EFFECTS OF CONTROL SENSITIVITY AND C.P. LOCATION ON LATERAL POSITION DEVIATION (RANDOM WIND GUST)

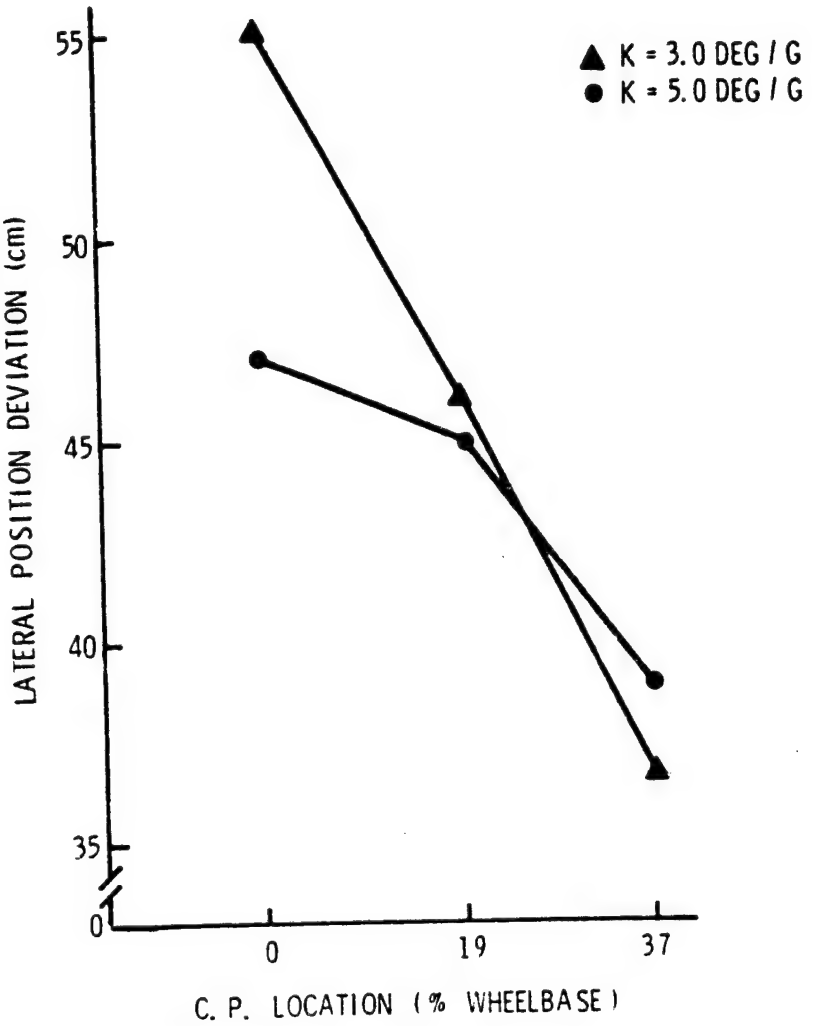

FIG. 5 COMBINED EFFECTS OF UNDERSTEER AND C.P. LOCATION ON LATERAL POSITION DEVIATION (RANDOM WIND GUST)

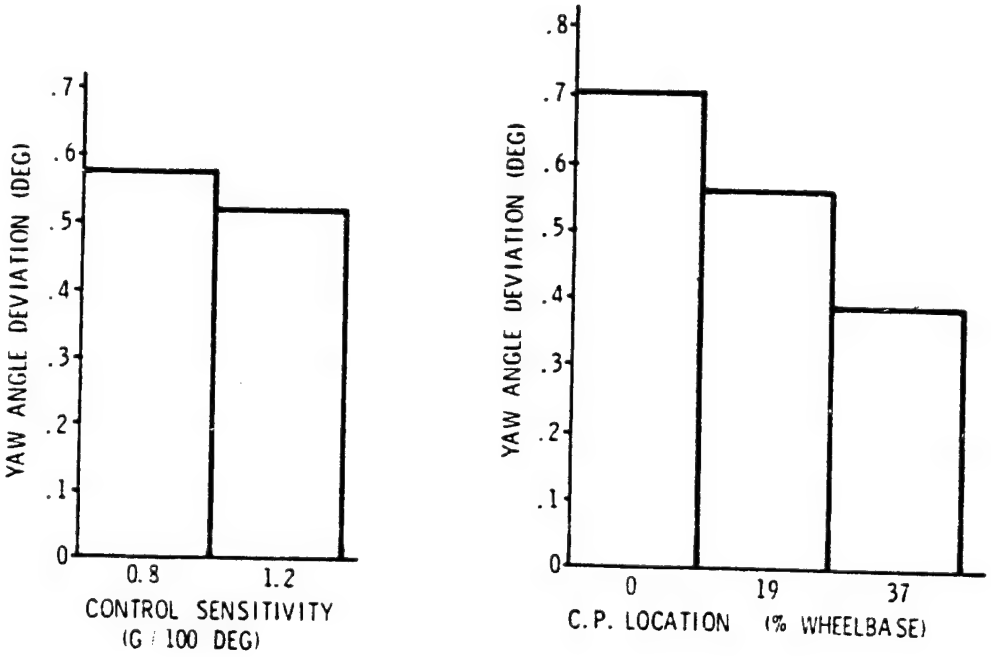

FIG. 6 EFFECTS OF CONTROL SENSITIVITY AND C.P. LOCATION ON YAW ANGLE DEVIATION (RANDOM WIND GUST)

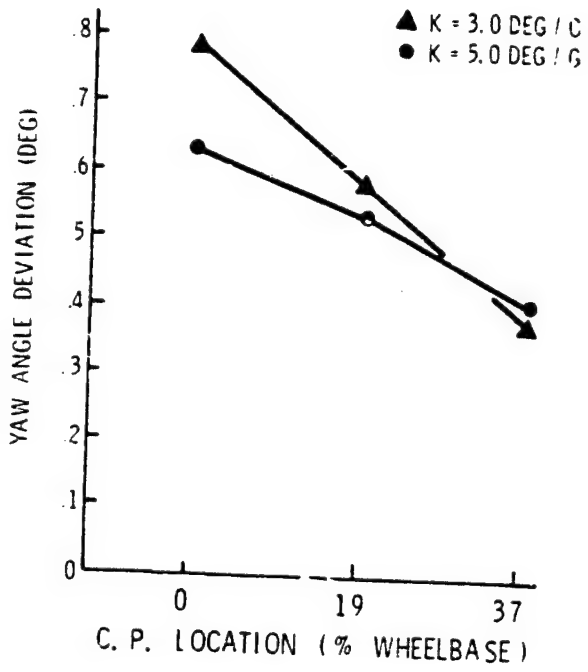

FIG. 7 COMBINED EFFECTS OF UNDERSTEER AND C.P. LOCATION ON YAW ANGLE DEVIATION (RANDOM WIND GUST)

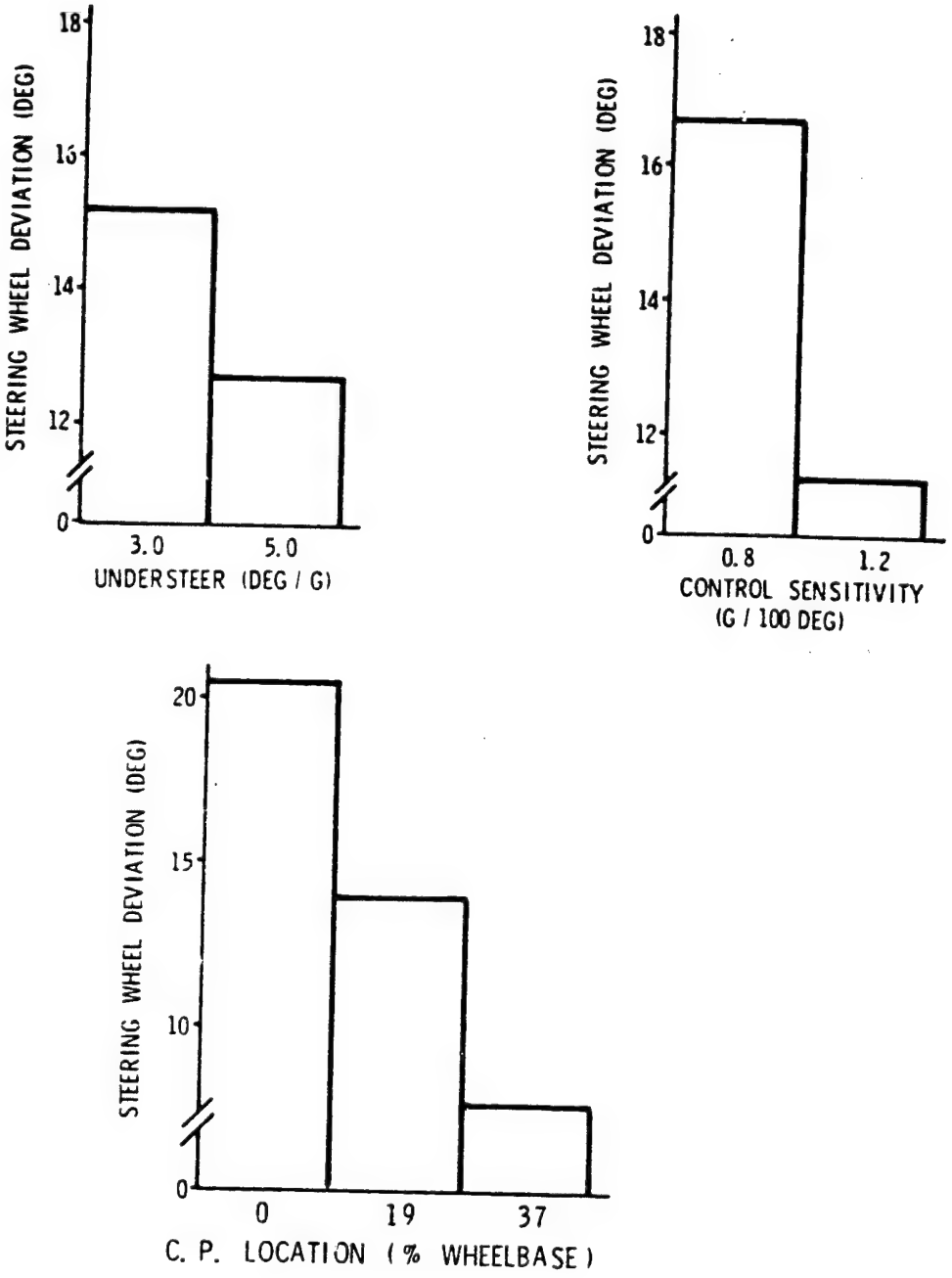

FIG. 8 EFFECTS OF UNDERSTEER, CONTROL SENSITIVITY, AND C.P. LOCATION ON STEERING WHEEL DEVIATION (RANDOM WIND GUST)

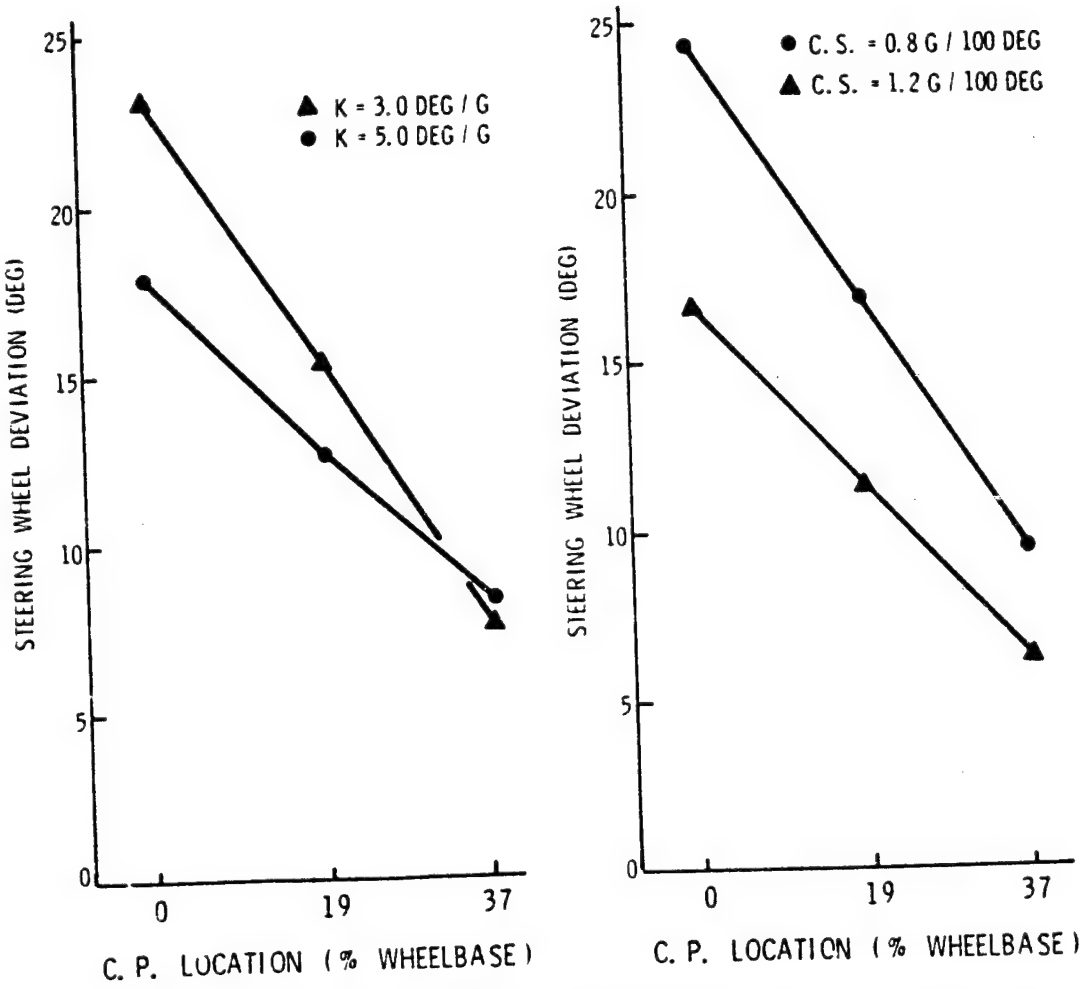

FIG. 9 COMBINED EFFECTS OF UNDERSTEER AND C.P. LOCATION AND OF CONTROL SENSITIVITY AND C.P. LOCATION ON STEERING WHEEL DEVIATION (RANDOM WIND GUST)

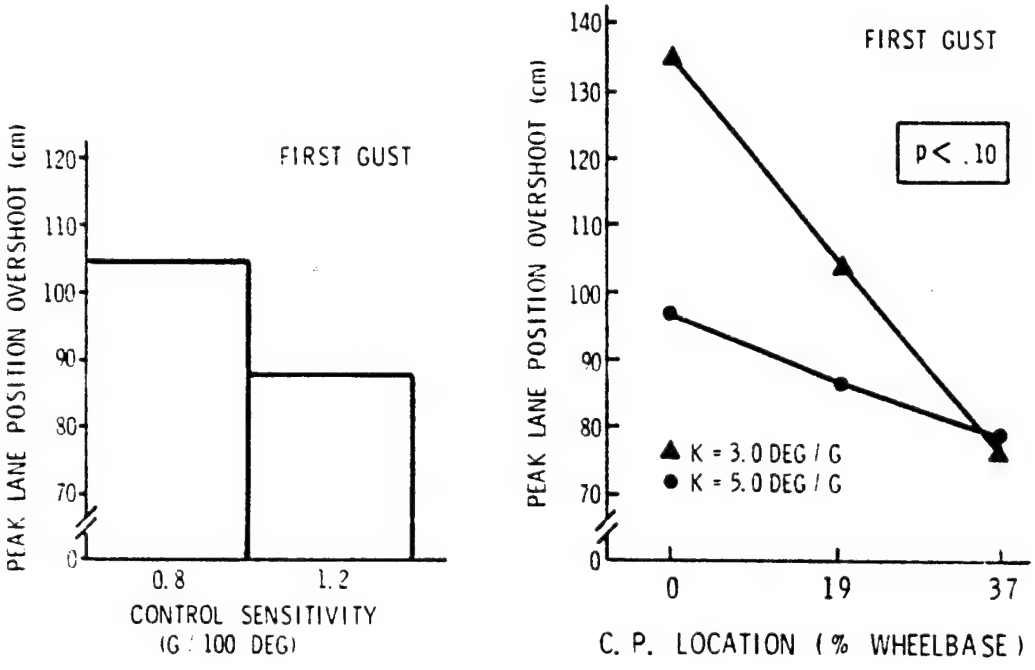

FIG. 10 EFFECTS OF C.P. LOCATION, CONTROL SENSITIVITY, AND UNDERSTEER ON PEAK LANE POSITION OVERSHOOT (STEP WIND GUST)

SESSION F: MANIPULATORS AND REMOTE MANIPULATION

Chairman: A. Freedy

N79-15609

THE DETERMINATION OF THE OPERATING RANGE OF A TWIN-GRIP CONTROL YOKE THROUGH BIOMECHANICAL MEANS

by Klaus-Peter Gärtner
Forschungsinstitut für Anthropotechnik (FAT)
(Research Institute for Human Engineering)
Meckenheim, F.R. Germany

Summary

A twin-grip control yoke was designed as an ergonomic case study that allows dual axis control inputs, both axes being rotational. Inputs are effected by rotating the grips. It will be reported how the handles were designed with respect to their shape and size and how the angular range of the control yoke in both rotational axes was evaluated.

The hand grip design is based on the anthropometric data of the hand. The main parameters for the layout are the breadth of the hand, the grip circumference, and the thumb length. The steering task for which the control yoke is designed requires that the grip shape takes into account task relevant grip characteristics, such as a rest for hand and thumb as well as a thumb operated switch button. One of the design requirements is the full use of the available motion range for steering inputs in the two rotational axes which is limited by the human arm-hand-system.

Using EMG activities, which were measured at the forearm, the permissible pitch and roll angles of the control yoke were evaluated to be $\pm 30^{\circ}$. The limitation stems exclusively from the combined limits of the radial and ulnar ranges of abduction of the human wrist joint. It should be pointed out that in this study the control range was not limited by muscle fatigue which is also measurable with EMG but rather by EMG levels which avoid painful loads on tendon and ligament structures. The experimental series is based on an isotonic rotation in both axes. EMG activities were only measurable under extreme angles of deflection. If the operator has to deflect the control element from its neutral position against a spring resistance a further reduction of the operational range will be expected.

Introduction

In this study, a control yoke which requires two-hand operation was tested to determine its operating ranges. The intention of this investigation was to find out the optimal form of the control yoke and the maximum permissible operating range in both rotating axes. In these experiments controls had no spring resistance. Future studies will involve controls with spring resistance.

296

PAGE INTENTIONALLY BLANK

The control yoke has two rotating axes. Vehicle direction changes to the left or right are accomplished by turning the yoke as with a steering wheel of an automobile, called here roll motion. Vertical vehicle direction changes are accomplished by rotating the yoke handles towards or away from the operator which will be called pitch motion.

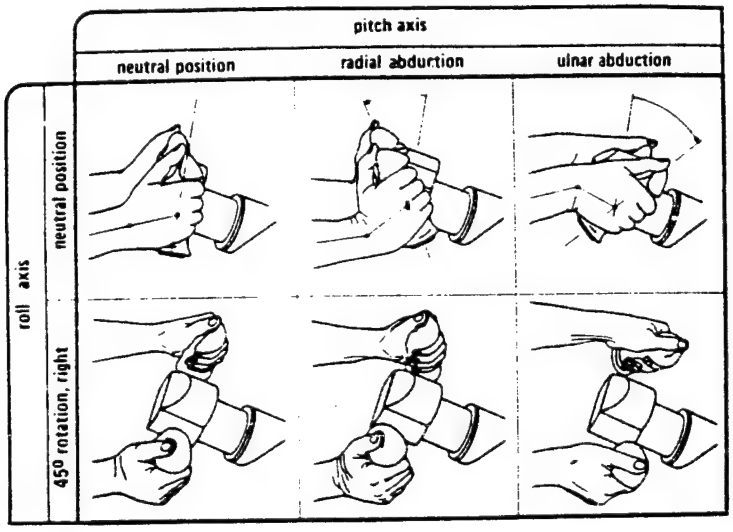

Figure 1 : Influence of roll axis rotation of a twin grip control yoke on radial and ulnar abduction angles of both hands

In the left of the upper row of figure 1 is to be seen the neutral position and in the middle and right pictures of this row the extreme excursion during the pitch movement. These two pictures illustrate the biomechanical position limits of the hand when rotating the yoke towards and away from the operator. The pitch motion of the hand towards the operator is accomplished by radial abduction ; pitch motion away from the operator is accomplished by ulnar abduction. Similar hand positions are shown in the lower row of pictures with a 45° roll angle position coupled with neutral, radial and ulnar pitch abduction.

With 0° pitch angle and roll motion to the right, radial pre-abduction will have occured in the right hand and some ulnar pre-abduction in the left hand, thereby restricting the available amount of further abduction for pitch command purposes. It can be shown that with increases in roll motion to the right pre-abduction will increase until biomechanical limitations make pitch commands impossible or very difficult. Similar pre-abduction occurs with left roll motions.

Biomechanical consideration of the arm-hand-system

Figure 2 illustrates the abduction range of the hand. In the left part of the picture there is shown a hand in two positions holding a stick. The hand rotates by an assumed axis of rotation through the wrist joint, as indicated by a small circle. This hand, turned 8 to 12°, corresponds to the normal resting position of the human hand.

If the prolonged center line of the forearm is considered as the reference line a natural pre-abduction of the hand can be noticed. The values given in the literature [e.g. 1] for the ulnar and radial abduction of the hand are based on this resting position. There is obviously no relationship between the angle at which the hand is in the natural resting position and the maximum range of abduction of the 5th to 95th percentile. On the right part of the figure the angle range is shown for the radial abduction with 35° and for the ulnar abduction with 53° measured from the resting position of the hand. This abduction angle of 88° is equivalent to the 90th percentile.

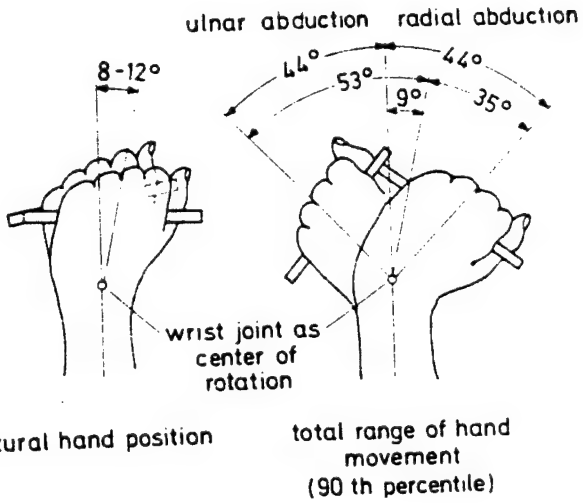

Figure 2 : Abduction range of the hand

If 9° is subtracted , which corresponds to the natural pre-abduction from the range of the ulnar abduction, a value of 44° both for the ulnar and for the radial angular range will be obtained. This consideration is important for practical applications in so far as there should be the same angular range in radial as in ulnar direction for the pitch movement, i.e. the up and down maneuver of the vehicle. If the total abduction ability of the hand is used for turning a control yoke, two

rotational axes can be selected. These two rotational axes of the control yoke cross in the steering column. In figure 3 the case is shown where the rotational axis of the wrist joint is equal to the axis of the control element. Consequently, there is hardly any motion of the forearm. The total range of abduction is used as pitch angle range, that is for radial abduction of 35° and for ulnar abduction of 53°, measured from the resting position. There is a light disadvantage of forearm movement when the rotational axis of the wrist joint does not correspond with the rotational axis of the hand grip for small and large hands. This effect does not occur if the rotational

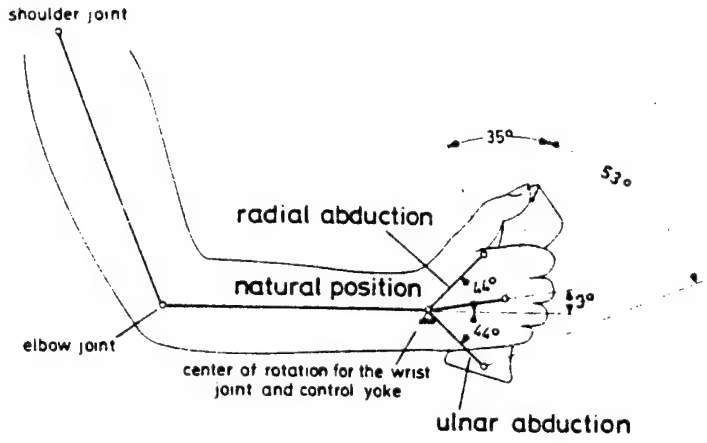

a) rotational axis through the wrist joint

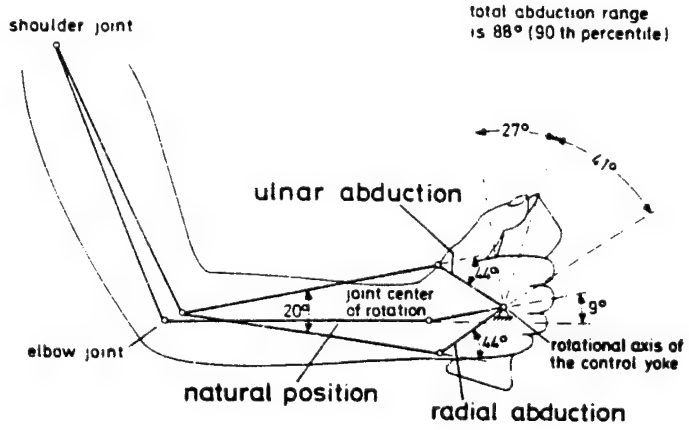

b) rotational axis through the volar hand

Figure 3 : The range of forearm motion for different rotational axes of the control yoke

axis of the hand grip corresponds with the center of the hand volar or palm as shown in the picture below. A pronounced up and down movement of the forearm which results during ulnar and radial abduction is illustrated in figure 3. Though, radial and ulnar abduction come to their limits at 88° for the maximal abduction of the 90th percentile, the maneuvering pitch angle range only reaches 68°, e.g. 27° for radial and 41° for ulnar abductions from the resting position.

Anthropometrical Design of the control grip

Figure 4 shows the operator sitting in front of the control console. The angle of inclination with respect to the body will be selected in a way so that the arm-hand-system of a 50th percentile operator measured from the shoulder reference point is in a position to turn the control yoke with the same angular values in ulnar and radial direction. A control yoke is shown, the rotational axis of which goes through the volar hand.

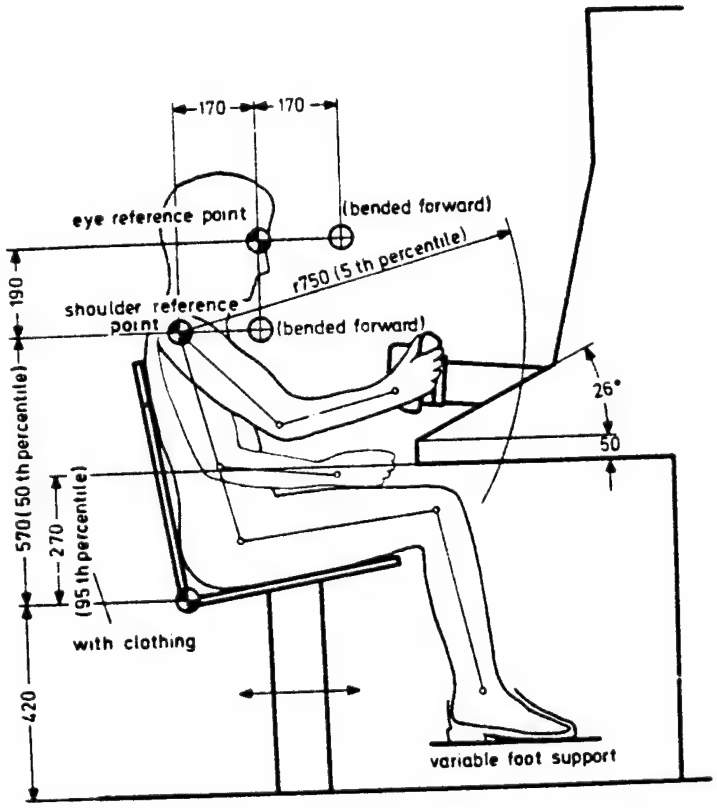

Figure 4 : Suggested anthropometric parameters for seated operator console

The control task for which the control yoke was designed requires a specially shaped grip which takes into account task relevant grip characteristics, such as a hand and a thumb rest and a switch button that is thumb operated (figure 5). The design of the grip was based on the 95th percentile hand. The dimension A of the palm was based on hand width. The hand fits between the hand rest and the top section of the grip. The fingers span the grip slantwise to the longitudinal axis of the grip and not in parallel fashion as they would with a cone.

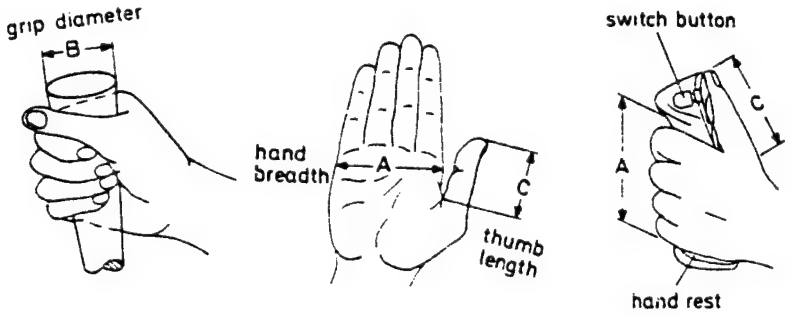

Figure 5 : Anthropometric parameters for designing a handgrip

So long as the switch button is not used, the operator can smoothly move his hands with the control yoke and follows its motions. Under these working conditions the hand of the 95th percentile man is resting on the hand support and the thumb is on its thumb rest. Smaller hands such as the 50th or 5th percentile hands can use either the hand rest or the thumb rest as a basic working position during the control task.

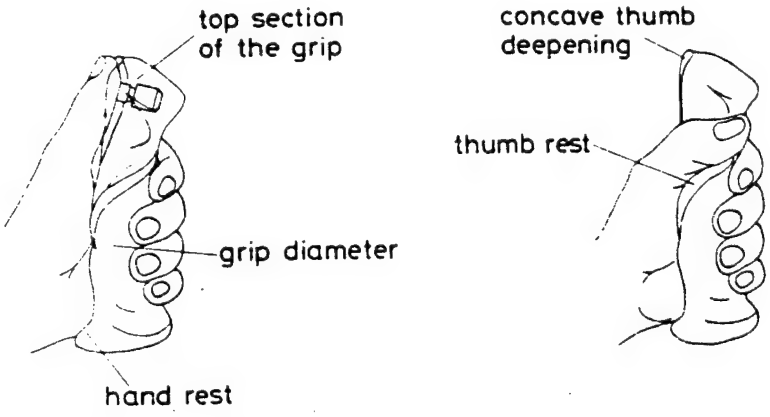

Figure 6 : Anthropometric parameters for designing a handgrip

The basic dimensions of the grip are the dimensions of an ideal conical bar which was first used by Henning. Henning suggests an increase in radius by 5 mm for each 80 mm in length. The grip is finger parallel and the forearm axis is vertical to the cone axis.The circumference is about 150 mm for a 95th percentile hand. As can be seen from the left picture of figure 6 the finger tips touch lightly the opposite part of the hand and the thumb rests on parts of the pointing finger. If the cone is closed the fingers are inclined to the longitudinal axis of the cone. A grip was designed using finger indentation and an appropriate deviation of the cone shape as may be seen in figure 5.

With this grip the finger tips of the 95th percentile hand are at small but constant distance from the opposite part of the hand. For the smaller hands like 50th or 5th percentile hands this distance becomes larger but still guaranties a good form closure. With this design a larger thumb rest was used which results in a separation of the possible touch between the thumb and the fingers. The location of a switch button in the grip head was based on the thumb length of the 50th percentile hand. Thumbs which are longer and shorter than 50th percentile are still in position to operate the switch button by use of lower or upper parts of the thumb respectively.A concave depression in the top section of the grip allows sufficient motion for larger thumbs when pressing the switch.

Biomechanical determination of the operating range of the twin-grip control yoke

For the layout of a control yoke both anthropometric and biomechanic qualities of the human hand-arm system must be considered. A method is proposed in this paper which permits a determination of a biomechanical range on the basis of surface electromyography activities which are involved in movement and force exertion. At the limits of movement, rather high EMG activity occurs together with such consequences as muscle, tendon, or ligament strain and/or pain.

For EMG measurements, subjects were instructed to grip the yoke lightly with both hands so that no forearm muscles were contracted. For each selected roll angle position of the yoke, the control was then slowly moved through both pitch directions. Raw EMG signals were processed with a double wave rectifier and a special averaging filter [2, 3, 4] .

EMG activity for the right hand in a number of different roll angle positions are illustrated in figure 7 as a function of pitch angles for roll angles in the right direction. The curves illustrated are only for EMG values recorded during increasing pitch angles as these represent the worst case for control evaluation.

The upper EMG value of "1" unit was arbitrarily given to the EMG level obtained when wrist joint pain was experienced after repeatedly holding an angle position for a few seconds. The maximum value of the curves (approx. .75 units) is obtained at the maximum pitch angle which was measured. The maximum pitch angle

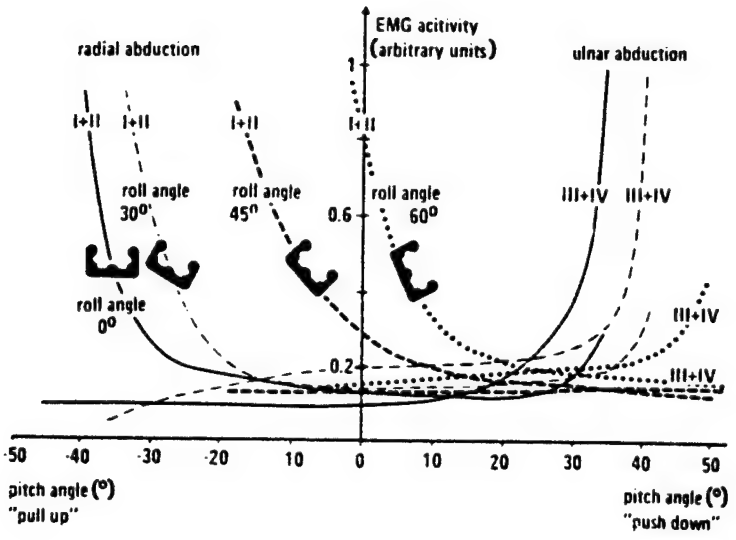

Figure 7 : EMG activities of radial and ulnar abductors of a right hand with 90th percentile wrist movement range as a function of pitch angle for various roll angles. Roll movement is in right

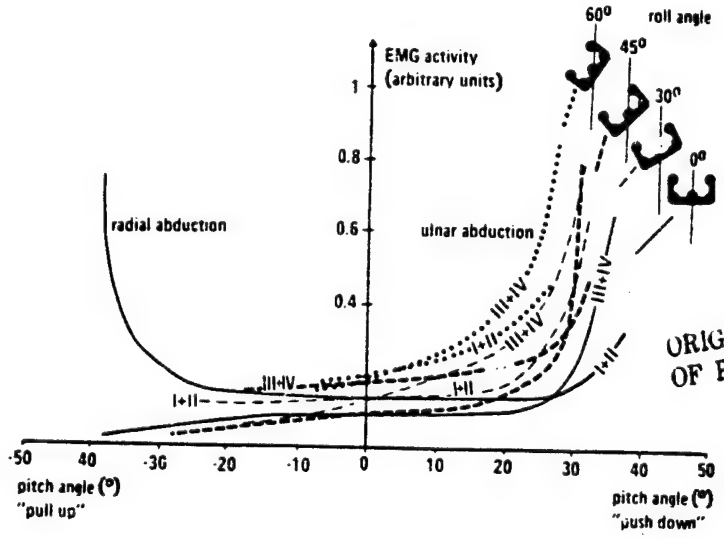

Figure 8 : EMG activities of radial and ulnar abductors of a right hand with 90th percentile wrist movement range as a function of pitch angle for various roll angles. Roll movement is in left

measured was selected after experimentally determining the maximum pitch angle at which no wrist pain build-up occured during fairly long measuring sessions. For any given pitch angle there is a tendency for pre-abduction to be larger with larger constant roll angles. It can be seen that at 0° roll angle the full range of possible wirst movement of the subject can be used for pitch commands in both directions because there is no pre-abduction. At 60° roll angle to the right, radial pre-abduction is so large that no pitch angle movement in this "pull up" direction is possible. In the right side of the figure the EMG curves for ulnar abduction i.e. in the "push down" direction is illustrated. The 45° and 60° roll angle permit relatively large "pull up" commands although the curves do not rise as high as those for radial abduction on the left side of the figure. The reason for this is that ulnar abduction of the left hand, which is not illustrated, reaches a limit at these pitch angles before the right hand, thereby preventing further ulnar abduction of the right hand. Of course, release of the control by the left hand would have permitted further movement.

EMG values for ulnar and radial abduction of the right hand is shown in figure 8 for left roll at various roll angles. As can be seen on the left side of the figure for left roll, right hand "pull-up" pitch commands or radial abduction movement is so severely limited by radial pre-abduction of the left hand in all roll angle positions except 0° that further movements are not possible. The range of ulnar abduction or "push-down" commands illustrated on the right side of the figure is slightly reduced by ulnar pre-abduction thereby allowing considerable movement before the ulnar abduction limits are reached.

Discussion of the EMG-measurements

In designing a range for this control device the following points are the most important to consider. 1. It should permit the largest possible pitch angle in both directions for each of the largest possible roll angles for subjects with 5th percentile wrist movement ranges. 2. Only lower levels of EMG activity should occur most of the time during control operations. Moderate EMG activity levels should occur very briefly and no high EMG activity at all.

As can be noticed in the figure 7 and 8 these requirements can be satisfied for the subject tested with roll and pitch angle ranges of approx. $\pm 30^{\circ}$ each (at which no more than 0,5 units of EMG activity are reached). It should be pointed out that in this study the control range was not determined by muscle fatigue limits which are also measurable with EMG but rather by EMG levels which avoid painful loads on tendon and ligament structures. The EMG measuring method presented proved to be a valuable objective aid for determining an advantageous control range.

References

[1] Damon, A., H.W. Stoudt, R.A. McFarland. 1966. The Human Body in Equipment Design. Havard University Press, Cambridge.

[2] Kreifeldt, J.G. 1971. Signal versus noise characteristics of filtered EMG used as a control source. IEEE Trans. Biomed. Eng. 18: 16 - 22.

[3] Rau, G. 1973. Ein verbessertes Meßsystem zur quantitativen Oberflächenmyographie (An improved measuring system for quantification of surface electromyography). Anthropotechnische Mitteilung No. 2/73. Forschungsinstitut für Anthropotechnik, Buschstraße, 5309 Meckenheim, Germany.

[4] Rau, G. 1974. Improved EMG quantification through suppression of skin impedance influences. In : Richard C. Nelson and Chauncey A. Morehouse (eds.) Biomechanics IV, pp. 322 - 327. University Park Press, Baltimore.

EVENT-DRIVEN DISPLAYS FOR MANIPULATOR CONTROL *)

A. K. Bejczy
Member of Technical Staff

G. Paine
Member of Technical Staff

Jet Propulsion Laboratory
California Institute of Technology
Pasadena, California 91103

SUMMARY

This paper considers the problem of constructing event-related information displays from multidimensional data generated by proximity, force-torque and tactile sensors integrated with the terminal device of a remotely controlled manipulator. Event-driven displays are constructed by using appropriate algorithms acting on sensory data in real time. The purpose of event-driven information displays is to lessen the operator's workload and to improve control performance. The paper describes and discusses several event-driven display examples that have been implemented in the JPL teleoperator project, including a brief outline of the data handling system which drives the graphics display in real time. One application shows the integration of a set of four proximity sensors with a JSC four-claw end effector for the shuttle manipulator training facility of JSC. The paper concludes with a discussion of future plans to integrate event-driven displays with visual (TV) information.

I. INTRODUCTION

The objective of this paper is to show and discuss display techniques aimed at reducing the dimensionality of proximity, force-torque and tactile sensor data, and conveying the sensory information to the operator of a remote manipulator in terms of significant events related to the control task. An event-driven display is a display which shows whether or not some desired state of the teleoperator effectors/sensors has been achieved. It may or may not show the details of the state itself, rather it displays the occurrence of the event. Hence, event-driven displays compress and explicitly indicate sensory data in terms of control goals or subgoals which require specific control decisions and actions.

The general problem of displaying information generated by proximity, force-torque, tactile and slippage sensors integrated with the terminal device of a mechanical arm has been treated in a previous paper (see Reference 1).

*) This work represents one phase of research carried out at the Jet Propulsion Laboratory, California Institute of Technology, under Contract No. NAS7-100, sponsored by the National Aeronautics and Space Administration.

The information generated by these sensors is basically non-visual: short (few centimeters) distances in given direction between terminal device and object; amount of force and/or torque exerted by the terminal device on objects along three orthogonal axes referenced to the terminal device; distribution and amount of contact area pressure between terminal device and object; or slip of an object in some direction on the inner surface of mechanical "fingers". Hence, the general problem and objective of displaying this type of information to the operator of a remote manipulator are to make non-visible events visible or, alternatively, to make non-visible events easily perceivable by using some appropriate means (e.g., audio tones).

The information generated by proximity, force-torque, tactile and slippage sensors has two specific features: it is multidimensional, and it requires quick (sometimes split-second) decision or control response. It is noted that, in general, the required decision or control response is also multidimensional. The use of multidimensional data with quick response requirements in a real time manual or computer control environment is a demanding perceptual and cognitive workload for the operator of a remote manipulator. It is a major source of errors, and can result in a general degradation of control performance. The purpose of event-driven sensory information displays is to lessen the operator's workload and to improve overall control performance of remote manipulators.

The concept of sensory information "events" is discussed in Section II. The general features of "event-driven displays" are briefly discussed in Section III. Section IV describes several event-driven display examples that have been implemented in the JPL teleoperator project. These include two uses of four proximity sensors and a single use of a six-dimensional force-torque sensor integrated with manipulator end effectors employing both audio and graphic display techniques. One application shows a set of four proximity sensors integrated with a JSC four-claw end effector to be used at the JSC Manipulator Development Facility. A simple touch sensor example is also described. The concluding Section V summarizes the results and outlines future plans to integrate event-driven displays with visual (TV) information. A brief description of the data handling system which drives the graphics displays in real time is presented in the Appendix.

II. SENSORY INFORMATION "EVENTS"

Proximity, force-torque and touch sensor data are inherently multidimensional. A six-dimensional force-torque sensor outputs the time trajectories of three orthogonal force and three orthogonal torque components normally referenced to a hand coordinate frame. The hand coordinate frame itself is a variable (i.e., has time trajectories) relative to a fixed "base" reference frame. A multipoint proportional touch sensor measures the area distribution and amount of contact pressure over a fixed surface. A single proximity sensor measures short (few centimeters) distances in a given direction relative to a hand coordinate frame. Several proximity sensors in a given emplacement geometry on the hand can measure several or all six position and orientation variables of the hand relative to objects.

A sensor-referenced or sensor-guided manipulator control task contains a goal or a set of subgoals. The control goal or subgoals are expressed as a combination of various sensory data. The simultaneous occurrence of time trajectories of various sensory data at a single point or within a given subvolume of a multidimensional data space can be called a sensory information "event". Hence, sensory information "event" is the projection or mapping of the control goal or subgoals into a multidimensional data space.

Figure 1 gives simple illustrations for the concept of sensory information "event". Equal length of two proximity sensor beams can be an "event" in the sense that it may signify, e.g., the roll, yaw or pitch alignment of a mechanical hand relative to an object. Equal magnitude of two orthogonal force components can be an "event" in the sense that it may signify, e.g., the push or pull of an object by a mechanical hand in a given direction. Or, for instance, half contact coverage of a touch-sensitive area on a mechanical finger can be an "event" in the sense that it may signify, e.g., that there is sufficient contact between hand and object for successful grasp.

The operator's attention in both manual and computer control is normally focused at the control goals or subgoals, that is, at the sensory information "events". Typically, when such "events" occur, some control action must be taken. It is to the operator's advantage to have these sensory "events" displayed in easily perceivable and unmistakably unique forms. In the absence of such "event" displays, the operator must determine the occurrence of the "event" by following and evaluating a multidimensional set of data in real time. This is not only a demanding task and heavy workload for the operator, but also a common source of errors.

III. DISPLAY OF "EVENTS"

Event-driven displays can be implemented by developing and/or employing appropriate real-time algorithms which (a) coordinate and evaluate sensor data in terms of predefined "events" and, (b) drive some appropriate information display in real time. Manipulator control tasks can be subdivided into a multitude of sensory "events", and each event may have a variety of characteristic parameters. Thus, the development of fairly general purpose event-driven displays requires that the logic/parametric structure of the algorithms be flexible in the sense that changing control goals or subgoals can be accommodated by simple call-changes in the algorithms in a given control/operation environment.

The actual event display can be implemented by alternative means, the selection of which depends on the application environment. For event displays, both audio and visual display techniques are suitable. An important consideration for selecting or designing event displays is the "warning effect" the display can or shall impose on the operator. By definition, the occurrence of a sensory event should call the operator's attention to some appropriate control decision or control action, without disturbing his normal visual attention directed toward the overall control task. Note that the control can require split-second decisions. Another important consideration

is related to the selection of the content of the display format. How much and what kind of detailed information the operator should be exposed to in addition to the "event information" within the same general frame of information? Too much information can be disturbing. Too little information can defy the purpose. The display of uncorrelated data, or the display of correlated data in uncorrelated form, may impose heavy cognitive load on the operator.

Properly designed event-driven displays are expected to have a number of benefits: (a) simplify on-line control decisions; (b) reduce errors caused by human factors; (c) reduce perceptual/cognitive workload on human operator in a real-time control environment; (d) improve overall control performance in control situations which many times require split-second type control decisions.

IV. EXAMPLES

A. Event-Driven Proximity Displays

Event-driven displays have been constructed for proximity sensors on two arms in the JPL teleoperator project, and also for a proximity sensor system developed at JPL and integrated with the four-claw end effector of JSC to be used at their shuttle manipulator training facility.

1. JPL Teleoperator Arms

Both the JPL/CURV and JPL/Ames arms are equipped with four proximity sensors, and the event-driven display developed recently is applicable to both sensor systems. Although the sensor hardware is quite different on the two arms, the sensor display drive software is common except for the routines that get the data. Similarly, the event logic is common. The details of the computer hardware and software are described in the Appendix.

The general format of graphics display of four proximity sensors data is shown in Figure 2. The display shows a view of the "bone" of a parallel jaw hand and four beams emanating from the hand, two from each jaw. The beam lengths are proportional to the sensitive length of the sensor beams. Each beam length is bound to 10 cm (4 in.).

Figure 3 summarizes the proximity events together with the event logic and event parameters that have been implemented. In the present implementation the parameter D is fixed at 5 cm. D is always defined parallel to and halfway in between the two beams which measure roll and yaw alignments, respectively, and relative to the line connecting the two fingertips. The tolerance, T, can be set by switch inputs on the computer's front panel. Values from 0.5 to 7.5 cm are allowed. Any combination of the four event logic equations may be selected to control the event success blinker. The success may be defined as X alignment with a tolerance, say, of 1 cm (corresponding to about 5 degrees when the hand is fully open). Or, the success may

be defined as Y range of 5 cm together with X alignment to within 0.5 cm tolerance (corresponding to about 2.5 degrees when the hand is fully open). This latter "success case" would be useful in moving the hand over a table to a wall while holding an object vertical. With this event logic, the hand roll angle would be small as the range measurement is made on both sensors and the object would be held with the hand 5 cm above the table. The final approach to the wall would be reached with the hand perpendicular to the wall.

The event indicator blinker has initially been placed in the top left hand corner of the monitor screen. Though all four sensor beams are shown on the monitor, the operator does not have to evaluate the four beams quantitatively in terms of a predefined event. This is done for him by the display drive logic automatically and in real time. He can take a more qualitative look at the four beams to determine, e.g., why the success blinker is "off"; that is, what to do in order to get the success blinker "on".

Figure 4 shows two uses of the event-driven proximity display. The first pair of photographs (Figure 4A) shows the hand above a table and skewed to a block. The task is to achieve alignment with the table and the block. The display shows the operator how to bring the hand perpendicular to the block while maintaining the hand level at 5 cm above the table. The second pair of photographs (Figure 4B) shows that this has occurred and the event blinker has come on. The third pair of photographs (Figure 4C) shows a different alignment problem. Here, it is desired to bring the hand in level over the plate on the table. There are no forward references. Following the required corrections as indicated by the display, the desired level state is achieved, and the event blinker comes on as shown in the fourth pair of photographs (Figure 4D).

While the two uses of the event-driven display shown in Figure 4 are simple, they do demonstrate the usefulness of the concept. As more complex tasks are performed and analyzed, a detailed examination of the benefits can be made. Future improvements in implementation are also planned to enable a broader variety of events to be defined. Ranges, alignment angles and tolerances could be individually defined rather than being commonly constrained as at present.

2. JSC Four-Claw End Effector

A proximity sensor has been developed for and integrated with a four-claw end effector of JSC. The purpose of this sensor system is to aid the operator to find the proper final depth positioning and pitch and yaw alignments of the four-claw end effector on a 16-m long manipulator relative to the grapple fixture of a large payload. The overall control is visually guided.

The sensor system, together with the grasp envelope and measurement definitions are shown in Figure 5. The use of the sensor system is presently restricted to the verification of a "successful grasp state" before grasp action is initiated. The "successful grasp state" is defined by the dimensions of the grasp envelope (see Figure 5) and by the dynamics of grasp.

When a "successful grasp state" has been reached, the data processing electronics automatically turns on a simple "success display" (a buzzer or a green light, or both), indicating to the operator that he is ready to grasp.

The data processing required to drive the "success display" has two modes: analog and digital. The analog drive logic implementation is quite simple as indicated in Figure 6. In fact, with this simple analog implementation the full capabilities of the sensor system cannot be utilized to account for all physically possible combinations of depth, pitch and yaw error states which, due to the dimensions of the end effector's grasp envelope, still would allow successful grasp. To achieve a full utilization of the sensor system capabilities versus all allowable depth, pitch and yaw error combinations, "success algorithms" have been developed and implemented using an Intel 80/20-4 single-board microcomputer together with an Intel single-board A/D converter.

For the purpose of experimentation, several "success algorithms" have been implemented in the digital computer to drive the displays. The algorithms are simple, and account for all (or for almost all) allowable error states combinations for successful grasp. Algorithms have also been implemented which utilize the outputs of any three out of the four sensors to indicate the "success states". This is useful if one sensor eventually fails, or if one sensor eventually misses the top (reference) surface of the grapple fixture due to allowable lateral alignment errors. (Note that the four-sensor configuration is redundant to define and compute depth, pitch and yaw errors. A triangular configuration of three sensors would be sufficient for that purpose.)

For the sake of brevity, only one "success algorithm" is shown in this paper, summarized in Figure 7. It is called "conic algorithm" since it condenses the individually allowable pitch and yaw errors into a simple allowable cone angle error condition. (See Condition 2 in Figure 7.) Three kinds of "success definitions" have been developed, each with three sets of "success parameters". All nine variations have been implemented for "all four" and for "three-out-of-four" sensors. All together 18 algorithms are stored in EPROM in the microcomputer. Any one of the 18 algorithms are easily callable by dialing the appropriate number between 1 and 18 on a BCD switch integrated with the microcomputer.

Very successful operational ground tests have been conducted with the sensor and simple display system at JSC using the 16-m long arm of the JSC Manipulator Development Facility in realistic large payload handling experiments. Fig. 8 shows a floor set-up scene (direct visual contact with target) for capturing a moving target. All together 112 test runs have been performed by 4 operators. The final result is that, when the "success display" (tone or green light) was on, the operators got a capture every time. There were no operator mistakes under sensor-indicated grasping conditions, and the sensors never indicated wrong conditions for grasping. Three of the four operators favored the buzzer for "success display". The utility of the display increased with task difficulty. The display was required to aid the operator to successfully complete the most difficult tasks without error.

The simple success display (tone or green light) does not show the details of the three-dimensional (depth, pitch and yaw) error states. Advanced graphics display concepts have been developed and implemented recently using the JPL teleoperator breadboard system to experiment with various formats. The advanced formats have been designed to convey to the operator not only the "success" information but also the details of the three (depth, pitch and yaw) errors so that the operator will know from the sensors "what to do" in order to get to the "success" state or to fine-control the grasp. Fig. 9 shows an advanced "success display" concept implemented in color graphics. Success is indicated here by all error bars turning green. The unsuccessful error combinations are indicated by all error bars turning red. The length of the error bars is proportional to the respective errors under both "green" or "red" conditions.

B. Event-Driven Force-Torque Display

Fig. 10 shows a six-dimensional force-torque sensor integrated with the JPL/CURV arm. The sensor mechanism has been built by Vicarm Inc. The sensor electronics and data handling have been developed at JPL. More details of this sensor system can be found in Ref. 2. Fig. 10 also shows a graphics display format: each force and torque component is displayed both numerically and graphically. The length of the bars is proportional to the value of the respective force or torque components. The bars originate from the center vertical line on the screen. To the left from this center line the force-torque field is negative, to the right it is positive. The force-torque components are referenced to a hand-based coordinate frame. The force-torque distribution seen on the graphics display of Fig. 10 actually shows the forces and torques felt at the hand base while the hand is pushing the object as indicated on the same figure. As seen, a simple push scene can generate a rather complex force-torque relation felt at the hand base.

The application of event-driven displays to force-torque sensor data will significantly enhance the use of that data type under manual or computer aided control. The events marked can show complex relationships between forces and torques alone or in combination. Further, when the desired force-torque events are not existing, the display format can be changed to show the operator what has to be done to reach the desired state. A simple example can best illustrate the concept.

Consider the task of sliding a block in a groove across a table by pushing it. (See Fig. 11) The applied forces must be in the direction of the groove if the block is to be moved efficiently and safely. Fig. 11 also shows an appropriate "event-driven" display. When the forces are applied correctly, the operator will know it by the event indicator. If not, the operator will see the force errors and be able to apply the needed corrections. Practical application and demonstration are needed before the benefits of this display concept can be fully documented.

An interesting use of even-driven displays is to signal the operator to switch displays. Say, for example, it is necessary to move a manipulator to an object and then move the manipulator into contact with the object without knowing the exact position of the object beforehand, or having specially positioned TV's showing all the necessary views.

With event-driven displays, the task could be performed as follows: using a proximity event display set in a position sensing mode, the operator moves the manipulator rapidly towards the object. When signalled that the manipulator is near the object, the operator slows its motion and switches the display to a force/torque even mode. When contact has been achieved, the operator is again signalled before the forces reach an unacceptable level. Thus, event-driven displays used in combination hold great promise for even greater benefits in that tasks can be performed more rapidly, more reliably and with lower expenditure of resources.

C. Event-Driven Touch Display

The touch sensor unit being used here has two 4 by 8 matrices of points that can sense applied pressures. These matrices, or perhaps some with higher point density, can be mounted on the inside of mechanical fingers (jaws) and used to sense contact areas or the location of points of contact between finger and object. Similar units could be mounted on other surfaces to sense other contact forces or patterns of contact areas. At each point of the sensor matrix the pressures applied locally are sensed by measuring the conductivity of a pressure sensitive plastic. The measurement concept and the actual sensing elements are shown in Fig. 12.

Fig. 12 also shows the basic touch sensor displays. The numeric representation of the sensor output gives a more quantitative impression of the applied forces distribution and is particularly useful for diagnostic work. The color or B/W shades displays are more graphic and are easier to understand at a glance although less information is presented.

A particular event-driven touch sensor display is planned to be implemented to further enhance the control context of data presented to the operator. The display concept (shown in Fig. 13) is aimed to give a quantitative indication to the operator when the contact area increases by predefined amount. While the pressures applied will still be shown as dark or light shades of a color, the color itself will be changed to reflect the total applied pressure over a given area. The matrix displayed may be red, if less than half the sensitive points have made contact; orange, if between 1/2 and 3/4 have; or green, if more than 3/4 have. Thus, a green condition will signify a safe grasp.

V. CONCLUSIONS

1) Performance tests conducted at JSC with a three-dimensional proximity sensor system and "go-no go" display have shown the basic utility of a simple event-driven display which conveys critical control information to the operator based on real-time algorithmic evaluation of multidimensional data.

2) In general, event-driven displays enhance the control context of sensory information since events can be defined with respect to critical control decisions or control actions.

3) Preliminary experiments strongly indicate the need of integrating visual and non-visual sensory information within a single perception format. This may require the development of TV monitors with sensory information overlayed to or cut into the camera information.

4) Extensive experimentation is needed with a multitude of event-driven display formats in order to develop a reliable rating of the different formats. The experimentation will by necessity encounter questions in human factors engineering. Presently it is not clear what kind of objective measures would be suitable to meet the challenges in the performance evaluation of event-related human factors.

ACKNOWLEDGEMENT

The contributions of Mr. E Shalom and Mr. K. W. Rudd to the software development is gratefully acknowledged.

REFERENCES

1. Bejczy, A. K., and Paine, G., "Displays for Supervisory Control of Manipulators," Proceedings of the 13th Annual Conference on Manual Control, Massachusetts Institute of Technology, Cambridge, MA., June 15 - 17, 1977.

2. Bejczy, A. K., "Issues in Advanced Automation of Manipulator Control," Proceedings of the 1976 Joint Automatic Control Conference, Purdue University, West Lafayette, Indiana, July 27 - 30, 1976.

APPENDIX

1. Computer System

A single computer system is used for software development and display driving. Its principal elements are shown in Fig. 14. The signals to be displayed can come from any of five sources: JPL/AMES arm proximity sensors, JPL/CURV arm proximity and force-torque sensors, touch sensors, or the JSC four-claw proximity sensors. (These last signals come through an Intel 80/20 processor.) The display computer processes these signals into the desired display format so that they may be seen in color or in B/W, with or without alpha-numeric text.

The display computer is an S100 bus based system and employes a Z80 based processor operating with a 4 MHZ clock. The computer communicates to the outside world through a 7 channel 8 bit A/D converter, 2 serial ports, 8 bit parallel ports, a dual floppy disk, and, of course, a graphics color/BW TV display. The operator interface is through an ADM-3A terminal, a TTY and the dual disk.

The graphics display is performed by DMA on a memory map. That is, the display driver circuitry timing operates independently from the main program and shares the memory storing to the screen image. Various display parameters are under program control: display on/off, point density, B/W or color, etc. The graphics densities employed are: 64 by 64 color and 128 by 128 B/W for the touch sensor; 128 by 128 B/W for the proximity sensors on the JPL/CURV and Ames arms and for the force-torque sensor on the JPL/CURV arm; and 64 by 64 color for the JSC four claw proximity sensors.

The signals from the JPL/Ames arm proximity sensor electronics are sent to the display computer on 4 analog lines. The A/D conversion is done inside the display computer by an 8 bit successive approximation converter. Each conversion takes about 5 μs.

The signals from both sensors (proximity and force-torque) on the JPL/CURV arm are converted to 12 bit digital words in the CURV vehicle electronics and then stored in a buffer memory associated with the Interdata M70 minicomputer which performs control and supervisory functions. The data is transferred in parallel to the display computer as two 8 bit words. The data to be transferred is specified by the address sent to the buffer memory from the display computer.

The signals from the touch sensor are converted to 12 bit digital words by the touch sensor electronics. The point of the sensor matrix to be sampled is under control of the display computer. An address is sent to the touch sensor electronics, the point is sampled, and the data is sent to the display computer as two 8 bit words. Due to the handshaking signals which are under software control, the whole process takes about 100 μs.

The signals from the JSC four-claw proximity sensors are processed by the Intel SBC 80/20-4 computer. Only the pitch, yaw, and range error signals and the "event" signal are passed over to the display computer. These signals are

encoded into three 8 bit parallel words. The two computers run asynchronously since the TV graphics display process is much slower than the event indication bulb and tone process (about 16 times per second versus about 100 times per second.)

2. Software System

The software for the display programs has been written in assembly language to maximize the signal processing and display formatting rate. This has been an effective approach since the processing and formatting are logically and mathematically simple. Typically, the symbolic language version of a program takes 10-15K bytes to store, and the machine language version 1-2K bytes.

The programs have been written in a structured subroutine format. The top level is a sequence of calls to subroutines. The first calls are to routines which initialize constants and set up the displays. These are followed by the main program loop which calls routines: to see if the display program should be exited, change parameters based on switch or keyboard inputs, input data, calibration of data, perform logic tests, format the data for the displays, etc. Each of these subroutines is a complete logical entity, so that new functions may be added by simply inserting new calls. A similar approach has been taken for the lower levels of subroutines. The program data structures have been designed so that they allow an EPROM version of the programs. Thus to perform tests only a small fraction of the computer system is needed. Further the operation of the system for demonstrations is simplified.

The program for displaying proximity sensor data from the sensors on the JPL/CURV arm and performing event logic is typical of the display computer programs. The first level structure is shown in part A of Fig. 15. The actual process for getting the data, processing and displaying it are shown in part B of Fig. 15. The modularity of the structure was a significant help in adding the event logic and display to the prior programs. All that was necessary was to add the two blocks which perform the event logic tests and which time and display the event blinker. Likewise, when changing the JPL/Ames arm proximity sensor program to accept data from the JPL/CURV arm proximity sensors all that was necessary was to change the "Read Sensor Data" subroutine. The subroutines, incidentally, were taken from a previous force-torque sensor program.

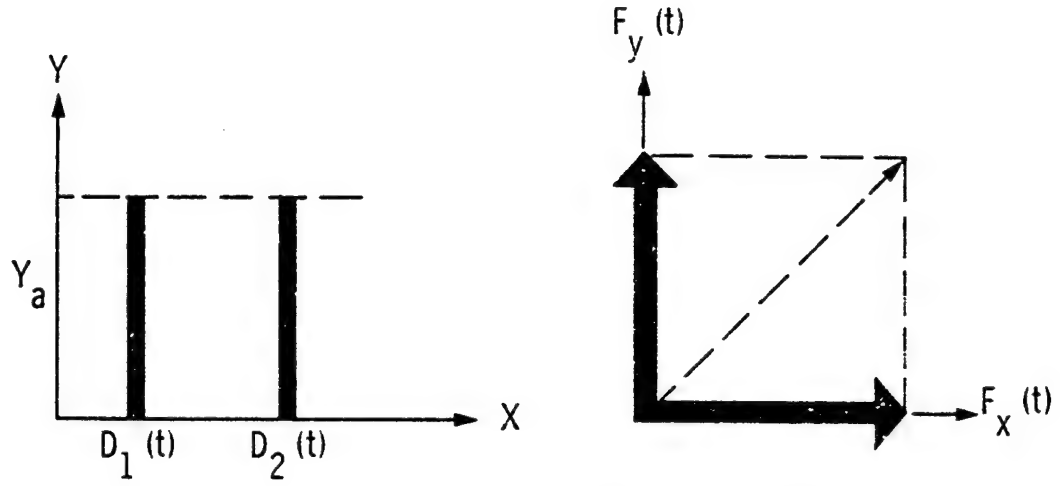

Figure 1. Examples for Event Definition

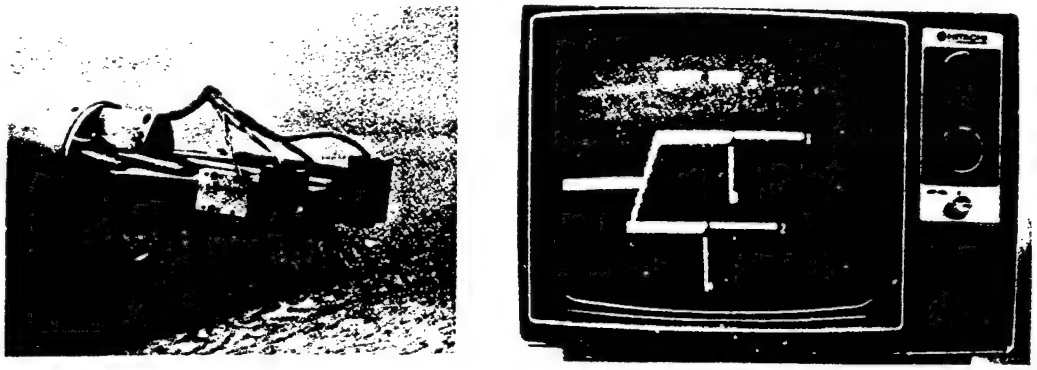

Figure 2. General Graphics Display of Proximity Sensor Beams

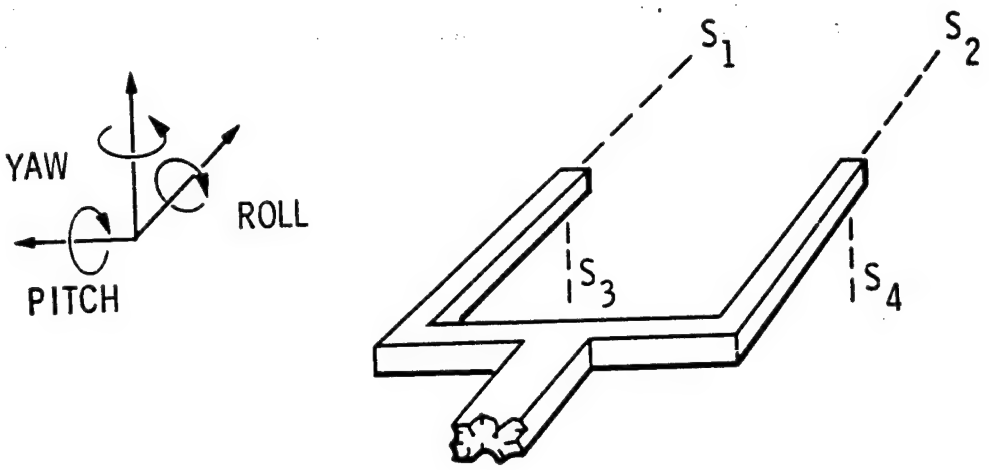

S_i = RANGE MEASURED BY SENSOR " i ", i = 1,2,3,4

D = DISTANCE
T = TOLERANCE
} PRESET PARAMETERS

LOGIC DEFINITIONS FOR EVENT E_i = {K}

E_i = 0 FOR K $\geq$ 0: EVENT ISN'T THERE, BLINKER "OFF"

E_i = 1 FOR K < 0: EVENT OCCURED, BLINKER "ON"

EVENTS	LOGIC EQUATIONS
1. YAW ALIGNMENT AT "D" WITH "T" TOLERANCE	$E_1 = \{\|S_1 - D\| - T > 0\} \bullet \{\|S_2 - D\| - T > 0\}$
2. YAW ALIGNMENT ONLY WITH "T" TOLERANCE	$E_2 = \{\|S_1 - S_2\| - T > 0\}$
3. ROLL ALIGNMENT AT "D" WITH "T" TOLERANCE	$E_3 = \{\|S_3 - D\| - T > 0\} \bullet \{\|S_4 - D\| - T > 0\}$
4. ROLL ALIGNMENT ONLY WITH "T" TOLERANCE	$E_4 = \{\|S_3 - S_4\| - T > 0\}$

Figure 3. Proximity Sensing Events Example

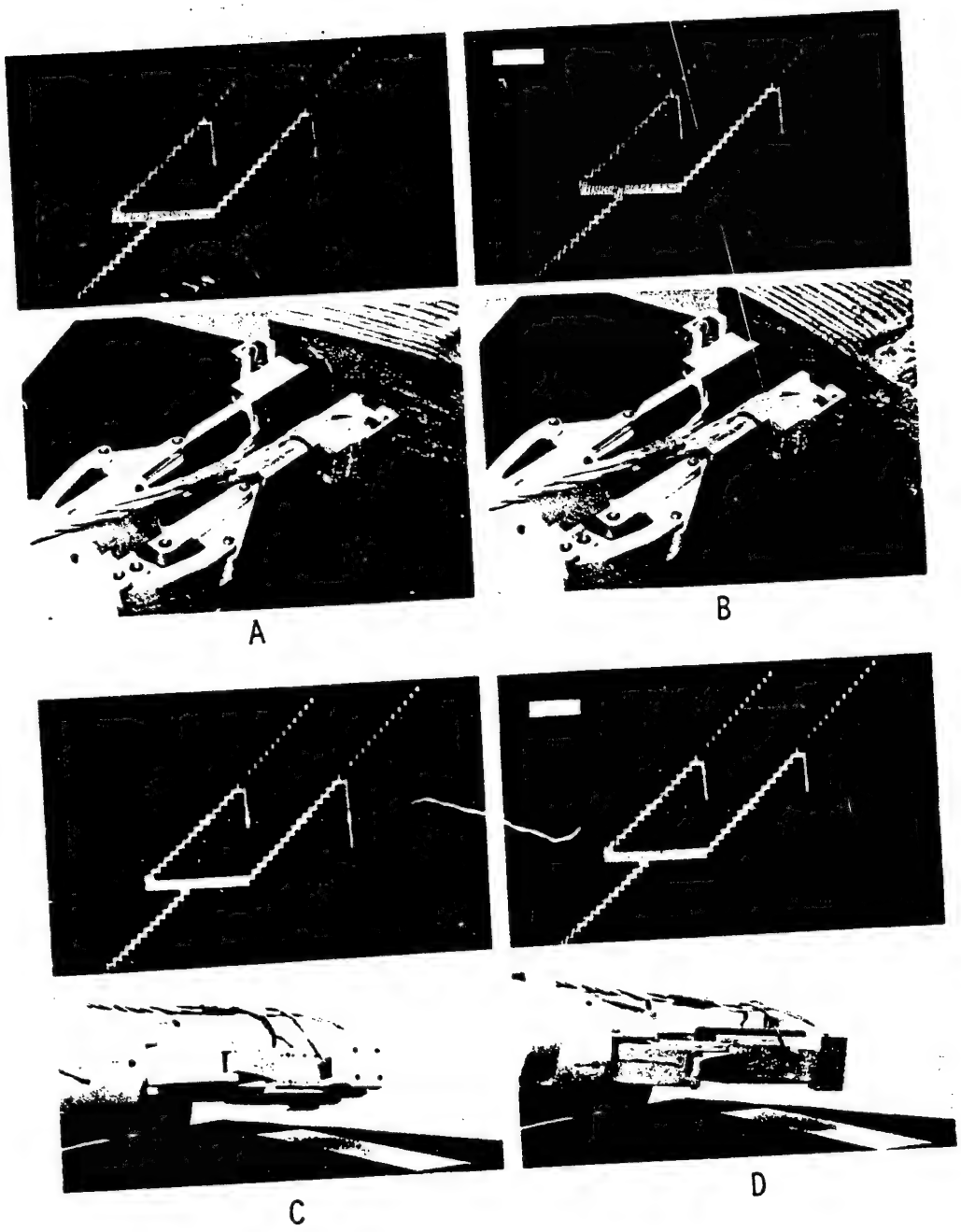

Figure .. Proximity Sensing Events Graphics Display

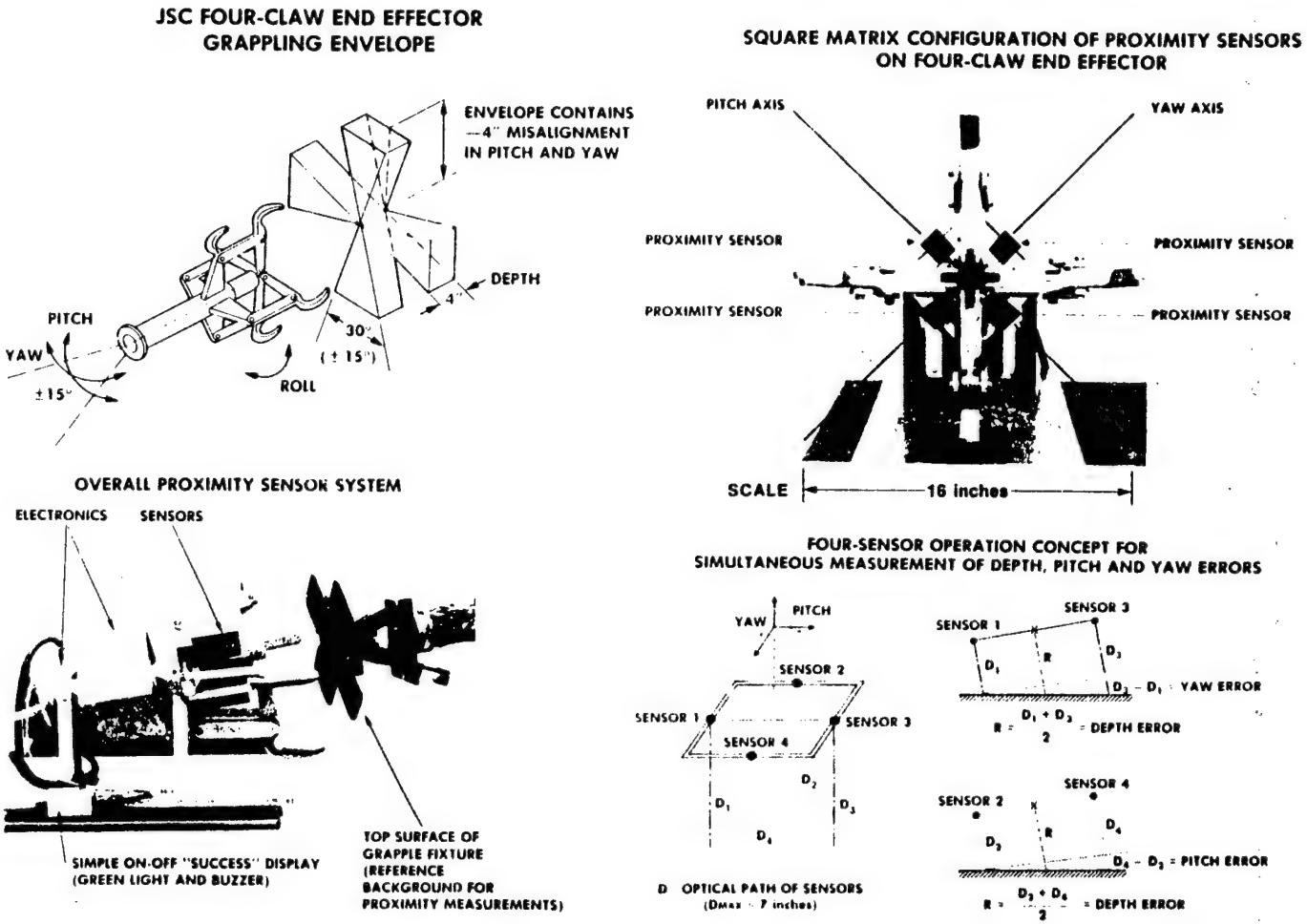

Figure 5. Four Proximity Sensors on JSC Four-Claw End Effector

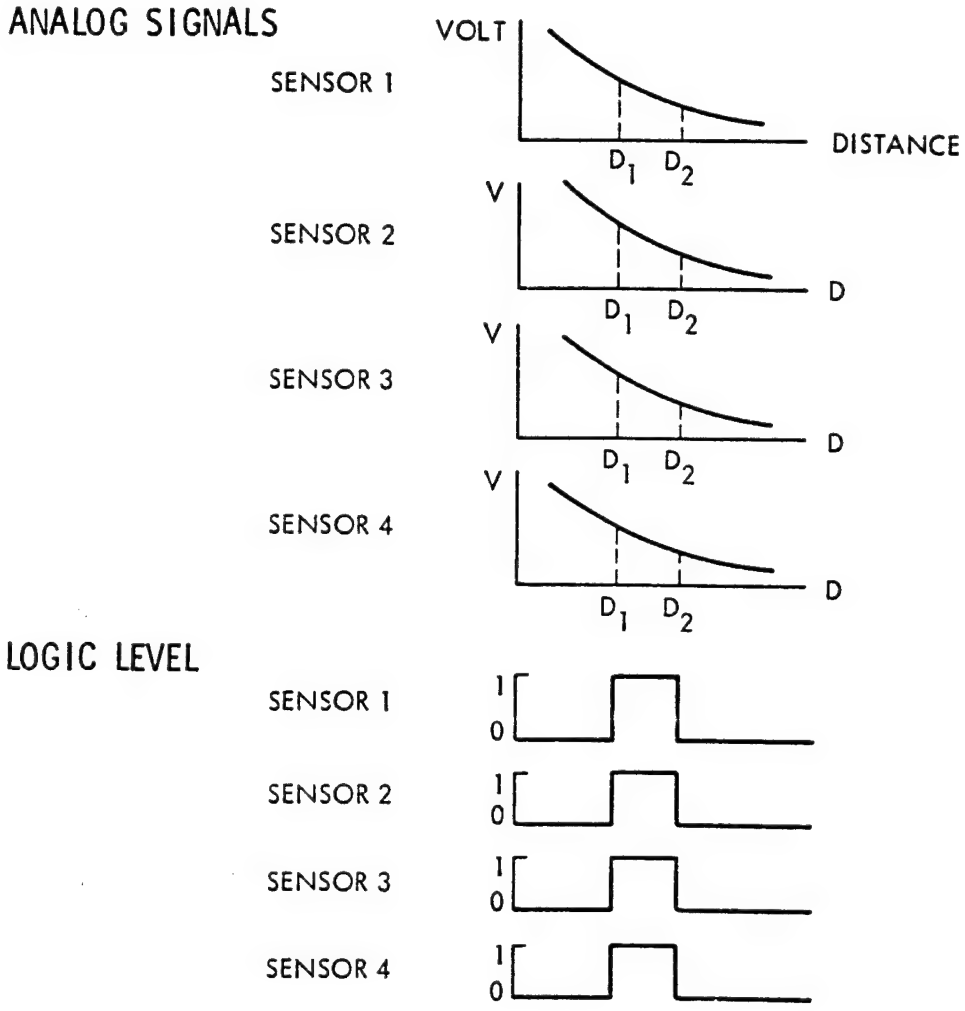

SUCCESS: EACH OF THE FOUR SENSORS OUTPUT IS IN LOGIC STATE "1" (THEN TONE AND/OR GREEN LIGHT ARE AUTOMATICALLY TURNED ON INDICATING TO OPERATOR THAT DEPTH POSITION AND PITCH AND YAW ALIGNMENTS OF END EFFECTOR ARE OK FOR SUCCESSFUL GRASP OF TARGET)

Figure 6. Analog "Event Logic" Indicating Acceptable Combinations of Range, Pitch and Yaw Errors for Successful Grasp Using Four Proximity Sensors Integrated with JSC Four-Claw End Effector

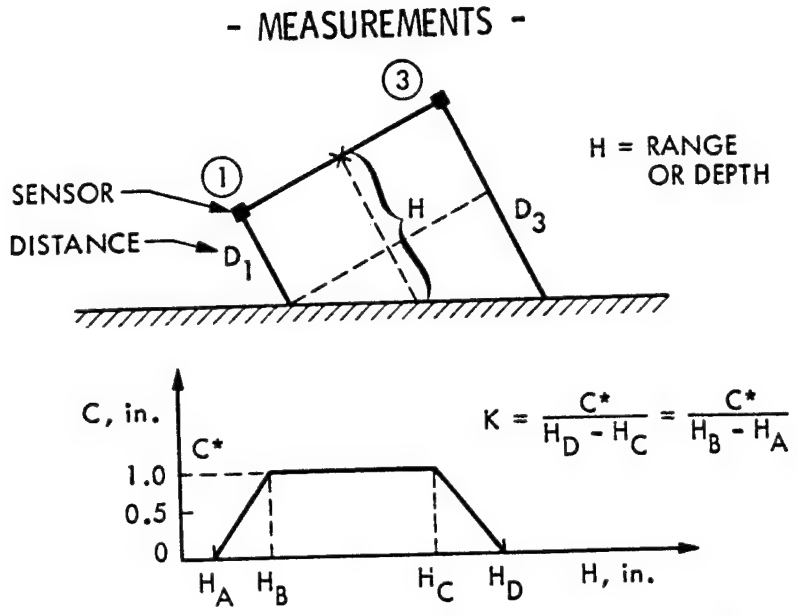

- SUCCESS LOGIC -

(1) $H_A \leq H \leq H_D$

WHERE $H = 1/2\,(D_1 + D_3)$ $1/2\,(D_2 + D_4)$

(2) $(D_1 - D_3)^2 + (D_2 - D_4)^2 \leq L$

WHERE $L = C^2 = [f(H)]^2$

IF BOTH CONDITIONS ARE TRUE THEN LIGHT/BUZZER ARE ON, OTHERWISE OFF

H_A, H_B, H_C, H_D AND K (AND IMPLICITLY ALSO C*) ARE PRESET CONTANTS

F(H) IS GIVEN BY THE TRAPEZOID FORMULA SHOWN ABOVE

Figure 7. Conic Algorithm Indicating Acceptable Combinations of Range, Pitch and Yaw Errors for Successful Grasp Using Four Proximity Sensors Integrated with JSC Four-Claw End Effector

Figure 8. Test Scenes at the JSC Manipulator Development Facility Using Four Proximity Sensors Integrated with JSC Four-Claw End Effector and Simple "Go-No Go" Event Display

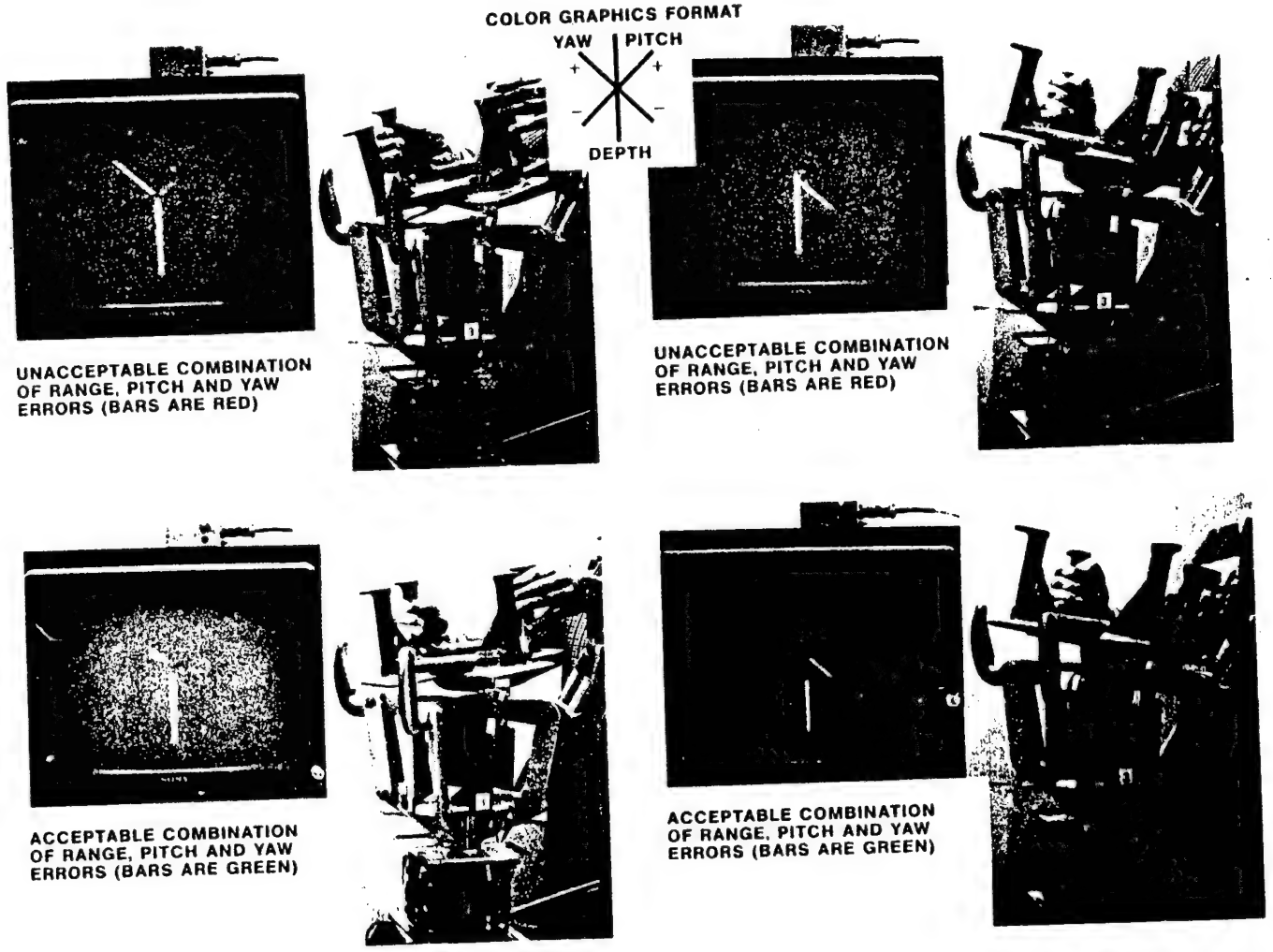

Figure 9. Graphics Display Concept Indicating Both Success and Details of Error States

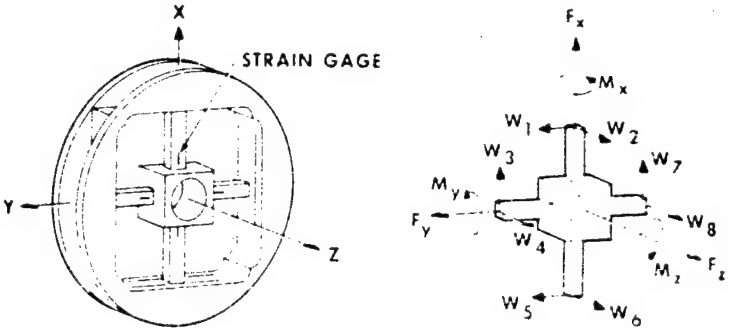

TRANSFORMATION MATRIX
UNDER IDEAL CONDITIONS

FORCES AND TORQUES REFERENCED TO X-Y-Z SENSOR COORDINATES

$$\begin{bmatrix} F_x \\ F_y \\ F_z \\ M_x \\ M_y \\ M_z \end{bmatrix} = \begin{bmatrix} 0 & 0 & k_{13} & 0 & 0 & 0 & k_{17} & 0 \\ k_{21} & 0 & 0 & 0 & k_{25} & 0 & 0 & 0 \\ 0 & k_{32} & 0 & k_{34} & 0 & k_{36} & 0 & k_{38} \\ 0 & 0 & 0 & k_{44} & 0 & 0 & 0 & k_{48} \\ 0 & k_{52} & 0 & 0 & 0 & k_{56} & 0 & 0 \\ k_{61} & 0 & k_{63} & 0 & k_{65} & 0 & k_{67} & 0 \end{bmatrix} \begin{bmatrix} W_1 \\ W_2 \\ W_3 \\ W_4 \\ W_5 \\ W_6 \\ W_7 \\ W_8 \end{bmatrix}$$

FORCES SENSED AT SPOKE ELEMENTS

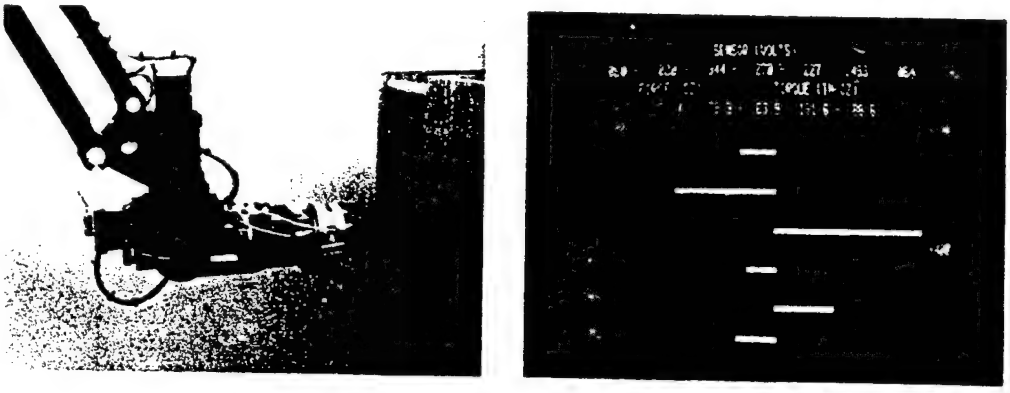

Figure 10. Force-Torque Sensor Measurement Transformation and Graphics Display

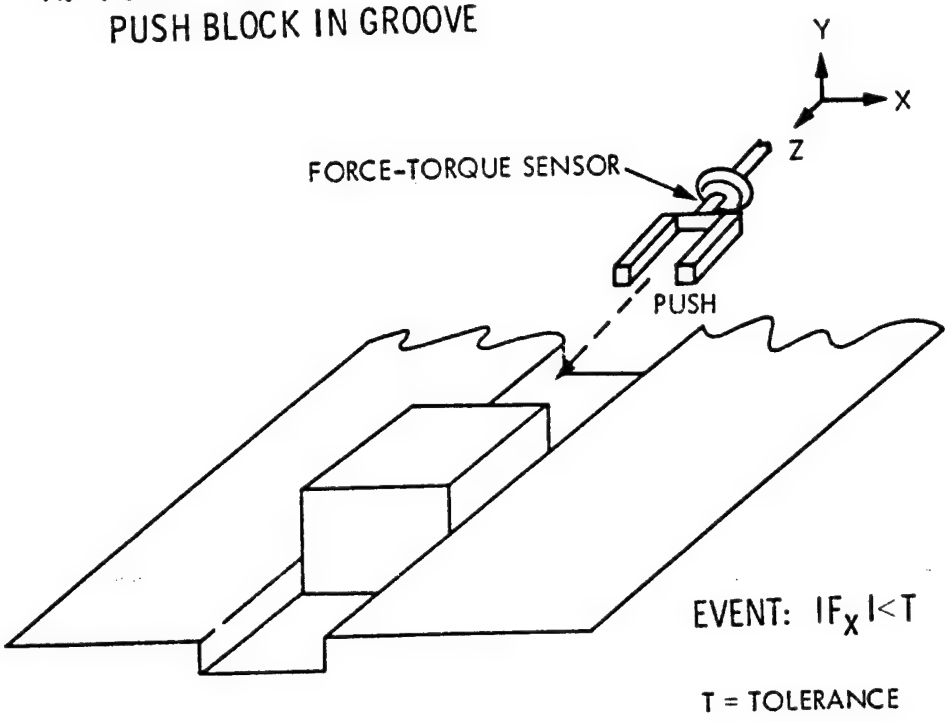

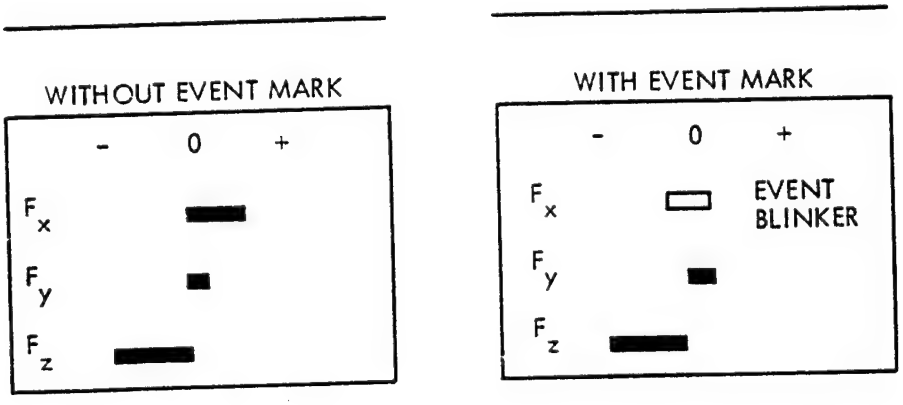

Figure 11. Force-Torque Sensing Event Example

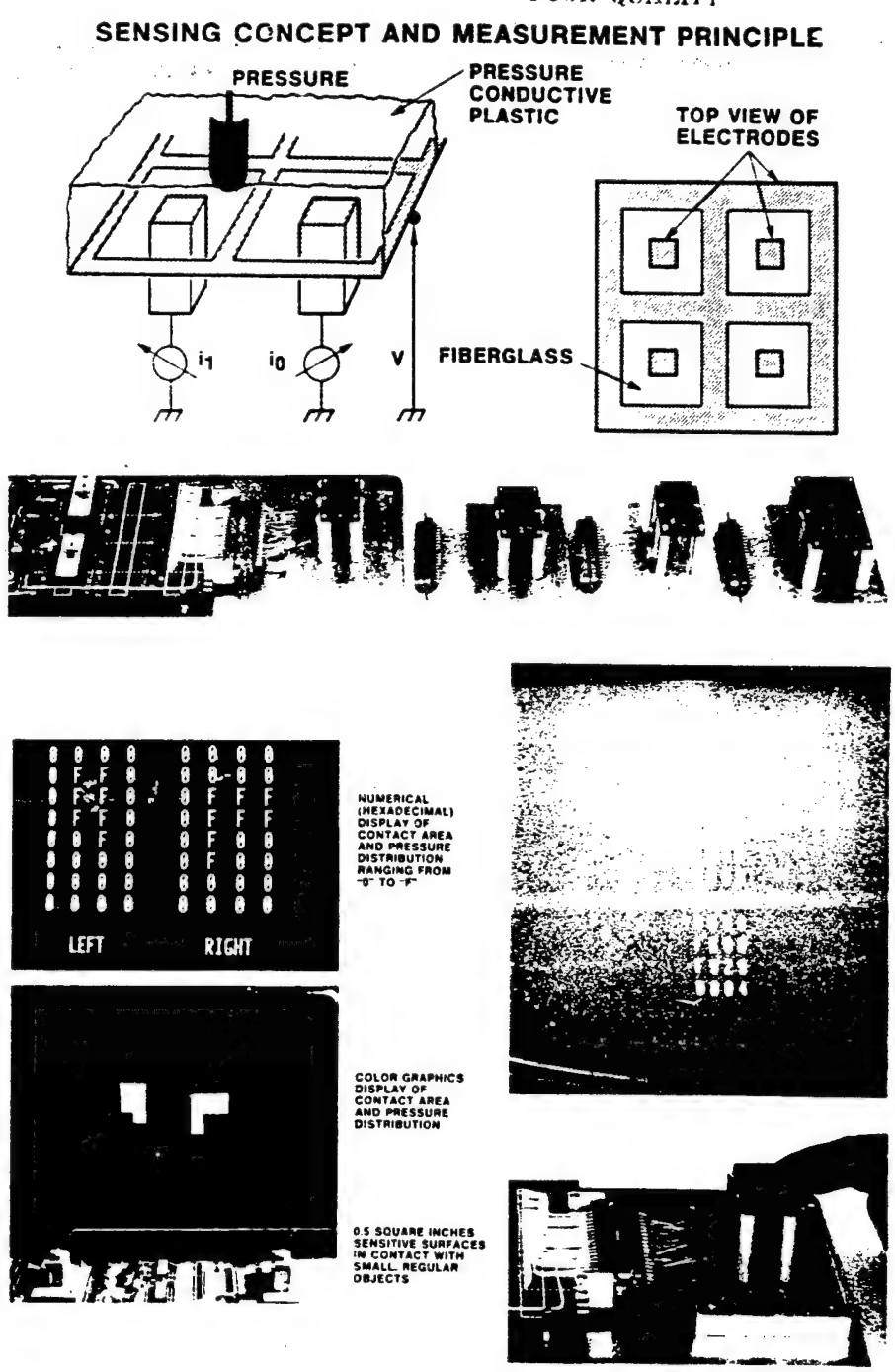

Figure 12. Multipoint Proportional Touch Sensors with Numeric and Color Graphics Displays

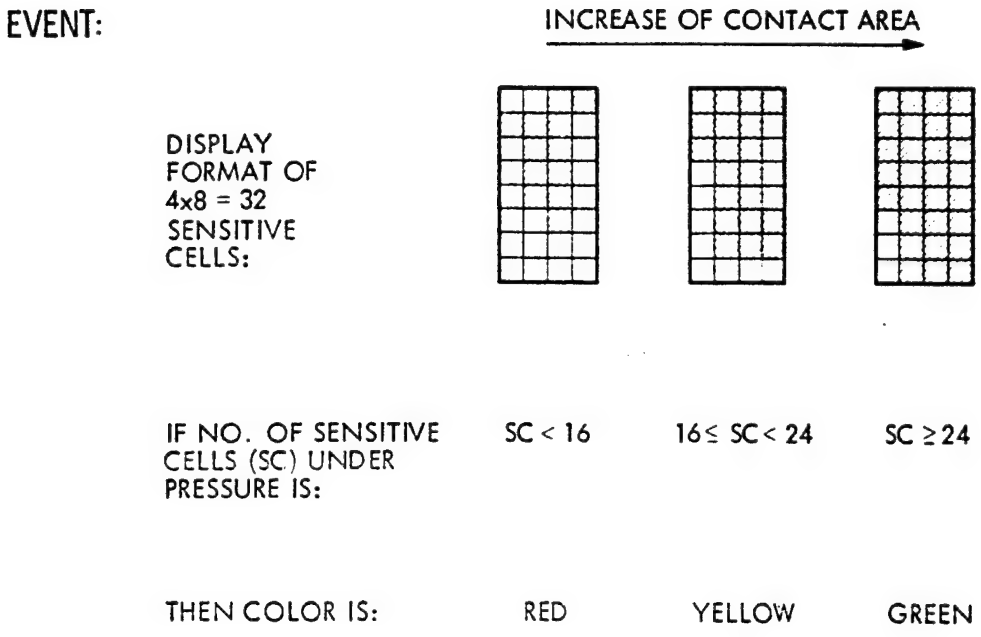

(NB: THE SHADED CELLS ARE THOSE UNDER PRESSURE. THEY HAVE TONES IN THE RESPECTIVE COLORS DARKER THAN THE UNSHADED CELLS.)

Figure 13. Touch Sensing Event Example

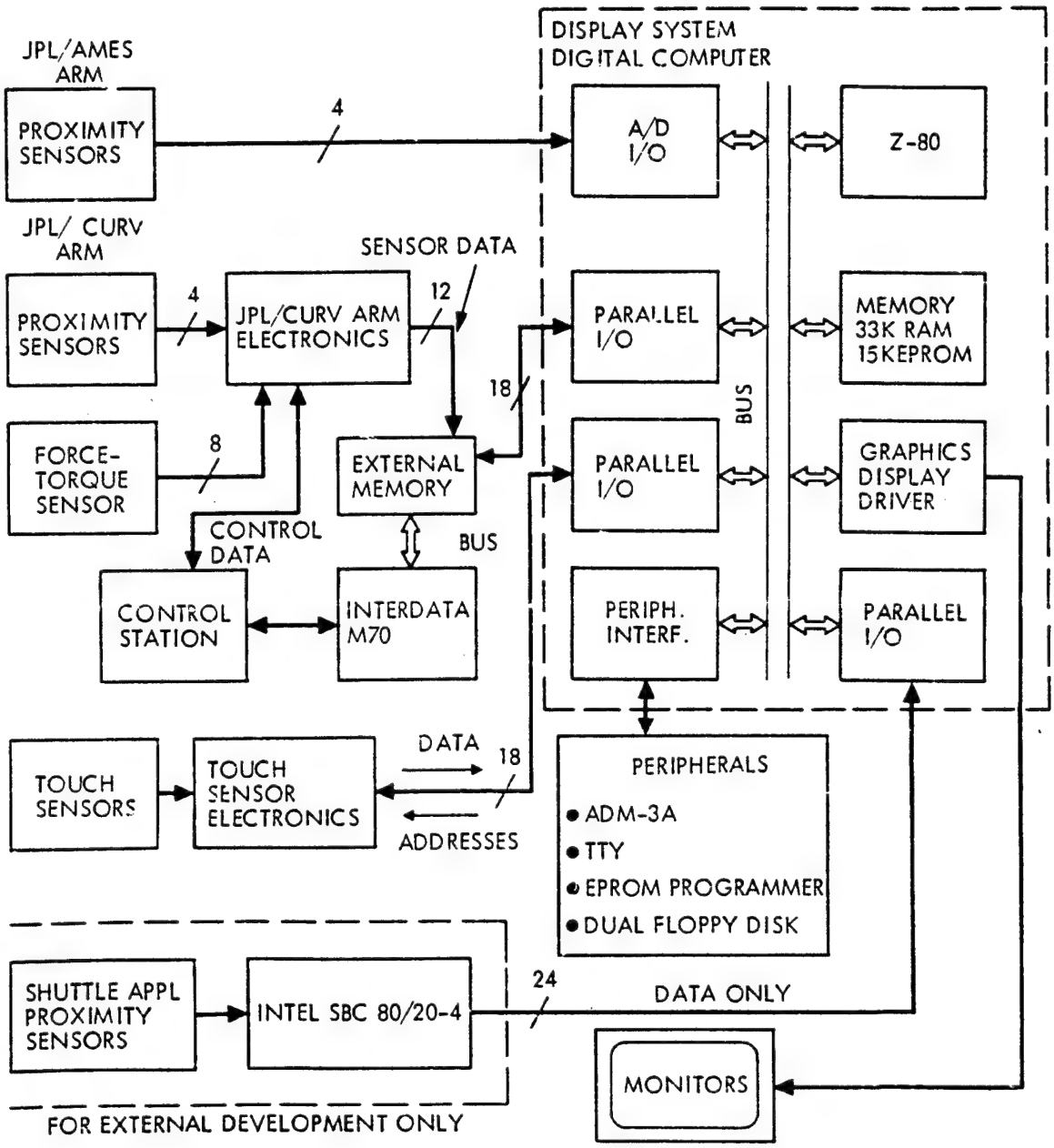

Figure 14. Computer System for Sensor Data Graphics Displays in the JPL Teleoperator Project

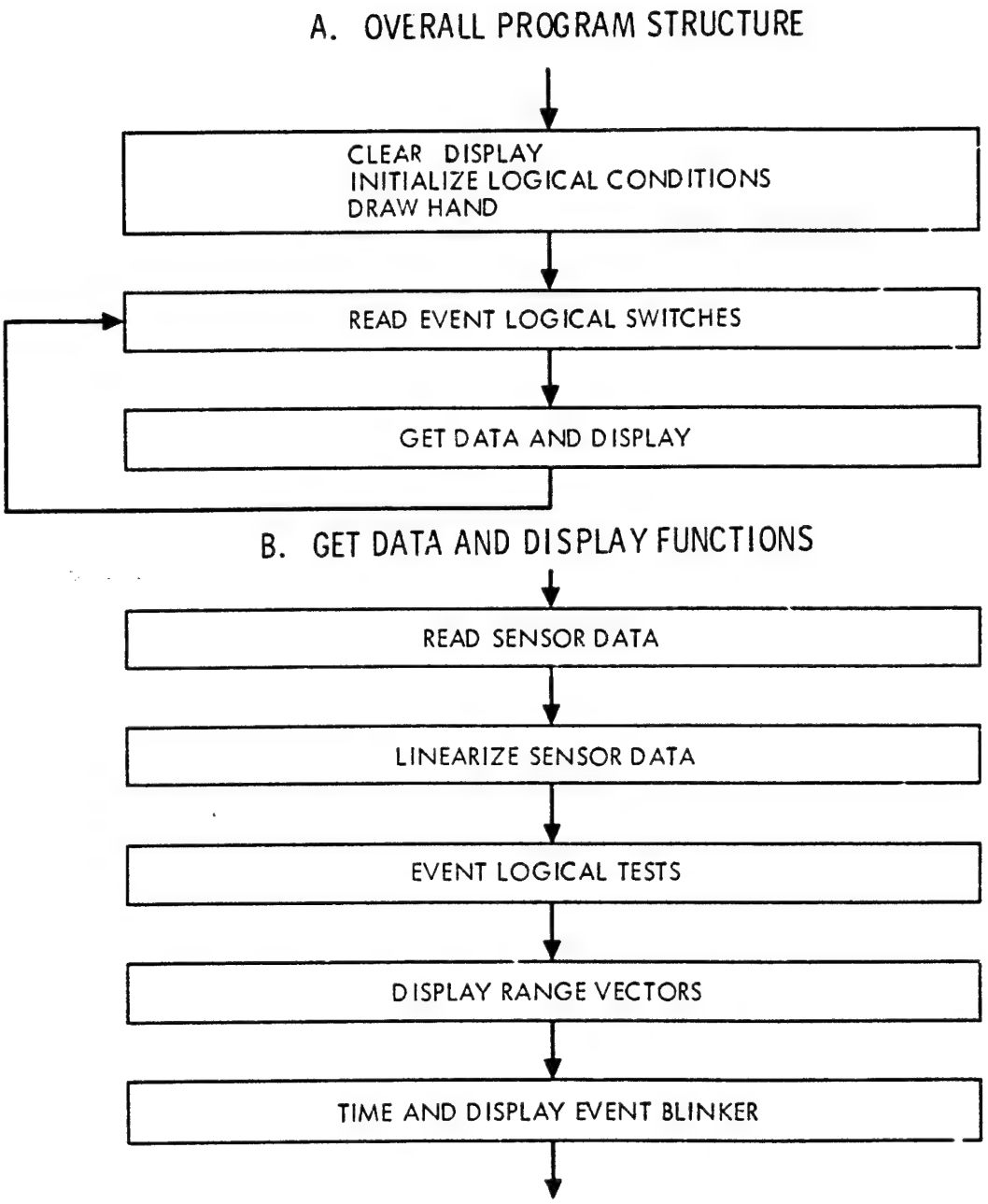

Figure 15. Software System Structure for Proximity Sensor Data Graphics Display in the JPL Teleoperator Project

N79-15611

MANNED SIMULATIONS OF THE SRMS IN SIMFAC

by

Andrew L. LIPPAY, Staff Engineer, Human Engineering, CAE Electronics, Montreal, Quebec, Canada

and

Graham D. WHITEHEAD, Ph.D. Engineering Specialist,

Dr. Claus G. WAGNER-BARTAK, Deputy Program Manager, RMS Division, SPAR Aerospace Products, Ltd, Toronto

INTRODUCTION

SIMFAC is a general-purpose real-time simulation facility currently configured with an Orbiter-like Crew Compartment and a Displays & Controls (D&C) Subsystem to support the engineering development of the Space Shuttle Remote Manipulator (SRMS).

The simulation consists of a software model of the anthropomorphic SRMS manipulator arm including the characteristics of its control system and joint drive modules. Structural flexibility is modelled by presenting the principal modes in six degrees of freedom.

The SRMS control system is normally operated in a Resolved Motion Rate Common mode, commonly known as the Manual Augmented or simply Manual mode. The point of resolution if just inside the tip of the End Effector of the arm, where the head of the Payload Grapple Fixture would fall when in the nominal position for legal capture. A Single mode is also available for selection, whereby the Operator individually commands each joint in turn. In both of these modes a Coarse/Vernier range may be selected, and Rate Hold function may be applied in the Manual mode.

Four coordinate systems may be selected which define the point of resolution and the spatial system response to hand controller inputs. The principal reason for this is to enable the Operator to move the End Effector (and the Payload when attached) in the most direct way possible and reduce the amount of mental transformation required.

Automatic sequences are available to manoeuvre the arm between fixed points. A terminal position and attitude may be determined by pre-programming or by detailed Operator input via a keyboard. The system will move in an optimized path to the terminal point, provided the initial conditions have been fulfilled.

SIMULATION & SCENE GENERATION SUBSYSTEMS

A master/slave computer pair (TI 980B), an Array Processor and floating-point hardware complex execute all computations under a simulator-oriented multi-task operating system (SIMTOS), driving a multi-process interface to which all displays, instruments and other input/output circuitry are connected. An extensive set of peripherals perform data gathering and software development/maintenance tasks.

Displays in SIMFAC are driven by a set of three Varian computers (V73), an array processor and picture generation hardware. An Aft and an Overhead out-the-window scene are presented on two large CRT screens equipped with pancake windows to approximate infinity optics. Two smaller monitors simulate CCTV scenes from six possible camera

positions in selected pairs. Of these the camera mounted on the wrist of the arm seems to carry the greatest impact and will be discussed in detail below.

The visual presentation is driven by a serial data link output from the simulation subsystem, delivered every 50 msec, the pictures are refreshed three times between the frame updates. Camera controls enable the Operator to zoom all cameras, and to pan and tilt all except the End Effector (Wrist) Camera.

Cockpit displays and controls resemble the Manipulator Station of the Orbiter. Mode selector switches, digital position/attitude/rate readouts and a comprehensive Caution & Warning annunciator panel are mechanized and driven by the main model outputs.

A Translational (THC) and a Rotational Hand Controller (RHC) are mounted to the left and right of the D&C panel. The THC has one linear and two pivoted axes in a package representing the flight article. It controls the rates of movement in the X, Y and Z freedoms of the point of resolution in the coordinates selected. The RHC has three pivoted axes and controls the attitude (angular) rates about the point of resolution. It also carries the Rate Hold, Capture/Release and Coarse/Vernier auxiliary controls. The THC has rate-dependent damping, both have spring return and breakout forces.

Caution/Warning annunciators include a Master Alarm coupled with an audio tone, and a lighted annunciator panel. The two most frequently activated are the Reach Limit Alarm, indicating that one of the joints is too close to its angular limit, and the Singularity alarm signalling a limited arm geometry such as that of the arm at rest in its latches, fully extended and unable to accommodate an applied load by yielding to excessive forces.

The manual control problem can be appreciated by considering that the design load limit of the arm is a deflection of 25.4 mm (1.0") under a lateral force of 4536 g (10) lbs, with the not-to-exceed limit being 4763 g 15 lbs. Software stops provide protection by refusing to drive a joint into its hard stops and arm movement ceases completely if the Reach Limit alarm does not result in the reversion of the manual inputs.

THE SRMS TASK IN SIMFAC

The principal task of the SRMS Operator is to manoeuvre the arm and its End Effector into a precise position and attitude with respect to the Payload in order to establish a rigid contact with the Grapple Fixture, and thence manoeuvre the Payload into the desired position and attitude with respect to the appropriate coordinate references, with zero residual energy remaining in the total system. In real life, the End Effector must not contact the Payload until the

latter has been secured against escape, and must not touch any other part except the grapple fixture. The Payload may initially be moving with respect to the Orbiter or it may be docked and secured in the Cargo Bay of the Orbiter. Relative velocity in excess of 0.061 m/s (0.2 fps) constitutes an illegal capture condition where contact must not be attempted. The arm must arrest the Payload within 608 mm (2.0 feet) after Capture. The positioning accuracy must be such that the maximum size Payload 18.24m long, 4.56 m dia (or 60 feet long x 15 feet diameter) can be placed into the Cargo Bay with an all-around clearance of 76.2 mm (3.0 ins).

In the case of the simulated moving Payload, the Operator must establish stable tracking with the End Effector before attempting to grapple, in approx. 80 secs. from the time the Payload enters the effective reach envelope of the arm. This phase is the most dynamic of the entire control task and will be the principal subject of discussion from here on. The tracking and eventual capture are based almost exclusively on the visual information provided by the CCTV camera carried by the arm. This scene is presented on a small CCTV monitor to the right of the Operator with a reticule applied to the glass envelope. This "gunsight" scene has a significant impact on the Operator; any high rate of movement or oscillatory behaviour generates a high gain condition in the external man-machine loop, increases the workload and may lead to PIO (Operation-Induced Oscillations). Among other things, it encourages capture attempts "on risk", i.e. without the assurance of being within legal limits. Since the camera is simulated as mounted on the wrist, a less than stable platform, arm flexibility effects generate just such visual dynamics, in addition to those produced by the real movement of the Payload with respect to the End Effector. Furthermore, the Operator is not positioned on the same platform, hence he will not receive motion cues to help him compensate for the lively visual scene.

A less dynamic but equally difficult situation ensues when the principal axes of the Payload or the End Effector are displaced from being parallel to those of the Orbiter. The four available coordinate systems recognized by the control algorithm are referenced to the End Effector, the Orbiter, and the Payload, respectively, and the fourth is divided between the Payload for attitudes and the Orbiter for translations. Euler sequences destroy the spatial correspondence between the hand controllers and system response where the coordinate system in use moves with the Payload or End Effector, but the Operator remains "frozen" to the Orbiter. Furthermore, a coordinate system, consistent in the engineering sense, will generate contradictory display increments and cause wrong-sign inputs unless its sign

convention is duly adjusted to conform with the aeronautical "positive" and "negative" in terms of switch or stick movements.

In summary, the SRMS command task is somewhat similar to flying a airplane by remote control, rather than that of piloting an aircraft.

OPERATOR TACTICS AND OPTIONS

Successful Operators in the SIMFAC simulations have quickly learned to accommodate the basic system responses and developed individual but similar command techniques. In the capture task they eliminate attitude errors first, in Coarse mode at a safe distance from the Payload, then use long, smooth approaches, maintain tracking. They apply ramped, well-damped command inputs to avoid flexibility effects and to reduce the image displacement rate on the End Effector gunsight scene. One attitude and one translational correction is applied as a pair to avoid roll-pitch cross-coupling and to minimize target displacement on the CCTV scene. Trained Operators maintain a good inner image of the arm geometry and are able to avoid joint angle limits, estimate the total arm performance available and even trade-off rotational vs. translational corrections for a smooth and efficient approach. The SIMFAC hand controller characteristics are said to make a significant difference against earlier models which had no damping and generally poor engineering quality.

Operator options such as Vernier selection which reduces the command authority to 10%, and Rate Hold, are used by all Operators, the former mostly to reduce the liveliness of the gunsight scene and to increase precision as required. The system applies Vernier automatically on Capture, i.e. during the transition between unloaded and loaded arm, and a manual selection reduces the Loaded Vernier velocity to 50%.

WORKLOAD

A peak is reached during the Track and Capture task. Arm flexibility effects appear in the CCTV reticule as elliptical oscillations, easily excited with high visual effects especially at close range. However, they damp out if not further excited and true PIO does not develop. The spare Operator capacity is significantly reduced, the gunsight scene is the focus of intense concentration. The selection of Vernier is easily predictable for most Operators, as a function of range from the Grapple Fixture, since it is determined by their acceptance of activity on the CCTV scene.

Other sources of increased workload include the necessity to make ramped inputs to command precision movements, to perform mental transformations in Payload manoeuvering and the management of the D&C subsystem, especially while operating in the Single mode, controlling each joint individually. Ramped inputs require high concentration over

many seconds; well-balanced and damped hand controller characteristics are essential. Coordinate transformations also require high mental effort during the final phases of Payload positioning, since a wrong-sign input will not only disturb a near-perfect deployment condition, but many cause collisions during the berthing task, with the Payload in close proximity with the Orbiter.

Displays and Controls Management involves mode selection and display selection, since all parameters cannot be simultaneously displayed; XYZ position and pitch-yaw-roll attitude must be selected for digital display readout. Mode selection must be followed by an Enter command to be accepted by the system. The Single mode involves not only display selection (associated with the tasks the mode is normally used) but also the selection of each of the six joints followed by the operation of a double-throw switch for positive or negative input.

In summary, the Resolved-Motion Rate Control system provides adequate means to control the manipulator arm by one Operator as specified for the SRMS tasks. Research work at MIT, NASA/JSC, NASA/Ames and NASA/Marshall have been compared with some experimental setups at Martin-Marietta, as well as Honeywell and CAE experience in fly-by-wire applications, and command philosophies such as the replica arm and force-stick controllers have been considered but later rejected in favour of the displacement stick and rate command with resolved-motion augmentation. A six degree-of-freedom controller would have been favoured for a single/command/input point but had to be abandoned for lack of cockpit space and because of higher design risk.

OPERATOR ERRORS AND SOURCES

Up to the time of this writing, the main SIMFAC effort was directed to validate the flexible arm and SRMS subsystems simulation, and to establish basic controllability and operability for the tasks specified. Initial work has been completed to simulate malfunctions and off-nominal conditions to verify procedures and indicate parameter sensitivities. No attempts have been made to simulate side-tasks, Orbiter environment and on-orbit workload. However, comments of Operators have been carefully recorded and analyzed, and their assessment of their own performance was elicited whenever practicable, both in terms of the simulation and the simulated SRMS tasks.

Short of malfunctions, the reference coordinate systems and sign conventions presented the greatest single problem as soon as human operators were inserted in the control loop.

The End-Effector CCTV scene with its reticule is essentially a fly-to display. One of the Alignment Aids (Payload target) resembled the

small aircraft symbol usually found on artificial horizons and flight directors. An Operator with long flying experience promptly reverted to the fly-from technique associated with that type of instruments and has had considerable trouble in readjusting his thinking during the demanding Track and Capture task. With a different target he had no difficulty.

Arm geometry causes non-linear responses due to limitations in the individual joint drives, necessary to ensure that the End Effector does not exceed certain velocity limits. Finite joint ranges and arm singularities also cause uncommanded stoppages. While most of these effects can be avoided or accommodated by trained Operators, the visual conditions in SIMFAC do not provide texture, hardware markings, shadows and other assistive side effects.

Visual conditions in the Space Shuttle are expected to vary between extremes, from sunshafting and specular reflections to near-total darkness. Wide variations in illumination will occur with every adjustment of the Orbiter attitude or Payload position. Judgement of depth or X-ranging is expected to be poor in real life as it is in SIMFAC, with its two-dimensional visual displays.

The dynamic aspects of the SIMFAC visual presentation are quite adequate. However, the SRMS task itself produces low-key visual cues with low dynamics, difficult to detect and monitor. A 18.24m (60 ft.) long Payload suspended say 15.2m (50 ft.) away from the Operator may have a very low yaw rate but its end bulkheads move with relatively high speed, and may contain great energy with the maximum Payload mass of 29,484 Kg (65,000 lbs). Furthermore, arm flexibility effects and control system responses are very similar in their visual aspects under certain circumstances near the Cargo Bay, potentially inducing the Operator into erroneous corrective action.

The SIMFAC Displays and Controls Subsystem resembles the Orbiter complement but is not completely representative of it and lacks some of the visual impact of the flight article. The hand controllers are engineering model quality but well engineered and have acceptable force characteristics and feel.

The harmony of manual input to system response is generally good, the controllers providing a one-to-one relationship with the desired Payload or End Effector movement. The displays follow the system responses adequately and present necessary and useful task information. However, the harmony between the command inputs and the display responses is not optimized in that the position and attitude information is referred to the Orbiter, while the command axes may be transferred to the End Effector or Payload. Hence, the same manual input will drive one display window or

another, depending on the Euler angles. The Operator then has to compensate with mental transformations and therefore is prone to errors and incorrect inputs. This effect is most noticeable in precision manoeuvres during Berthing and Payload Deployment, when the Operator is "flying the Payload on instruments", i.e. making final adjustments by the digital displays. This observation on SIMFAC resulted in a change of SRMS coordinate systems and displayed values.

The management of displays and controls is a significant side task with some peak workloads occurring in parallel with other high-activity periods.

AREAS FOR FURTHER WORK

Visual improvements are being planned for SIMFAC. Full hidden line removal and additional scene contents are considered. As noted above, the dynamics of the visual scenes are largely satisfactory and carry a high impact.

Orbiter-SRMS interaction, namely reactive forces and the operation of the Orbiter attitude control systems, have not been fully simulated in SIMFAC.

Man-machine integration and rigorous Operator modelling work would be most desirable from the resarch point of view, since these are outside the scope of an industrial development. Multi-axis hand controllers, computer-driven active force feel systems, integrated displays may be needed for future generations of Remote Manipulators. The loop dynamics exhibited by the wrist camera in this simulation in connection with the human visual and neuromotor channels is peculiar to large manipulators and presents a set of interesting modelling tasks in itself.

GENERAL OBSERVATIONS

The simulation as a whole is considered successful, judging from the reaction of Operators to computer glitches and malfunctions. These indicate that the experienced Operator is very much in the simulation picture and is using his best efforts to perform the task.

Learning curve effects are readily visible and repeatable, well documented. The task presented in SIMFAC, that of capturing a free-flying satellite and berthing it into the Cargo Bay is deemed equivalent to the worst case task expected to be attempted in real life.

Quick setup and initialization capability of SIMFAC facilities manned simulation under reasonably consistent conditions.

The observed command strategy and Operator behaviour, as well as individual performances, clearly indicate not only the existence of an "inner model" but the necessity of one even in the static sense, whereby some Operators manage to maintain a picture of arm configuration regardless of arm visibility, and avoid potential

joint limits, singularities and collisions.

Some Operators perform equally well in dynamic and precision manoeuvres, others exhibit a distinct preference and success in one or the other. No explanation is offered at this time except the possibility that the force characteristics of the hand controllers may have enhanced competence in some cases by matching the individual neuromotor systems.

The flexibility of the dynamic arm presented a distinct increase of task difficulty compared to the kinematic arm model, but all operators managed to adapt their input rates and control strategies to overcome these effects. It may be noted that both the increased dynamics in the wrist camera scene due to flexibility, and the absence of an alignment aid target, led to attempts to capture with less than proper alignment or at a questionable capture distance.

Simulated malfunctions presented in SIMFAC generated three distinct phases of response in each Operator participating in the tests. At first, a malfunction was immediately considered on the SIMFAC system, i.e. a simulation error. No corrective action was attempted. In the next phase, most Operators blamed themselves, claimed Crew Error and tried to rectify it until they realized that the corrective commands were ineffective. Finally, absolutely everything out of line was suspect, and immediately questioned as to which malfunction is being presented.

From the point of view of man-machine integration, the external loop composed of the Operator, the Wrist Camera display and the behaviour of the End Effector due to flexibility effects and arm geometry present a intricate problem. It is impossible to analyze these relationships on paper and understand the wide range of factors involved, many of which are intangible, such as the aeronautical control conventions ingrained in Operators with piloting experience. SIMFAC has some shortcomings; to be sure; the visual scenes lack texture, reflections and shadows, contrast and similar effects, but the dynamics of the presentation are sufficiently convincing to point out flaws in the man-machine interface and to validate system stability and operability with man in the loop.

HUMAN/COMPUTER CONTROL OF UNDERSEA TELEOPERATORS

T.B. Sheridan, W.L. Verplank and T.L. Brooks

Man-Machine Systems Laboratory
Department of Mechanical Engineering
Massachusetts Institute of Technology
Cambridge, Massachusetts 02139

Abstract

This paper discusses the potential of supervisory controlled teleoperators for accomplishment of manipulation and sensory tasks in deep ocean environments, and discusses one such system. Teleoperators and supervisory control are defined, the current problems of human divers are reviewed, and some assertions are made about why supervisory control has potential use to replace and extend human diver capabilities. The relative roles of man and computer and the variables involved in man-computer interaction are next discussed. Finally, a detailed description of a supervisory controlled teleoperator system, SUPERMAN, is presented.

1. Teleoperators and Supervisory Control

Many future undersea tasks may be accomplished by "teleoperators". We define teleoperators to be general purpose submersible work vehicles controlled remotely by human operators and with video and/or other sensors, power and propulsive actuators for mobility, with mechanical hands and arms for manipulation and possibly a computer for a limited degree of control autonomy. A manned submersible is not a teleoperator vehicle, but its attached manipulators are certainly teleoperators, requiring control through a viewing port or through closed-circuit video. Sometimes the term "teleoperator" is restricted to telemanipulator, excluding the system for remotely positioning and orienting a sensor, but for the sake of generality we include this important function.

This paper focuses on those aspects of undersea teleoperation which concern the human operator and the man-machine interface, and within this still relatively broad domain, it concentrates on the prospects for utilization of "supervisory control". Supervisory control is a hierarchical control scheme whereby a system (which could be a teleoperator, but could also be an aircraft, power plant, etc.) having sensors, actuators and a computer, and capable of autonomous decision-making and control over short periods and in restricted conditions, is remotely monitored and intermittently operated directly or reprogrammed by a person.

The distinction between direct human control of a teleoperator and supervisory control of a teleoperator is made graphically in Figure 1. In

+ This work was supported by Office of Naval Research (Contract N00014-77-C-0256) and by the MIT Office of Sea Grant (National Oceanographic and Atmospheric Administration).

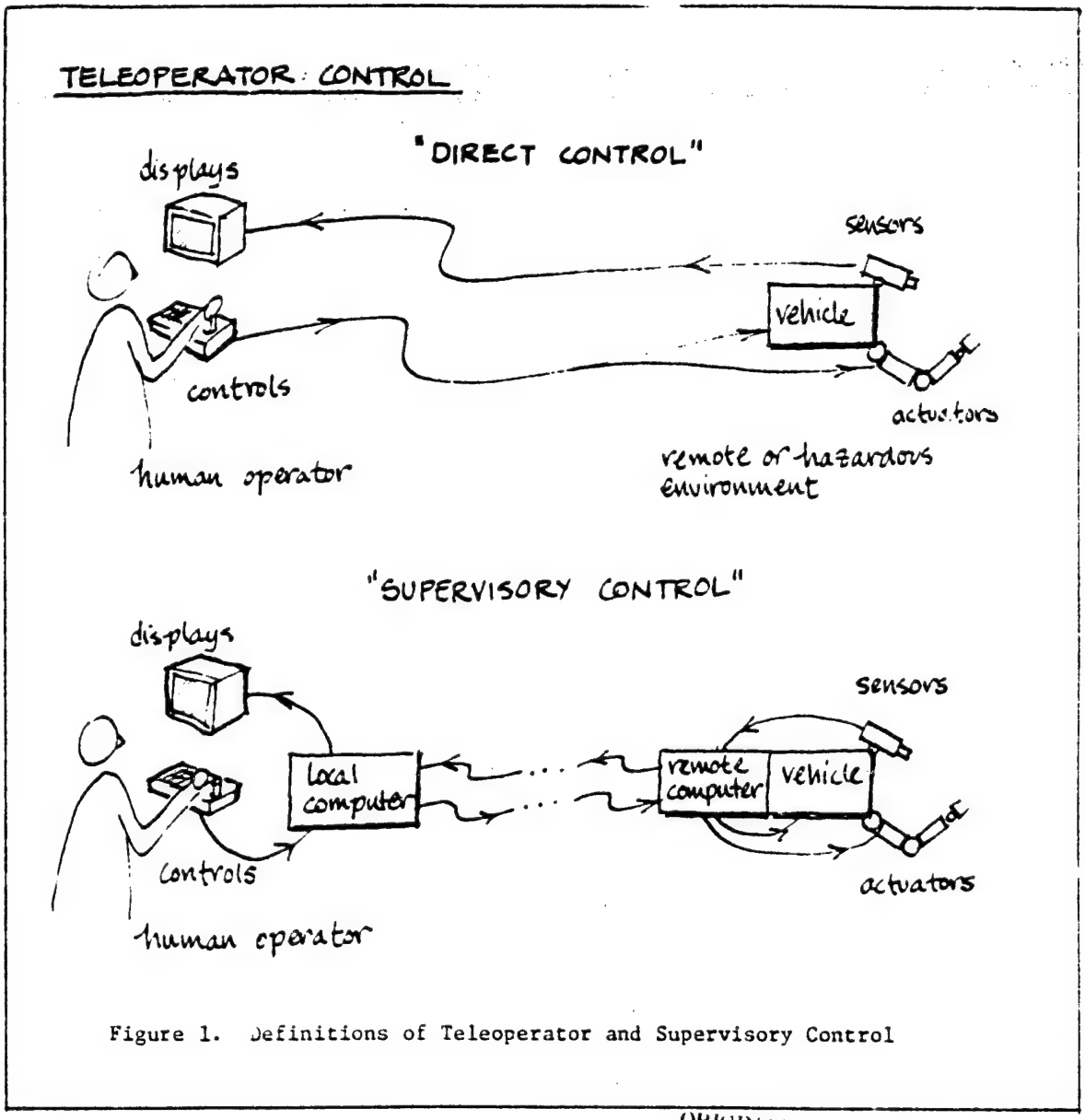

Figure 1. Definitions of Teleoperator and Supervisory Control

Definitions

TELEOPERATOR

A vehicle having sensors and actuators for mobility and/or manipulation controlled by a human operator, and thus enabling him to extend himself to physically remote or hazardous environments.

SUPERVISORY CONTROL

A heirarchical control scheme whereby a device having sensors, actuators and a computer, and capable of automomous decision making and control over short periods and restricted conditions is remotely monitored and intermittently operated directly or reprogrammed by a person.

the upper figure the human directly controls, over either a wire or sonic communication link, the separate propulsive actuators of the vehicle, the actuators for the separate degrees of freedom of the manipulator, and the pan and tilt actuators of the video camera. The video picture is sent back directly to the operator. The "hand control" can be a master-slave positioning replica or a rate joystick.

In the lower figure a computer is added to the teleoperator, and for short periods and limited circumstances this teleoperator may function autonomously.

At the bottom are generic definitions of teleoperator and supervisory control. The upper drawing portrays the former without the latter. The lower drawing is the combination.

In supervisory control the teleoperator's (remote) computer communicates at high bit-rate with the teleoperator's sensors and actuators. But because of bandwidth constraints on the signal transmission link, or because of teleoperator sensing limitations, communication may be restricted to low-bit-rate with the human operator's (local) computer. For this reason, and also because of the intermittent nature of human monitoring and reprogramming of commands on a keyboard (and possibly joystick or other controls), the human supervisor's communication with the teleoperator tends to be at a slow rate, i.e., intermittent symbol strings or movement sequences on a master-controller with relatively many bits per instruction package. His communication with the local computer to refresh TV images or to edit or "dry run" his commands on a model before committing them to action may be constrained only by his own speed limitations.

The physical separation of local and remote computer is not necessary in aircraft, industrial plants or other systems where the operator is physically nearby, and where supervisory control is used for reasons other than physical remoteness and limited communication channel capacity between human operator and the object of control. In such situations supervisory control may be advantageous, nevertheless, to achieve faster or more accurate control, or to control simultaneously in more degrees-of-freedom than the operator can achieve by direct servo-control, or to relieve him of tedium. The latter reasons for supervisory control can apply to undersea vehicles when the human operator is not physically distant (as with manned submersibles) or to undersea teleoperators when a reliable high-bandwidth communication channel (wire or optical tether) is available.

2. Why Teleoperators Underseas? The Limits of Divers and Manned Submersibles.
The principal reasons for interest in using teleoperators for underseas tasks are dollar costs and safety.

Operations, including exploration, inspection, construction, maintenance, salvage and rescue, are having to be performed at increasing depths. At such depths - below, say 300m. (depending upon the paticular task) the time required for divers - mostly compression/decompression time - becomes excessive; factors having to do with depth per se, including life support equipment,become increasingly costly; personal safety is more and more difficult

to maintain. These assertions are borne out by rather alarming mortality figures for commercial divers in the North Sea.

Water turbidity and other depth-related factors may require greater bottom-time, thus compounding the decompression-time factor. Under such conditions, a fixed-capability teleoperator, which sometimes is seen as too clumsy by comparison to a human diver at shallower depths, becomes much more attractive economically.

Happily, there is progress in the development of teleoperators, and they are becoming less clumsy. Inspection and manipulation tasks which simply could not be accomplished a few years ago are now achievable, due to steady progress in the design of video systems, mechanical valves and actuators, etc. For the immediate future, however, the primary technological factor which is changing the prospects for undersea teleoperation is the computer.

Circa 1970 divers seemed to have the edge on manned work-vehicles with manipulators in terms of maneuverability, manipulation, tactile sensing, and covertness. Because of smaller unmanned vehicles and eventually through unmanned untethered vehicles, however, the diver (especially the tethered diver) is losing his edge. Manipulation, sensing and cognition remain the primary advantages for the diver, but the computer is changing these also.

The comparison between teleoperators and manned submersibles is more clear-cut. The fact is that television cameras can now "see" with less light than the human eye, and new sonic imaging systems can see through densely turbid waters where neither human vision nor video can function. Spatial resolution of video can be made to approximate that of the eye by focusing. Present advantages of manned submersibles or teleoperators as work vehicles (neglecting for the moment personnel rescue) are: steropsis for close-up objects, and the ability of a human observer with a wide angle of view to keep track of the relative location of different objects. As the communication channel improves, to the point where the manipulator itself is the limiting factor, a man in a submersible can control manipulators or video pan-tilt controls just as well as a man on the surface. The major difference remaining between manned submersible and teleoperator are then cost and safety, as with the diver. The pressure vessel and life-support equipment make the manned submersible much more costly than the same vehicle without the pressure vessel and life-support equipment but with remote control instead. The factors of quality and reliability of communication and remote control then become the key factors.

3. Why Supervisory Control of Teleoperators Underseas? Some Assertions about the Problem.

a. Demands are increasingly stringent in terms of depth, sensory resolution, speed and accuracy of power of response for accomplishment of undersea tasks. Some of these tasks are always the same and are amenable to fixed automation, but many are different each time they occur and therefore cannot be done by fixed automation.

b. In terms of depth and skill human divers are reaching their limits, or when they go beyond these limits they do so at significant risk to life and cost in support equipment and personnel.

c. Teleoperators, i.e.,submersibles having video and other sensors, actuators for mobility and manipulation, and remotely controlled by human operators, offer much promise for extending man's flexible, adaptable, perceiving and control capabilities into remote and hazardous environments.

d. Present teleoperators are quite limited in sensory capability (e.g.,in turbid water), in manipulation capability (in speed and dexterity as compared to human hands), and in dealing with distortion in man-machine communication (misorientation of teleoperator to human body, time delays and noise).

e. Computers are rapidly getting smaller in size and power requirement and cheaper in cost for a given computing capability.

f. While accomplishment of one-of-a-kind undersea tasks by intelligent and completely autonomous robots may have appeal, we simply do not have available at this time such devices or the understanding to build such devices.

g. Undersea systems, like aerospace systems, demand conservative design because unreliability poses severe costs.

h. The most immediate and reliable approach would appear to be to add modest computer aiding and "artificial intelligence" to teleoperators, retaining human sensing, motor, memory and decision capability, at least for higher level planning, decision-making, and control.

i. Over a longer period of years, as computer control and artificial intelligence become more sophisticated, certain human functions in teleoperation may be replaced, but greater need and demand will be placed upon other human functions, and in these respects the need for improved man-computer interaction will increase, not diminish.

4. Relative Roles of Man and Computer, and Man-Computor Communication.

In analyzing the relationship between human operator and computor in teleoperation, it is useful to consider how human behavioral components, through two basic forms of communication are used in four human supervisory roles. Figure 2 summarizes the situation by arrows indicating causality between descriptors.

Commanding the computor is done by either typing strings of symbols or pushing dedicated buttons or switches (symbolic commands) or moving a joystick or replica controller, where there is a geometric isomorphism between control movement and its meaning (analogic commands). Observing can also be of symbolic displays (alphanumerics) or analogic displays (pictures or geometric diagrams). Imagining(internal mental visualization) may also be symbolic or analogic.

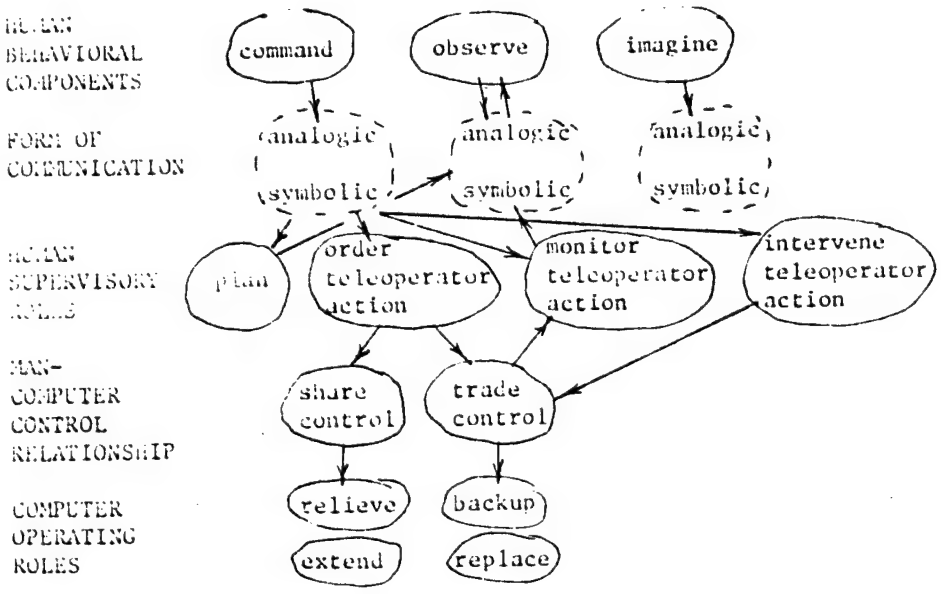

Figure 2. Relative Roles of Man and Computer

Supervisory commands may be for purposes of planning information, such as referencing computer memory or testing a potential future action on a model; they may be for ordering teleoperator action; they may be for making computer adjustments while monitoring teleoperator action; or they may be for intervening in teleoperator action to assume direct manual control. Observation of displays is indicated in both the planning and the monitoring role of the operator.

As shown in the fourth row, the teleoperator may be ordered to act in two different ways. One is where the man shares control with the computer, i.e. the two work on the same task at the same time. The other is where the man trades control on all or some of the tasks, i.e. for those tasks he gives over complete control to the computer. Intervention means that the computer trades control back to the man. When control has been traded to the computer, part of the act of monitoring is to observe (analogic and symbolic) displays of its performance, as shown by the upward arrows.

The computer's alternative operating roles when sharing control with the human operator are relieve, i.e. do things which make his work easier, and extend, i.e. pushing his performance beyond where it would normally be. When control is traded to it the computer may backup the operator by being ready to take over in case he fails, or it may replace him altogether.

While this taxonomy of relationships at the present has no corresponding quantitative theory, it has been useful to the authors in thinking about what is desirable for man-computer control of teleoperators. In particular it has helped us think through the various forms of computer aiding which might be programmed into an experimental system. And it has clarified for us the potential of using a combination of general purpose typewriter and dedicated on special-purpose keyboard commands (symbolic)and force-reflecting master-slave and rate commands (analogic).

5. SUPERMAN: A System for Supervisory Manipulation

A brief description of a thesis by T.L. Brooks in progress at the Man-Machine Systems Lab at MIT is given on the following pages as an example of a supervisory manipulator system. This system is called SUPERMAN. Figure 3 shows the general relationships between the multiple inputs (keyboard, dedicated symbolic keys, and analog inputs), the computer states (STANDBY, DEFINE, EDIT, EXECUTE, AND TAKEOVER) and the control modes (RATE, MIXED MASTER/SLAVE AND RATE, MASTER/SLAVE, and COMPUTER control).

STANDBY State - When the computer is in this state, control resides with the main program and the operator. By pressing the proper button on the control console, the user can enter a particular manual control mode or another computer state (see Figure 4).

Manual Control Mode - A manual control mode is the method through which the user analogically interacts with the arms. A control mode is independent of the state. For example, the control mode might be MASTER/SLAVE while the state is EDIT. There are three kinds of modes:

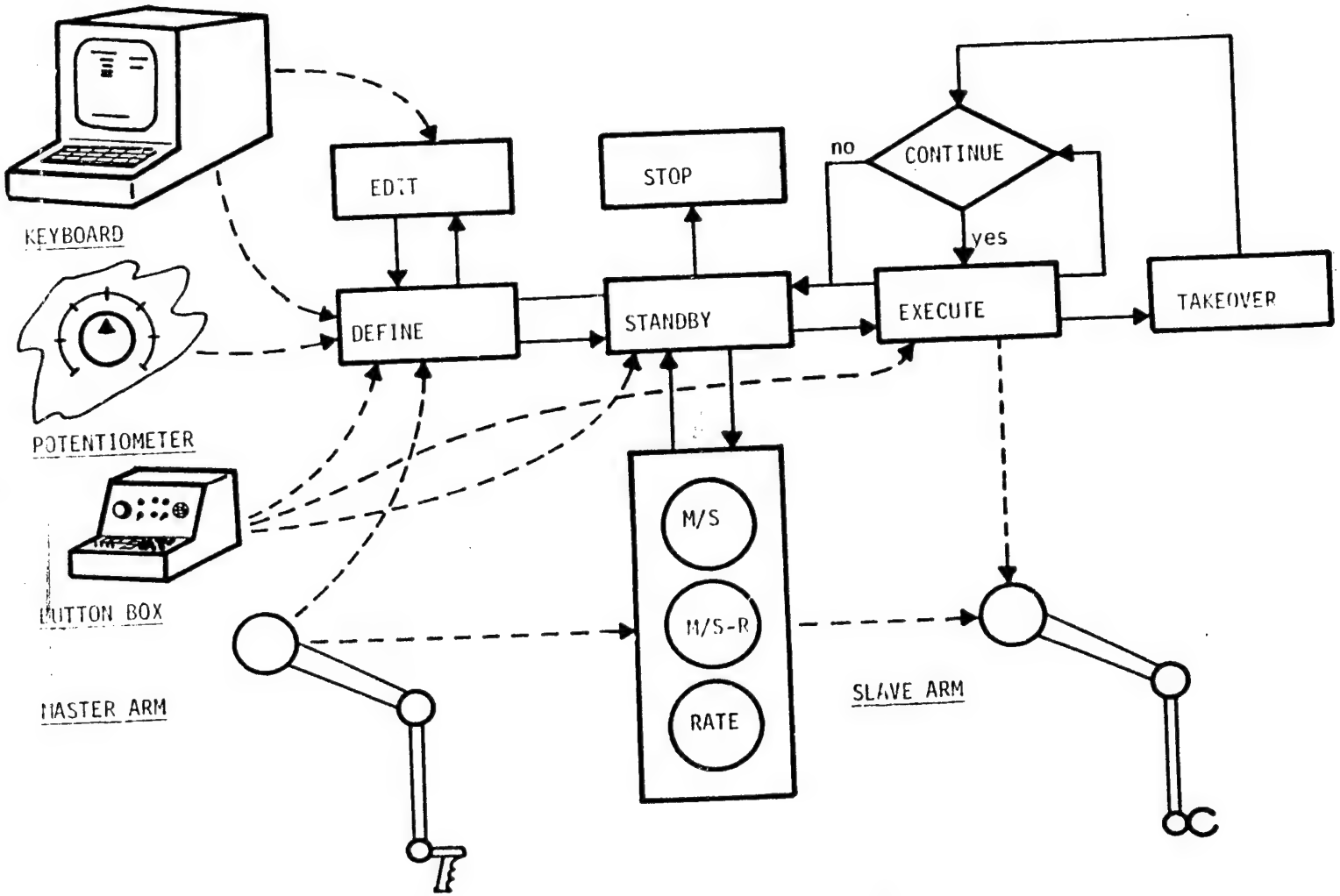

Figure 3. Block Diagram of SUPERMAN System

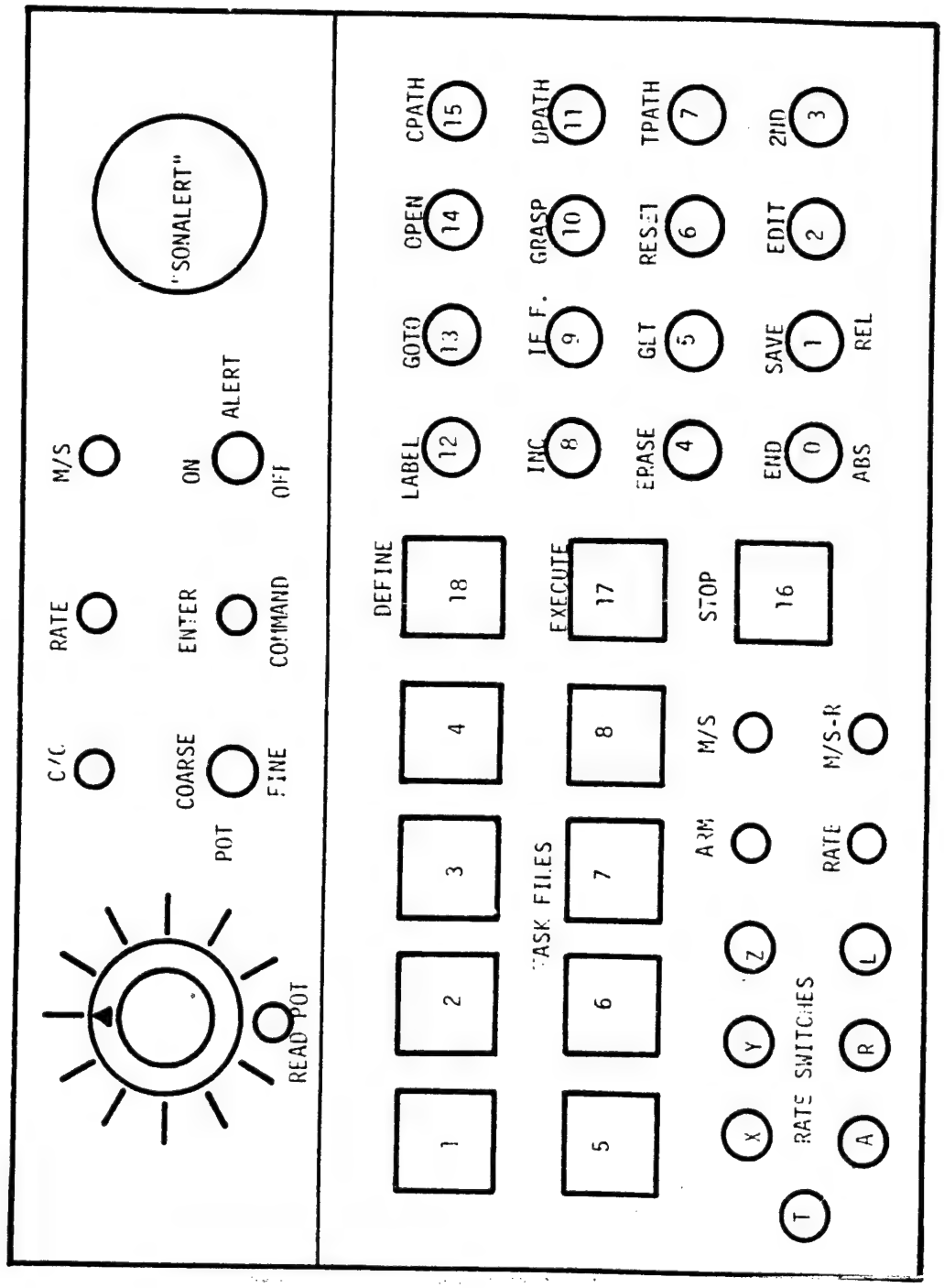

Figure 4. Special Control Console for SUPERMAN System

a) RATE - The individual degrees of freedom are controlled through rate commands by switches on the control console and a potentiometer for rate adjustment. Both rate and resolved-motion rate are available.

b) MIXED MASTER/SLAVE AND RATE - The master acts as a spring-loaded joystick in the X, Y and Z axes, giving rate commands to the X, Y and Z axes of the slave proportional to displacement of the master. (The rate of the slave arm is then reflected in the force feedback level which the operator feels in the master.) Both rate and resolved motion rate control are available. The remaining degrees of freedom, the left and right elevation, the azimuth and the end-effector are controlled in a master/slave mode.

c) MASTER/SLAVE - The slave arm is driven to duplicate in position the action of the master. Any force felt by the slave is reflected to the master giving the operator force feedback (i.e. proportional to position disparity between master and slave).

DEFINE - DEFINE is the primary state through which the operator enters a string of commands to be executed. Commands are entered by pressing specially dedicated buttons for each function. All of the buttons used in the DEFINE state have dual functions (see Figure 4 - dual function buttons are 0-15).

EXECUTE State - As the title implies, the string of commands is executed through this state. During the execution of the command register, if the operator desires to take control, there are two methods available. The operator can take immediate control: (1) by pulling on the appropriate control stick (i.e. the MASTER in the case of MASTER/SLAVE or MIXED MASTER/SLAVE AND RATE modes or the rate switches in the RATE mode), or (2) by pressing the STOP button (all action ceases after the STOP button has been pressed until the operator signals for continuation or return to STANDBY). The operator can execute a string of commands which have been saved as a task file by pressing one of the lighted TASK FILE buttons. The operator also has the option of executing the current command register by pressing the EXECUTE button. This allows the operator to define a string of commands and immediately execute them to determine if any modifications are necessary. After the operator is sure the command string performs the desired function correctly, that function can then be saved as a task file or a named file.

TAKEOVER State - TAKEOVER is a transition state between control modes, i.e. from computer control to the control mode in effect before the EXECUTE command. Special problems result during this state due to the mismatch between the master and the slave at the time of the takeover. The diamond in Figure 3 signifies that after the mismatch has been dissolved, the operator has the option of moving into the STANDBY state or continuing the EXECUTION state.

The detailed meanings of the DEFINE buttons 0-15 are given below:

BUTTON Number	Command
0	END Final command used to signal completion of DEFINE state.
1	SAVE Used to save the command register on the disk as either a task file or a named file. A task file can be recalled only by one of eight buttons in the STANDBY state, whereas a named file is saved under a user-designated title and can only be recalled by the same name through the GET button (6) in the DEFINE state.
2	EDIT The EDIT command allows the user to modify the command register. The following options are available through the keyboard after entering the EDIT state: a) CHANGE A LINE b) INSERT A LINE c) DUPLICATE A LINE d) DELETE A LINE e) LIST COMMAND REGISTER f) RETURN TO DEFINE
3	2ND Used to enter the second function of dual command keys. The first function of each key is printed in black letters above the button. The second function is written below the button in gold letters. To enter a second function command, press the 2ND key and then the desired second command.
4	ERASE LAST LINE [ERASE] Used to erase the last entry in the command register.
5	GET Used to retrieve a named command file from the disk. GET asks for the name of the command file to be recalled and then locates the file, reads it into the command register (and returns to DEFINE state).
6	RESET Used to initialize the necessary internal variables and the command register to zero.

7 THROUGH PATH [TPATH]

Records the present position of the arm for use in EXECUTE as a through point. (A through point is a position which the operator desires the arm to move through without stopping, i.e. non-zero velocity point.)

8 INCREMENT (DOF) (XXXX)

Makes an incremental motion in the desired degree of freedom by a selected value. The user enters the INCREMENT command, then the degree of freedom (DOF), adjusts the desired increment (XXXX) through the potentiometer and presses the READ POT VALUE button directly beneath the potentiometer.

9 IF (DOF) FORCE.GT.
EXECUTE NEXT COMMAND

If the force level in the desired degree of freedom (DOF) is greater than the level set by the operator (XXXX) the following command is executed. If the force level is less than the level set by the operator, the command immediately following the IF FORCE.GT. statement is skipped during execution. The user enters the IF FORCE.GT. command, then the desired degree of freedom, adjusts the force level through the potentiometer.

10 GRASP WITH FORCE (XXXX) [GRASP]

The user enters the GRASP command and adjusts the force level through the potentiometer.

11 DISCRETE PATH [DPATH]

Records the present position of the arm for use in EXECUTE as a stopping point. During execution, the slave arm is moved from its current position to the recorded position with zero final velocity.

12 LABEL (XXXX)

Labels a position in the command register which can be returned to through a GOTO command. The user presses the LABEL button and then the number (XXXX) of the desired label.

13 GOTO (XXXX)

GOTO is a conditional command which moves to label (XXXX), unless the operator signals during execution to change the branch to (YYYY) by pressing a different button. To enter the command the operator presses the GOTO button and then the number (XXXX) of the label to which GOTO should branch.

14 OPEN

Open jaws.

15 CONTINUOUS PATH [CPATH]

Records the position of the master manipulator every 0.1 second for use in EXECUTE. A continuous path is achieved by interpolating between the recorded positions.

2ND - 0 ABSOLUTE

Informs the execution compiler that the command register is to be executed exactly as recorded (see RELATIVE). The user enters the absolute command by pressing the 2ND button (#4) and then the ABSOLUTE button (#0).

2ND - 1 RELATIVE

Informs the execution compiler that the positions in the command register are to keep the same relative displacement with respect to each other, but are to be transformed so that the first position following the RELATIVE command corresponds to the position of the slave at the time of execution. A RELATIVE command can be cancelled by an ABSOLUTE command, with the result that only the positions between the RELATIVE and ABSOLUTE commands are transformed. The user presses the 2ND button (#4) and then the RELATIVE button (#1) to enter the command in the register.

2ND - 2 through 2ND - 15 not assigned.

As an example program consider a string of commands to take a nut off of a bolt and put it in a box. This program can be broken down into two major sections, one removes the nut and the other places it in the box. Since the user would prefer one nut removal program to be used for all nuts regardless of the orientation of the nut, a RELATIVE command should obviously be the first command in the register (the RELATIVE command and all of the following commands are briefly described under DEFINE). The entire command register for the nut removal program would be as follows. The following general formats will be followed throughout this example:

[BUTTON PUSH]
(POT READINGS)
"KEYBOARD COMMANDS"
COMPUTER REPLIES.

1	[RELATIVE]	
2	[LABEL] [1]	
3	[DPATH]	Place the slave on a nut and record that position by pressing the DPATH button.
4	[GRASP](200)	
5	[DPATH]	Turn the end effector 180° and record the position.
6	[INCREMENT] [Y](300)	Increment the slave by 300 counts in the direction that would pull the nut off.
7.	[IF FORCE.GT.][Y] (100)	If the force is greater than 100 in the Y direction, the nut is still on the bolt, therefore execute the next command.
8	[GOTO] [2]	
9	[GOTO] [3]	If the force had been less than 100 in the Y direction, the nut is free and this command would be executed.
10	[LABEL] [2]	
11	[INCREMENT] [Y] (-300)	Return the arm to position before incrementing in #6.
12	[OPEN]	Release the nut.
13	[GOTO] [1]	Return to LABEL 1 and continue turning the nut.
14	[LABEL] [3]	End of the first part of task - nut is off.
	[SAVE] "NUT-OFF"	Save command register as the named file "NUT-OFF" (typed in at the keyboard).

The second part of the task requires the manipulator to place the nut in a box. The entire command register for the program to put the nut in the box would be as follows:

1.	[ABSOLUTE]	The box would always be in the same place.
2	[TPATH]	Move the slave to a position just over and above the outside edge of the box and record this position by pressing the TPATH button.
3	[DPATH]	Move the slave to a position over the center of the box and record the position.
4	[OPEN]	
5	[TPATH]	Enter same position as in #2 by duplicating line 2.

[SAVE] "NUT-IN-BOX"

At this point the operator could call either program and execute it. The NUT-OFF program would simply take the nut off and return control to the operator as soon as the nut was free. But the present status of each file (i.e., a named file) requires that the operator type in each name to obtain the file to execute it. If the operator performs the following commands the file will be saved as a task file which is immediately executed at the touch of a button:

[GET] "NUT-OFF"

[GET] "NUT-IN-BOX"

The computer will reply by stringing the two files together as one file. Then enter:

[SAVE] "TASK-FILE"

and press the button which will retrieve the file (e.g., button #1). To remove a nut and put it in the box the operator simply presses the same button, the execution compiler transforms the first half of the register relative to the position of the slave at the instant the button is pressed and then executes the program. After the nut is removed and placed in the box the slave returns to the operator's position and the computer relinquishes control.

SESSION G: DISPLAYS

Chairman: H. Jex

DISPLAY AIDS FOR REMOTE CONTROL OF UNTETHERED UNDERSEA VEHICLES*

W. L. Verplank

Man-Machine Systems Laboratory
Department of Mechanical Engineering
Massachusetss Institute of Technology
Cambridge, Massachusetts 02139

Abstract

A "predictor" display superimposed on slow-scan video or sonar data is proposed as a method to allow better remote manual control of an untethered submersible. Simulation experiments show good control under circumstances which otherwise make control practically impossible.

1. Introduction

Untethered, unmanned submersibles have been limited to automatic control on simple pre-programmed or target-seeking trajectories. More precise navigation and obstacle avoidance will require increasingly sophisicated automatic control and/or direct control from the surface. Direct human control through a sonic communication channel will be difficult because of the low bandwidth and the signal travel time. Probably the most productive approach will be a combination of elementary automatic control such as is possible with some present-day tethered submersibles (e.g., altitude or depth and heading control) plus display aids which make control easier for the operator. This paper proposes a display aid which is particularly applicable to the problems of time-delay and slow frame-rate.

2. The Problem

For remote control, there are two sources of difficulty with sonar communications: time-delay and slow-frame-rate. Round trip time-delay is the time for a command to travel to the vehicle and the first indication of response to travel back. At a minimum this will be two times the distance divided by the speed of propagation, 2T. For example, T = 1 second at about 5,000 feet.

Pictorial information from television camera or obstacle avoidance sonar will be further delayed because of limited channel capacity. Assuming a low resolution picture of 80 K bits and a channel capacity of 10K bits/sec., there would be at most, one picture every 8 seconds (S = 8 seconds).

The effects of trying to navigate with just this pictorial information are illustrated in Figure 1.

* This work was supported in part by ONR Contract N00014-77-C-0256. The untethered vehicle control problem was suggested in discussions with the Harbor Branch Foundation and the M.I.T. Office of Sea Grant.

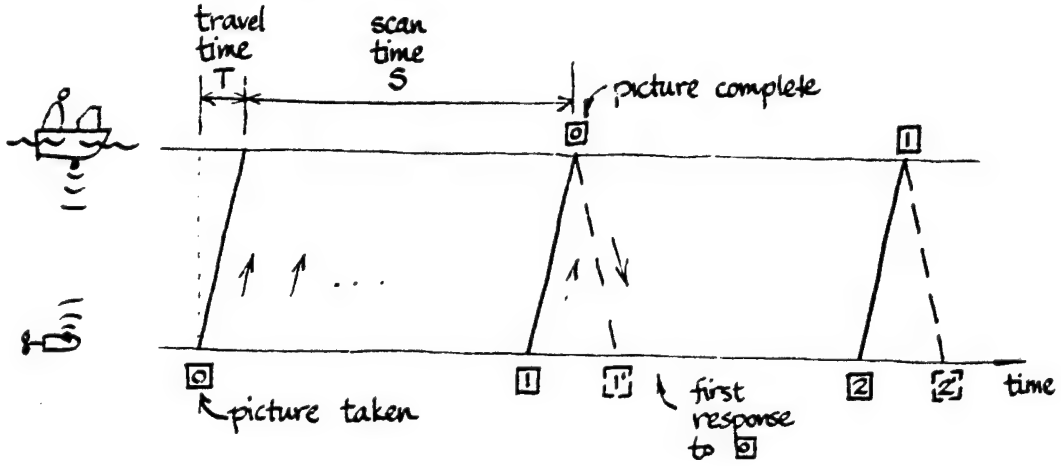

Figure 1a. Effect of delays from transport time (T) and scan time (S).

The picture from 0 is received T + S seconds after it is taken; the first operator response is received by the vehicle at least T seconds later, for a total delay of 2T + S seconds. While the operator is looking at the still picture from 0 the commands he is sending are actually moving the vehicle from 1' to 2', as illustrated in Figure 1b.

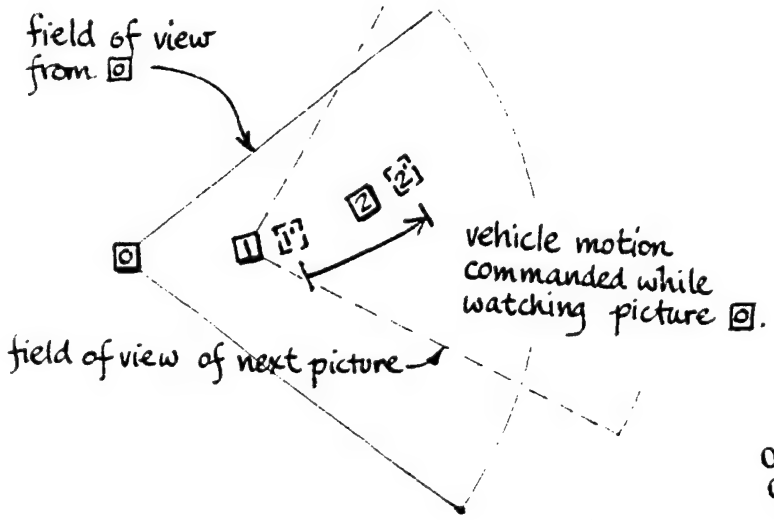

Figure 1b. Positions of vehicle at times in Figure 1a.

3. Predictor Display

Predictor displays were first used for submarine control (Kelley, 1968). NASA considered predictor displays for remote control of unmanned lunar roving vehicles (Arnold, 1963) but sent men instead.

The predictor display proposed here presents a symbol superimposed on the slow-frame-rate and time-delayed picture from the vehicle's television camera. The symbol responds instantansously and continuously to the operator's commands predicting "future" positions of the vehicle. For example, refering to Figure 1b, when 2 is complete the predictor symbol would show the position 1'. Before the next picture from 1 arrives, the symbol will be moved, in response to the operator's commands, to position 2'.

The position of the vehicle is computed from a local model of the vehicle response and the operator's commands u(t), as shown in Figure 2.

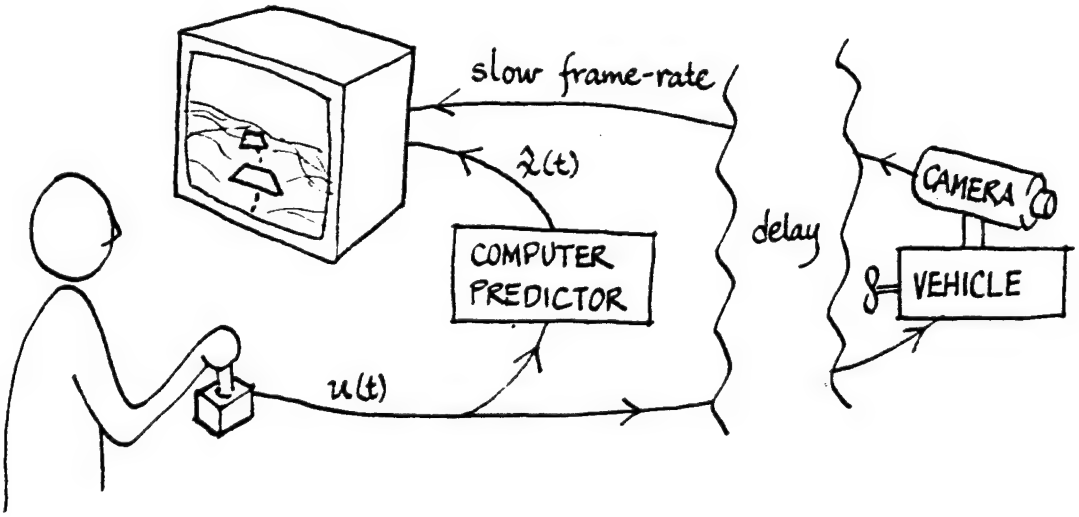

Figure 2. Predictor display superimposed on pictorial data

Pictorial or Map Displays

The predictor symbol may prove useful both on pictorial displays (superimposed on television or obstacle-avoidance sonar) and on map-like position displays. Map displays would avoid one difficulty of pictorial displays, which is loosing the predictor symbol when it moves out of the field of view of the camera (for example, moving sideways or backward).

Auxiliary Position Data

If position data is available from transponders or locator beacons, it could be used to update the vehicle model. With just the pictorial data, the open-loop prediction would have to span an interval of (at least) 2T + S to (at most) 2T + 2S seconds. With auxiliary feedback the open-loop estimate will only need to span the delay of that auxiliary data (at minimum 2T). The signals and corresponding delays are shown in Figure 3. (u(·), command vector; x(·), vehicle location data).

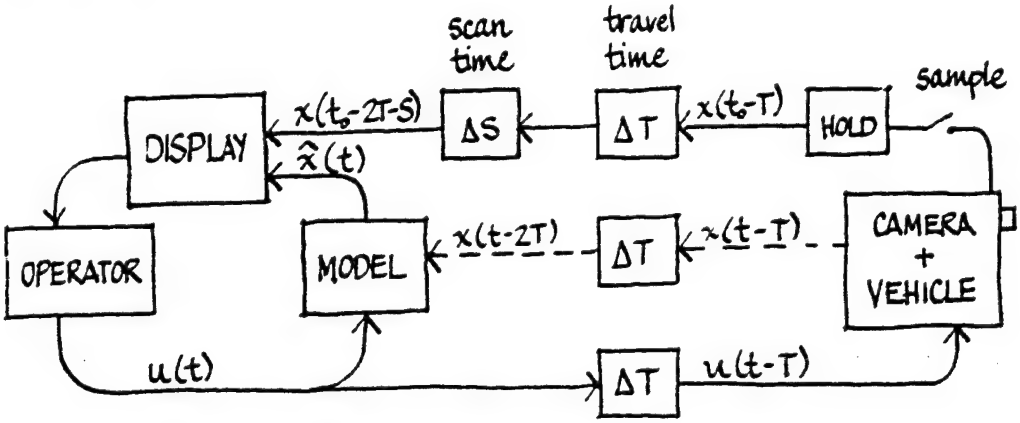

Figure 3. Delays associated with predictor calculation

Adaptive Estimation

Another feature that could be built into the local model of the vehicle is some estimate of the disturbances (such as current). The current model as well as the vehicle model could be updated on the basis of the mismatch between predicted and measured vehicle position.

4. A Demonstration Experiment

In order to explore the effects of the predictor display, an interactive simulation was written on an Interdata 70 computer and Imlac graphic display. A random terrain was generated and displayed in perspective, updated every 8 seconds, to simulate the pictorial information. A moving predictor symbol was generated respresenting the vehicle as a square in perspective. Two straight ridges were added to the random terrain to serve as a test course. (Figure 4).

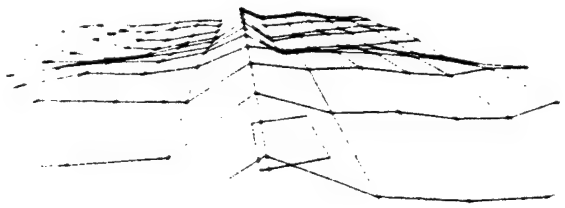

Figure 4. Computer-generated terrain with predictor symbol

The simulated vehicle was controlled by the operator with a spring-centered 2-degree-of-freedom joystick. The dynamic response of the vehicle was simple integration with forward speed proportional to forward-back position of the stick and turn-rate proportional to left-right position of the stick. The vehicle was always the same height above the terrain (simulating automatic altitude hold). No disturbances such as currents were simulated. Also, it was found important to have a good detent and dead-zone on the sitck to avoid inadvertent commands.

A stationary "table" was drawn to indicate where the next picture was to come from while the "real-time" predictor continued to move in response to the operator's commands (Figure 5). Dotted lines were added to this table to indicate the field of view. This reduced the considerable confusion about how the picture was expected to change and served as a guide for keeping the vihicle within its own field of view, which is the best strategy for using this kind of predictor on the pictorial display.

Figure 5. Predictor plus "table" showing from where next picture will come

Results

A typical path, without the predictor, is shown in Figure 6. The dotted lines represent ±1 terrain-unit from the ridge. The circles represent the vehicle's position every 2 seconds. V's represent the field of view of each picture sent. Quite often there is no movement between successive dots (2 secs.) or successive pictures (8 seconds.)

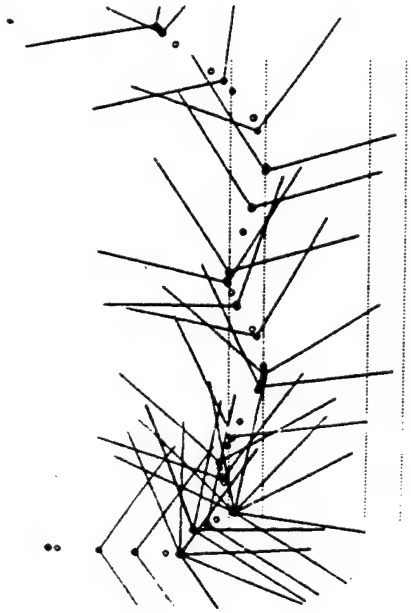

Figure 6. Typical path with no predictor

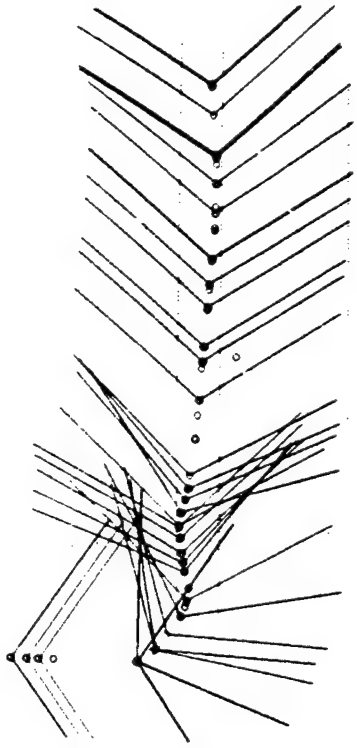

Figure 7. Success at slow speed with no predictor

Only with extremely slow speed was it possible to keep track of the ridge. Approximately five minutes and 40 pictures were required to traverse just one of the ridges (half the course). This is shown in Figure 7.

With the predictor symbol, practically continuous motion was possible. A typical path is shown in Figure 8. The course was completed in 3 minutes and 23 pictures.

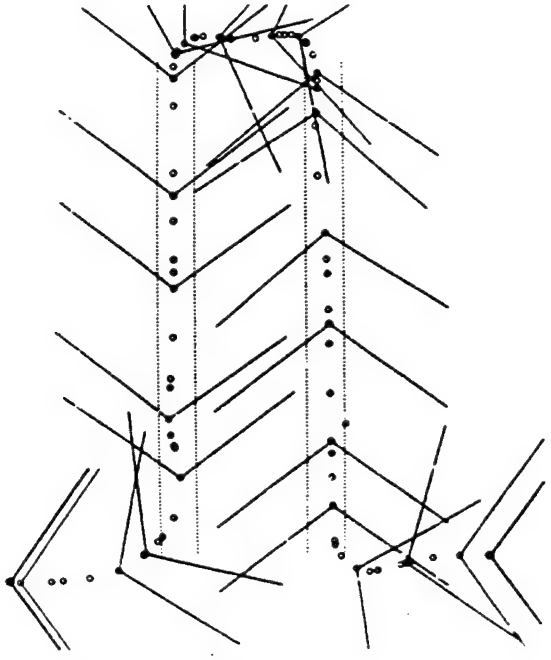

Figure 8. Path with predictor display

Request Mode

One unexpected finding from these experiments was that rather than sending the picture periodically every eight seconds, sending the picture only upon the operator's request reduces the total number of pictures necessary and encourages a "move and wait" strategy which avoids confusion. The difference is illustrated in Figure 9.

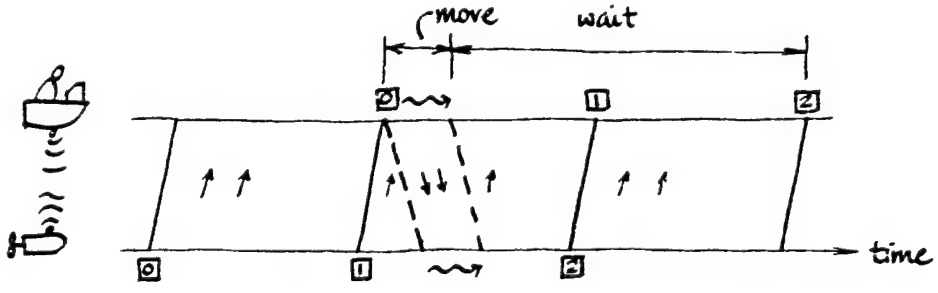

Figure 9a. New picture every 8 seconds: "periodic mode"

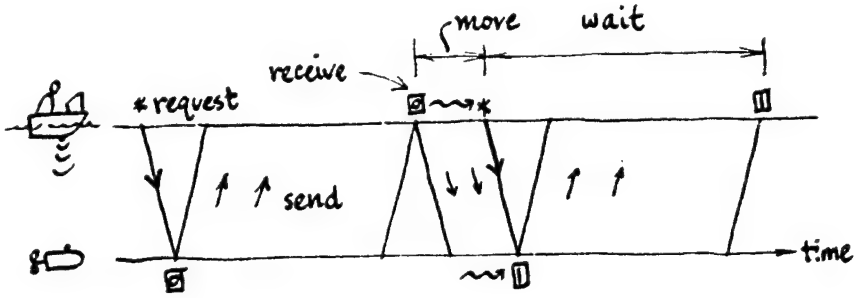

Figure 9b. New picture upon request: "request mode"

In the periodic mode (Figure 9a) a short move starting with the receipt of picture 0 will not be reflected in the next picture, 1 , as the operator might expect; instead he has to wait for 2 . In request mode (Figure 9b), the wait for pictorial confirmation is minimized.

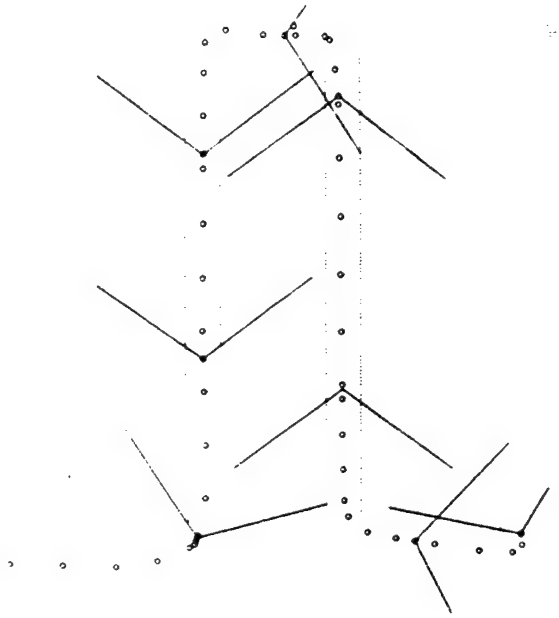

Figure 10. Typical path in the request mode

A typical path in request mode (using the predictor) is shown in Figure 10. Compared to periodic mode, the time is about the same but the number of pictures used in one-half to one-third; velocities are higher but there is a wait for 10 seconds as each picture is taken and sent.

On an actual vehicle, probably both modes should be available with the request mode used when move-and-wait strategy is appropriate (for precise positioning based on pictorial feed-back, and when environmental disturbances are small). Periodic mode is probably more appropriate for less precise navigation and continuous motion when the predictor symbol can be relied upon.

Another trade-off that should probably be built into the pictorial feed-back is variable frame-rate/resolution. In a more dynamic and uncertain environment (i.e., larger bandwidth disturbances or target motion) sampling rate will want to be higher at the expense of resolution.

6. Conclusions and Recommendations

For the conditions studied (T = 1 sec., S = 8 sec.) manual control is not feasible without display aids such as the predictor symbol. The request mode is preferred as it seems to avoid confusion and reduce the number of pictures necessary.

The present results are at best preliminary. We studied only very simple vehicle dynamics and only one set of delay conditions. Further study with laboratory simulation can investigate:

1) more realistic vehicle dynamics,

2) environmental uncertainties such as drift,

3) a broader range of delay conditions and

4) various degrees of partial automation.

Also, the predictor displays (both pictorial and map) could be used on existing tethered vehicles to simulate untethered operation and evaluate the potential for untethered operation.

References

Kelley, C. R., Manual and Automatic Control, Wiley, New York, 1968.

Arnold, J. E., and Braisted, P. W., Design and Evaluation of a Predictor for Remote Control Systems Operating with Signal Transmission Delays, NASA TN D2229, 1963.

A SAFETY MARGIN AND FLIGHT REFERENCE SYSTEM AND DISPLAY FOR POWERED-LIFT AIRCRAFT*

by Robert K. Heffley
Systems Technology, Inc.

and Gordon H. Hardy
NASA Ames Research Center

SUMMARY

A study was conducted to explore the feasibility of a safety margin and flight reference system for those powered-lift aircraft which require a back-side piloting technique. The main objective was to display multiple safety margin criteria as a single variable which could be tracked both manually and automatically and which could be monitored in order to derive safety margin status. The study involved a pilot-in-the-loop analysis of several system concepts and a simulator experiment to evaluate those concepts showing promise. A system was ultimately configured which yielded reasonable compromises in controllability, status information content, and the ability to regulate safety margins at some expense of the allowable low speed flight path envelope. It was necessary, however, to utilize an integrated display of two variables — one to be tracked in a compensatory manner and one to be monitored. The variables themselves consisted of linear combinations of the computed critical safety margin and pitch attitude, and the proportions of the combinations were definable in terms of the aforementioned compromises.

SYMBOLS

k	Weighting coefficient for pitch attitude
N_H	Engine rpm
V	Airspeed
V_{min}	Minimum airspeed at approach thrust
V_{min_m}	Minimum airspeed at maximum thrust
α	Angle of attack
α_{max}	Maximum allowable angle of attack
γ	Aerodynamic flight path angle
θ	Pitch attitude

* This study was performed under Contract NAS2-9418.

PAGE INTENTIONALLY BLANK

INTRODUCTION

The pilot's control technique for a powered-lift aircraft in the approach flight phase is inherently different from that for a conventional aircraft. The pilot (or autopilot) of the powered-lift aircraft cannot simply use 1.3 times the power-off stalling speed (for the approach configuration) as the target airspeed or "flight reference" and be guaranteed adequate safety margins. Since a powered-lift aircraft derives a significant part of its lift from a thrust vector which is inclined nearly perpendicular to the flight path, the minimum speed is determined to a large extent by the thrust or power setting. This is in dramatic contrast to the characteristics of a conventional aircraft as shown in Fig. 1. Note that the approach speed for a powered-lift aircraft may be in the neighborhood of the idle thrust stalling speed (Point A in Fig. 1).

In addition to the problem of selecting a suitable speed (or other parameter) to use as a flight reference which will ensure adequate safety margins, the pilot may have to cope with some other unusual flight characteristics. For example, most powered-lift aircraft approach at speeds on the "backside" of the thrust required curve. Consequently, a "backside" or "STOL" control technique is usually used, i.e., the pilot uses pitch attitude to regulate airspeed and modulates thrust to control flight path. A typical flight characteristic resulting from this mode of control and from the thrust vector being inclined nearly perpendicular to the flight path is shown in Fig. 2. That is, if the pilot is using airspeed as a flight reference (i.e., maintaining a constant airspeed), it can be seen that to steepen the descent path angle the pilot must increase pitch attitude! This is contradictory to all normal practice and can make airspeed a very confusing flight reference.

Because of these problems, the pilots of airplanes such as the NASA Augmentor Wing Jet STOL Research Aircraft (AWJSRA) must use a combination of airspeed, angle of attack, and pitch attitude as a flight reference. Only through extensive experience are these pilots able consistently to maintain adequate safety margins. While this use of a complex flight reference has been acceptable in the research environment, it would not be acceptable operationally.

OBJECTIVE

The objective of the program, therefore, was to find a single display to be used for maintaining a safe flight condition in powered-lift aircraft. Several features needed to be considered, however, which significantly complicated the design of such a system. These are shown in Fig. 3.

The present study was primarily a feasibility study and was limited to an analysis and simulation phase. The results to be presented were obtained in the context of (1) an existing powered-lift STOL airplane (NASA AWJSRA),

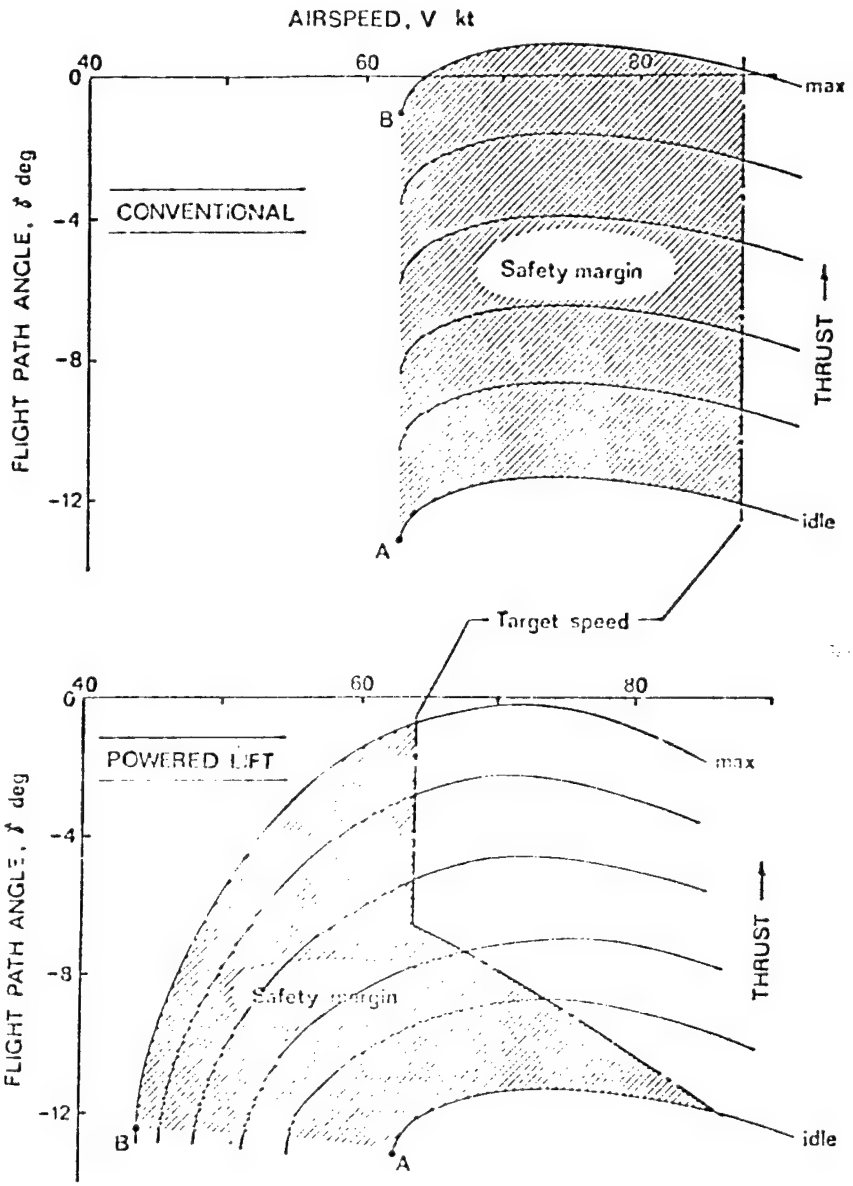

Figure 1. Comparison of γ - V Plots Between a Conventional and a Powered-Lift Aircraft.

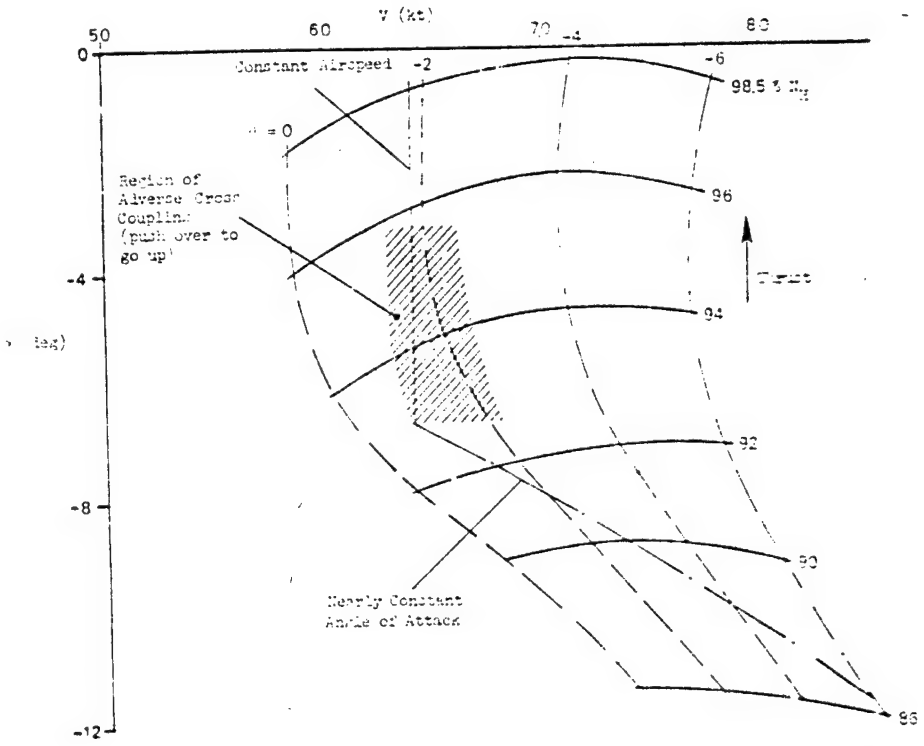

Figure 2. γ - V Curve Showing Region of Adverse Cross Coupling Along Trajectory of Desired Airspeed.

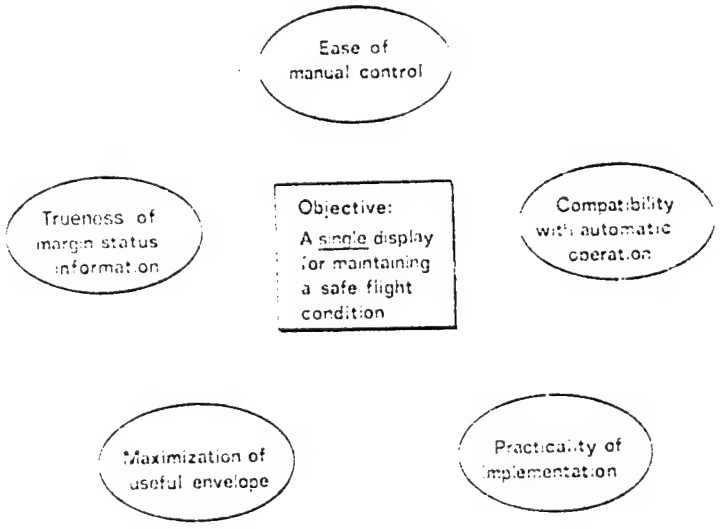

Figure 3. Tradeoffs Involved in the System Design.

C-5

(ii) existing avionics hardware (STOLAND guidance, control, and navigation system, Ref. 1), and (iii) severe atmospheric disturbances encountered during the landing approach flight phase.

TECHNICAL APPROACH

An extensive study of airworthiness requirements which is described in Refs. 2 and 3, defined the required safety margin criteria for powered-lift aircraft in terms of the instantaneous angle of attack and airspeed. The suggested criteria from Ref. 2 are listed in Table 1. Figure 4 shows these criteria superimposed on the AWJSRA flight envelope. The present study assumed these safety margin criteria for the purpose of defining the available flight envelope. Note that only two criteria dominate, i.e., airspeed must be greater than the minimum speed at maximum thrust plus 20 knots and the angle of attack must be such that a 20 knot vertical gust will not result in exceeding the maximum allowable angle of attack. The resulting flight envelope is bounded in Fig. 4 by the lines labeled "minimum safe airspeed."

Table 1. Safety Margin Criteria.

(All Engines Operating)

$V > 1.15\ V_{min}$ (approach thrust)	
$V > V_{min} + 10$ knots (approach thrust)	
$V > 1.3\ V_{min_m}$ (maximum thrust)	
$V > V_{min_m} + 20$ knots (maximum thrust)	Most Critical Criteria
$\alpha < \alpha_{max} - \sin^{-1} \frac{20 \text{ knots}}{V}$ (vertical gust margin)	

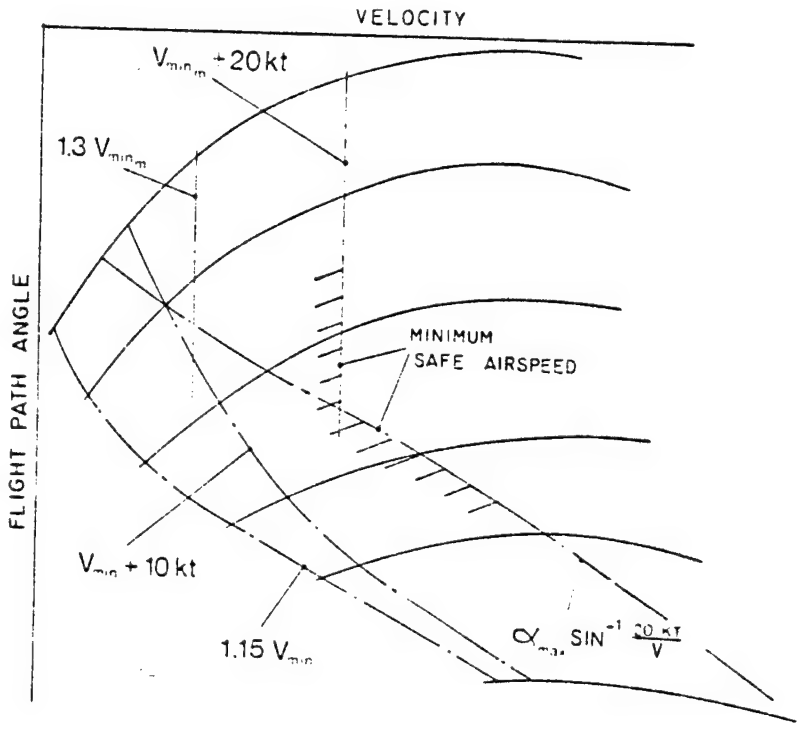

Figure 4. Relationship of Various Safety Margin Criteria. (Corresponding to Table 1 for the AWJSRA)

A large number of possible flight reference and safety margin mechanizations that were consistent with this flight envelope were examined and are described in detail in Ref. 4. The analysis utilized multiloop control system analysis methods and considered: (1) ease of control, (2) display of safety margin status, (3) pilot and automatic system performance in maintaining safety margins, and (4) system mechanization as they relate to sensor and computational requirements. The purpose of the analysis was to sort through the large number of possibilities to find a few which would be worthwhile examining during the simulation phase.

RESULTS

From the large number of implementation concepts considered, one was found to meet design objectives satisfactorily. Although it consisted of a single display, two variables were involved. One variable was actively tracked and thus served as a flight reference. The other variable was simply

monitored in order to obtain high quality status information. This implementation can be summarized as:

$$[\text{Tracked Variable}] = [\text{Actual Margin}] + k \cdot [\text{Pitch Attitude}]$$

$$[\text{Monitored Variable}] = [\text{Actual Margin}]$$

where the actual margin is taken as the most critical of applicable airspeed and angle of attack safety margin criteria from Table 1.

It is significant that the tracked variable was composed of a simple linear combination of actual margin and pitch attitude. This implementation permitted a direct tradeoff between ideal status information and easy controllability depending upon the weighting factor, k. A single value of k was found to provide satisfactory compromises in the various tradeoffs shown previously in Fig. 3*.

The manner in which the two variables were displayed was important to the success of the system. The main hardware element of the display was the STOLAND Electronic Attitude Director Indicator (EADI) shown in Fig. 5. Safety margin information was presented along the vertical scale on the far left-hand side.

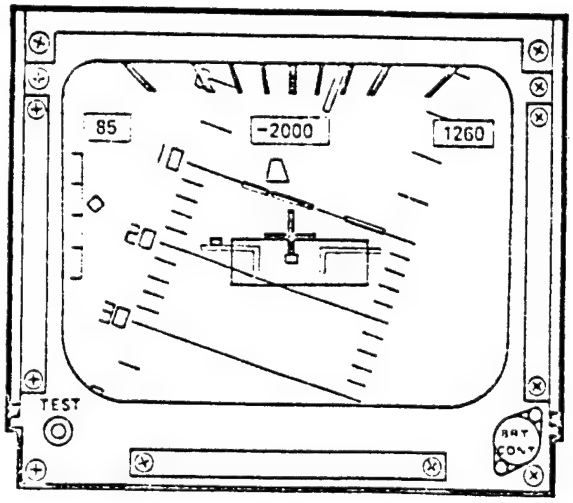

Figure 5. Overall EADI Presentation.

* This value amounted to 10% safety margin change per degree pitch attitude change where the nominal operating point was at 100% allowable safety margin.

Details of the safety margin system presentation are described in Fig. 6. Note that the tracked variable is displayed directly on the moving pointer, but that the monitored variable is displayed as the distance between the moving pointer and a moving scale "floor." This configuration provided good relative emphasis on the two variables and did not confuse their respective roles in the pilot's mind.

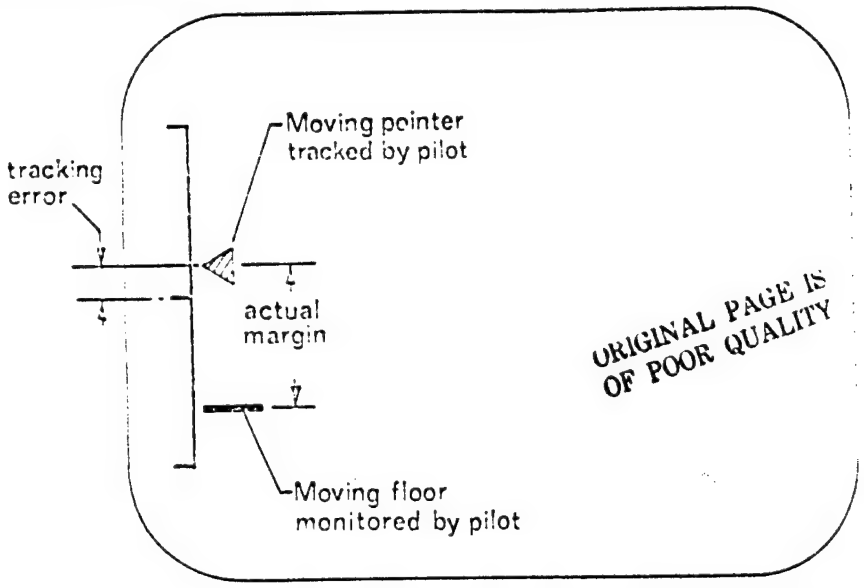

Figure 6. Details of Safety Margin System Display on HADI.

CONCLUSIONS

The study reported in this paper was successful in evolving a useful safety margin system and display for a powered-lift aircraft. The flight reference implementation found most effective involved a blend of the safety margin and a linear function of pitch attitude. This concept provided (i) an easily controlled variable, (ii) correct sensitivity to gusts, (iii) a guide to correct control action for obtaining good safety margin performance, (iv) acceptable performance in the presence of large atmospheric disturbances, and (v) the concept was relatively easily implemented. The main compromise resulting from the use of this concept was a reduction in available flight envelope in order to enhance certain controllability features. (The nominal operating point was approximately 5 knots faster than the minimum approach speed permitted by applicable safety margin criteria.) The envelope compromise was, however, controllable in a rational and predictable way by the flight reference weighting coefficient. Finally, the results of the study have provided the necessary groundwork for a flight investigation.

REFERENCES

1. Irgurich, John; and Bradbury, Peter: STOLAND Final Report. NASA CR-137972, 1976.

2. Scott, Barry C.; Martin, Paul W.; Hynes, Charles S.; and Bryder, Ralph B.: Progress Toward Development of Civil Airworthiness Criteria for Powered-Lift Aircraft. FAA-RD-76-100, 1976.

3. Hefley, Robert K.; Stapleford, Robert L.; and Rumold, Robert C.: Airworthiness Criteria Development for Powered-Lift Aircraft. A Program Summary. NASA CR-2791 or FAA-RD-76-195, 1977.

4. Hefley, Robert K.; and Jewell, Wayne F.: Study of a Safety Margin System for Powered-Lift STOL Aircraft. NASA CR-152139, 1978.

N79-15615

A HEAD-UP DISPLAY FOR MID-AIR DRONE RECOVERY

W. L. Augustine, E. L. Heft

Air Force Flight Dynamics Laboratory
Wright-Patterson AFB, Ohio 45433

T. G. Bowen

11th Tactical Drone Squadron
Davis-Monthan AFB, Arizona 85707

and

R. L. Newman

Crew Systems Consultants
Yellow Springs, Ohio 45387

SUMMARY

During mid-air retrieval of parachute packages, the absence of a natural horizon creates serious difficulties for the pilot of the recovery helicopter. A head-up display (HUD) was tested in an attempt to solve this problem. Both a roll-stabilized HUD and a no-roll (pitch only) HUD were tested.

The results show that fewer missed passes occured with the roll-stabilized HUD when the horizon was obscured. The pilots also reported that the workload was greatly reduced. Roll-stabilization was required to prevent vertigo when flying in the absence of a natural horizon. Any HUD intended for mid-air retrieval should display pitch, roll, sideslip, airspeed, and vertical velocity.

INTRODUCTION

One of the most successful ways to recover drones is the mid-air retrieval system (MARS). During these recoveries, a parachute system is deployed from a descending drone prior to retrieval. A typical parachute system consists of an engagement parachute connected by a load line to the drone and a main parachute canopy supporting the drone. The main canopy is designed to release when the load line from the drone to the engagement parachute is under tension. The load line is routed up the main canopy risers to a break-tie at its apex, then up to the engagement parachute.

To recover the drone or other object, the pilot flies the helicopter to approach the engagement parachute from the side opposite the load line.

This location is shown by an aiming panel on the main canopy. The helicopter has three hooks rigged below it which catch load carrying members in the engagement parachute. These hooks are connected to an energy absorbing winch aboard the helicopter. As the load line absorbs the tension after engagement, the apex tie releases, followed by main canopy separation, and the drone is carried by the load line supported from the helicopter. Figure 1 shows the helicopter and parachute system just prior to engagement.

Safe and consistent MARS operations depend on the pilot's ability to match the helicopter's vertical velocity with the parachute's while closing with the top of the engagement parachute. At the same time, the helicopter must approach from a specific direction to ensure that the load line will not be pulled through the main canopy.

The pilot's primary visual cue is the alignment of the helicopter, the top of the engagement parachute, and the horizon. If the horizon is obscured by smoke, haze, or clouds, or if false horizons are present, the pilot has extreme difficulty in judging his position relative to the target. Under these circumstances, attempted recovery can be dangerous and fruitless.

Variations in the size of the parachute canopies can produce illusions of being too high or too low relative to the engagement parachute. The pilot must allow the canopy top to pass beneath the fuselage as the helicopter closes with the engagement parachute. The apparent change in position from level to approximately twelve feet below the helicopter can make engagement difficult to judge. These visual problems are compounded by the need for precise heading and roll control since any degree of uncoordinated flight is magnified in the pole position. Airspeed must be maintained within a small band (45 to 60 knots) for proper operation of the energy absorbing winch.

The head-up display has been used to assist pilots during visual tracking tasks. The HUD is an outgrowth of the reflecting gunsight and presents flight instrument data in the pilot's field of view as he looks at external visual cues. To date, HUDs have been applied to two main areas: weapons delivery(1) and landing approach(2,3). A survey of HUD technology is also available(4).

HUDs serve to combine real world visual cues with derived data. These data sources are complementary. It would be difficult to reproduce the real world cues artificially. At the same time, the derived data presents information that the pilot cannot perceive directly, or only with great difficulty. One must be careful, however, to ensure that both data fields are compatible. As Singleton points out(5), there is a basic incompatibility between the redundant, analogue data of the real world and the symbolic, often digital data of artificial displays. The problem is further complicated by the need for careful attention to retain proper balance, so that the proper display (real world or artificial data) dominates. During visual tracking, the real world must dominate with the flight instrument data providing supplementary information. The roles reverse during instrument flight. However, the HUD must not be such a compelling sight that the pilot fixates on it to the exclusion of the real world. This has definite implications on pilot learning and has been reported elsewhere(2). These comments were verified by conversa-

tions with HUD-qualified pilots prior to the development of the test plan for this study, as well as during preliminary HUD flights.

EQUIPMENT DESCRIPTION

The particular HUD evaluated in this study is a modified electro-mechanical unit manufactured by Sundstrand Data Control. The system consists of two pilot display units, a control module, and a computer. The HUD was developed from a commercial transport display known as the Visual Approach Monitor (VAM). The VAM presents pitch and longitudinal flight patch information to the pilot. No roll or heading information is supplied. The VAM was designed to minimize the problems of judging final approach path angles during visual approaches. It is presently in operational use with Pacific Western Airlines in their arctic support flights(3). It has also been evaluated in several military and civilian airplanes.

Roll information is not considered essential since the VAM was designed for use on final approach in visual conditions only. Later VAMs incorporate an airspeed index showing deviation from a reference speed. A color-coded index shows deviation with a red S for slow, a yellow F for fast, and a green O for correct airspeed. This peripheral cue is similiar to the angle-of-attack indexes on some military airplanes.

The Light Line is a further development of the basic VAM display. Developed under support from the AFFDL, the Light Line presents both pitch and roll information as well as a flight path angle display appearing as a beam of light emanating from the airplane to the projected impact point. This display was evaluated as an approach aid in USAF T-38 airplanes at the Instrument Flight Center(6).

The HUD used in this study is a further development of the VAM/Light Line displays. At the start of the program, it was not clear if roll-stabilization would be required. Therefore a roll/no-roll option was provided through a roll cut-out switch. Airspeed data was provided with a VAM-type airspeed index, and a "ball bank" indicator showed sideslip information. Figure 2 shows the symbology of the test MARS HUD.

SCOPE OF EXPERIMENT

The overall purpose of this program was to determine whether a HUD will assist the pilot of a MARS helicopter with recoveries in low visibility conditions and will also enhance training and standardization. The experimental objective was to determine whether a no-roll presentation is acceptable for MARS operations. If not, is a roll-stabilized horizon bar acceptable? Specific questions to be answered were: (1) What changes in MARS performance (precision and smoothness of control, airspeed control, and maintenance of the sight picture) are attributed to the HUD? (2) What is the pilot workload change induced by the HUD? (3) What are pilot preferences for, and potential

operational problems associated with roll-stabilized and non-roll-stabilized HUD formats? and (4) What changes in HUD format, data, or procedures will help improve MARS performance?

The evaluation was originally planned to be conducted in two phases, both to be flown from Davis-Monthan AFB, Arizona, in visual flight conditions. Phase I was to be flown using 80 lb weights with modified personnel parachutes (TWs) as targets. Actual engagement was not planned. A counterbalanced experiment was designed using the two HUD presentations (roll-stabilized - RH, and no-roll - NR) and a no HUD control (NH). The experiment was arranged to yield useful data with as few as four subjects and six sorties, although the planned numbers were six subject pilots and ten sorties.

Phase II was to follow and consist of two MARS recoveries of 1800 lb dummy vehicles (DVs) with tandem parachutes (main and engagement parachute system described above). This phase was intended to validate the results of Phase I which used single parachutes as targets with no recoveries. During Phase I, the advantages of the HUD were so obvious that Phase I was curtailed at the minimum allowed in the experimental design. Phase II was expanded to include a thirty day operational evaluation at an operating location (OL). During this evaluation, eighteen operational drones were recovered using the HUD.

PHASE I: INITIAL TESTING

Each subject pilot flew on one or two sorties. A sortie consisted of approximately thirty minutes of familiarization with the HUD, followed by up to twelve simulated MARS passes to TWs. All three HUD configurations were used on a given sortie: RH, NR, and NH. The order was varied to minimize the effect of learning. Each subject pilot completed a pre-experiment questionnaire, rating cards after each series of passes, a post-flight questionnaire, and a post-experiment questionnaire. The safety pilot completed a rating card after each pass.

A total of six sorties were flown using four subject pilots. All four subjects were well qualified in CH-3 MARS operations. CH-3 flying experience ranged from 800 to 1800 hours with a total flying experience range of 2500 to 2950 hours. All pilots were CH-3 instructor pilots. The safety pilots were also CH-3 instructor pilots. One of the subjects also served as a safety pilot after he completed his flights as a subject. None of the pilots had flown any HUD-equipped aircraft prior to this evaluation.

Pre-experiment Questionnaire

In addition to establishing the subjects' qualifications, the questionnaire asked for their assessment of the MARS mission. Counting the safety pilot and the copilot on one Phase II DV recovery, six questionnaires were completed. The consensus was that the most significant visual problem was determining the position relative to the engagement parachute in the absence

of a natural horizon. The pilots also commented on the difficulty of transitioning from keeping the parachute on the horizon to passing over the canopy just prior to engagement. Two pilots felt that roll information would be very important in a MARS HUD, but not essential. Three felt that it would be desirable, and one pilot had a neutral opinion.

Subjective Workload

There was no major change in overall subjective workload as reported by the pilots. However, sideslip was perceived as easier to control with either HUD than with no HUD. Roll was reported to be easier with the RH configuration than with the NR HUD. Table I shows the data.

Need for Additional Data

The pilots all felt a need to come "inside" for more data than was shown on the HUD. All reported a need for airspeed until they adapted to the airspeed indexes. All required vertical velocity data. Most required sideslip information with NH, but either HUD provided this data to the pilots' satisfaction. Roll and pitch data were required in the absence of a HUD by some pilots; the RH configuration eliminated the need to come inside for either. One pilot felt a need for torque or RPM.

The need for additional data is summarized in Table II. The HUD was felt to be useful only during final approaches since the horizon bar was displaced beyond the limits of the combiner glass during the turns to final approach.

No focus or visual conflict was reported. Two pilots reported difficulty with the airspeed cue. Comments were also made about the HUD blocking the view of the parachute as it passed beneath the helicopter.

Performance

Under the excellent visibility conditions present at Davis-Monthan AFB, there was no difference in the miss rates (reported by the safety pilot or by the pole operator) between the RH and the NH configurations. Both had miss rates of 22% (4 misses in 18 passes). The absence of roll data causes the miss rate to increase to 28% (4 misses in 14 passes). This is not statistically significant.

Concern Over High or Low Passes

The pilots were generally less concerned over high or low passes with the HUD than without. One pilot commented that while he was less concerned in general, the loss of sight of the parachute on short final (blocked by the HUD hardware) did bother him. (Note: this subject pilot also flew as a safety pilot and as a subject pilot during Phase II and felt that it was not a problem after adaptation.) Either HUD configuration caused the "hits" to be concentrated at the pole tips.

Other Comments

Additional comments were made. Significant comments (paraphrased) are: (1) Airspeed too far from center (3 subjects), (2) Display should be moved closer to pilot (3 subjects), (3) HUD would help training by providing a common sight picture to instructor and student (3 subjects), (4) Practice time was too limited (3 subjects) and the learning curve was slow for airspeed control (1 subject), and (5) The horizon line should be made more intense than the aiming V (1 subject).

PHASE II: OPERATIONAL EVALUATION

Following the decision to conduct an operational evaluation at the OL, the two pilots chosen to fly the evaluation each flew a training sorties consisting of practice MARS approaches to two TWs, followed by a sorties with an actual recovery of an 1800 lb DV. The two pilots were already experienced with the HUD, having flown as safety pilots in Phase I (one also flew as the first subject).

The HUD was removed from the helicopter used for Phase I and for the four sorties described above. It was then taken to the OL and installed in another CH-3. Eighteen operational recoveries were made at the OL during the month of April 1975. Only the RH display was used for recoveries during this phase, although the NR mode was briefly evaluated during other flying in the haze conditions prevalent at the OL.

Both DV recoveries at Davis-Monthan AFB were made on the first pass. Of the eighteen HUD-assisted engagements at the OL, sixteen were made on the first pass*, one on the second, and one on the third pass. One mission had a no-HUD recovery (4th pass) because of excessive display vibration. The miss rate using the HUD was 14% (per pass).

Benefit of HUD

The second operational sortie typifies the benefit of the HUD. On this sortie, the load line break-ties had separated from the main canopy resulting in the engagement parachute lying over and remaining at the same altitude as the main canopy. With the horizon obscured by haze, rain, and clouds, the HUD allowed a successful recovery on the first pass. The pilots felt that in the absence of a HUD, there would have been multiple missed passes and very likely a lost drone.

The pilots felt that pilot workload was much lower with the HUD.

Visual Illusions

Both pilots commented on an illusion during passes with the HUD in marginal weather. They had the illusion of being correctly lined up with the engagement parachute, but the HUD showed them to be high. Confidence in the

---

* Counting one tear-out as a successful pass

HUD from their experience in Arizona allowed them to use the HUD to correct their flight paths and make consistent catches.

Need for Roll-Stabilization

The HUD proved to be highly satisfactory under adverse weather conditions with roll-stabilization; but without roll a serious problem was encountered. Both pilots felt that manuevering in haze induced vertigo. They considered that roll-stabilization was an essential requirement for use in reduced visibility.

DISCUSSION

Operational Effectiveness

There were 77 MARS passes during the evaluation. Of these, fifty passes were made to 80 lb TWs and success/failure was estimated by the safety pilot or pole operator. The remaining 27 passes were made to DVs or to actual drones with success being defined as an engagement (or a tear-out). Of the 77 total passes, twenty-five were made during drone recoveries in haze at the OL. The remaining passes (50 TWs and 2 DVs) were made in good weather in Arizona.

We must further separate the data into learning and steady-state performance. To do this, we shall classify all no-HUD passes as steady-state since all subjects were considered to be highly qualified by their organizations. All Phase I passes with either HUD should be considered as learning passes. The actual recoveries made using the roll-stabilized HUD, both DVs and operational drones, can be classed as steady-state performance. Thus we have 32 learning passes and 45 steady-state performance passes.

The performance comparison between the two HUD versions can only be based on the learning data. Because of the small sample size, the difference in miss rates is not significant.

To compare the performance of the RH and the no-HUD baseline, we must use steady-state performance and, as a result, equate the difficulty of making passes to TWs and to tandem parachutes, although the motion of the tandem parachute system makes actual recoveries harder. Likewise, we must equate the difficulty of operating in Arizona in good visibility to the difficulty of operating at the OL in haze and smoke. Since the NH passes were mostly made to TWs at Davis-Monthan AFB, these assumptions are heavily weighted against the HUD.

Nevertheless, the miss rates were much lower with the HUD (3 misses in 23 passes or 13%) than without the HUD (32% missed). Again the limited data precludes any statistical test ($\chi^2=2.29$, df=1, $0.2>p>0.1$). However, in view of the heavily biassed test conditions, this difference in miss rates should be considered valid.

Mission Success Rate

To convert from miss rate (i. e., fraction of passes missed) to mission success rate (i. e., fraction of drones recovered), we use the familiar parallel redundancy formula:

$$\text{MISSION SUCCESS RATE} = 1 - (\text{MISS RATE})^{n}$$

where n is the number of passes possible before the drone is too low for a safe pass. With a typical value of n = 3, we can compute the mission success rates. For the roll HUD, the learning curve performance is 98.9% and the steady-state performance in 99.8% of all drones recovered. The steady-state baseline (no HUD) performance is 96.8%.

Again, the assumptions favor the no HUD case. If we look at the one sortie where the HUD malfunctioned (3 misses out of four passes), the corresponding mission success rate for no HUD in haze would be 58%. This figure is consistent with mission recovery rates of less than fifty percent which have been reported in no-horizon conditions.

Flight Safety

The primary hazard during MARS operations is collision with the parachute. During Phase I, it was noticed that the successful passes with the HUD were concentrated at the pole tips. This effect is probably the result of the aiming V helping the pilot to make a smooth transition to allow the parachute to pass beneath the helicopter into the engagement window. While this effect was only noticed with passes to TWs, it will undoubtedly reduce the number of nose or belly slaps during training and certainly minimize the risk of a catastrophic collision. It is not clear whether the aiming V should be adjustable to accommodate different size parachutes. The pilot opinions were divided and no tests were conducted.

While no particular problems with the no-roll HUD were noted during flights in good weather, the pilots at the OL did report a strong tendency toward vertigo when flying the no-roll HUD in restricted visibility. This represents an unacceptable hazard.

One sortie was cancelled because of invalid pitch data on one HUD. This can be a serious hazard in instrument weather conditions or if the horizon is not visible. Serious consideration should be given to incorporating an instrument comparator to warn against invalid data. Failing this, crew procedures must be developed to ensure that discrepancies are noted. However, it will be difficult for the non-flying pilot to crosscheck his HUD with his panel instruments.

Displayed Data Requirements

The basic MARS HUD was intended to display pitch, sideslip, and airspeed with an optional roll display. The pitch display was the primary display needed for MARS. Since sideslip and airspeed were critical for successful engagements, they were also included. Part of the experimental design was to

evaluate the need for roll. The HUD also included an aiming V to assist the pilot during the transition just prior to engagement. During the evaluation, pilot comments suggested that vertical velocity data be added.

Pitch. Lack of adequate pitch cues from the horizon was the original reason for the HUD. We can, therefore, presume that pitch is a requirement for a MARS HUD. However, with a pitch malfunction, the airspeed, sideslip, and vertical velocity data would still be useful. Pitch failure, then, need only extinguish the pitch and roll displays (and the aiming V).

Roll. Roll can be considered a requirement primarily as a vertigo avoiding measure. Roll failure must extinguish the pitch and roll displays.

Airspeed. No test without airspeed was conducted. We conclude from pilot comments that it is required. Airspeed failure need only extinguish the speed indexes.

While the use of the three symbol airspeed display is adequate for determining both the actual airspeed and trends, some learning over and above the normal HUD familiarization seems to be needed.

Sideslip. Likewise, no specific evaluation of a no-sideslip HUD was done. Based on pilot comments, we conclude that it is a requirement. The original ball bank display was too hard to read for small sideslip angles. As a result, the opaque ball was changed to a triangular shaped sideslip index. The display, as modified, is adequate for the MARS mission. Bad sideslip data need only extinguish the ball bank display.

Vertical Velocity. The original display had no vertical velocity data. However, the majority of the pilot comments indicated a need for such data. The reason for this can be found in the Air Force handbook on instrument flying(7). This approach divides the flight instruments into control and performance instruments. The pilot makes his control inputs be reference to the control instruments (such as ADI or power/thrust) and monitors the aircraft's response by reference to the performance instruments (airspeed, heading, or vertical velocity).

The MARS pilots, having made a pitch or power correction to fly up or down relative to the parachute, felt the absence of a vertical performance instrument to monitor their corrections. This explains the need for vertical velocity data. Apparently, they felt able to do without a power control instrument. Perhaps, kinesthetic feedback from the collective position was sufficient. One pilot did comment on the absence of torque or RPM data.

During the recovery after engagement, the pilot must, at maximum torque, trade altitude for airspeed. During this transition, the vertical velocity data is also needed. A torque display is not needed since the pilot can sense maximum torque from the RPM droop. As a result of these observations, the production MARS HUD incorporates a vertical velocity display. Preliminary pilot comments to this addition were favorable.

Aiming V. The aiming V was commented on favorably by the subject pilots. However, no concensus could be reached on the need for different Vs for different sized parachute canopies.

Modified Display. As a result of the testing and pilot comments, the symbology was changed for the production MARS HUD hardware. The revised format it shown in Figure 3.

CONCLUSIONS

The HUD system (with roll) will enhance MARS performance during periods of reduced visibility. It will also enhance safety during training by causing the passes above the target parachute to be higher — reducing the chances of the helicopter's striking the parachute. Roll stabilization is a safety-of-flight requirement to avoid vertigo in no-horizon weather conditions. Roll-stabilization appeared to improve performance over the no-roll case; however insuffient data was available for a statistically valid test.

Pilot workload is much lover when using the HUD. Training to use the HUD should require practice passes to 2-4 training weights, assuming a MARS-qualified pilot. The ability to make full use of the airspeed cue on the HUD may require additional time. The airspeed learning curve seems to be quite variable from pilot to pilot.

The MARS HUD should display pitch, roll, sideslip, airspeed, and vertical velocity data. A reliable self-test circuit is highly desirable. The horizon line should be more distinct than the aiming V.

While the HUD should enhance crew training and standardiza[illegible] well as mission performance, operational flight procedures should be rev[illegible]rtly after fleet use begins.

REFERENCES

1. A-7D Navigation/Weapon Delivery System, Vought Report 2-14000/412-10, 1974

2. Naish, J. M., Properties and Design of the Head-Up Display (HUD), McDonnell-Douglas Report MDC-J1409, 1968; revised 1970

3 Mackie, R.. Jet Transport Operations in the Arctic, presented at the Aircraft Operations in the Canadian Arctic Meeting of the Canadian Aeronautics and Space Institute, Edmonton, 1973

4 Augustine, W. L., Head-Up Display Area Survey, AFFDL-TM-72-11-FGR, 1972

5 Singleton, W. T., Display Design: Principles and Procedures, ERGONOMICS, 12, 1969, 519-531

6. Tapia, M. and Intano, G., Light Line Visual Landing Head-Up Display Evaluation, USAF IFC-TR-76-1, 1976

7. Instrument Flying, USAF Manual AFM-51-37, 1971

8. Partial (MARS) Flight Manual, USAF CH-3E Helicopters, USAF Technical Order 1H-3(C)C(I)-1, 1974

HUD	Controlled Parameter	Number of Responses 1 Very Easy	2 Easy	3 Medium	4 Hard	5 Very Hard	Mean Value
No HUD	Airspeed		1	2	1	1	3.4
	Vertical Velocity		1	2	1	1	3.4
	Pitch		2	3			2.6
	Sideslip		2	2	1		2.8
	Roll		3	2			2.4
	Overall		1	2	1	1	3.4
Roll HUD	Airspeed		1	3	1	1	3.33
	Vertical Velocity			4	1	1	3.5
	Pitch		3	2	1		2.67
	Sideslip	1	4	1			2.0
	Roll		5	1			2.17
	Overall		1	3	1	1	3.33
No-Roll HUD	Airspeed		2	1	3		3.17
	Vertical Velocity		2	1	3		3.17
	Pitch		3	2			2.4
	Sideslip	1	4	1			2.0
	Roll		4		1	1	2.83
	Overall		1	3	2		3.17

TABLE I

SUBJECTIVE DIFFICULTY OF MAKING PASSES

Configuration	Number of Questionnaires	Number of Times Parameter Cited by Pilot						
		Airspeed	Pitch	Roll	Sideslip	Altitude	Vertical Velocity	RPM or Torque
No HUD	6	6	2	3	4	1	6	1
Roll HUD	6	3				1	3	1
No-Roll HUD	5	3		2		1	2	1

TABLE II

NEED FOR ADDITIONAL DATA

NOT SUPPLIED BY HUD

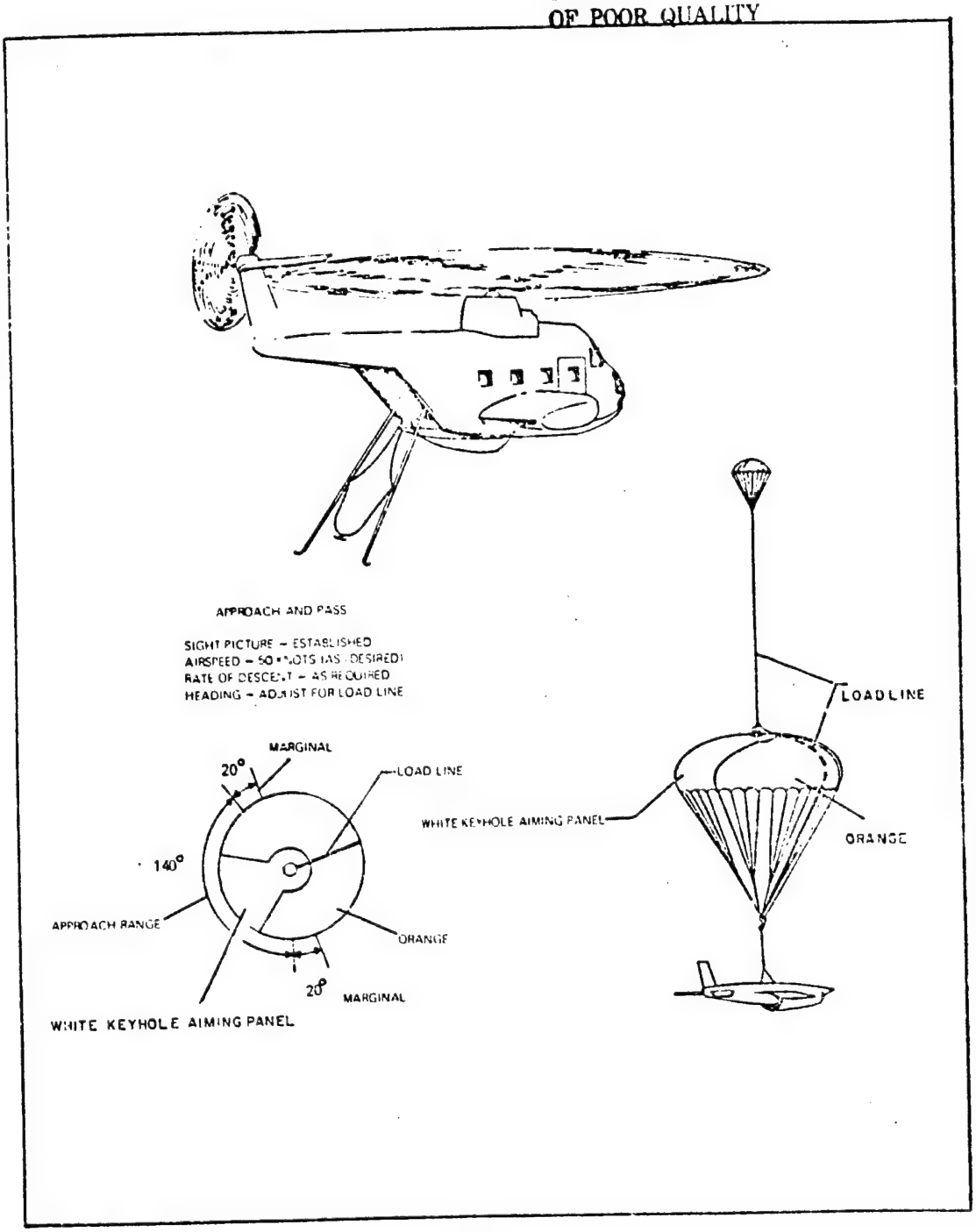

Figure 1

Helicopter Approach and Pass

From Reference 8

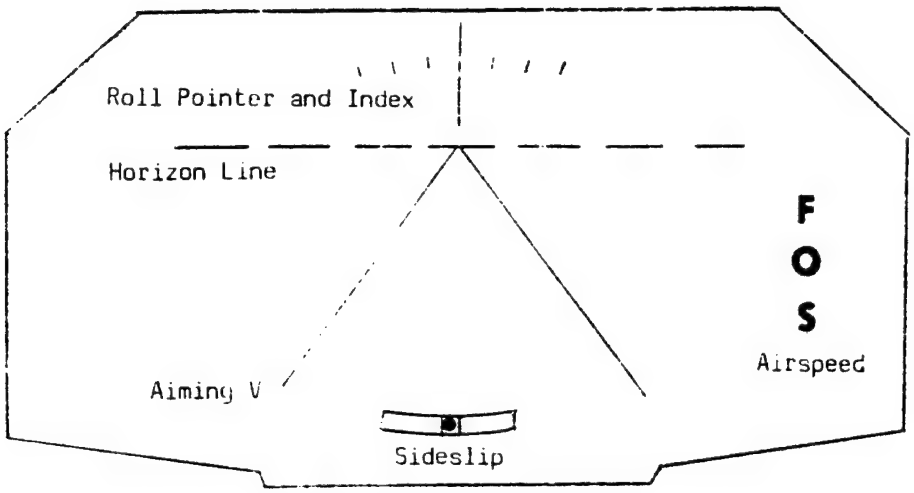

Figure 2

MARS HUD Display Format

(As Tested)

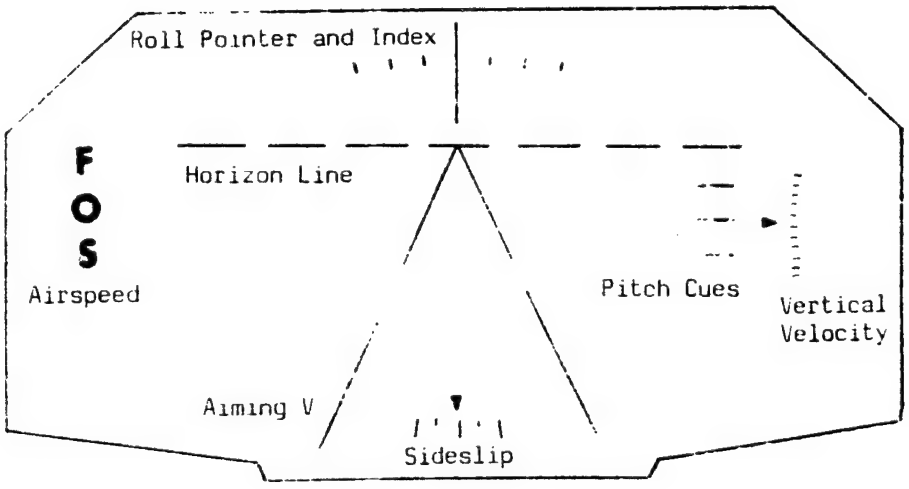

Figure 3

Revised Display Format

N79-15616

EVALUATION OF DISPLAY AND CONTROL CONCEPTS FOR A TERMINAL CONFIGURED VEHICLE IN FINAL APPROACH IN A WINDSHEAR ENVIRONMENT*

William H. Levison
Bolt Beranek and Newman Inc.
Cambridge, Mass. 02138

Presented at the fourteenth Annual conference on Manual Control, University of Southern California, April 25-27, 1978.

ABSTRACT

The effects of display and control parameters on approach performance of a simulated Terminal Configured Vehicle (TCV) were explored experimentally in a manned simulation study and analytically using a state-of-the-art pilot/vehicle model. A revised treatment of nonrandom inputs was incorporated in the model. Response behavior was observed for two display configurations (a pictorial EADI presentation and a flight-director configuration requiring use of a panel-mounted airspeed indicator), two control configurations (attitude and velocity control wheel steering), and two shear environments, each of which contained a head-to-tail shear and a vertical component.

In general, performance trends predicted by the model were confirmed experimentally. Experimental and analytical results both indicated superiority of the EADI display with respect to regulation of height and airspeed errors. Velocity steering allowed tighter regulation of height errors, but control parameters had little influence on airspeed regulation. Model analysis indicated that display-related differences could be ascribed to differences in the quality of speed-related information provided by the two displays.

*This research was supported by the National Aeronautics and Space administration under contract No. NAS1-13842.

INTRODUCTION

Windshear constitutes one of the major threats to flight safety in approach and landing operations. This threat is enhanced not only by the potential severity of the shear (defined as a wind whose velocity changes with altitude), but also by the tendency of the shear profile to change rapidly over time. This lack of predictability has led to the need for control and display aids to help pilots better cope with the presence of windshears.

This paper summarizes the second phase of a program to analyze display-control configurations for the Terminal Configured Vehicle (TCV). This work was performed for NASA Langley Research Center and was intended to augment a simulation study conducted there.

The first phase of this study explored the effects of certain control and display configurations on approach performance in a zero-mean, random turbulence environment. The LRC simulation was augmented by an analytic study performed at Bolt Beranek and Newman Inc. using the "optimal-control" pilot/vehicle model to explore both performance and workload differences among control/display configurations of interest. The reader is assumed to be familiar with the features of this model, which has been well documented in the literature. Frequent reference is made below to the report by Levison and Baron [1] which documents the results of the first study phase and which demonstrates application of the pilot model to analysis of TCV approach performance.

Approach performance of a TCV in windshear environments was studied in the second study phase, with control and display configuration (along with windshear profile) the major variables of interest. The existing pilot/vehicle model was modified to allow a revised treatment of nonrandom inputs; because the longitudinal and vertical components of the shear have greatest impact on path and airspeed regulation, only longitudinal-axis performance was explored in the analytic study. The results of the windshear study are documented in [2].

PROBLEM DEFINITION

Description of the Flight Task

The flight task of interest was the standard straight-in (3 degree) approach of a simulated TCV. The simulated atmospheric environment contained low-level zero-mean gusts plus a wind shear consisting of a rotating horizontal component and a brief interlude of either an updraft or a downdraft.

Speed and flight path were controlled manually. Flight-path control was aided by one of the following control augmentation schemes: "Attitude Control Wheel Steering (ACWS) or "Velocity Control Wheel Steering" (VCWS). Basically, these modes provide attitude-rate stabilization and allow the pilot, in effect, to command either attitude (ACWS) or path angle (VCWS). A more detailed description of control wheel steering is given in Levison and Baron [1]. In order to use the existing man-machine model, the track-hold feature of the CWS was approximated by continuous linear feedback law as shown in Figure 1.

Displays

Flight control information was provided primarily by an electronic attitude/director indicator (EADI). Two display configurations were considered: (1) "advanced" display, which presented information in an integrated (pictorial) format, and (2) the flight director display, which provided director information based on path, path angle, and attitude errors.

The advanced display provided the following flight-control information (as diagrammed in Figure 2): (a) an aircraft symbol to serve as x-axis airframe reference, (b) an artificial horizon and pitch attitude scale, (c) a roll attitude scale and pointer, (d) a pair of so-called "gamma wedges" to indicate path angle, (e) a dashed line to indicate a point 3 degrees below the horizon, (f) a perspective runway symbol, (g) an extended runway center line to aid in lineup regulation, (h) a symbol to indicate track angle, (i) a glideslope indicator, (j) a localizer indicator, and (k) a so-called "potential gamma" symbol to provide information pertaining to speed management.

Except for the potential gamma symbol, this display was indentical to the advanced display described in [1], to which the reader is referred for additional details on the structure and use of this display. A weighted sum of airspeed error and rate of change of vehicle velocity was used to drive the potential gamma symbol, relative to the gamma wedge, in the vertical dimension.

The "flight director display" consisted of a raw status display plus director information. The EADI provided attitude information, glideslope and localizer errors in symbolic format, and director information. Airspeed and rate-of-climb were displayed by conventional panel meters. Perspective runway, gamma wedges, and potential gamma were omitted from the EADI in this display configuration.

Director information was provided with a pair of crossbars

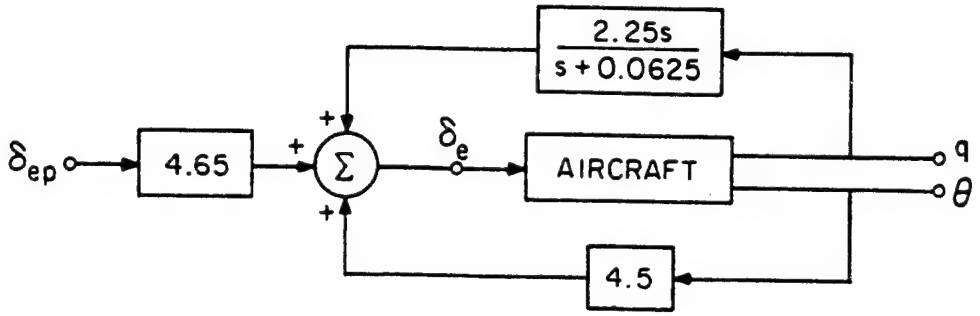

(a) ATTITUDE CWS

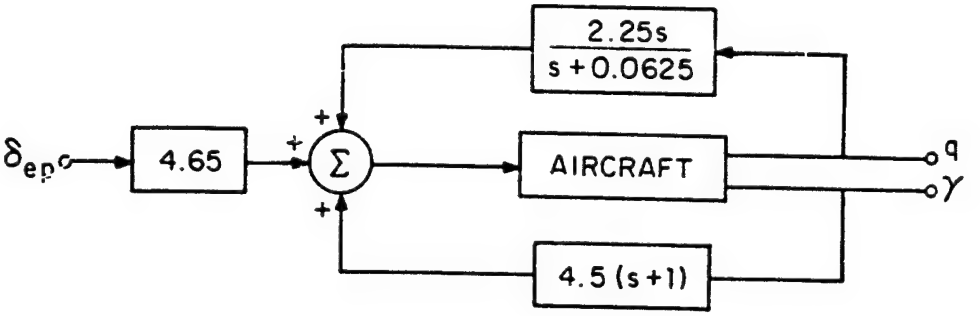

(b) VELOCITY CWS

Figure 1. Linear Approximation to Control Wheel Steering

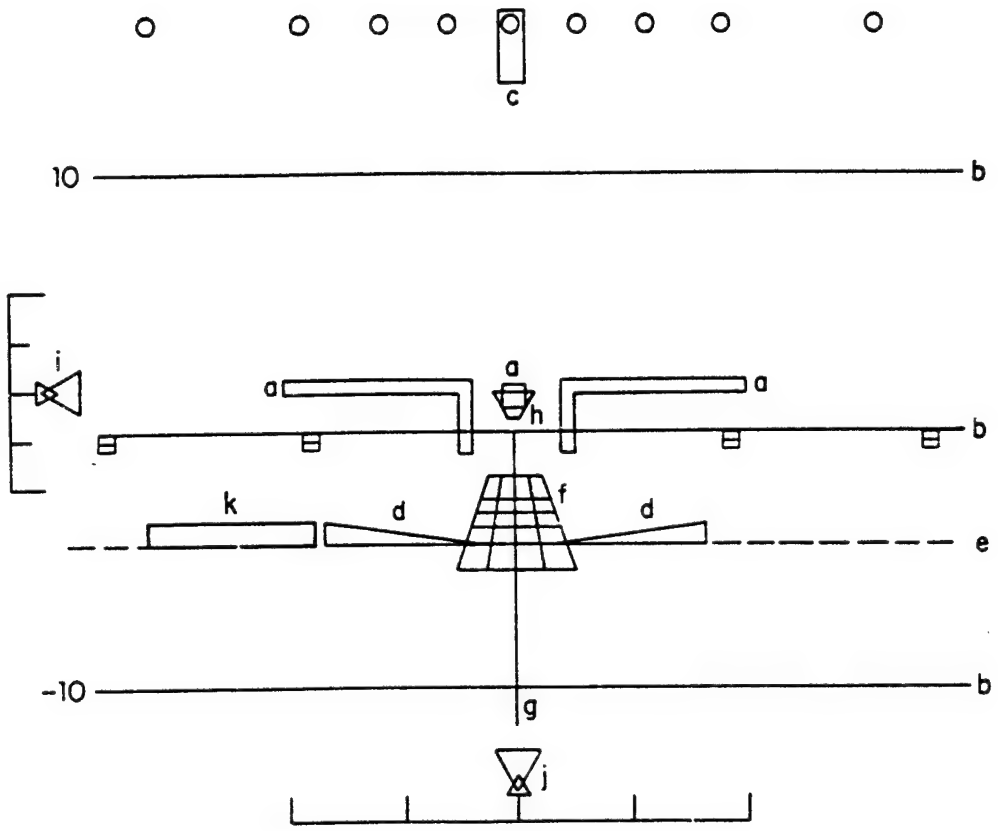

Figure 2. Sketch of the EADI Display
(Display elements defined in the text)

that deviated from the x-axis reference symbol in a "fly-to" mode. The director indicator was driven by a weighted sum of height, path angle, and pitch-rate errors as described in [2].

Wind Environment

Wind shears as well as zero-mean random gusts were simulated in the NASA-LRC experiments. In order to simplify problem formulation and reduce computational requirements, the effects of these simulated gusts were approximated in the bulk of the model analysis by including wide-band disturbances added in parallel with the control deflections. Preliminary model analysis was conducted to select disturbance levels that would give nearly the same predicted path and airspeed errors as would be obtained from a more faithful representation of the simulated gust inputs [2].

Each of the simulated windshears used in the experimental and analytical study contained a rotating horizontal component plus a brief vertical component. Figure 3 shows the relationship between wind speed and range for points along the nominal 3 degree glide path for two of these shears.* (Note that the horizontal and vertical wind components have been scaled differently in this figure.)

METHODS

Model Analysis

The model employed in this study was basically the so-called "optimal-control model" described extensively in the literature, modified to treat non-zero-mean (i.e., deterministic) inputs. As the treatment of the deterministic input (i.e., the windshear) was different from that used in previous studies (3-5), a brief discussion of this treatment is given below. A more detailed exposition of this aspect of the pilot model is given in the appendix to [2].

Modeling the pilot's response to a deterministic input involves two basic considerations: (1) the degree to which the

*Since windspeed is an explicit function of altitude, rather than range, deviation of the aircraft from the desired glide path would modify somewhat the range dependency shown in Figure 3.

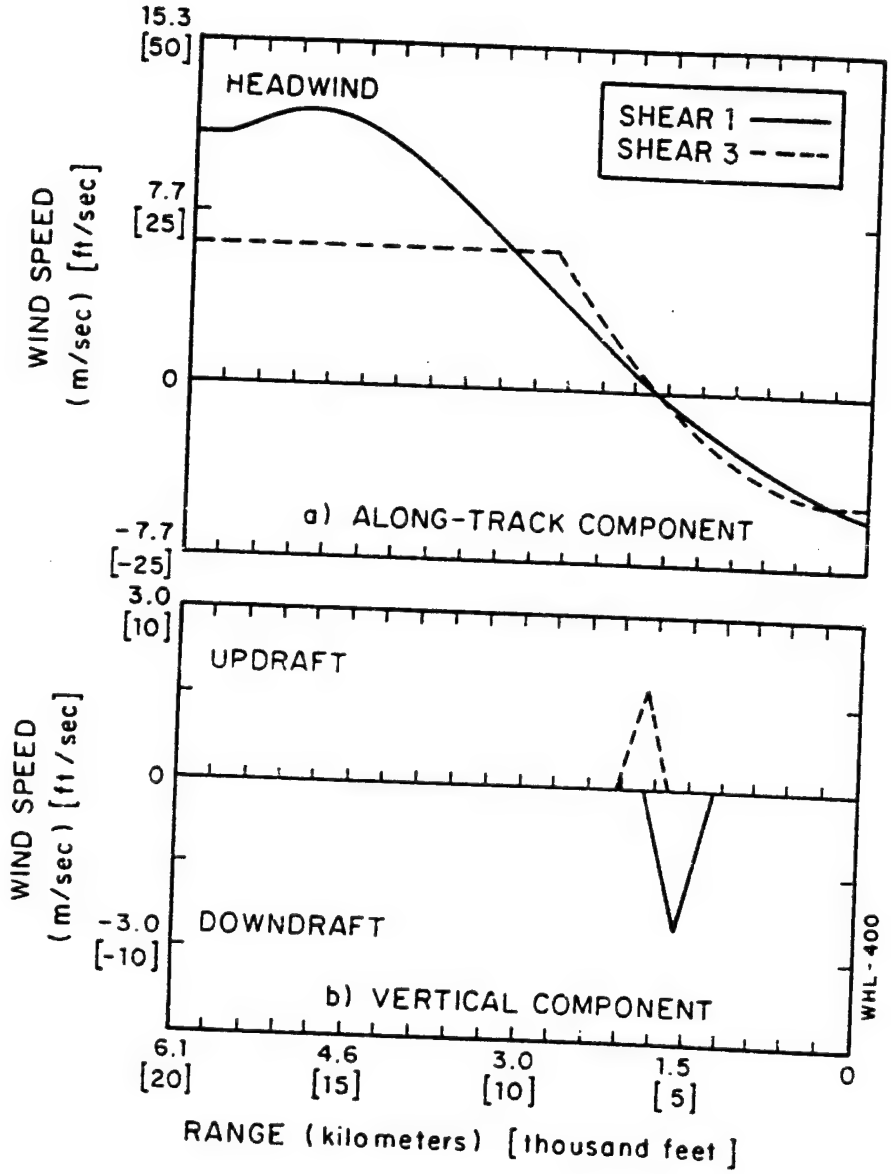

Figure 3. Windshear Profile

pilot understands the nature of the input (i.e., his "internal model"), and (2) the way in which the pilot detects and responds to the input. A simple representation of the pilot's knowledge of the windshear was adopted for the study; basically, we assumed no specific knowledge of the shear, only the knowledge that a non-zero-mean wind might exist. We assumed that the pilot would not try to anticipate changes in the wind, but would, at best, attempt to estimate the current wind vector. This level of pilot knowledge was modeled by simply implementing a stepwise-constant representation of the wind. Since the wind varied relatively slowly with time, an integration time step of 1 second was sufficiently fine to allow an adequate representation of the continuously-varying wind speed.

The pilot/vehicle model was modified to reflect the following assumptions concerning pilot behavior in a non-zero-mean input environment:

a. The pilot continuously anticipates the behavior of the display variables he is utilizing, given his current estimates of system states and his internal model of system parameters.

b. The pilot performs a short-term average on the difference between expected and actual behavior of each display variable.

c. If average prediction error is sufficiently large with respect to the variability of this error, the pilot becomes additionally uncertain about his estimates of system state variables, and he attempts to upgrade these estimates.

Implementing this set of assumptions led to the following additional pilot-related model parameters: (1) the short-term averaging time, (2) the magnitude of the prediction error considered large enough to warrant special action, and (3) specific state variables to which the pilot attributes his uncertainty. In addition, an algorithm had to be formulated for relating prediction errors to increased uncertainty.

Model predictions were obtained with the assumptions that (1) prediction errors were averaged over about two seconds, (2) an average deviation of two standard deviations from the expected value warranted special consideration by the pilot, and (3) uncertainty could be associated with any of the principal state variables, including the state variables representing the horizontal and vertical shear components.

To obtain a model solution it was necessary to describe the task environment in a suitable mathematical format and to assign values to model parameters related to pilot limitations. System dynamics were modeled as described in [1], with the modification indicated in Figure 1 of this paper to account for control wheel steering augmentation.

The pilot was assumed to adopt a control strategy that minimizes a weighted sum of mean-squared response variables. In this study, the "cost function" included height error, sinkrate error, airspeed error, angle-of-attack error, control deflection, and rate-of-change of control deflection. Because the results of the previous study suggested that pilots tended to regulate height error in terms of an angular, rather than a linear, criterion, weightings associated with height and sinkrate errors were varied inversely with range. Weightings for other variables were kept fixed throughout the "flight" as documented in [2].

When tracking with the advanced display, the pilot was assumed to perceive height error, sinkrate error, pitch and pitch rate, flight path angle and path angle rate, and potential gamma. Because movement of the perspective runway with respect to the nominal glideslope was proportional to error in angular terms, the thresholds for height and sinkrate errors (in terms of feet and ft/sec) varied linearly with range. The height error threshold was based on an "indifference threshold" of 1.4 meters at the 30 meter decision height as determined from previous analysis. Other threshold values were based on considerations of visual resolution as described in Levison and Baron. The noise/signal ratio of -17 dB associated with use of the advanced display reflects a moderate-to-high level of workload with no interference among display elements (i.e., we assume integration of the displayed information).

When tracking with the director display, the pilot was assumed to rely primarily on the director symbol and the airspeed indicator for continuous flight-control information, with a negligible amount of time spent scanning the status information for monitoring purposes only. The threshold of 1.0 m/sec. on airspeed was based on the assumption that the pilot was indifferent to airspeed errors smaller than the calibration increments of the airspeed indicator (2 kts); threshold values for perception of director displacement and rate were based on visual resolution limitations. The noise/signal level of -14 dB reflects the same overall level of attention to the task as before, with the requirement to share attention between the director and airspeed indicators. For simplicity, equal sharing of attention between the two displays was assumed, and loss of visual inputs associated with eye movements was neglected.

Experimental Procedures

The experimental task was to track a 3° ILS beam to touchdown. Each experimental trial began at a simulated range of 5700 m from the runway threshold at an altitude of approximately 366 m. The aircraft was initially trimmed on the desired glide path for a 3° path angle in its approach configuration: 120-knot airspeed laps, gear down. Rudder was automatically controlled.

Zero-mean random gusts and wind shears were both simulated during each experimental trial. Three shear environments were explored, including those designated as "Shear 1" and "Shear 3", profiles of which are given in Figure 3.

Gust disturbances having an rms variation of 0.3m/sec were simulated for all three translational axes. Gust spectral characteristics were varied with altitude according to the wind models suggested by Chalk et al. [6].

Data were obtained from three NASA test pilots. Practice trials were provided using shears other than those specified for data collection. Each pilot "flew" two sessions of 18 approaches each for data collection; each session consisted of two replications of 3 control/display configurations and 3 shear environments presented in a balanced order. Thus, four replications per experimental condition per pilot were obtained.

Ensemble statistics were computed for selected response variables for each experimental condition. First, within-subject replications were analyzed to provide trajectories of mean response and of the standard deviation of the response. These measures were processed further to provide across-subject averages of the mean and standard-deviation response trajectories. Mathematical definitions of these statistical variables are given in Levison and Baron.

For purposes of data presentation, statistical analysis was performed for height and airspeed errors, sampled at 305 meter intervals beginning at a range of 4572 m from the ILS origin.

SUMMARY OF RESULTS

Considerations of space preclude an extensive presentation of either theoretical or experimental results. A sampling of results is presented to demonstrate three applications of the pilot/vehicle model in the context of this study: (1) prediction, (2) diagnosis, and (3) extrapolation. Additional results are documented in [2].

Prediction

The following four figures compare display and control trends for predicted and experimental mean response trajectories for the "Shear 1" environment.* Because the experiment was not full factorial, display differences are shown for the Attitude CWS configuration only, and control differences are compared for the advanced display configuration.

Effects of display on mean height error and mean airspeed error are shown, respectively, in Figures 4 and 5. In general, the trends predicted by the model are confirmed, but the differences observed experimentally are smaller than predicted. Model and experimental correlation is generally better for height than for speed response.

As predicted, experimental height error is generally more negative for the director than for the advanced display. The data also confirm the prediction that the director display leads to a larger swing in error over the course of the approach. There was also a tendency (not predicted) for the pilots to fly above the nominal glide path.

Figure 5 shows that the test pilots flew the director display with less negative (or more positive) airspeed errors than achieved for the advanced display--a trend the reverse of which was predicted by the model. Given the reported tendency of pilots to fly approach speeds greater than nominal when windshears are anticipated [7], we suspect that the test subjects attempted to compensate for the lack of good airspeed information from the director configuration by intentionally carrying excess airspeed. Experimental results confirm the prediction of greater swings in error with the director display, although the magnitudes of the display-related differences are less than predicted.

Figures 6 and 7 confirm the major trends predicted for control effects; namely, tighter regulation of height error was observed for velocity CWS, whereas control configuration had little effect on regulation of speed error.

Results for the Shear 3 environment, documented in [2], showed similar types of correlation between predicted and measured mean error trajectories.

---

*Model results shown in these figures are true predictions in the sense that they were obtained before the experimental data were analyzed. Pilot-related model parameters were not adjusted to provide a best match to the data.

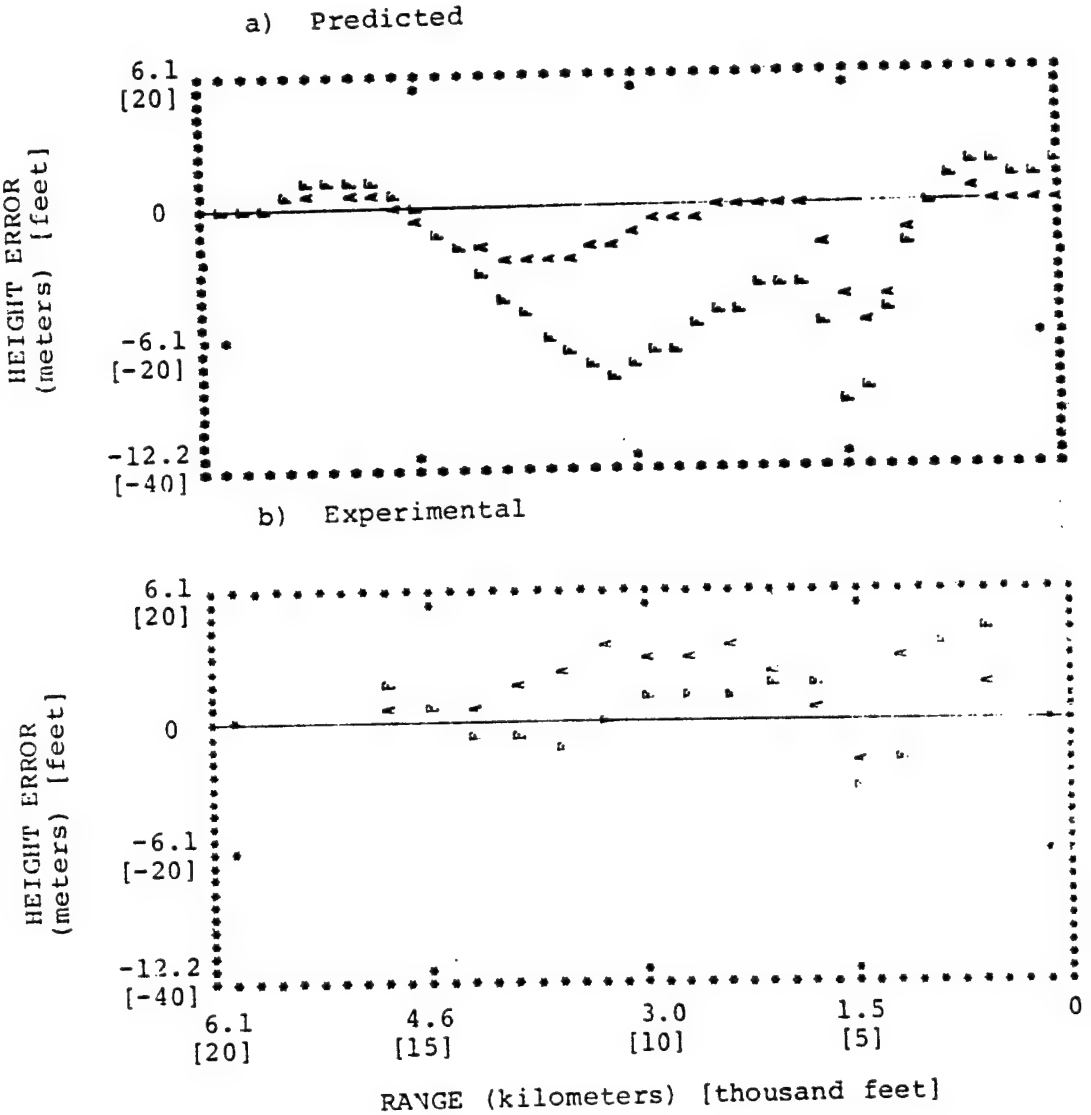

Figure 4. Effect of Display on Mean Height Error, Shear 1 Attitude CWS.
A = advanced display, F = flight director

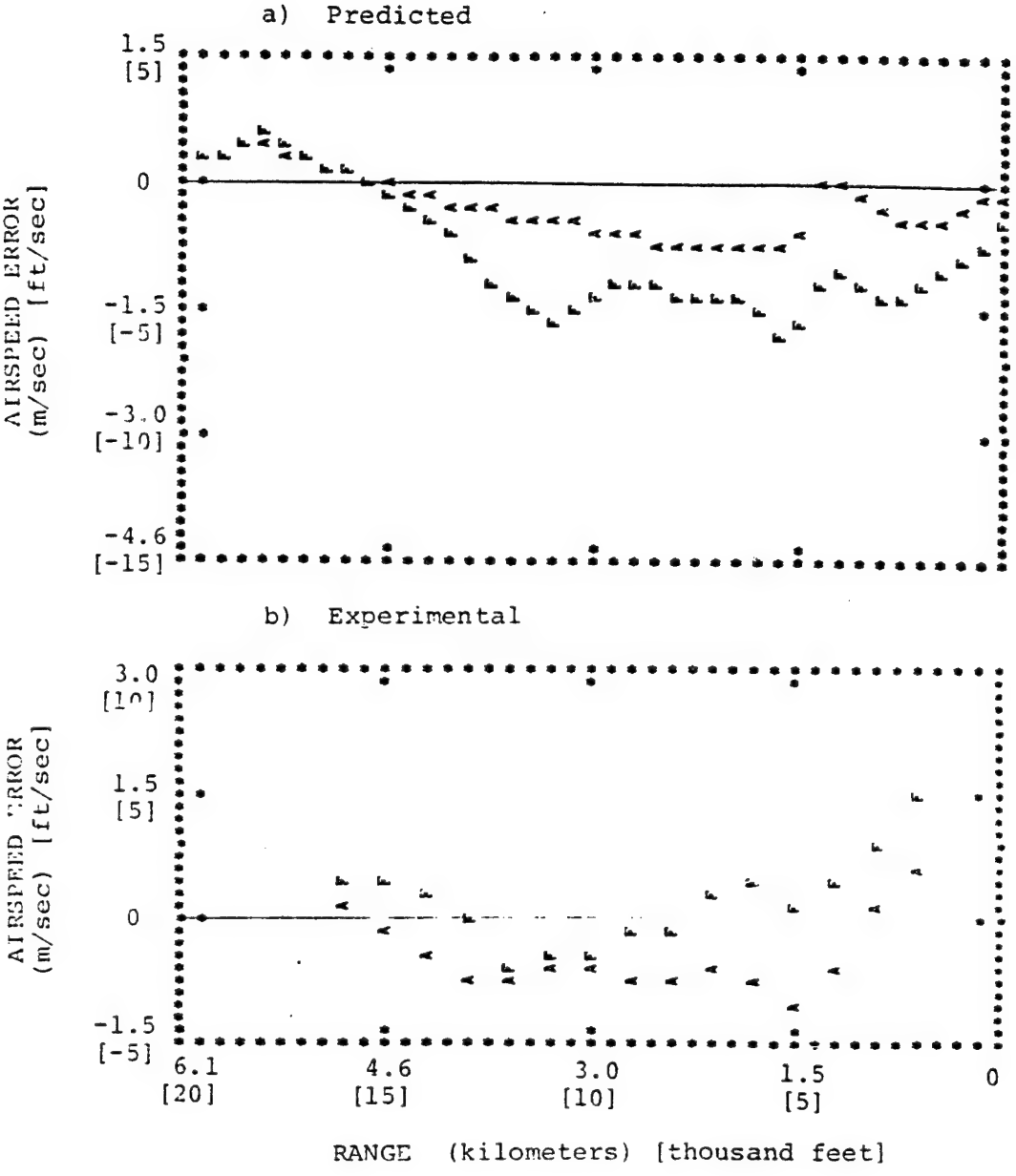

Figure 5. Effect of Display on Mean Airspeed Error, Shear 1

Attitude CWS.
A = advanced display, F = flight director

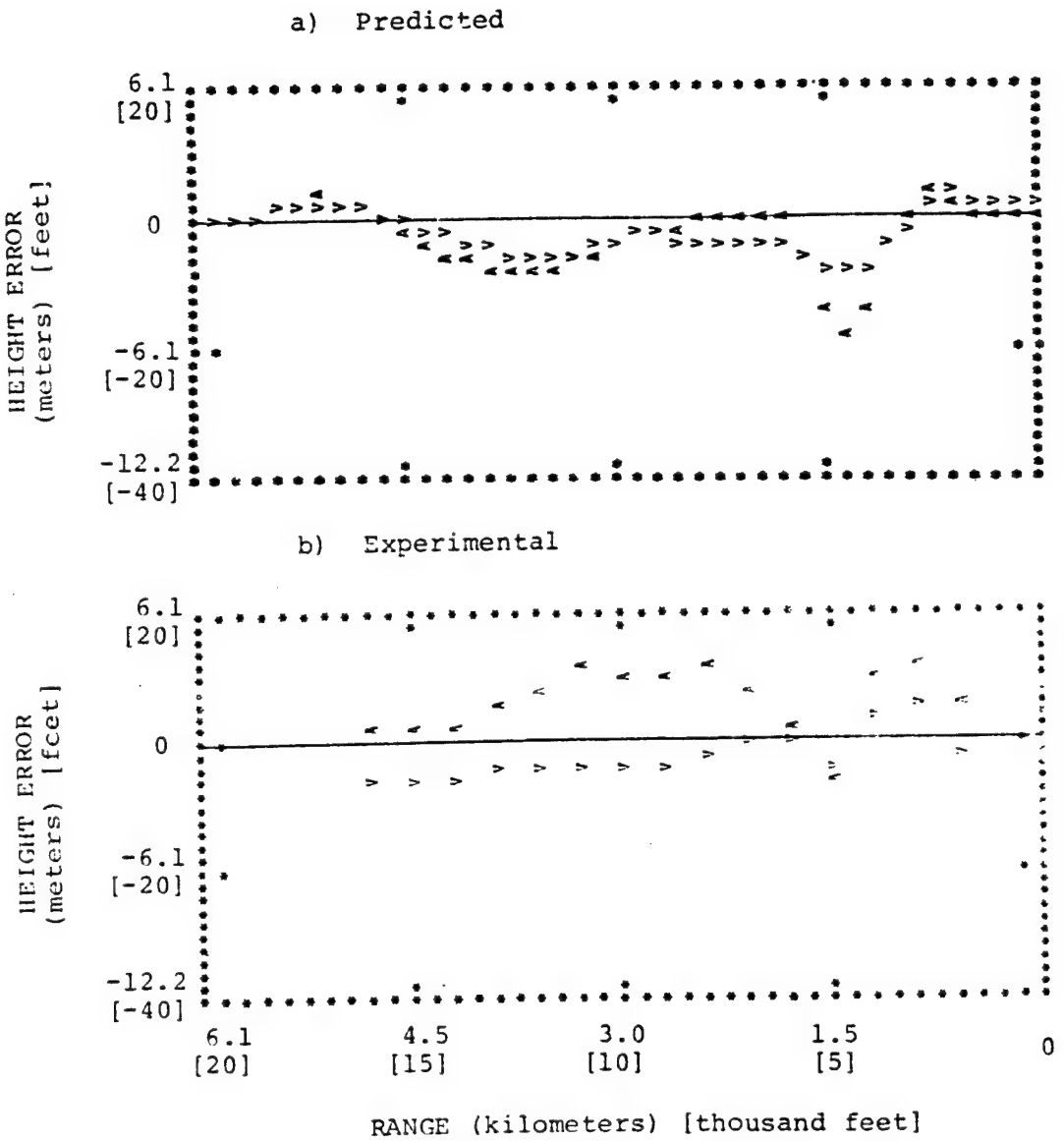

Figure 6. Effect of CWS on Mean Height Error, Shear 1

Advanced Display.
A = attitude CWS, V = velocity CWS.

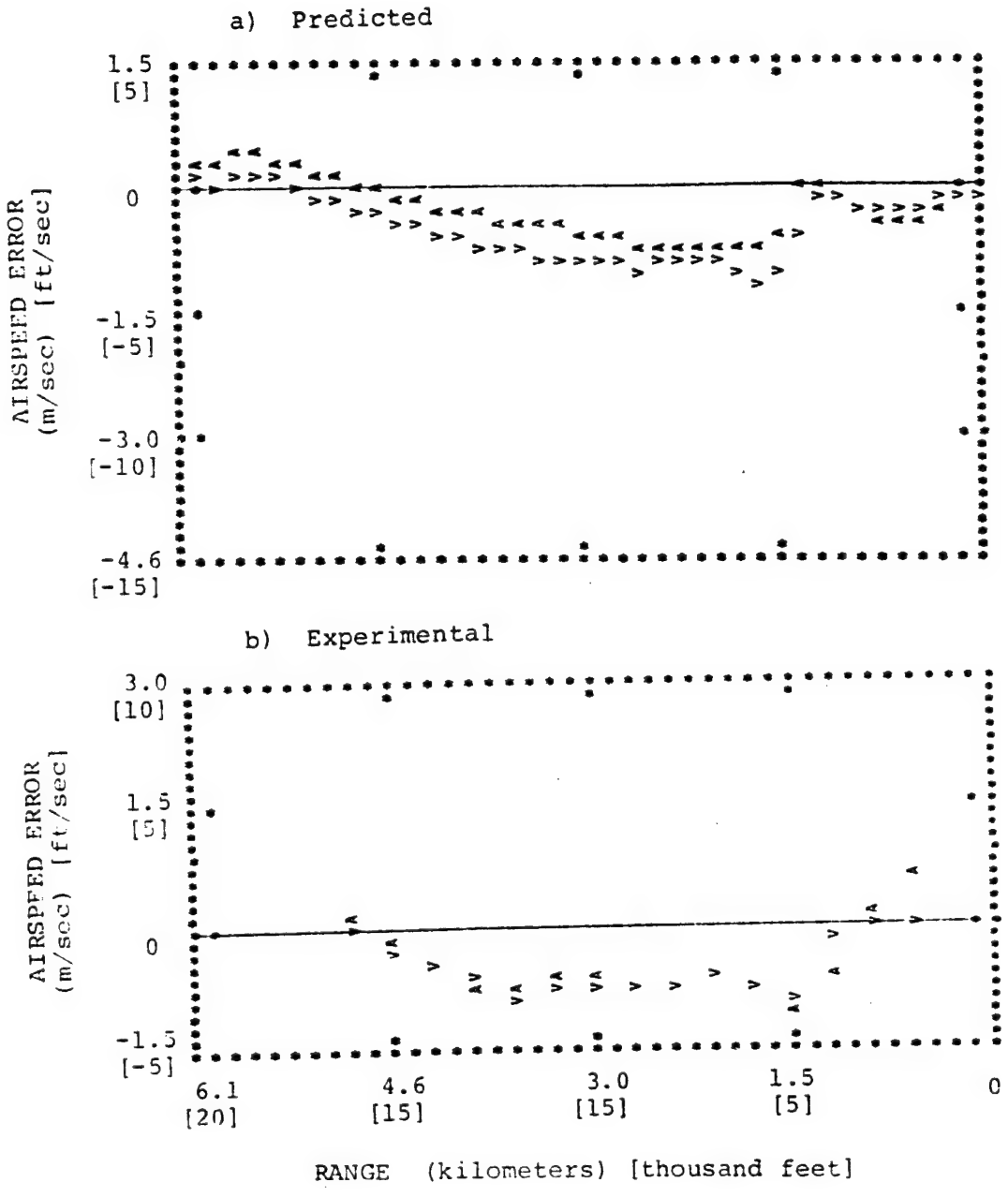

Figure 7. Effect of CWS on Mean Airspeed Error, Shear 1 Advanced display.
A = attitude CWS V = velocity CWS

Diagnosis

In order to ascertain the cause of the performance differences observed for the two display configurations, the director display configuration was reanalyzed with the threshold of 0.024 m/sec (as opposed to 1.0 m/sec assumed previously). This reduced threshold was equivalent to that which would be associated with the potential gamma indicator of the advanced display if potential gamma were driven solely by airspeed error. Director laws and scaling were unchanged, and, as before, the pilot was assumed to share attention equally between the director and speed indicators.

Figure 8 shows that predicted performance with the director display, given improved airspeed resolution, is comparable to that achievable with the advanced display for the Shear 1 environment. Thus, reducing the perceptual threshold on airspeed should substantially improve performance with the flight director.*

Extrapolation

A reliable pilot/vehicle model provides a convenient tool for answering various "what if" questions that may not be readily explored experimentally. In this study we used the model to explore the consequences of providing the pilot with better knowledge of the wind environment. Specifically, the "advanced" display was considered with additional, direct, displays of horizontal and vertical wind assumed. Thresholds relating to perception of wind velocities were neglected, and an integrated display was assumed (i.e., noise/signal ratios remained at -17 dB for all display quantities). The intent here was not to simulate a physically realizable display, but to determine the performance potential associated with improved estimation of the wind environment.

Figure 9 shows that predicted performance with the two displays is nearly identical over most of the approach. Thus, it would appear that little overall improvement in performance can be expected from a display which provides the pilot with improved estimates of the instantaneous wind environment.

This latest result is contingent on the assumption that the pilot does not attempt to estimate the altitude- (hence, time-) varying nature of the shear but attempts only to estimate the current wind vector. It is possible that performance could be improved if the pilot were to attempt to extrapolate the wind--

*As of the writing of this paper, this prediction has not been tested experimentally.

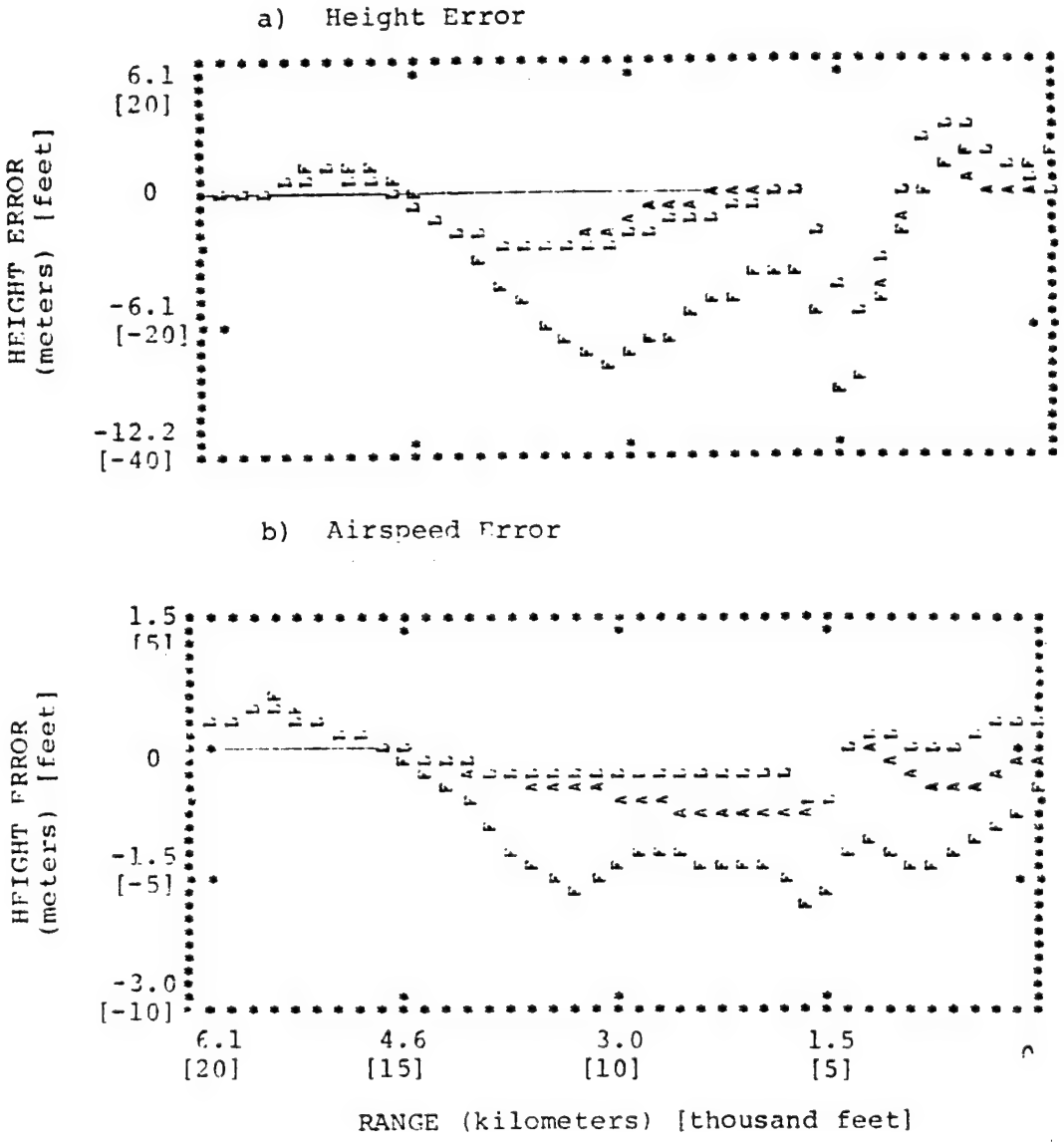

Figure 8. Effect of Reduced Threshold for Perception of Airspeed Error

Shear 1, attitude CWS
A = advanced display, F = flight director,
L = director with lowered perceptual threshold.

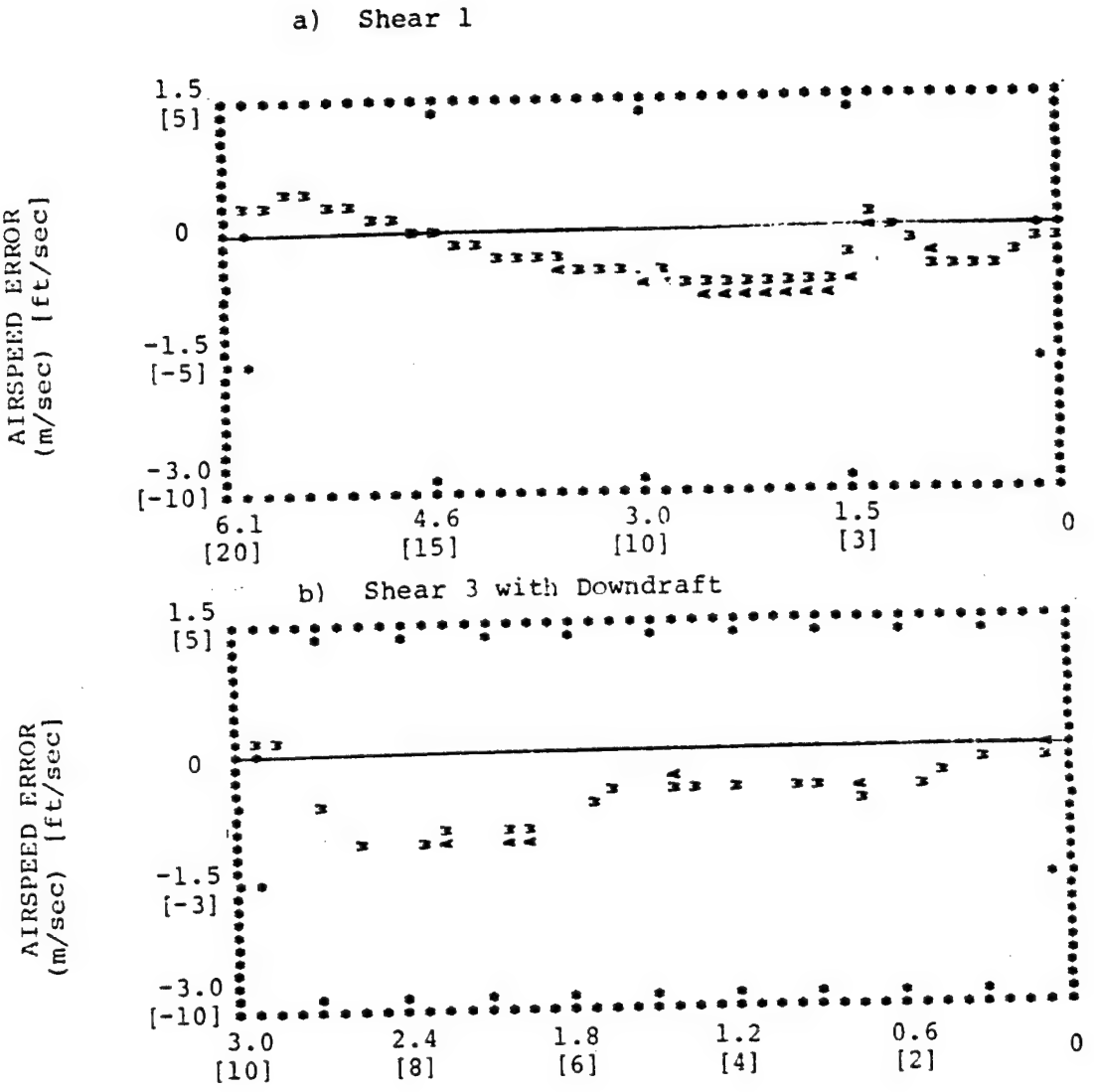

Figure 9. Effect of Explicit Display of Wind on Predicted Mean Height Error

Attitude CWS
A = advanced display, W = additional wind display

especially if the display were augmented to provide such predictive information. The potential for predictive capabilities of both pilot and display is a relevant area for future study.

DISCUSSION

In general, performance trends predicted by the model were confirmed experimentally. Experimental and analytical results both indicated superiority of the "advanced" display with respect to regulation of height and airspeed errors. Velocity steering allowed tighter regulation of height errors, but control parameters had little influence on airspeed regulation. Model analysis indicated that display-related differences could be ascribed to differences in the quality of speed-related information provided by the two displays.

Predictions were most accurate with regard to display-and control-related differences in the total swing of the mean error over the course of the approach, and least accurate with regard to response variability and absolute levels of mean error. Experimental run-to-run variability was from 2 to 3 times as great as predicted for both height and speed errors, [2], and mean errors tended to be less negative (or more positive) than predicted. The relatively large experimental variability may have been, in part, a result of keeping the data base small to prevent the pilot's learning of the shear profile. In addition, there appeared to be a tendency for the pilots to fly high and/or fast on some trials and not on others, a factor that could contribute to predictive inaccuracies.

With regard to future application of the pilot/vehicle model to the study of approach performance in windshears, one might profitably address questions relating both the pilot's conception of the behavior of the wind as well as to the wind information explicitly displayed. For example, one can assume that the pilot knows that the wind will change with altitude (and thus with time) in a smooth manner, and one can explore the consequences of displaying (a) the same variables displayed in this study, (b) additional variables relating to the current wind state, and (c) additional variables relating to the rate-of-change of wind. Furthermore, one can explore the interaction of these factors with the type and severity of shear. Additional factors that can be explored are the relation between performance and workload for candidate controls and displays, as well as the utility of motion cues in detection of windshears.

In conclusion, the model employed in this study has been validated with regard to its ability to predict important performance trends related to controls and displays in windshear environ-

ments. Because of the operational necessity of understanding performance in windshears, we suggest that the pilot/vehicle model be applied further to aid in the design of simulation experiments and to explore a variety of factors that cannot be readily studied in the laboratory. While we cannot guarantee accurate predictions of absolute performance levels at this stage of model development, the model should provide reliable indications of the nature of performance and workload improvements that can be achieved with candidate controls and displays in a variety of windshear environments.

REFERENCES

1. Levison, W. H. and S. Baron, "Analytic and Experimental Evaluation of Display and Control COncepts for a Terminal Configured Vehicle", Report No. 3270, Bolt Beranek and Newman Inc., Cambridge, Mass., July 1976.

2. Levison, W. H.; "Analysis and In-Simulator Evaluation of Display and Control Concepts for a Terminal Configured Vehicle in Final Approach in a Windshear Environment", Report No. 3632, Bolt Beranek and Newman Inc., Cambridge, Mass., August 1977. To be published as NASA CR-3034, 1978.

3. Baron, S. and W. H. Levison, "Analysis and Modelling Human Performance in AAA Tracking", Report No. 2557, Bolt Beranek and Newman Inc., Cambridge, Mass., March 1974.

4. Kleinman, D. L. and W. R. Killingsworth, "A Predicative Pilot Model for STOL Aircraft Landing", NASA CR-2374, March 1974.

5. Kleinman, D. L. and T. Perkins, "Modeling the Human in a Time-Varying Anti-Aircraft Tracking Loop", Trans. of the First NWC Symposium on the Application of Control Theory to Modern Weapons Systems, China Lake, California, June 1973. Also IEEE Trans. on Auto. Control, Vol AC-19, No. 4, pp. 297-306, August 1974.

6. Chalk, C. R., T. P. Neal, T. M. Harris, F. E. Pritchard and R. J. Woodcock, "Background Information and User Guide for MIL-F-8785B(ASG), "Military Specification - Flying Qualities of Piloted Airplanes." AFFDL-TR-69-72, U.S. Air Force, August 1969. (Available from DDC as AD 860 856.)

7. Foxworth, T. G. and H. F. Marthinsen, "Another Look at Landing and Stopping Criteria", AIAA Paper No. 74-956, AIAA 6th Aircraft Design Flight Test and Operations Meeging, Los Angeles, California, August 13-14, 1974.

SESSION H: EYE/HEAD TRACKING AND SCANNING

Chairman: K. Ziedman

TWO DIMENSIONAL EYE TRACKING: SAMPLING RATE OF FORCING FUNCTION

John P. Hornseth, Donald L. Monk, James L. Porterfield
Crew Station Integration Branch
Human Engineering Division
6570 Aerospace Medical Research Laboratory
Wright-Patterson AFB, Ohio 45433

Robert L. McMurry
Systems Research Laboratory
2800 Indian Ripple Road
Dayton, Ohio 45440

INTRODUCTION

This study was conducted to determine the minimum update rate of a forcing function display required for the operator to approximate the tracking performance obtained on a continuous display. Previous studies (see review by Frost, 1972, p. 287) using time on target as a measure of performance, obtained a breakdown in performance around 15 samples per second. In this study, frequency analysis was used to determine whether there was an associated change in the transfer function characteristics of the operator. It was expected that as the forcing function display update rate was reduced, from 120 to 15 samples per second, the operator's response to the high frequency components of the forcing function would show a decrease in gain, an increase in phase lag, and a decrease in coherence.

APPARATUS

The forcing function, in each dimension, consisted of the sum of nine sine waves and simulated a Gaussian noise passed through a second order filter with a roll-off frequency at 1 Hz. The forcing function was generated at rates of 120, 60, 30, or 15 samples per second and presented on the screen at these update rates. An optical projection system consisting of a low power laser and a pair of galvo-mirrors rear projected the forcing function onto a cloth screen in the form of a spot of red light randomly moving in two dimensions about a center spot marked on the screen. The maximum excursion of the forcing function was $\pm 5°$ visual angle in azimuth and elevation, as viewed by the subject (S). The $\pm 5°$ visual angle positions were also marked on the screen and, along with the center spot, served as

calibration points for both the forcing function and S's eye movement response. The subject tracked the forcing function from a position on the opposite side of the screen from the optical projections system and equidistant from the screen.

The subject's eye line-of-sight was computed using the AMRL Honeywell Remote Oculometer. For a complete description of the Oculometer, see Merchant, et. al., 1974. Calibration of the Oculometer prior to each tracking run was accomplished by using a second optical projection system positioned adjacent to the forcing function optical projection system. The movement of the laser spot generated by this second system corresponded to the subject's eye line-of-sight. The Oculometer-driven laser spot was turned off during the tracking run.

Five channels of a seven channel 1/2-inch Ampex 300 instrumentation tape recorder were used to record: (1) time code, (2) horizontal forcing function, (3) vertical forcing function, (4) horizontal eye movements, and (5) vertical eye movements.

PROCEDURE

Four students, two male, two female, from the University of Dayton served as subjects for this study. Each subject tracked the forcing function twice at each sampling rate (eight tracking runs per subject) in a partially balanced design. The data for each subject was collected in two test sessions of four tracking runs each. After seating the subject, the operation of the Oculometer was checked and calibrated. The subject was instructed to sit in a natural, comfortable position. The only constraint placed upon the subject was the instruction to refrain from making large head movement. The subject was instructed to follow (pursue) the moving spot of light with his eyes as the spot moved on the screen. The subjects were screened for uncorrected 20/20 vision. Between runs subjects were given a short rest.

RESULTS

Frequency analyses of the data from the four subjects were accomplished using an IBM 370 Computer and the BMD X92 program. For each run the power spectral density of the forcing function, the power spectral density of the eye response output, the cross power spectral density, the cross correlation, the coherence, and the transfer functions in gain and phase were computed. The data for the two runs for a given sampling rate condition were averaged, for each subject, at each of the nine sine wave component frequencies of the forcing function.

The average transfer function gain, averaged across subjects, for each of the four sampling rates, are presented in Figure 1 (Horizontal) and Figure 3 (Vertical). No differences attributable to sampling rate are present.

The average transfer function phase, averaged across subjects, for each of the four sampling rates, are presented in Figure 2 (Horizontal) and Figure 4 (Vertical). An increase in transport delay of approximately 30 msec was observed at the 15 samples per second update rate for both the horizontal and vertical tracking data.

The coherence data averaged around .98 with a slight drop off at the high frequencies and showed no differences attributable to the sampling rate of the forcing function.

DISCUSSION

The lowest update rate used in this study (15 samples per second) was not low enough to have an appreciable effect upon the transfer function characteristics of the operator. Further research is planned using lower update rates. Expected changes at the high frequency sine waves components of the forcing function not observed in this study may be observed at lower update rates. A time on target analysis of the data is planned to determine whether the results of this study correspond with the results previously reported.

REFERENCES

1. Frost, G., Man-Machine Dynamics. In Vancott, H.P. and Kinkade, P.G. (Eds), Human Engineering Guide to Equipment Design, (Revised Edition), McGraw-Hill, 1972.

2. Merchant, John, Morrissette, Richard, and Porterfield, James L., "Remote Measurement of Eye Direction Allowing Subject Motion Over One Cubic Foot of Space," IEEE Transactions in Biomedical Engineering, Vol BME-21, No. 4, July 1974.

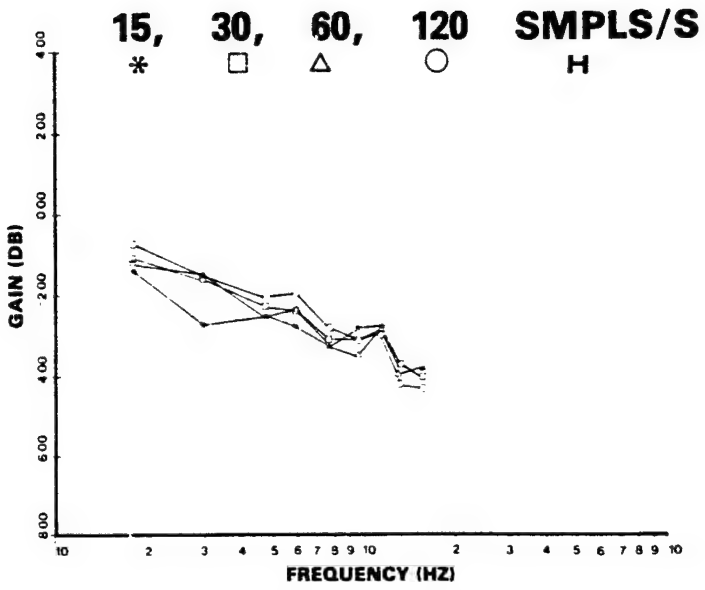

Figure 1. Horizontal Gain as a Function of Update Rates

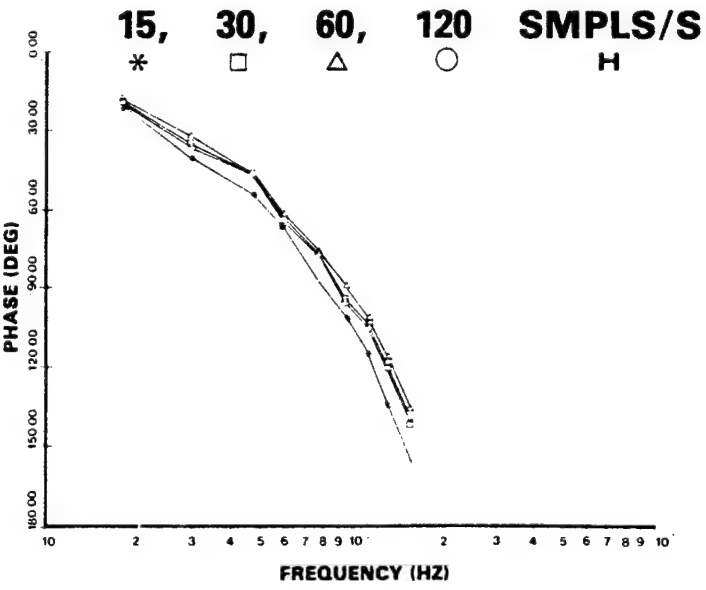

Figure 2. Horizontal Phase as a Function of Update Rates

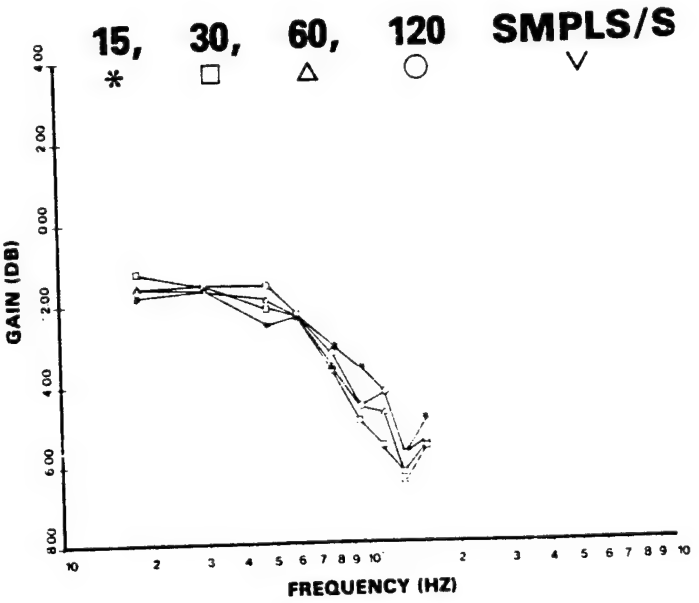

Figure 3. Vertical Gain as a Function of Update Rates

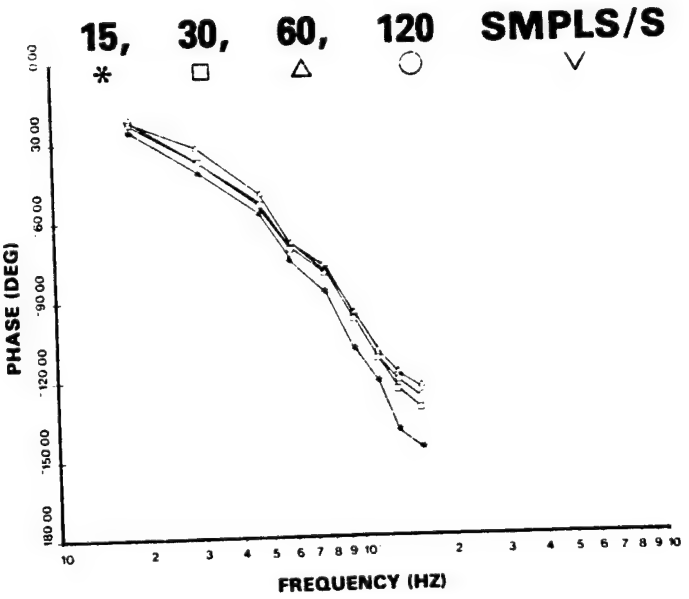

Figure 4. Vertical Phase as a Function of Update Rates

HEAD TRACKING AT LARGE ANGLES FROM THE STRAIGHT AHEAD POSITION

Donald L. Monk, James L. Porterfield, John P. Hornseth
Crew Station Integration Branch
Human Engineering Division
6570 Aerospace Medical Research Laboratory
Wright-Patterson AFB, Ohio 45433

Robert L. McMurry
Systems Research Laboratory
2800 Indian Ripple Road
Dayton, Ohio 45440

INTRODUCTION

The basic purpose of this experiment was to compare head tracking performance at various angles from the straight ahead position. In our previous laboratory studies (e.g. Shirachi and Black, 1975; Hornseth, Stanley, and Carson, 1976; and Shirachi, Monk, and Black, 1976) head tracking was performed within a $\pm$ 15° or less cone about the straight ahead or boresight position. Honeywell has conducted studies in which the subjects aimed their heads as far off boresight as 40° (Hughes, et al, 1970). Their subjects slewed their heads in the direction indicated by an arrow, on the head position display they were using, until a target came into the field of view of the helmet mounted display. At this point their task became that of laying a reticle over the target to achieve lock on. The length of time the subjects were actually tracking was only a few seconds. Flight test studies conducted at Tyndall AFB and China Lake (Dietz et al, 1971 and Grossman, 1974) investigated head tracking performance which included large off-boresight angles. The target motion in these two studies was highly predictable.

One of the big advantages of a helmet sight in a high performance aircraft is its off-boresight capability in aiming a fire control system. However, tracking data using a target that is moving rapidly and randomly for an extended period of time is missing. This study is intended to provide data in this area that will be of value to engineers in designing head control systems.

METHOD

Apparatus:

A PDP 11/34 minicomputer with floating point hardware was used to generate the forcing function, digitize and record 4 analog data channels (azimuth and elevation of both the target and head motion), and perform some data analyses. A Honeywell helmet mounted sight (HMS) was used to sense the subject's head angles as he tracked the target. This helmet system weighed 1.65 kg. A Hughes, side mounted, helmet display was used to present the moving target and head position reticle to the subject's right eye. This helmet mounted display weighed .54 kg. An IMLAC PDS-4 computer graphics display generated the target and reticle symbology using the forcing function and the head position signals to position the target symbol relative to the reticle. An Ampex FR-1300 instrumentation tape recorder was used to record the subjects' responses, the forcing function, and a time code. An IBM 370/155 was used for data analysis and plotting.

The forcing function was updated at a 90 Hz rate. The HMS provided head azimuth and elevation angles at a 30 Hz rate. The IMLAC was "free running" at approximately a 1000 Hz refresh rate.

Forcing Function:

The forcing functions were generated from a sum of sine waves with the amplitudes scaled to simulate white noise passed through a second order filter with a break frequency of 0.7 Hz. More information on the forcing function can be found in Appendix A. The phase relationships between the sine waves were randomly varied from subject to subject but remained constant across a given subject's conditions. Pilot study data indicated that there was negligible learning across 6 runs with the same forcing function.

Procedure:

Each subject performed the head tracking under 6 head position conditions. The following mean azimuth and elevation angular positions were used:

0°, 0° (center-center); 0°, +30° (center-up); 0°, -30° (center-down); -45°, 0° (left-center); -45°, +30° (left-up); and -45°, -30° (left-down). Because of symmetry of the left-right neck muscles and pilot study data, only the left hemisphere of head motion was investigated. Performance at angles further off-center were not selected for examination because pilot study data suggested that the limits of head and neck motion may be exceeded at larger angles for some subjects. Other supporting data give the average limit of male neck movement for up flexion at 61° with S.D. of 27° down

flexion at 60° with S.D. of 12°, and left or right rotation at 79° with S.D. of 14° (Van Cott and Kinkade, 1972). The maximum excursion of the target from each of the 6 head positions was ±10°. This small excursion was used to increase the probability the target would remain on the subjects' display at all times and not require the subject to search for it. Also, the small target excursions constrained the subjects to track at various mean angular positions within the head motion envelope to provide an adequate representation of head tracking at the specified off-center positions.

Each tracking run was 100 seconds long. The first 9 seconds of tracking were not scored to allow the subject to overcome the initial "start up" error induced by the target suddenly jumping to a random starting position and beginning to move. The following 91 seconds of tracking data were recorded and scored. At the end of each run a rest period of 1 minute was given. After each group of 3 runs, the rest period was extended to 5 minutes. The first 6 runs were practice runs, allowing for the subjects to adjust to head tracking at each angular position. All practice runs were presented to each subject in the same order. The data runs were presented in a randomized order to reduce any possible ordering effects. All subjects' scores asymptoted to an acceptable level of performance during the practice runs.

Subjects:

Fourteen male subjects were used with ages ranging from 16-40. Eye dominance was tested for each subject with about half reporting right eye dominance. The subjects' instructions are given in Appendix B.

RESULTS & DISCUSSION

A subject's performance scores were computed from his radial error data. Radial error is the visual angle from a subject's line of sight to the target at each instant in time. The Duncan's New Multiple Range Test (NMRT) was used to test for statistical differences in performance at the 6 head angle positions. Table 1 shows the 3 homogenous subsets of head positions found using the 50% circular error probability (CEP) metric (a 50% CEP refers to that radius, about the target, within which the subject tracked 50% of the time). The best performances (lowest CEP), denoted by the A subset, was found when the head faced center-center, left-center, and left-down. The next best performance, the B subset, was obtained when the head faced center-center, left-up, left-down, and center-up. The worst performance, subset C, was found when the head faced center-down, center-up, and left-up. It should be noted that the differences between the best position (-45°, 00°) and the worst position (00°, -30°) is small, .15° or 6%. While this difference is statistically significant, it is left up to the designers/engineers to determine if the difference is of practical significance.

Establishment of on target gate rings were done as an analysis procedure after data collection. However, during the experimental runs, the subjects were not required to keep the target within a gate ring, nor were they shown any rings. In analyzing the data, a subject was considered on target if his radial error was less than a specified tolerance. Six on target tolerance rings were used in analyzing the data collected in this experiment. They ranged from 1° to 6°, in 1° increments. Gate times were computed for each tolerance ring. Gate time was defined to be the amount of time a subject kept the target inside the ring. As soon as the target was outside the ring, that gate time ended. If the target was again inside the ring, another gate time was started. To reduce "noise" effects in this gate time measure, an arbitrary dead time zone of .1 seconds was used. This meant that not only must the target be within the ring to start a gate, it must also be within for .1 second. Likewise, it must be outside of the ring for .1 second to end the gate. The mean gate times for each ring, averaged over all positions, are shown in figure 1. Using the Duncan's test, the gate time metric did not prove to be a sensitive measure for distinquishing among the angular positions (Tables 2-7). For all of the tolerance rings, except the 4° ring, performance at the 6 head positions did not differ significantly from each other. The 4° ring indicated that the longest gate times were obtained at all positions except left-up and center-down. The next subset included all positions except left-center.

The time on target (TOT) scores, for each tolerance ring, were computed by multiplying the mean gate times by the number of times the target stayed within the ring. The mean TOTs for each ring, averaged across all positions, is shown in figure 2. The Duncan's test was applied to each of the 6 rings to determine homogenous subsets. As shown in Table 8 for the 1° tolerance band, there are no significant differences among any of the 6 angular positions. As the task becomes easier, by increasing the tolerance ring to 2°, the Duncan's test indicates that 3 homogenous subsets exist. As with the CEP metric, the TOT with a 2° ring has the best scores at the center-center, left-center, and left-down (Table 9). Next best scores are center-center, left-up and down, and center-up. The worst scores are center-center, left-up, and center-up and down. Increasing the ring size to 3°, there are still 3 homogenous subsets (Table 10). The best and second best scores remain the same, while the worst score is found to be the center-down position. With the rings at 4° and 5°, only 2 homogenous subsets are found (Tables 11 and 12). The best scores are the same positions as those in the 2° and 3° rings. The second best positions are also the same as in the 2° and 3° ring plus the center-down position is included in this subset. The 6° tolerance ring, the easiest task, also has 3 homogenous subsets (Table 13). The best positions were found to include all positions except center-down, while the next best included all positions except left-center. For this condition, both significantly different subsets have almost merged into a single subset.

A two way analysis of variance was used to test for significances in RMS error scores. No significant difference was found between azimuth versus elevation RMS errors (Table 14). Significance at the p = .001 level was found between the 6 angular positions. The head position by azimuth-elevation dimension interaction was also found to be significant at p = .001 level.

A Duncan's test was performed to compare RMS error scores between the 6 angular positions for both azimuth and elevation. Two homogenous subsets were found with the azimuth scores (Table 15). The best performance was the center-center and all left positions. With the elevation RMS error scores, 3 homogenous subsets were found, but with a different grouping than the other metrics have found (Table 16). The best performance was at left-center, left-down, and center-down. This was the only time that the center-down position was in the best performance grouping when multiple groups were found. The next subset contained the left-down, center, center-up, and center-down conditions. The worst position was the left-up position.

CONCLUSIONS

The 3 primary metrics, CEP, TOT, and gate times, all emphasize a different aspect of tracking performance, but they are not independent of each other. Thus, it is not surprising that the Duncan's test should generally designate the same position subsets. In almost all the tests, the best position was the left-center, followed by the center-center and left-down positions. Again, it should be emphasized that all of the differences found were small but statistically significant. However, they may or may not be practically significant. The helmet mounted sight and helmet mounted display used for this experiment were early prototypes. The later models of each unit are lighter and have a much improved center of gravity. Both of these factors may eliminate even the statistical significant differences among the positions within the envelope $\pm 45^{\circ}$ azimuth and $\pm 30^{\circ}$ elevation.

APPENDIX A

The sum of sine wave input was chosen such that it simulated white noise passed through the second order system $\left(\frac{A}{S+A}\right)^2$. Eleven sine frequencies, for azimuth were selected on the basis of being equal spaced between 0.10 Hz and 2.00 Hz on a $\log_{10}$ scale. For elevation, the 11 sine frequencies were also spaced equally on a $\log_{10}$ scale with the frequencies being midway between the azimuth frequencies. Their frequencies ranged from 0.12 Hz to 2.32 Hz. An additional requirement placed upon frequency selection was that the resultant input must complete a full cycle at the run's end. Thus, all frequencies must be a harmonic of the fundamental frequency. For this experiment, the fundamental frequency, f_o = $\frac{1}{91.02 \text{ seconds}}$ = .01099 Hz.

APPENDIX B

Subject Instructions: "Your task in this experiment will be to head track a rapidly moving target. In the head mounted display, located in front of your right eye, you will notice a reticle at the center of the display. This reticle will always remain at the center of the display as you move your head. Please move your head around a little so that you can see which of the two objects is actually the reticle. The object that moves around on the display, as you move your head, is the target. During the test runs, the target will move around in a rapid, random pattern. Your task will be to move your head so as to keep the center of the reticle as near the center of the target as you can. The test runs will last 90 seconds. After each test run, you will be given a 1 minute rest period before the next run. Please remain seated during these short rest periods. Each test run will require you to track the target with your head aimed in a different direction. You will first be given some practice in tracking at each of the 6 head positions used in the experiment. Then you will be given the experimental runs. After each group of 3 runs you will be allowed to get up out of the chair to stretch and walk around. If at any time you have any questions about what you are to do, be sure to ask for additional instructions or clarifications. Do you have any questions at this time?"

REFERENCES

Dietz, F. and Wise, J., "Evaluation of the Helmet Mounted Sight" (Title Unclassified, Confidential Report) ADC/ADWC, Project 69-19, December 1971.

Grossman, J., "Flight Evaluation of Pilot Sighting Accuracy Using a Helmet-Mounted Sight, "NWC TP5638, Naval Weapons Center, China Lake, California, April 1974.

Hornseth, J., Stanley, G., and Carson, P., "Head Tracking: A Fatigue Study," NASA TMX-73 170, Twelfth Annual Conference on Manual Control, Ames Research Center, Moffett Field, California, May 1976.

Hughes, J., Henke, A., and Schultz, R., "Helmet Mounted Sight/Display Applications," AFFDL-TR-69-118. Air Force Flight Dynamics Laboratory, Wright-Patterson AFB, OH, April 1970.

Shirachi, D., and Black, J., "Head-Eye Tracking in Two-Dimensional Pursuit Tasks," NASA TMX-62-464, Ames Research Center, Moffett Field, California, May 1975.

Shirachi, D., Monk, D., and Black, J., "Effects of Headgear and Visual Angle on Head Rotation Spectral Characteristics," NASA TMX-73-170, Ames Research Center, Moffett Field, California, May 1976.

Van Cott, H., Kinkade, G., Editors; Human Engineering Guide to Equipment Design", Superintendent of Documents, U. S. Government Printing Office, Washington, D.C., 20402, 1972.

FIGURES AND TABLES

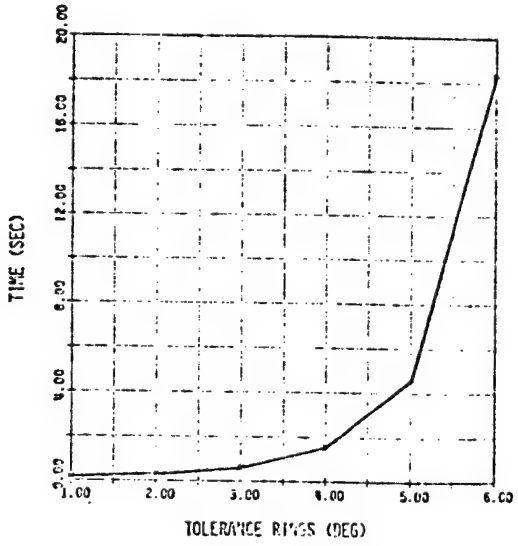

FIGURE 1

MEAN GATE TIMES FOR EACH GATE TOLERANCE RING, AVERAGED ACROSS ALL HEAD POSITIONS

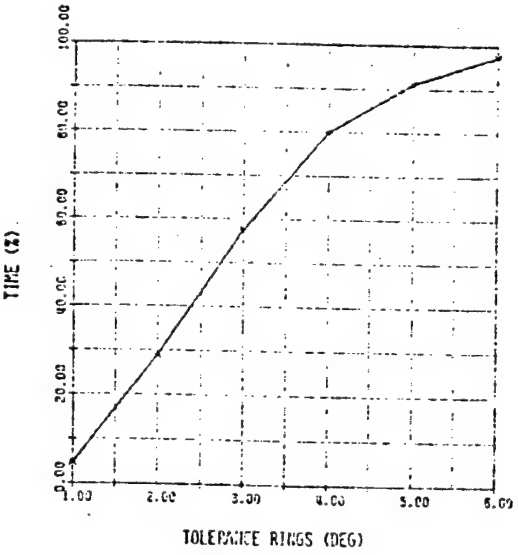

FIGURE 2

MEAN TIME ON TARGET FOR EACH TOLERANCE RING, AVERAGED ACROSS ALL HEAD POSITIONS

TABLE 1

DUNCAN'S NMRT FOR THE MEAN CEP SCORES AT THE 6 HEAD POSITIONS

CEP (DEGREES)		
EL (DEG)	AZ (DEG)	
	-45	0
+30	2.60 BC*	2.61 BC
0	2.51 A	2.55 AB
-30	2.57 AB	2.66 C

TABLE 2

DUNCAN'S NMRT RESULTS FOR THE 1° GATE TIME SCORES AT THE 6 HEAD ANGLE POSITIONS

1° GATE TIMES (SEC)		
EL (DEG)	AZ (DEG)	
	-45	0
+30	0.15 A	0.16 A
0	0.16 A	0.15 A
-30	0.16 A	0.15 A

TABLE 3

DUNCAN'S NMRT RESULTS FOR THE 2° GATE TIME SCORES AT THE 6 HEAD ANGLE POSITIONS

2° GATE TIMES (SEC)		
EL (DEG)	AZ (DEG)	
	-45	0
+30	0.28 A	0.28 A
0	0.29 A	0.28 A
-30	0.29 A	0.28 A

TABLE 4

DUNCAN'S NMRT RESULTS FOR THE 3° GATE TIME SCORES AT THE 6 HEAD ANGLE POSITIONS

3° GATE TIMES (SEC)		
EL (DEG)	AZ (DEG)	
	-45	0
+30	0.60 A	0.59 A
0	0.64 A	0.62 A
-30	0.62 A	0.58 A

* For all Duncan's NMRT tables in this report, letters represent homogenous subsets. The mean performance scores contained in a subset do not differ significantly from other means contained in that subset. The means not contained in the same subset are significantly different at the p = .05 level. A given mean can belong to more than one subset.

TABLE 5
DUNCAN'S NMRT RESULTS FOR THE
4° GATE TIME SCORES AT THE
6 HEAD ANGLE POSITIONS

4° GATE TIMES (SEC)		
EL (DEG)	AZ (DEG)	
	-45	0
+30	1.44 B	1.52 AB
0	1.85 A	1.57 AB
-30	1.59 AB	1.33 B

TABLE 6
DUNCAN'S NMRT RESULTS FOR THE
5° GATE TIME SCORES AT THE
6 HEAD ANGLE POSITIONS

5° GATE TIMES (SEC)		
EL (DEG)	AZ (DEG)	
	-45	0
+30	4.54 A	4.62 A
0	5.12 A	4.59 A
-30	4.42 A	4.13 A

TABLE 7
DUNCAN'S NMRT RESULTS FOR THE
6° GATE TIME SCORES AT THE
6 HEAD ANGLE POSITIONS

6° GATE TIMES (SEC)		
EL (DEG)	AZ (DEG)	
	-45	0
+30	17.2 A	19.2 A
0	20.0 A	20.3 A
-30	19.5 A	13.6 A

TABLE 8
DUNCAN'S NMRT RESULTS FOR THE
1° TIME ON TARGET SCORES AT
THE 6 HEAD ANGLE POSITIONS

1° TOT (%)		
EL (DEG)	AZ (DEG)	
	-45	0
+30	4.52 A	4.56 A
0	5.15 A	4.73 A
-30	5.22 A	4.66 A

TABLE 9
DUNCAN'S NMRT RESULTS FOR THE 2° TIME ON TARGET SCORES AT THE 6 HEAD ANGLE POSITIONS

2° TOT (%)		
EL (DEG)	AZ (DEG)	
	-45	0
+30	28.2 BC	28.4 BC
0	30.7 A	29.3 ABC
-30	29.6 AB	27.4 C

TABLE 10
DUNCAN'S NMRT RESULTS FOR THE 3° TIME ON TARGET SCORES AT THE 6 HEAD ANGLE POSITIONS

3° TOT (%)		
EL (DEG)	AZ (DEG)	
	-45	0
+30	57.4 B	56.8 B
0	60.3 A	58.7 AB
-30	58.3 AB	55.7 C

TABLE 11
DUNCAN'S NMRT RESULTS FOR THE 4° TIME ON TARGET SCORES AT THE 6 HEAD ANGLE POSITIONS

4° TOT (%)		
EL (DEG)	AZ (DEG)	
	-45	0
+30	79.2 B	78.2 B
0	82.0 A	80.5 AB
-30	79.9 AB	78.3 B

TABLE 12
DUNCAN'S NMRT RESULTS FOR THE 5° TIME ON TARGET SCORES AT THE 6 HEAD ANGLE POSITIONS

5° TOT (%)		
EL (DEG)	AZ (DEG)	
	-45	0
+30	91.5 B	91.7 B
0	93.6 A	92.5 AB
-30	92.2 AB	91.0 B

TABLE 13

DUNCAN'S NMRT RESULTS FOR THE 6° TIME ON TARGET SCORES AT THE 6 HEAD ANGLE POSITIONS

6° TOT (%)		
EL (DEG)	AZ (DEG)	
	-45	0
+30	97.2 AB	97.4 AB
0	98.2 A	97.7 AB
-30	97.7 AB	96.9 B

TABLE 14

ANALYSIS OF VARIANCE TABLE OF RMS ERROR

Source of Variation	DF	Sum of Squares	Mean Square	F	P
A (AZ-EL Dimension)	1	.17	.17	4.53	>.05
B (Angular Positions)	5	.46	.09	5.01	<.001
C (Subject)	13	7.16	.55	65.82	
A X B	5	.27	.05	6.42	<.001
A X C	13	.50	.04	4.56	
B X C	65	1.19	.02	2.19	
A X B X C	65	.54	.01		
Total	167	10.30			

TABLE 15

DUNCAN'S NMRT RESULTS FOR THE AZIMUTH RMS ERROR SCORES AT THE 6 HEAD ANGLE POSITIONS

AZ RMS E (DEG)		
EL (DEG)	AZ (DEG)	
	-45	0
+30	2.23 AB	2.25 B
0	2.15 A	2.15 A
-30	2.23 AB	2.31 B

TABLE 16

DUNCAN'S NMRT RESULTS FOR THE ELEVATION RMS ERROR SCORES AT THE 6 HEAD ANGLE POSITIONS

EL RMS E (DEG)		
EL (DEG)	AZ (DEG)	
	-45	0
+30	2.29 C	2.20 B
0	2.05 A	2.16 B
-30	2.11 AB	2.13 AB

N79-15619

LIGHTWEIGHT HELMET-MOUNTED EYE MOVEMENT MEASUREMENT SYSTEM

John A. Barnes

US Army Human Engineering Laboratory
Aberdeen Proving Ground, Maryland

We first realized the need for a simple, easy to use, lightweight device to determine the aircrewman's fixation points and paths of eye movement between fixation points when we performed our initial eye movement measurement work. We used a Mackworth EMC-2 device, figure 1, to determine a helicopter pilot's visual work load during actual flight.

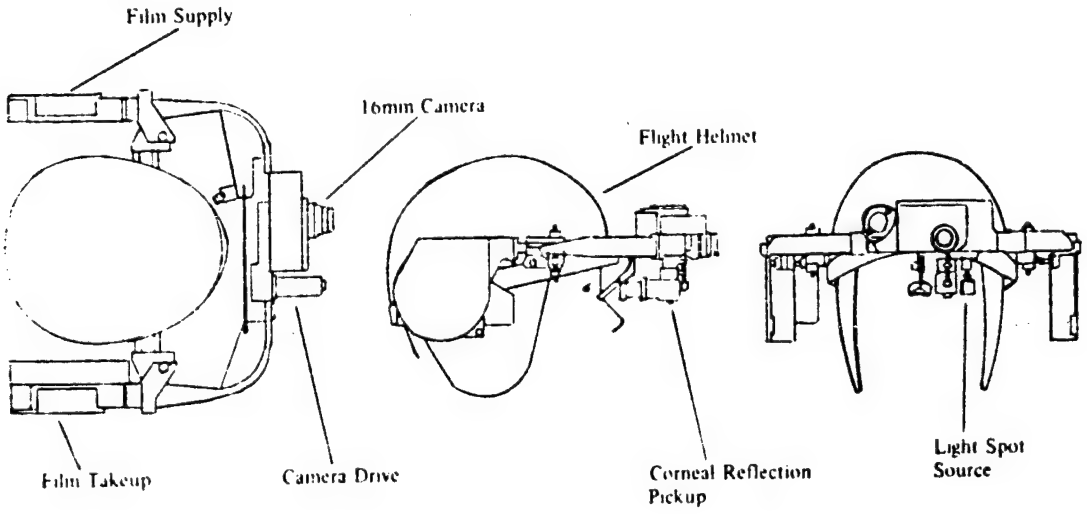

Figure 1. EMC-2 Eye-Movement Camera

The development of the present system has been a "spare-time" project since 1971. The components have been procured whenever funds were available or a particular project required their use. The interface components were constructed by our shop personnel during slack periods in their work schedules. There are no custom designed components in the present system; every item is, or is made up from commercially available components.

The helmet we used is the type that preceded the present US Army aviators' helmet. It has been modified slightly; a small amount of material has been removed from immediately above the brow to accommodate the camera case, the visor has been removed and the suspension system has been replaced with a removable, subject-fitted, molded plastic foam inner helmet similar to the one used in the USAF HCU-2 flight helmet. The fitted helmet

stabilizes the optical head and helps to keep the system in calibration during use. The helmet-mounted eye movement measuring system, figure 2, weighs 1,530 grams; the weight of the present aviators' helmet in standard form with the visor is 1,545 grams.

Front view of the system.

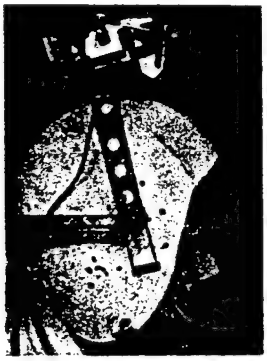

System in the stowed position.

Figure 2. Lightweight Helmet-Mounted Eye Movement Measurement System

The optical head is a standard NAC Eye-Mark. This optical head was mounted on a magnesium yoke which in turn was attached to a slide cam mounted on the flight helmet. The slide cam allows one to adjust the eye-to-optics system distance quite easily and to secure it so that the system will remain in calibration. The design of the yoke and slide cam is such that the subject can, in an emergency, move the optical head forward and upward to the stowed and locked position atop the helmet. This feature was necessary for flight safety.

The television camera that is used in the system is a solid state General Electric TN-2000 with a charged induced device (CID) imager used as the vidicon. This particular device has 45,000 cells which form the video picture. The charged coupled device (CCD) solid state imagers are also available but the CID imagers have an advantage in that they do not "bloom" as badly when they are struck by a bright light. Fairchild now offers a CCD imager which contains 185,440 cells and produces a more detailed video picture; this was not available when our system was assembled. The CID imager is mounted on the NAC optical head in place of the standard fiber optics. The camera electronic package which measures 7½ x 2 x 4 inches and weighs less than two pounds is placed in the pocket of a vest worn by the subject. The imager and electronic package are connected by a very thin ribbon cable which is 42 inches long.

The output of the system can be sent to the video monitor and recorder by direct wire or by the use of video transmitter. It can be transmitted over a range of 3,000 feet. The video transmitter measures 7½ x 3 x 3¼ inches and weighs 1½ pounds; it can be placed in another pocket of the subject's vest.

All components of this system operate on 12 volts or less. The power can be supplied from a belt-type battery pack or can be taken from the vehicle electrical system; the total power requirement for the subject mounted equipment is less than three amperes.

A coupling lens is required to match the optical output from the NAC optical head to the CID imager. The design of the lens used determines the distance between the optical head and the CID imager.

For applications where the helmet is not necessary, the system's video components can be used with the standard EYE-MARK face mask mount. For our own laboratory use we have replaced the snap fasteners of the face mask mount with VELCRO for easier and faster adjustments.

This system is not without its difficulties; the video presentation is not as precise as a film rendition of the same scene but the instant feedback is worth the degradation of the presentation. For most purposes little or no information is lost by using the video recordings. When the system is used to investigate visual behavior where the fixation points will be at distances greater than 100 meters, there is an inherent problem in the EYE-MARK. The light marker that indicates the subject's fixation point is a fixed size, .5 mm, and as the scene lens presents an increased scene area this fixed mark increases in size relative to the rest of the presentation. We have had limited success in decreasing the size of the light marker by reducing the size of its aperture. This also decreases the marker's brightness and it will no longer be visible on the scene presentation. The minimum aperture size that we have been able to use is .11 inches (normal is .16), this reduces the light marker size by about one-third. One further problem that might bother some is that the video presentation is a mirror image of the real world, the fiber optics systems contains a mirror which is not used with this video system. We rectify this by placing a front surface mirror at some comfortable angle in front of the monitor and view the video picture from a position above and behind the monitor.

The Fiscal Year 1977 cost to the Government for the system components was:

NAC EYE-MARK Optical Head	$ 3,420.00
GE TN-2000 CID Video Camera	2,925.00
Sony AV-3400 Video Recorder	888.75
Sony CVM-115 Monitor/Receiver	252.00
VM-2200 Video Transmitter 15 mw	1,584.00
Coupling Lens	400.00

The "off-of-the-shelf" cost of the complete system was $9,469.75. This cost does not reflect the cost of interfacing these components into a system; this will vary with the user's support resources but should not exceed $500.00.

We have field tested the system to check its performance with the performance specifications given by NAC for the optical head. The subject's

head was fixed in position so that all recorded movement was pure eye movement and the recorded errors were from eye movement only. The targets were set at a distance of 100 meters from the subject and extended in an arc of 11^{o} either side of the center target. The NAC specifications indicated a maximum error of 2^{o} of arc at 10^{o} either side of the center position; this is 3.5 meters error at 100 meters range. We measured 3.6 meters at 10^{o} on a smoothed curve of the 42 data points recorded. We have found in our work that a 3^{o} eye movement will be tolerated before the head is moved, thus with this system for 3^{o} of eye movement we have an error of 1 meter at 100 meters range, 10 cm at 10 meters range and 1 cm at 1 meter range.

The listing of trade name products in this article is not to be taken as an indorsement of these products. They were the products that were available at the time of procurement which met our requirement that all elements of the system operated on 12 volts DC. They were the least costly items that met that requirement and that were compatible with, or could easily be made compatible with, the other elements of the system.

SESSION I: MOTION SIMULATION AND EFFECTS

Chairman: R. Stapleford

THE EFFECTS OF CLOSED LOOP TRACKING ON A SUBJECTIVE TILT THRESHOLD IN THE ROLL AXIS

By Marvin Roark* and Andrew [illegible]**

*Systems Research Laboratories, Inc.
Dayton, Ohio 45440

**Aerospace Medical Research Laboratory
Wright-Patterson Air Force Base, Ohio 45433

SUMMARY

The indifference thresholds for the perception of tilt in the roll axis were experimentally determined in a moving base simulator under three tracking task difficulties. The threshold level determined in this experiment is approximately 5 to 7 degrees (.1g).

INTRODUCTION

In ground based simulators, unlike aircraft, false tilt cues may occur when they are rolled. The amount of tilt which can be detected by the pilot in the simulator, defined as the indifference threshold, appears to be a function of the task being performed. To eliminate the false tilt cues that occur when the indifference threshold is exceeded, washout schemes are used to limit the motions of the simulator. This is often accomplished by limiting the amount of roll of the simulator while still allowing the acceleration and other helpful cues to be felt by the pilot. In the past the washouts used were based on what felt good to the pilot in the simulator. Very little data is available relative to what this threshold is, see reference 1, and what factors, if any, alter the level of indifference. Data in the past has dealt with determining the absolute threshold. One set of data, see reference 2, does show that the "absolute" threshold increases when workload is increased. This prompted an investigation to determine the effect of workload on the indifference threshold level for use in washouts and in motion related parameters of pilot modeling.

An experiment was performed to determine the indifference threshold and the interactive effect of the tracking task on the threshold value. This experiment and associated results are presented in this paper.

METHOD

The basic idea behind the experiment was to have a subject track a closed loop disturbance nulling task and then superimpose a random appearing ramp (tilt input) to the motion loop of the simulator. Figure 1 is a block diagram

of the motion and visual systems used in the experiment showing the location of the disturbance input and the tilt input to the motion plant in the system. The only input was the disturbance input so the display was the negative of the simulated plant position. When the subject could detect the tilt input, he was to indicate the direction of the tilt via a hand-held indicator containing a left and a right thumb actuated pushbutton. The subject was instructed to hold the pushburton down until he no longer felt that he was tilted. The time histories of the chair position, the tilt input and the hand-held indicator signals were recorded and later analyzed.

The experiment was run on the Roll Axis Tracking Simulator (RATS) at the Aerospace Medical Research Laboratory at Wright-Patterson Air Force Base. The RATS is capable of simulating the roll dynamics of a high performance aircraft, in this case, an F-16. The plant dynamics are described by equation 1 with limits of 180°/sec and 400°/sec^2. The cab contains a CRT mounted at the axis of rotation which is through the head of the subject. The subject viewed the display shown in figure 2 which was 26 inches away. The subject used a force stick mounted on the right side of the cab to control the tracking task. To prevent the subject from experiencing any external cues, a shroud inclosed the cab, white noise was injected in the helmet and the room lights were extinguished. In addition, a harness was used to keep the subject in his seat while the cab was in motion.

Three sum of sine inputs, simulating white noise passed through a low-pass filter with a double pole at 2 radians, were used with RMS values of .933, 1.40, and .467 pounds which resulted in 14, 21, and 7 degrees/second root mean squared (RMS) variance in the visual error. A group of ten subjects were exposed to the inputs in the order mentioned above. They ran 4 runs a day for 3 days, with each run lasting 165 seconds. The subjects had been trained from a previous experiment, therefore, minimum training was required. Data from the last two days was used for subsequent analysis. An example of a data run can be seen in figure 3. The top trace is a time history of the negative visual error (simulated plant position) seen by the subject. The negative of the visual error is shown so that it can easily be compared to the actual motion plant seen in trace 3. This was the tracking task he was trying to null out by keeping the wings on the display level with the dashed reference line. The second trace shows the offset signal that was added to the cab position. The resulting cab position during the tracking task is shown in trace 3. A run consisted of from zero to four of the offset signals to maximize randomness between runs. The offset signal itself occurred at a rate of 1°/sec with limits of ±20 degrees. The 1°/sec value was chosen because it is below the roll velocity threshold of 2°/sec, see reference 1. The last graph is the output of the hand-held indicator the subject used to indicate when the tilt was felt.

In addition to the tracking data taken, a set of baseline data for each subject was recorded. This data provides a baseline indifference threshold, comparable to the absolute threshold data taken in previous experiments. The subject was asked to sit quietly in the cab while the cab was tilted, using the same tilt input described earlier. The subject was to indicate the direction of tilt as he did before. The tracking task was not present and the

display remained fixed on the screen.

RESULTS

The results are shown in figures 4 through 7 and summarized in figure 8. For each group, the offset angle, at the point when the indicator button was pressed was recorded and placed in groups of half degree increments. The number of points recorded in each half degree group was then plotted in histogram form with the mean and standard deviation shown for each group. The mean values for the indifference threshold increases with the difficulty of the task. Fewer data points were needed for the baseline data due to the smaller amount of variance across subjects.

The summary shows a baseline level of 3.48° (.06g) which jumps to 6.46° (.113g) with the least difficult task and 7.56° (.132g) with the most difficult. These results are discussed in the following section.

DISCUSSION

From the baseline data, the indifference threshold level is 3.48° (.06g). This value can be compared to data taken from other experiments where the absolute threshold was determined but, the results from this experiment are 3 to 30 times higher, see reference 1. This is due to the conditions under which the experiment was run. These conditions added extra loading to the subjects tilt detection, similar to the kind of loading he would receive when running in a simulator. Under these "real world" conditions, the simulator environment, a useful measurement of the indifference threshold is made and can be directly applied to washout designs and used in pilot modeling.

Figures 5 through 7 show the results when tracking tasks of varying difficulties are added to the baseline conditions. The results of all four conditions, summarized in figure 8, contained the type of trend as expected, see reference 2. The summary shows a sharp jump from the baseline to the least difficult of the three tracking tasks and then increasing threshold levels with the difficulty of the task. The various difficulties were obtained by increasing the tasks RMS value which had the effect of changing the signal to noise ratio of the system. This change accounts for part of the increase in the threshold levels as well as the increase in the variance of the data. The relatively large jump from the baseline is due to the initial loading of the subject by the tracking task.

CONCLUSIONS

In this paper, an experiment to investigate the effects of the tracking task workload on the indifference threshold is described. Based on the results and the discussion, the following conclusions can be drawn.

1) The indifference threshold increases with task loading.

2) The tilt indifference threshold while performing a tracking task is approximately .1g.

REFERENCES

1. Zacharias, G.: Motion Cue Models for Pilot-Vehicle Analysis. Technical Memorandum, Bolt Beranek and Newman Inc., Cambridge, Mass., under Contract No. F33615-77-C-0506, September 1977.

2. Hosman, R.J.A.W., van der Vaant, J.C.: Thresholds of Motion Perception Measured in a Flight Simulator. Proc. of the Twelfth Annual Conference on Manual Control, Ames Research Center, Moffett Field, California, May 1976.

3. Peters, R.A.: Dynamics of the Vestibular System and Their Relation to Motion Perception, Spatial Disorientation and Illusions, NASA CR-1303, 1969.

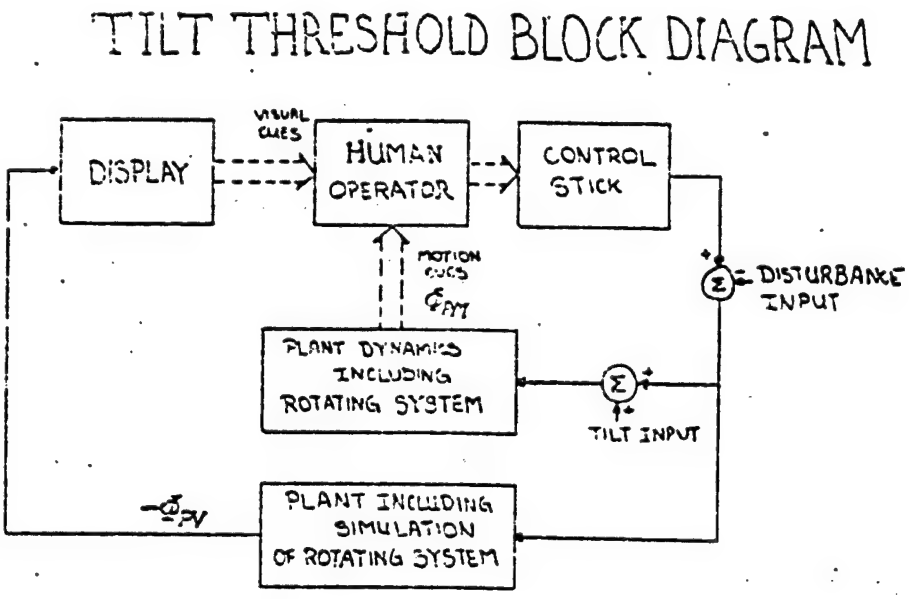

Fig. 1. Experimental Block Diagram

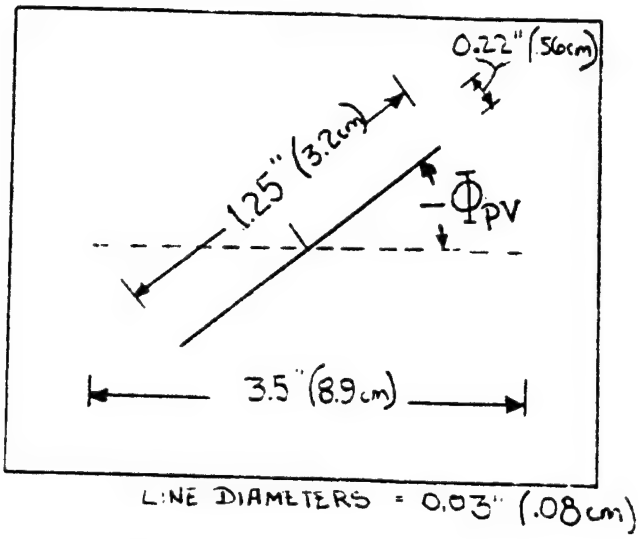

Fig. 2. Visual Display

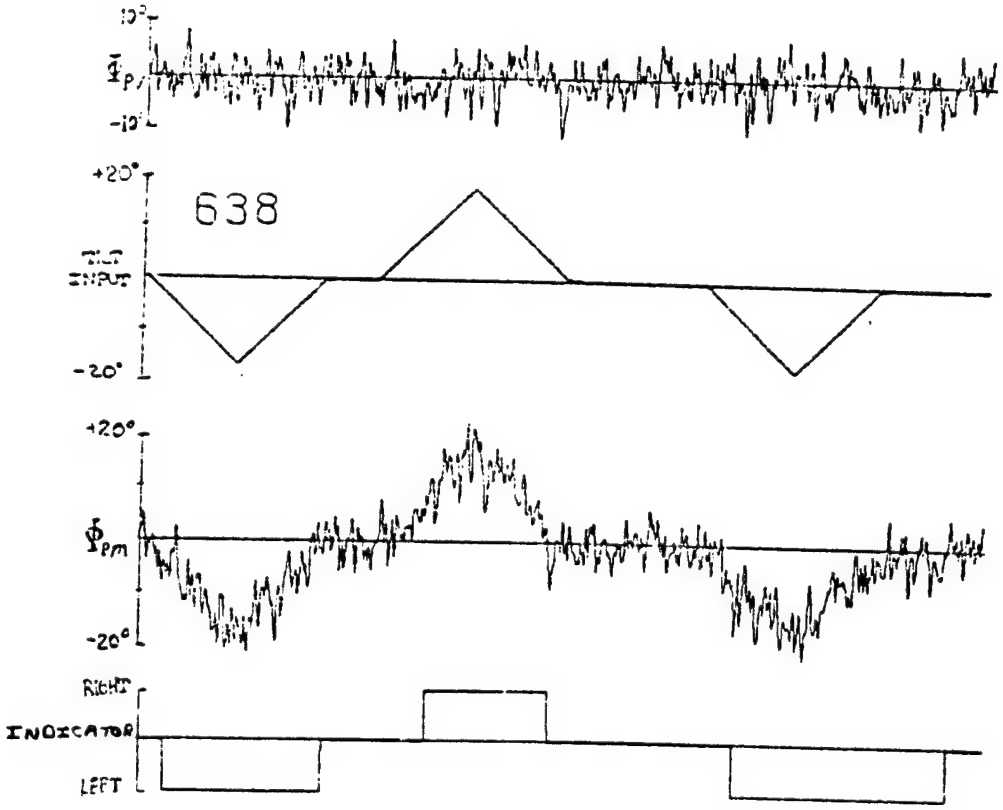

Fig. 3. Sample Data

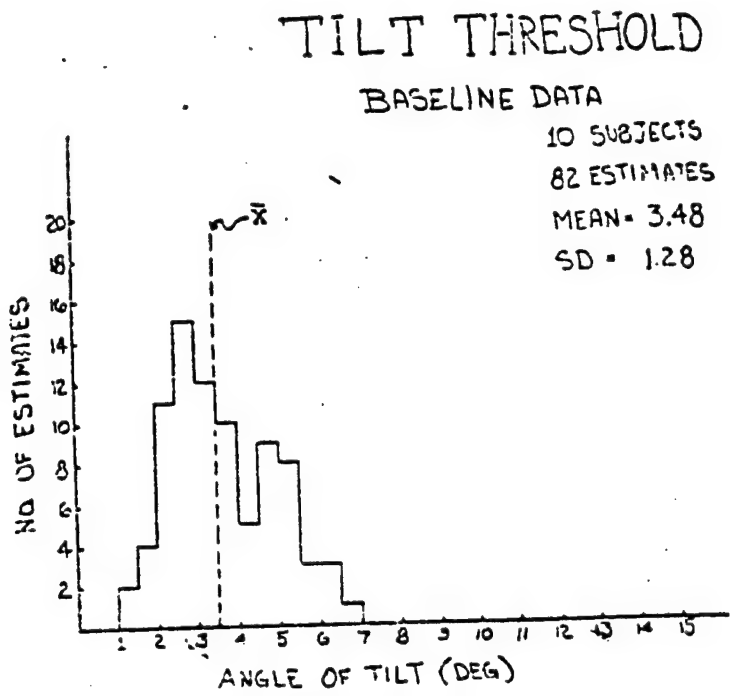

Fig. 4. Results of the Baseline Data

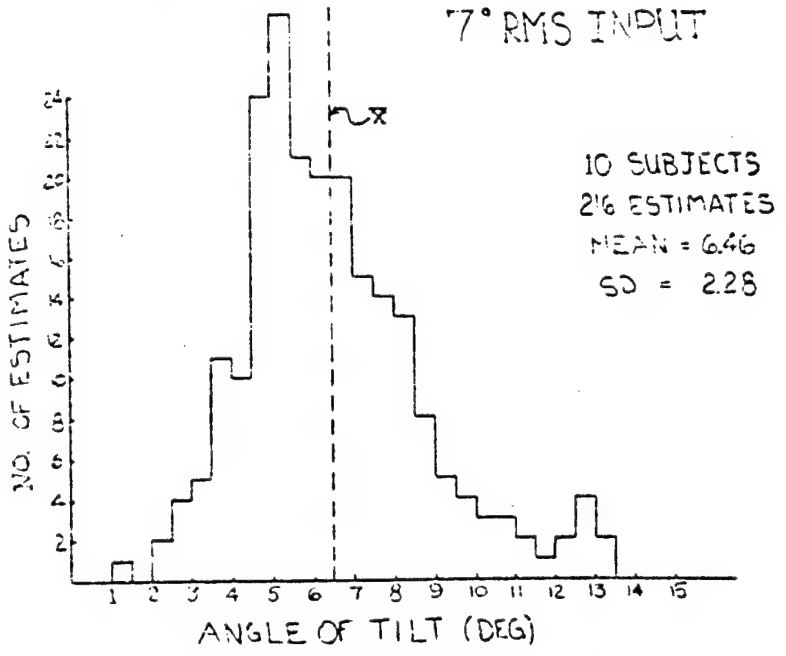

Fig. 5. Results of the 7° PMS Tracking Task

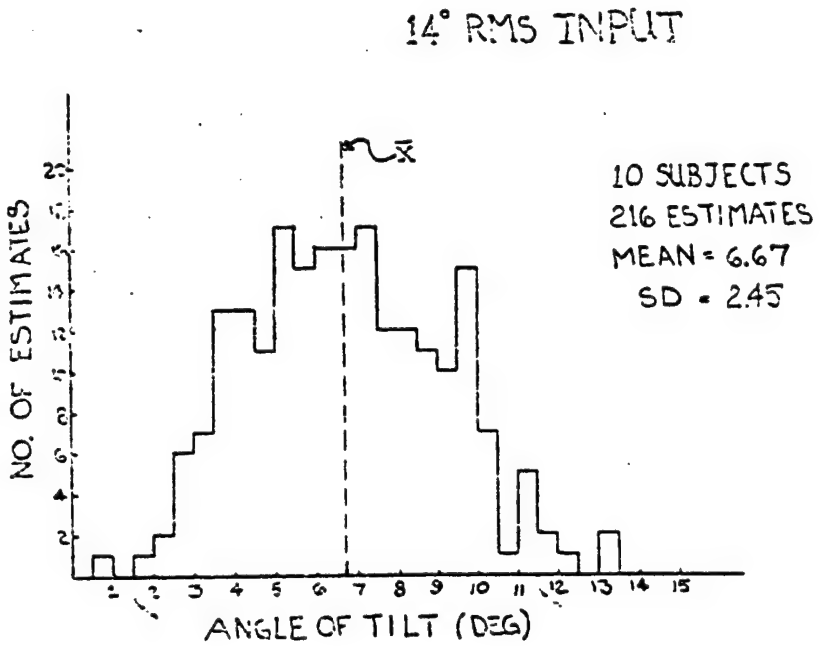

Fig. 6. Results of the 14° RMS Tracking Task

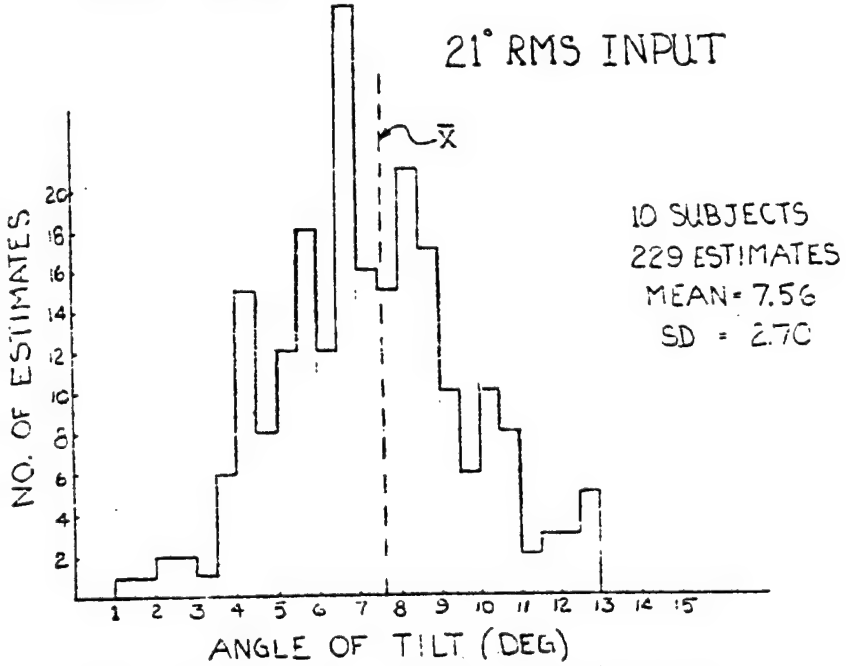

Fig. 7. Results of the 21° RMS Tracking Task

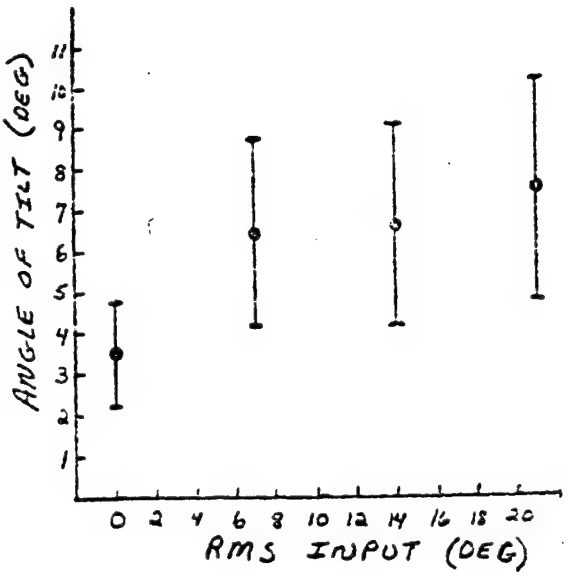

Fig. 8. Data Summary

USE OF THE TILT CUE IN A SIMULATED HEADING TRACKING TASK*

William H. Levison
Bolt Beranek and Newman Inc.
Cambridge, Mass. 02138

and

Andrew M. Junker
Aerospace Medical Research Laboratory
Wright-Patterson AFB, Ohio

Presented at the Fourteenth Annual conference on Manual Control, University of Southern California, Los Angeles, California, May 25-27, 1978.

ABSTRACT

An experimental and analytical study was undertaken jointly by the Aerospace Medical Research Laboratory and Bolt Beranek and Newman Inc. to explore the effects of the tilt cue on pilot/vehicle performance in a simulated heading tracking task. The task was performed with subjects using visual-only cues and combined visual and roll-axis motion cues. Half of the experimental trials were conducted with the simulator rotating about the horizontal axis; to suppress the tilt cue, the remaining trials were conducted with the simulator cab tilted 90° so that roll-axis motions were about earth vertical.

The presence of the tilt cue allowed a substantial and statistically significant reduction in performance scores. When the tilt cue was suppressed, the availability of motion cues did not result in significant performance improvement. These effects were accounted for by the optimal-control pilot/vehicle model, wherein the presence or absence of various motion cues was represented by appropriate definition of the perceptual quantities assumed to be used by the human operator.

* This research was supported in part by AFOSR under Contract No. F44620-74-C-0050.

INTRODUCTION

One of the problems associated with ground-based motion simulation is the introduction of unwanted or "false" cues that are not present in three dimensional flight. The particular set of such false cues present in a given simulation depends both on the nature of the flight task and the degrees of freedom of the moving-base simulator.

This paper reviews the results of a recent experimental and analytical study to explore the pilot's ability to use the "tilt cue" (i.e., the deviation of the effective "gravity vector" from the usual head-to-seat orientation). Such a cue is "false", for example, if it is present in the simulation of a constant rate coordinated turn. This study was performed as part of a multi-year collaborative effort between Bolt Beranek and Newman and the Aerospace Medical Research Center to develop a model of the pilot's use of roll-axis motion cues. Results obtained in the preceding phases of this program have been reported in References [1-5]; documentation of the study reviewed below is in preparation.*

DESCRIPTION OF EXPERIMENTS

Preliminary model analysis was conducted using the optimal-control pilot/vehicle model to search for an experimental task for which performance would be sensitive to the presence or absence of the tilt cue. This analysis revealed that simple roll-axis tasks of the type explored previously would not be sufficiently sensitive. When the addition of another integration to the system dynamics was found to provide the desired predicted sensitivity, the heading tracking task diagrammed in Figure 1 was adopted for this study. In all experimental trails the subject was provided with a visual display of heading error as sketched in Figure 2.

Motion about the roll axis was provided by the Dynamic Environmental Simulator (DES). When the roll axis of the simulator was in the normal horizontal orientation, a roll displacement provided the subject with a tilt cue. The tilt cue was suppressed by rotating the DES 90 degrees so that the pilot was in the supine position. In this position gravity acted normally to the plane of rotation and could not provide the pilot with information related to the tracking task. Motion was provided only in the roll axis; yaw motion was absent.

Vehicle dynamics were of a higher order than those explored in the preceding study. The DES itself provided approximate dynamics of a single pole

* Levison, W. H. and A. M. Junker "Modeling the Pilot's Use of a Roll-Axis Tilt Cue", BBN Report No. 3802, Bolt Beranek and Newman Inc., Cambridge, Mass. (in preparation).

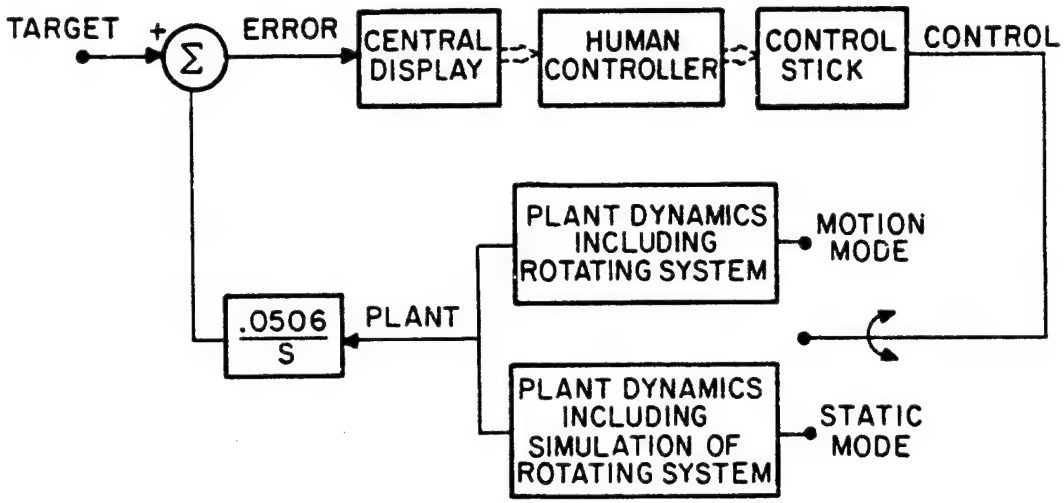

Figure 1. Block Diagram of the Tracking Task

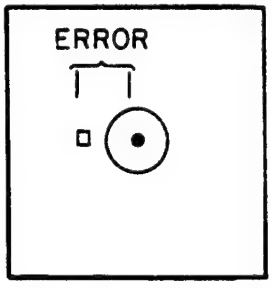

Figure 2. Sketch of the Central Visual Display

at 2 rad/sec and a complex pole pair having a natural frequency at about 10 rad/sec. "Target" motion was provided by a sum of sinuscids designed to approximate a second-order noise process.

Subjects were instructed to minimize a weighted sum of mean squared heading error and mean squared roll acceleration and were trained to near asymptotic performance on each of the four experimental conditions.

SUMMARY OF RESULTS

The comparison between predicted and measured rms performance scores presented in Figure 3 shows that the model predicted the major trend of the experiment: namely, that motion cues would benefit performance to a greater extent when the tilt cue was present (i.e., horizontal roll axis). This comparison is perhaps better illustrated in Figure 4 in which static-motion differences in rms scores are shown for all performance measures. For the most part, predicted differences were within one standard deviation of the difference scores obtained experimentally. For roll axis horizontal, the model predicted a smaller decrease in the error score and a greater decrease in the acceleration score than revealed by the data. Predicted static/motion performance differences were generally less than observed experimentally for roll about the vertical; however, observed differences were largely not statistically significant.

Model predictions shown in Figures 3 and 4 were obtained with pilot-related parameters selected as indicated in Table 1. On the basis of results obtained in a study of simulator washout effects [3], a "residual noise" of 15 degrees was associated with perception of plant roll angle from the tilt cue. Because of the relatively large roll rates and accelerations required to perform the tracking task, perceptual thresholds and residual noise terms for other motion-related cues were considered negligible.

The informational analysis adopted in previous studies was used to account for the presence or absence of motion cues. For roll about the horizontal axis, moving-base simulation was assumed to provide the pilot with information related directly to vehicle roll angle, roll rate, roll acceleration, and roll acceleration rate. We further assumed that attention would be shared between visual cues as a group and motion cues as a group and that the pilot would allocate attention between these two sets of cues in a way that would minimize the objective performance cost. A similar treatment was adopted for roll about the vertical axis, only in this case the pilot was assumed to obtain no cue related directly to plant position, and zero attention was ascribed to this variable. The model for static tracking was

* The reader is directed to References 1-5 for a review of the optimal-control model and its treatment of motion cues.

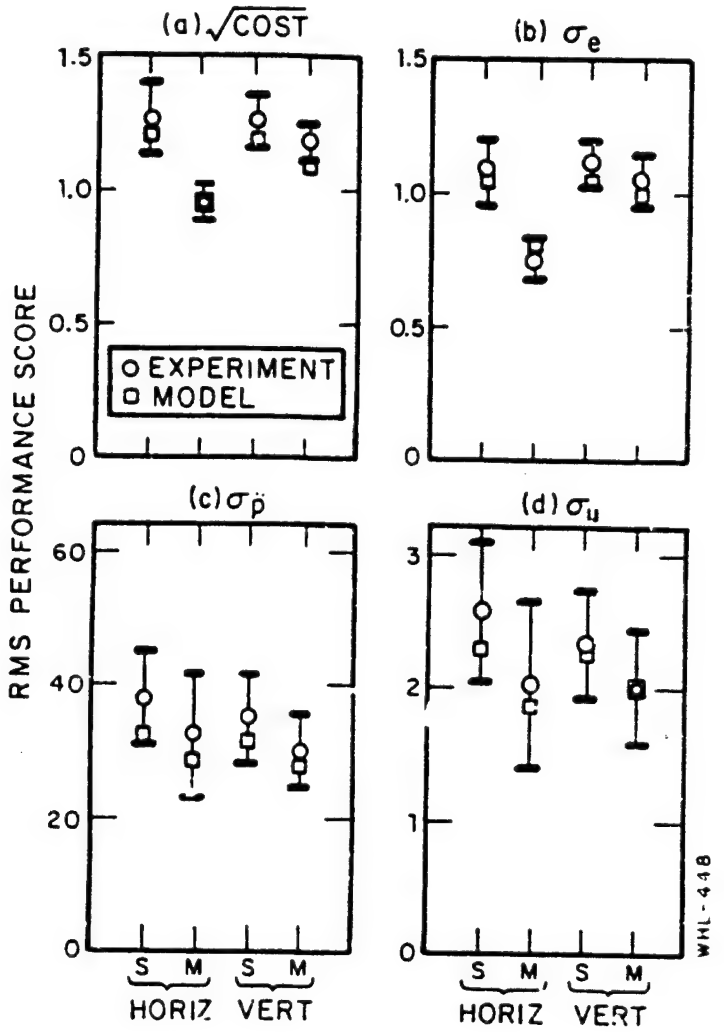

Figure 3. Comparison Between Model and Experimental Performance Scores, Nominal Parameter Values

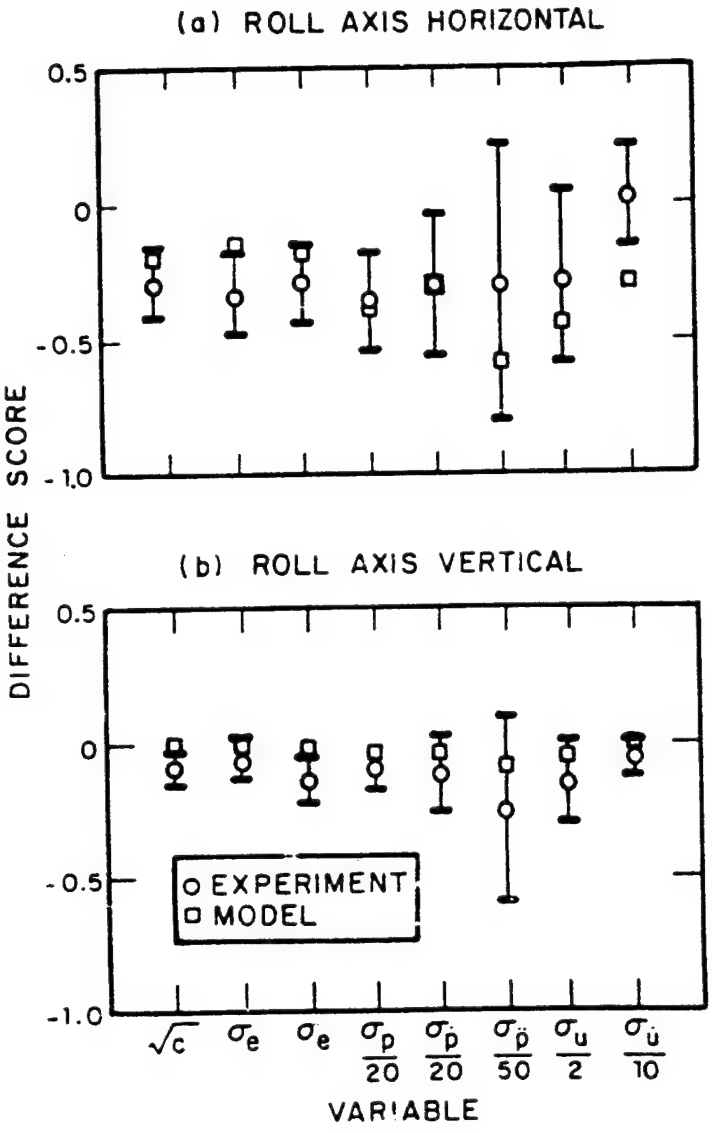

Figure 4. Differences Between Motion and Static Performance Scores

identical for the pilot in the upright and supine positions. Relative attentions of 0.5 and 0.2 to motion variables were predicted, respectively, for the cases of tilt cue present and tilt cue absent.

Table 1

Nominal Values for Pilot-Related Model Parameters

Motor time constant	0.1 seconds
Time delay	0.2 seconds
Driving motor noise/ signal ratio	(negligible)
Pseudo motor noise/ signal ratio	-35 dB. relative to control variance
Observation noise/signal ratio for "full attention"	-20 dB relative to signal variance
Perceptual threshold, indicator displacement	0.05 degrees visual arc
Perceptual threshold, indicator velocity	0.05 degrees/second visual arc

Figure 5 shows that the model correctly predicted many of the detailed changes in pilot response behavior induced by the moving-base simulation. For roll about the horizontal, the model showed a substantial increase in low-frequency phase shift, a small decrease in amplitude ratio, and a decrease in input-correlated control power at low frequencies. For vertical-axis roll, the model correctly predicted a small increase in low-frequency phase and, in general, no appreciable changes in other frequency-response measures.

The model also predicted the following effects that were not observed experimentally: decreased input-correlated and remnant-related control power at high frequencies for horizontal-axis roll, and increased low-frequency remnant power for roll about the vertical. Errors in predicting the effects of motion simulation on low-frequency remnant power arose primarily from the tendency of the model to predict considerably less remnant in the static case than was observed experimentally.

The subjects used in these experiments were instructed only to minimize total "cost"; they were not instructed as to the desired control strategy. One might, therefore, expect the subjects to have adopted strategies different from that predicted by the model, provided such non-optimal behavior had neglible effect on total cost.

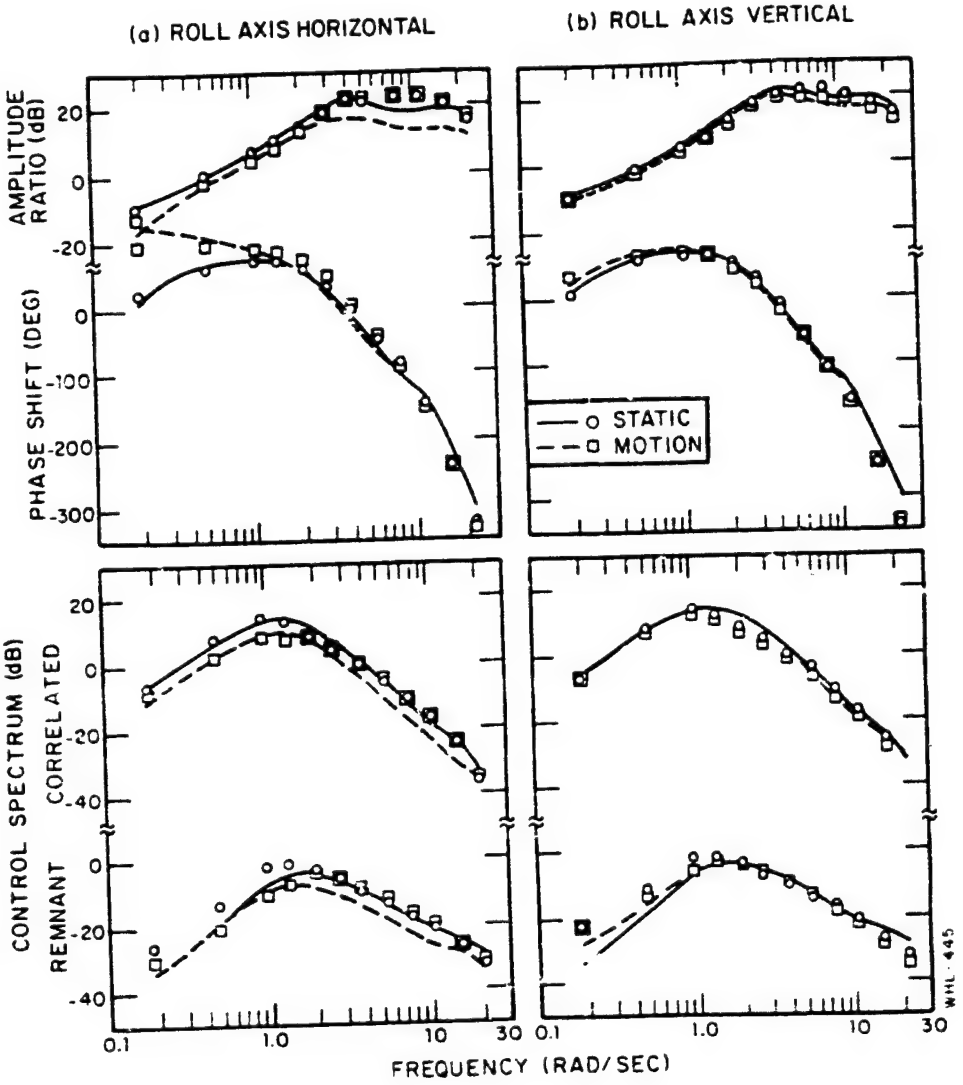

Figure 5. Comparison Between Model and Experimental Frequency-Response, Nominal Parameter Values

Selected pilot-related parameters were varied to determine the extent to which matching errors could be attributed to performance insensitivity. Specifically, time delay and cost weightings were modified in such a way that total cost was virtually unchanged (an increase of less than 3%.) Figure 6a shows that the ability of the model to match pilot response behavior at high frequencies was substantially improved by this procedure. To this extent, differences between predicted and observed measurements can be attributed to "pilot preference" of the type that does not noticeably affect performance.

Errors in modeling low-frequency aspects of response behavior could not be attributable to pilot preference, however. Low-frequency remnant power for static tracking was matched only by an increase in observation noise - specifically, noise associated with perception of heading error. The match to low-frequency phase shift for the motion case was improved by assuming less than optimal attention to motion cues. The resulting improvement in model-matching capability is demonstrated in Figure 6b.

DISCUSSION OF RESULTS

The results of this study indicate that a simple informational analysis is sufficient to account for much of the influence of the tilt cue in tasks involving roll-axis motion. Specifically, one assumes that the pilot directly perceives the bank angle of the (moving) vehicle if the tilt cue is present; otherwise, this element is omitted from the pilot's "display vector". The remaining motion-related cues of roll rate, roll acceleration, and roll acceleration rate are assumed available in both situations.

One should not interpret the results of this study as indicating that the tilt cue will generally be of significance in a task involving roll-axis motions. On the contrary, the degree to which the tilt cue provides usable information to the pilot depends on the details of the tracking task. (In fact, considerable pre-experimental model analysis was required to design an experimental task in which performance would be significantly influenced by the presence or absence of the tilt cue.)

The "residual noise" of 15 degrees associated with perception of the tilt cue is not to be interpreted as a detection threshold, but rather as a measure of uncertainty associated with this perceptual variable in the context of a continuous tracking task. Since a "residual noise" is roughly equivalent to a "threshold" of one-third the value in terms of the optimal-control pilot model [6], the residual noise of 15 degrees is consistent with an indifference threshold of about 5 degrees recently obtained in an experiment requiring simultaneous detection of tilt and continuous roll-axis control [7].

To some extent, insensitivity of performance to pilot response strategy appears to have allowed the subjects to "trade" acceleration score for error score when performing the tracking task with roll motion about the

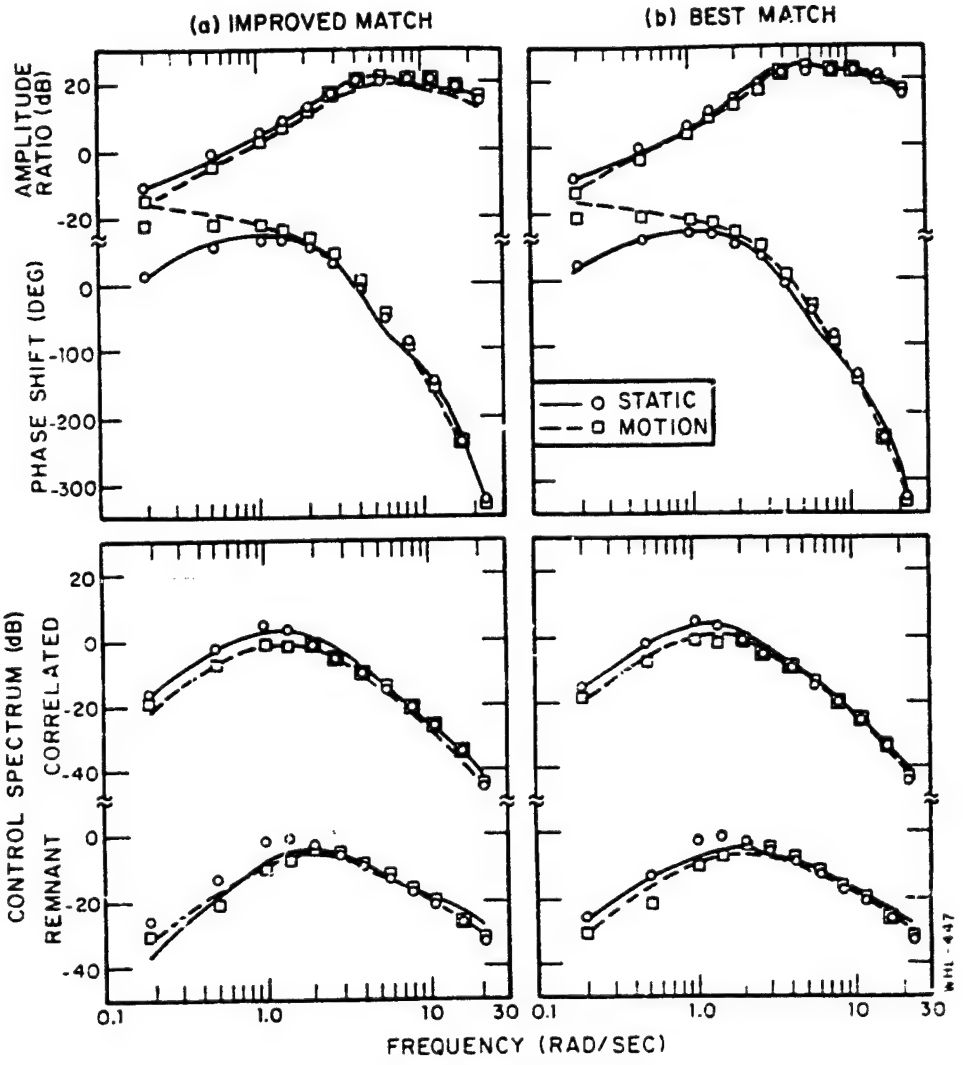

Figure 6. Comparison Between Model and Experimental Frequency Response, Parameter Values Adjusted for Better Match

horizontal axis. However, performance insensitivity does not explain the relatively large noise/signal ratio (equivalently, low attention) associated with perception of heading error in the fixed-base tracking task. Increasing this parameter from the nominal -20 dB to -5 dB to provide the best match to the experimental results increased the predicted total cost by about 20% - an increase too large to ascribe to pilot indifference.

A more consistent explanation of these results is that the high noise level may have reflected increased uncertainties about vehicle response characteristics caused by the relatively high order of the plant dynamics (two pure integrations plus additional lags to represent the dynamics of the rotating simulator). When motion cues were present, the controllers may have obtained sufficient additional information about the state of the controlled plant to minimize this uncertainty; hence, the ability to match moving-base response behavior with nominal noise levels. Improved modeling of pilot response behavior in situations involving high-order dynamics is a possible area for future research.

REFERENCES

1. Levison, W. H., S. Baron and A. M. Junker, "Modeling The Effects of Environmental Factors on Human Control and Information Processing," AMRL-TR-76-74, Wright-Patterson Air Force Base, Ohio, August 1976.

2. Levison, W. H. and A. M. Junker, "A Model for the Pilot's Use of Motion Cues in Roll-Axis Tracking Tasks," AMRL-TR-77-40, Wright-Patterson Air Force Base, Ohio, June 1977.

3. Levison, W. H., "A Model for the Pilot's Use of Roll-Axis Motion Cues in Steady-State Tracking Tasks", Bolt Beranek and Newman Inc. Report No. 3808, May 1978.

4. Levison, W. H., "Use of Motion Cues in Steady-State Tracking", NASA TM X-73, 170, Twelfth Annual Conference on Manual Control, Urbana, Illinois, May 1976.

5. Levison, W. H. and A. M. Junker, "Use of Motion Cues in Two Roll-Axis Tracking Tasks", Proceedings of the Thirteenth Annual Conference on Manual Control, M.I.T., Cambridge, Mass., June 15-17, 1977.

6. Kleinman, D. L. and S. Baron, "Analytic Evaluation of Display Requirements for Approach to Landing", NASA CR-1952, November 1971.

7. M. Roark and A. Junker, "The Effects of Closed Loop Tracking on a Subjective Tilt Threshold in the Roll Axis", Proceedings of Fourteenth Annual NASA-University Conference on Manual Control, University of Southern California, April 25-27, 1978.

ROLL TRACKING EFFECTS OF G-VECTOR TILT AND VARIOUS TYPES OF MOTION WASHOUT

Henry R. Jex and Raymond E. Magdaleno
Systems Technology, Inc.
Hawthorne, California

and

Andrew M. Junker
6570th Aerospace Medical Research Lab, EM Branch
Wright-Patterson AFB, Ohio

SUMMARY

The aim of this research was to discover the basic effects on pilot roll tracking behavior, performance, and impressions for several types of motion-reducing logic ("washouts") used in moving-base simulators. It was a joint program between the 6750 Aerospace Medical Research Laboratory (AMRL-EM Branch) and Systems Technology, Inc.

The experiments were performed on the AMRL Dynamic Environment Simulator (DES), in the roll degree of freedom only. The g-vector was oriented both normally (pilot erect, tilt cue present) and 90 deg nose-up (pilot supine, no tilt cue). Washout filters included: second order, first order, attenuated first order, attenuated, and static (fixed base).

In a dogfight scenario, the task was to follow the target's roll angle while suppressing gust disturbances. The two independent inputs (interleaved sum-of-sines) enabled identification of both the visual and motion response parameters of the pilot by the STI Model Fitting Program (MFP'77). A 12-parameter multiloop model structure fitted includes separate visual and roll motion sensing channels, with a common neuromuscular actuator block.

Excellent describing function and performance data as well as subjective impressions were obtained on four non-pilot subjects, each well trained in the "real-world" case (full motion; 90 deg nose-up). All subjects adopted the same behavioral strategies in following the target while suppressing the gusts, and the MFP-fitted math model response was generally within one "data symbol width."

The results include the following:

- Comparisons of full roll motion (both with and without the spurious gravity tilt cue) with the static case. These motion cues help suppress disturbances with little net effect on the visual performance. Tilt cues were clearly used by the pilots but gave only small improvement in tracking errors.

- The optimum washout (in terms of performance close to "real world," similar behavioral parameters, significant motion attenuation (60 percent), and acceptable motion "fidelity") was the combined attenuation and first-order washout.

- Various trends in parameters across the motion conditions were apparent, and are discussed with respect to a comprehensive model for predicting pilot adaptation to various roll motion cues.

The detailed data base (spectra, remnant, describing functions, model fits) are compiled in a separate document available to interested researchers through AMRL-EM.

INTRODUCTION

Objectives and Background

A joint experimental/analytical effort by the Aerospace Medical Research Laboratory (AMRL/EM) and Systems Technology, Inc. (STI) was conducted to define a pilot's use of motion cues in moving-base simulators free to rotate only in the roll degree of freedom. This situation provides the pilot an intrinsically spurious roll attitude or "tilt" cue. This effect can be reduced by "washing out" the cab motion so the cab always tends to return to an upright orientation, although this distorts the true angular motions. The optimization of the washout dynamics to achieve the best compromise between realistic roll rate cues and suppression of the spurious tilt cue is an important facet of the immediate future work to be done in the AMRL/EM laboratory.

The basic objective was to determine what form and degree of washout dynamics achieves the highest simulation realism, while engendering true-to-life behavior of the pilot, and producing the correct performance effects due to environmental stressors. Longer range objectives include the possible correlation of these experiments with other ground-based simulations and later with in-flight experiments.

To accomplish the above objectives this investigation had to consider two basic problems in moving-base simulation: the use of motion cues by the pilot in the actual ("real world") case and the effects of spurious motion cues in modifying that usage in the simulator. A brief examination of the piloting task involved in the first problem is useful before proceeding to the second.

Consider a situation of primary interest to the Air Force — air-to-air combat — and focus upon the pilot's response to the dynamic (non-steady) components of motion. Assume that, initially, the pilot has his wings lined up with those of a target aircraft that he perceives against a murky or night-time background (no horizon visible). In this "impoverished display" situation he can visually perceive only the difference (error) between the target's wings and his own. Further, the pilot has two tasks to perform, from simultaneously:

a. Regulate (suppress) disturbances, e.g., due to gusts or swirls from the target's wingtip vortices. In this task the pilot's role is to reduce motions, and if he suppresses the gusts with small error, the physical motions become small.

b. Track (follow) the target roll motions (e.g., by keeping one's wings parallel with the target). In this task the pilot's role is to produce motions, and if he tracks with small error, the physical motions become larger (approaching the target motions).

In the general case, where both inputs are present, the pilot is faced with a continual conflict between reducing disturbance motion and producing correct following motions. The figure-of-merit (at least in air combat and landing tasks) is primarily low roll error (and, perhaps, limited roll acceleration or its rough equivalent — aileron control deflection). Because multiple sensory feedbacks are involved, with more than one input, the problem is a multiloop one, and this greatly complicates the control system analysis as well as the attempt to infer the pilot's behavioral "structure" and parameters, as will be demonstrated, herein.

Most of the earlier research in measuring the use of visual and motion cues, such as that of Stapleford, et al (Ref. 1) and Shirley (Ref. 2), tended to have either the target input or disturbance, as dominant, such that the possible cue conflicts were minimized. Stapleford, et al were able to infer the separate visual and motion pathway dynamics by using mathematically independent target and disturbance inputs comprising sums-of-sinusoids interleaved in frequency, then interpolating between frequencies to solve the simultaneous vector equations required to untangle the loops (this process will be shown later herein). However, these pioneering results were not fitted in any form suitable for efficient use. Thus, the secondary objectives of this program were to improve the reduction and analysis of multisensory manual control data, and to structure and parameterize the results. Here, where the target following and disturbance motions were comparable, in bandwidth and amplitude, new techniques were required.

Such a situation seems natural for an optimal control model of the human operator, and Levison, working with AMRL experimenters has put forth a first-cut at just such a model in Refs. 3 and 4. The forcing functions were either target inputs or disturbances, and effects similar to Stapleford's and Shirley's were obtained. Whether or not their (implicitly) assumed feedback structure is valid is hard to say without more data on the all important dual-input case treated here.

In another approach Zacharias (Ref. 5) has tackled the problem of sensory conflict of visual and vestibular sensors in conjunction with regulation of purely visual, purely motion or conflicting cue situations, and has speculated on a cue-conflict resolving model for the human operator, in the yaw-only degree of freedom. Testing the validity of such cue-conflict-resolution approaches as these requires a very solid data base to exercise one's model against, and this is still largely lacking. In light of the above needs, a

third objective was to establish a very solid and comprehensive data base, using inputs, controlled elements, and washouts that were analytically tractable and fairly linear, so that future validation of cue-utilization models would be facilitated.

Scope

To meet these objectives, the AMRL Dynamic Environmental Simulator (DES) was employed, which permits pilot rolling motions with his rolling axis horizontal (normal spurious tilt cues present) as well as vertical (tilt cues absent). Details are given later. The scenario selected was that of air-combat with a set of fairly sluggish aircraft roll dynamics, so that motion cues would be useful. As will be described, the target and disturbances were carefully designed to provide strong motion-usage conflicts as well as easy analytical modeling. Several motion cases, ranging from full motion, various washouts to fixed base were included. Based on prior work, a plausible structure for the pilot's use of visual and motion inputs was proposed, and a newly developed technique was used to fit these model parameters quite precisely to the frequency-domain data.

We show how some of the past results are explained on the basis of differences in the apparent "opened-loop" transfer functions for target vs. disturbance inputs, despite identical pilot behavior with respect to either by itself.

To obtain reliable measurements, worth fitting by the relatively high-order models selected, extremely consistent pilot behavior is necessary. This was obtained by a combination of the sluggish controlled element (which had a fairly well-defined optimum strategy) and very well-trained subjects.

The results show clear answers to the questions raised earlier, when analyzed with respect to various performance and behavioral 'dynamic' parameters, and some interesting trends are evident in the pilot parameters vs. motion measures, even for fairly small motions. Nevertheless, this report does not attempt to interpret these covariations in terms of an overall model of operator adaptation to pure and distorted motion feedbacks.

EXPERIMENTAL DESIGN

Approach

As noted in the introduction, there were two facets of roll motion-cue usage to be investigated: "real-world" motion vs. no-motion and distortions of real-world motion by various washout filters. In the actual flight case, where gradual bank angles result in translation of the aircraft, there is no way to tell vertical by seat-of-the-pants or other vestibular sensors. A set of realistic rolling cues were provided by tipping the roll-axes of the simulator 90 deg nose upward so that the spurious tilt cues were absent. This full-motion at 90 deg inclined roll axis (F-90) case was given the most

practice and became the "real-world" reference for all other motion cases. By comparing it with the static case, the basic effects of motion were revealed. To check effects of the conflicts between target following vs. disturbance regulation, both forcing functions were given alone and together (dual input) for the F9C case. If the dual case gave similar data as either input alone, then the dual input could be used throughout, with consequent savings in runs and data analysis.

The washouts in roll-only simulators are used for two main purposes, a) to reduce the tilt cues (largely a low frequency effect) and b) to reduce any or all motions (accelerations, rates, displacements) to fit into a limited capability simulator, always with a horizontal orientation of the roll-axis. Consequently the effects of simulated roll only motions were covered by the full motion at 0 deg roll axis inclination and various washouts — all selected to give substantial reduction in roll displacement.

To keep the number of runs within bounds, it was decided to keep constant the plant and the spectrums of forcing functions; and to try only one variation of each washout filter scheme.

Control Task

Block Diagram — a scenario with high face validity relevant to Air Force problems is air-to-air gunnery. In a modern high thrust/weight fighter, combat maneuvers take place at all flight path angles, hence the horizon is relatively unimportant. The main criterion for accurate tail chase is to match the roll angle of the target aircraft. The pilot is attempting to follow an evasive target while at the same time he may be buffeted by gusts, a component of which could be wing tip vortices of the target. To simplify the simulation and subsequent modeling and interpretation, a compensatory display (error only) was used and the subjects were instructed to minimize the bank angle error.

Fig. 1-a illustrates the basic elements involved: the Human Operator, Controlled Element, and Washout dynamics. The multiloop nature is evident in that the Motion Path senses physical (inertial) bank angle while the Visual Path senses the error between target and task bank angle. (The four-character "names" on the signals in Fig. 1 represent the Fourier coefficients and are used to label some power spectra and describing functions later in this report).

Controlled Element

The controlled element (Eq. 1 on Fig. 1-b) represents an approximation to the roll dynamics of a fighter. The Roll Subsidence mode, having a time constant of $1/1.6 = 0.63$ sec, is typical of a loaded fighter (i.e., with external stores). This value was selected as it would require a significant amount of lead generation by the pilot, because the Crossover-Law for human operator equalization (e.g., Ref. 5) predicts that in such cases the ideal pilot lead

a. Block Diagram Showing Definitions of Elements and Signals

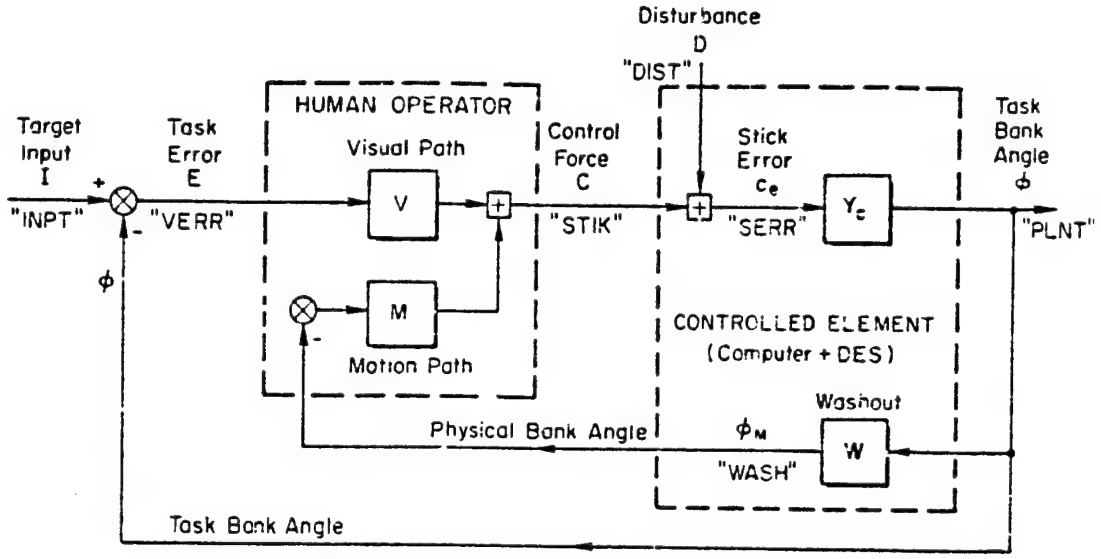

b. Controlled Element Transfer Function

$$Y_c(s) \equiv \frac{\dot{\phi}}{c_e} = 17 \; \frac{(-s/2.5 + 1)}{s\left(\frac{s}{1.4} - 1\right)\left(\frac{s}{\quad} - 1\right)\left[\frac{s^2}{11^2} + \frac{2(.3)s}{11} + 1\right]} \quad \left(\frac{\text{deg/sec}}{\text{lb}}\right) \quad (1$$

Lags

Spiral Mode | Roll Subsidence | "Servo" Lag | "Structural" Mode

Figure 1. Roll Tracking Task Block Diagram and Transfer Function

C-6

would be about $T_L \doteq T_R \doteq 0.5$-$0.7$ sec. The "Structural Mode" and "DES lags" represent the unavoidable and measured response characteristics of the DES motion simulator, while the "Servo" Lag represents actuation lags of a (poor) aircraft control system. It was raised to 0.2 sec to prevent excessive acceleration or rate commands to the DES which would cause its drives to operate in a partly saturated (hence nonlinear) manner.

Analysis of this controlled element showed that it requires a fairly tightly constrained pilot equalization, with some lead to offset the roll-subsidence lag, but not too much or else the structural mode and lag elements would destabilize the system. Thus, there was a clearly optimum control strategy for the subjects to learn, which was important because they were not experienced pilots.

Forcing Functions

Quasi-random target and disturbance inputs were constructed from eight sinusoids each (Table 1). The frequencies were selected so as to have an integer number of cycles in the run length as shown. To assure statistically independent inputs, target and disturbance frequencies were interleaved, yet each was approximately evenly spaced on a log-frequency plot. After these choices were made the amplitudes were "shaped" to simulate a random noise process that would result from white noise being filtered by the shaping filter forms given in Table 1. Finally, these "shaped amplitudes" were scaled so as to give the listed rms and peak amplitude values.

The target's shaping filter was selected to simulate a low pass spectrum typical of an evasive target. The disturbance's shaping filter was selected so that under static conditions (and, as further shaped by the controlled-element) the spectral content and rms values would be nearly equal to that of the target, as seen on the error display. Thus the pilot could not use input frequency properties to separate target motions from disturbance motions.

Multiloop Pilot Model and Identification Procedure

Analysis. — The measurement problems involved in the multiloop system of Fig. 1-a can be illustrated by examining the task error components resulting from target and disturbance inputs, shown in Fig. 2.

First consider the static case, where the Motion Path is inoperative: $M(j\omega) = 0$. Then the task error vector (frequency response function) becomes that given by Eq. 2 in Fig. 2. For convenience, we have dropped the arguments $s = j\omega$ in each of the inputs and transfer functions; $K_{j\omega} = K$, etc.).

Equation 2 has been written in the form of a conventional single loop system, wherein the [ ] term is the closed-loop error-to-input describing function, so the product $V \cdot Y_c$ is recognized as the open-loop describing

TABLE 1. FORCING FUNCTIONS FOR DUAL INPUT RUNS

TARGET (rms = 7.1 deg)*			DISTURBANCE (rms = .74 lb = 3.4 N)*		
Cycles / Run Length†	ω (rad/sec)	A_{dB} 0 = 1. deg	Cycles / Run Length	ω (rad/sec)	A_{dB} 0 = 1. lb
5	0.19	15.6	9	0.35	−20.6
13	0.50	11.6	17	0.65	−17.5
23	0.88	8.7	30	1.15	−15.6
37	1.42	5.6	49	1.88	−11.4
65	2.49	1.0	85	3.18	− 9.7
107	4.10	− 5.8	141	5.41	− 9.2
182	6.98	−14.4	241	9.24	−10.0
309	11.85	−24.4	410	15.72	−11.7
SHAPING FILTER FORM					
$\frac{1}{(s+0.5)(s+1.7)(s+5.0)}$			$\frac{s}{(s+0.5)(s+5.)}$		

* For single input runs the values were increased by $\sqrt{2}$:1
† Run length = 163.84 sec

function, G_{CL} for purely visual feedbacks. Recall that increasing the magnitude of G_{CL} reduces tracking errors, etc.

Similarly, in hypothetical situations where the operator would close his eyes and operate solely on motion cues (V = 0), the task errors would be given by Eq. 3 in Fig. 2. The input is unaffected, while the disturbances are suppressed.

When both visual and motion paths are active the multiloop relationships become more complex, but can still be written so as to reveal the effective opened-loop dynamics (similar to Eqs. 2 and 3), as shown in Eq. 4. Now, however, the "opened-loop" describing function for target errors G_I, of Eq. 4a) contains the closed-motion loop $1/(1 + MWY_C)$, while G_D for the disturbance errors contain the sum of motion and visual effects $(V + MW)Y_C$.

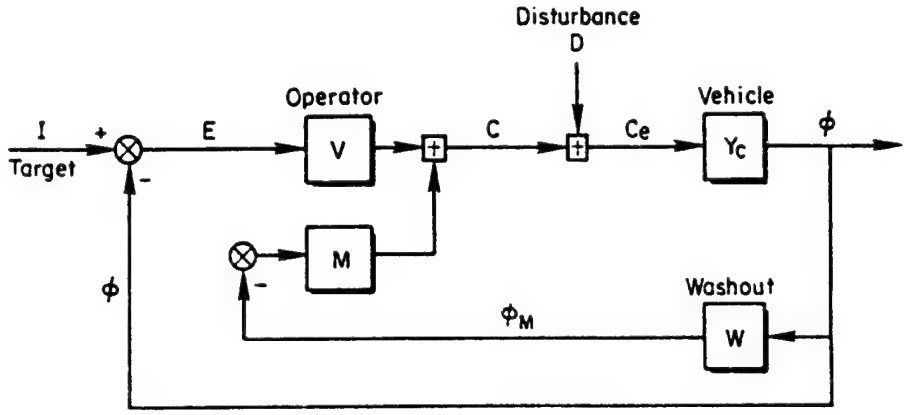

Note: All blocks and signals are vector functions of frequency: $V = V(j\omega)$ etc.

For Visual only: (Static; $M \equiv 0$)

$$E = (I - DY_c)\left[\underbrace{\frac{1}{1 + VY_c}}_{(E/I)_{CL}}\right] \qquad (2)$$

Open-loop DF: "G_{OL}" for Visual Loop alone

For Motion Only: (Eyes closed; $V \equiv 0$)

$$E = I - DY_c\left[\underbrace{\frac{1}{1 + MWY_c}}_{G_{OL}}\right] \qquad (3)$$

Open-loop DF: G_{OL} for Motion Loop alone

For Visual-Plus-Motion:

$$E = I\left[\frac{1}{1 + G_I}\right] + (-DY_c)\left[\frac{1}{1 + G_D}\right] \qquad (4a)$$

where "Opened-loop" DF's

$$G_I = \frac{VY_c}{1 + MWY_c} \qquad (4b)$$

$$G_D = (V + MW)Y_c \qquad (4c)$$

Figure 2. Closed-loop Error Relationships to Target and Disturbance Inputs for Various Single and Multiloop Structures

In the single loop cases of Eqs. 2 and 3 a high-gain (V or M) reduces errors, but in the multiloop case there is a conflict:

- A high-gain motion feedback (large M) reduces the disturbance errors via Eqs. 4a and 4c, but increases the target errors via 4a and 4b.
- A high-gain visual loop (large V) reduces both error components.
- The optimum strategy (to minimize E) is a complicated function of the spectra of I and $D \cdot Y_c$, as well as of Y_c and M.

These are the analytical expressions for the qualitative motion/visual cue conflict mentioned in the introduction. Further, notice that analytically opening the loop for either target or disturbance inputs will give different apparent "opened-loop" describing functions (Eqs. 4b vs. 4c even with identical V and M operations in both equations. This has led in the past to some misinterpretation of results for mostly-target or mostly disturbance inputs.

Finally, it can be seen that, knowing the vehicle and washout dynamics (Y_c and W) and with simultaneous independent inputs I and D, the independent estimates of the visual and motion operations (V and M) are theoretically possible if the signals are not confounded with noise. The temptation to measure V and M from static and motion-only runs, respectively, is precluded by the adaptive nature of the human operator. In general, the pilot will adopt different parameter values for his gains, leads and lags in the above special cases compared to the combined case, as will be shown later.

Model Structure and Parameters. — The criteria for selecting the model structure were that it be:

1. The simplest form capable of capturing all of the significant frequency-domain characteristics of the measured data, both with and without motion.
2. Have components structurally related to previously well known visual-motor elements, such as neuromuscular (NM) and, central-nervous system (CNS) components, as well as motion sensing elements from afferent vestibular and proprioceptive signals.
3. Compatible with prior manual-control models, e.g., those in Ref. 5.

Figure 3 details the assumed pilot model structure and forms for the Visual and Motion paths of Fig. 2. The rate and displacement elements in the "VISUAL PROCESSES" group are used to generate a lead time constant ($T_L = K_R/K_D$) which pilots typically adopt to cancel the roll-subsidence mode in the controlled element (Ref. 3). The "integral" term is sometimes needed to represent the pilot's trimming actions and other low frequency behavior. (e.g., the so called "α-effects" in the Extended Crossover Model of Ref. 5

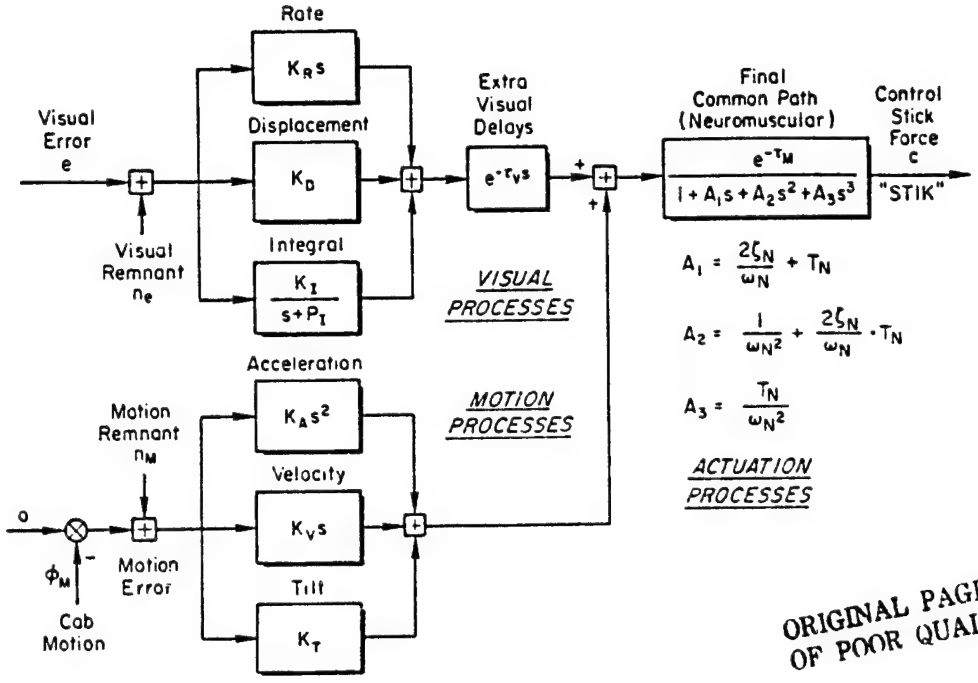

Figure 3. Assumed Pilot Model for Roll-Only Tracking

The extra visual time delays account for retinal and central (e.g., rate) processing as well as computational and display lags.

The tilt, velocity and acceleration terms in the "MOTION PROCESSES" are the simplest possible descriptors of the pilot's use of physical bank angle. These are not intended to represent motion sensors directly although the velocity term is very similar to the output of the semicircular canals over the forcing function frequency region. The tilt angle cue K_T is actually due to the lateral specific force due to the tilted g-vector.

The "ACTUATION PROCESSES" include a time delay and a third order neuromuscular system, the latter readily simplified to a second or even a first order approximation, as noted in the figure (e.g., for a second-order system set $T_N = 0$, whence $A_3 = 0$, $A_2 = 1/\omega_N^2$ and $A_1 = 2\zeta_N/\omega_N$). The delay terms τ_V and τ_M were actually modeled as first-order Pade polynomials, and by breaking up the net delays into two small portions the Pade roots (at $2/\tau$) are at sufficiently high frequency to give an excellent fit up to over 10 rad/sec.

Identification. — The two "opened-loop" expressions in Eq. 4a can be used to identify the two unknown paths (Visual and Motion) only if the Target and Disturbance inputs are independent. For signals constructed as a sum of sine waves this means that there can be no common frequencies. However this precludes the direct solution for the unknowns (V and M) since the "opened loop" expressions cannot be evaluated at the same frequencies. This dilemma was dealt with in Refs. 1 and 2 by linearly interpolating the measurements at the interleaved frequencies. This can lead to difficulties and inaccuracies in the vicinity of lightly damped modes, where the transfer functions are not smooth. A different technique is used where specific model forms are assumed for the Visual and Motion paths and the equations of motion are written for all elements and loops, so that in effect the "interpolations" are made with appropriately shaped math models. The unknown parameters are then adjusted by the STI Model Fitting Program (MFP; described below) so as to fit simultaneously the closed loop error and stick describing function responses to the Target and Disturbance inputs.

The STI Model Fitting Program was developed to fit high order multiloop models to frequency domain data (e.g., from Fast Fourier transforms and is described in Ref. 7. It evaluates selected transfer functions from fixed-form adjustable-parameter equations-of-motion written in a special way such that each adjustable parameter appears only once in the "matrix-of-equations." Thus, the influence of each parameter on any system response to any input is available. The program minimizes the vector difference between model and data transfer function responses using a variety of steepest descent techniques to minimize a cost function. This cost function is evaluated by squaring and amplitude weighting the difference in the real and imaginary parts of the data and model responses. In the present case, five frequencies of the task error-to-disturbance, four of the stick-to-disturbance and five of a linear sum of error- and stick-to-target were fit. The amplitude-weighting was the inverse of the data magnitude, thus each frequency was uniformly represented except that the highest frequency of the stick-to-disturbance was weighted 10 dB less.

Since the target and disturbance are sums of sinusoids, the effective "opened-loop" expressions in Eq. 4 were estimated using ratios of Fourier coefficients:

$$\hat{G}_I(j\omega)\Big|_I = \frac{P}{E} = \left(\frac{PLNT}{VERR}\right) \quad \text{at Target frequencies, } \omega_I \tag{5}$$

$$\hat{G}_D(j\omega)\Big|_D = \frac{-C}{C_e} = \left(\frac{-STIK}{SERR}\right) \quad \text{at Disturbance frequencies, } \omega_D \tag{6}$$

where the four character names PLNT, VERR, STIK and SERR are defined in Fig. 1 and will be used to identify various responses in the remainder of this report.

To check the accuracy of this procedure an analog "autopilot" operation on both task error and measured motion was mechanized on the DES setup and the recorded signals were processed thru MFP. Table 3 summarizes the results of

TABLE 3. ORIGINAL AND RECOVERED PARAMETERS FOR DUAL AUTOPILOT

$$\text{Visual Path:} \quad V = \frac{K_R s + K_D}{T_V s + 1} e^{-\tau_V s}$$

$$\text{Motion Path:} \quad IM = \frac{K_V s + K_T}{T_M s + 1}$$

CASE	"VISUAL LOOP"				"MOTION LOOP"		
	K_D	K_R	T_V	τ_V	K_T	K_V	T_M
Original	.133	.067	.100	.018	.040	.100	.100
Recovered by MFP	.134	.062	.098	.023	.040	.104	.092

this check, using the forms indicated. The time delay shown is an approximation to the net phase effects of various hybrid computation delays and high-frequency anti-aliasing filter lags. Some errors could be due to the fact that the "dialed-in" computer settings did not accurately represent the effective parameters. Generally the recovered parameters in Table 3 are quite close to the nominal, such that a transfer function plotted from the recovered parameters would be indistinguishable from one plotted for the original parameters.

Washout Dynamics

In addition to the static (no motion) case ("ST"), and full-motion cases with roll axis at 0 deg inclination "F0", and nose up 90 degrees, "F90"; four different washout schemes were tested:

- Purely Attenuated, "A" wherein the plant motions at all frequencies were multiplied by 1/2 in commanding the DEC.
- First-Order, "W1"; where the low frequency motions are attenuated by a first-order high pass filter of the form:

$$\left.\frac{I_M}{\ddot{\gamma}}\right|_{W1} = \frac{K_{hi}\, s}{s + 1/T} \qquad (7)$$

where

K_{hi} = high frequency gain (near 1.0)

T = time constant ("break frequency" = 1/T)

With this washout a step bank angle command returns experimentally to zero with a time constant of T sec.

- First-Order, Attenuated, "W1.A"; a combination of the two foregoing washouts, with different gains and break frequencies.

- Second-Order "W2"; the low frequency terms are washed out by second order high pass filter of the form

$$\left.\frac{\varphi_M}{\varphi}\right|_{W2} = \frac{K_{hi}\, s^2}{s^2 + 2\zeta\omega s + \omega^2} \qquad (8)$$

where

ω = the break frequency, and
ζ = the damping ratio (typically .7)

With such a second-order washout an initial step bank angle returns with minimal overshoot with an effective delay (to half amplitude) of $(2\zeta/\omega)$ seconds. A constant roll rate input still ends up at zero bank angle.

The various washout parameters were originally selected to produce a reduction in rms roll amplitude to about 50 percent of the full motion case, based on a more-or-less arbitrary a priori assumption of a typical, invariant, second-order closed-loop pilot-simulator response to roll commands, characterized by a bandwidth of 3.6 rad/sec and a closed-loop damping ratio of $\zeta_{cl} \doteq 0.5$. It was realized that in practice the pilot might change his response characteristics for different washouts, but this procedure was used to select the different parameters on a more rational basis than (say) fixed break frequencies of all the washouts.

In the simulation, inadvertent problems with mechanization of the filters and DES response properties slightly modified the intended wash-out dynamics. The actual response properties of the washout plus DES combination were fitted by the appropriate forms of Eqs. 7 and 8 and the effective washout-filter parameters were extracted. These are summarized in Table 4. Most of the effective parameters were close to the intended ones, except for the W2 high frequency gain which was 1.2 instead of the 1.0 desired. In Table 4 the cases are arranged in order of decreasing magnitude of rms physical roll angle, and this order will be used throughout the presentations to follow.

Measurements

A comprehensive set of measurements were made in an attempt to quantify all aspects of the pilot's performance, behavior, and effort.

TABLE 4. MOTION CONDITIONS AND WASHOUT DYNAMICS

Case:	F_{90}	F_0	W2	W1	W1, A	A	ST
Washout Type:	"Full Motion" at 90°	"Full Motion" at 0°	"Second Order"	"First Order"	"First Order, Attenuated"	"Attenuated"	"Static"
High Frequency Gain	1.0	1.0	1.2	1.0	0.7	0.53	0
Break	—	—	ω = .85 r/s ζ = .7	1.0 r/s	.40 r/s	—	—

1. Performance Measures: Overall statistics (mean, variance, rms) of all signals, with emphasis herein on: tracking error stick force and physical roll-angle and rates.

2. Pilot Behavior Measures: Describing functions are the primary indicators of pilot behavior. The fitted parameters are useful for encoding efficiently the data, but the actual plots are often most informative. We use the "opened-loop" describing function, as they are the most useful and tie in with past experience on single loop systems.

3. Subjective Evaluations: Each subject was given a questionnaire about his tracking strategy, effects of motion cues and. differences due to washouts. Because these were not experienced pilots, no comparison to actual flight could be made; instead, subjects were asked to compare the motion cues with those of the F90 "real world" case.

APPARATUS AND PROCEDURES

Apparatus

The experiment was performed on the Dynamic Environmental Simulator (DES) at the Aerospace Medical Research Laboratory at Wright-Patterson Air Force Base. The DES is a man-rated centrifuge with independent roll and pitch cab control. For this experiment only the roll tracking motion was used, with the roll-rate limited to 90 deg/sec and the roll acceleration limited to 90 deg/sec^2. There are no limits on roll angle in the DES.

Within the cab, the subject seat was mounted such that the roll axis of rotation was roughly through the subject's head. Mounted on the seat was a right-side-mounted force stick for vehicle control. The elbow was braced, so that when the roll axis was 90 deg nose up, the hand was still comfortably over the stick. The cab contained a computer generated display, Fig. 4,

which was centered in azimuth a distance of approximately 17 inches from the subject's eyes. Subject's sitting height were such that the display was within 0 to 10 degrees of eye level. The "inside-out" display of target tracking error consisted of a 3.5 inch long rotating "target wing" whose center was superimposed upon a stationary horizontal dashed line nine inches in length. A .25 inch perpendicular "fin" at the center of the rotating line provided upright orientation.

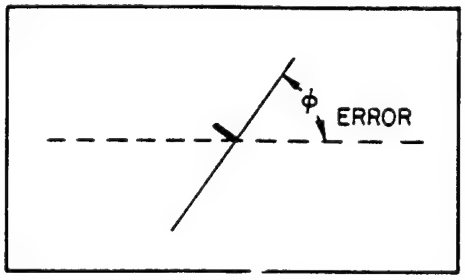

Figure 4. Sketch of the Roll Tracking Display

The DES is configured such that the pitch gimbal is outside of the roll gimbal. Thus it is possible to pitch the simulator nose up 90 degrees without affecting the roll axis tracking system. The cab pitched up 90 degrees was used for the "real-world" condition, as noted earlier.

Experimental Procedure

Four healthy college students between 18 and 25 years of age were used for the experiment. None were experienced pilots, so extensive training was necessary. Training was first accomplished for the static and two Full-Motion conditions. Tracking under each condition was considered one run. Each run lasted 165 sec and the three conditions or runs were presented in a random order each day. At the end of each run, subjects were presented their mean-squared-error score for that run. Training continued for approximately three weeks, three to six runs per day, at which time error scores began to reach asymptotic levels. Once performance leveled off, four more runs per subject per condition were performed and time history data was recorded for subsequent analysis.

For the second part of the study in which we investigated washout filter effects, we used the experimental design philosophy stated earlier — that washout filter effects should be compared to the "real-world" motion cues as encountered in the full motion no-tilt-cue case (F90). Therefore at the start of the evaluation of each washout filter, we let each subject first track in the F90 condition for one day. Following this we had each subject track normally (roll axis at 0 deg) with a given washout filter for three days, four runs per day. The last four runs for each subject with the washout filter were saved for data analysis. The procedure was followed for each washout filter investigated. As in the first part of the study, subjects were told their scores for motivational purposes.

Data Collection

A hybrid computer system was used for: display generation, forcing function creation, on-line error score computation, and time history data collection. From the time history data, root-mean-squared values and Fast Fourier Transforms (FFT) of each time signal were computed. From the FFT's power spectral densities and opened-loop describing functions (e.g., Eqs. 7 and 8) were computed. The frequency response data reduction, based upon the sum of sine waves generation, was similar to that employed in a preceding study (Ref. 5).

Comparisons among individual data showed good consistency, once sufficient training had occurred. Therefore, for each motion condition, the last four runs of every subject were averaged (16 runs total) by AMRL to give mean ± standard deviation values for model fitting by CTI. It is these averaged data that are analyzed in the following section on Results.

RESULTS

Limited space precludes the presentation, here, of all the reduced and averaged data. Instead we present typical time histories for one subject, averaged spectra and describing functions for a typical motion case, and then, after demonstrating that the fitted transfer functions truly represent the data, we present the "opened-loop" curves for various cases, and analyze the resulting performance and behavioral measures to answer the questions in the Introduction.

Typical Time History

A pair of time-histories of the various inputs and outputs for corresponding segments of static and full-motion runs, is given in Fig. 5. For these plots, identical target and disturbance inputs (top and bottom traces) were used in each run, so reveal the differences more clearly. The following features of the time histories should be noted:

- The disturbance input, which is summed downstream of the stick (and shown to the same scale) is effectively integrated by the vehicle dynamics to yield roll motions comparable in amplitude and frequency to the target input.
- In the static case the roll angle does not follow the target very well, because of these simultaneous, large disturbance inputs.
- Comparison of the E and C traces for the static case (where only the visually displayed error can be used) shows that the pilot is using both error displacement and rate in his compensating control actions.

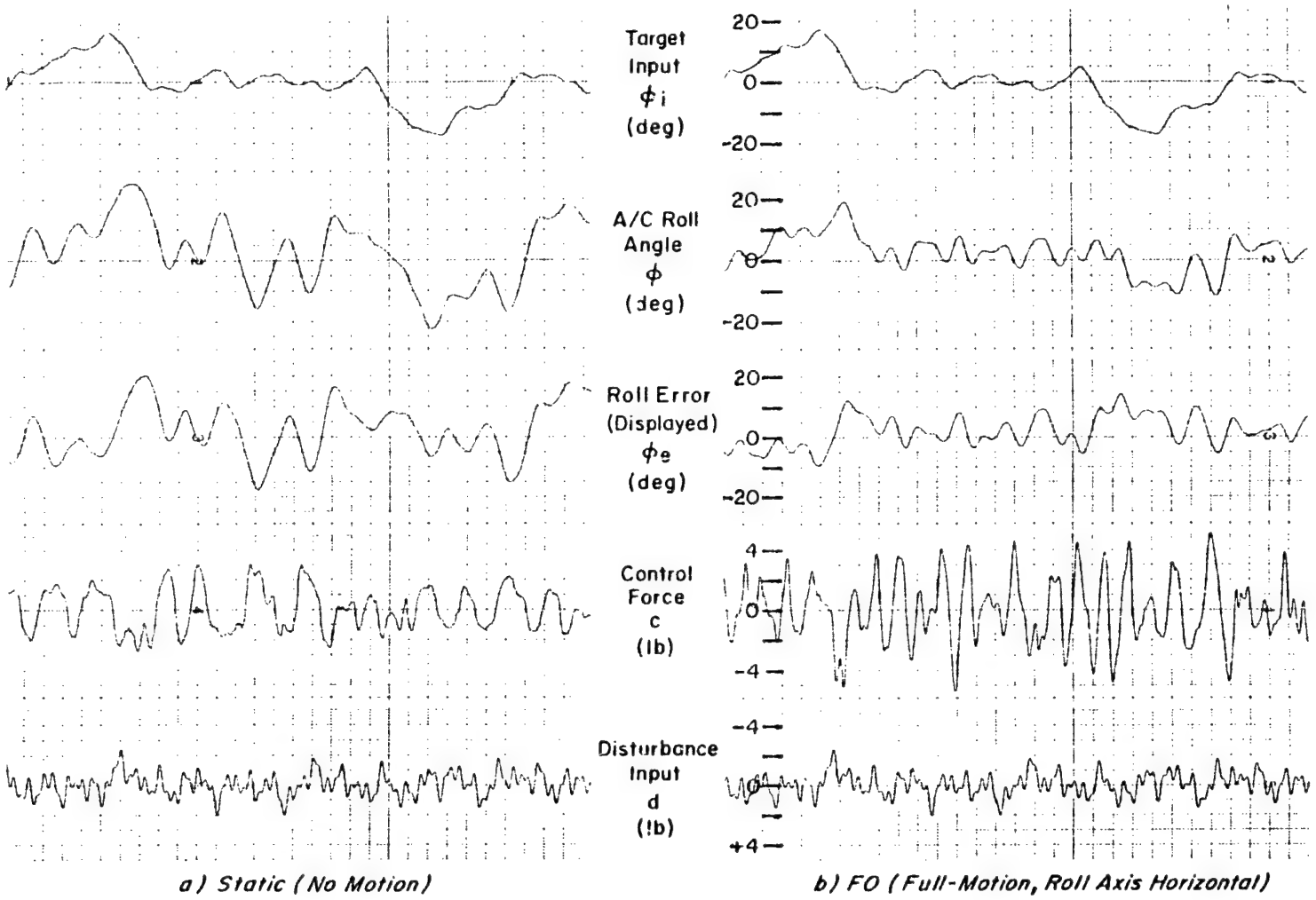

Figure 5. Typical Time Histories with N- and Full-Motion

- Comparing the motion case to the static case, the control response is obviously a more aggressive and higher bandwidth (due to motion cues), while the tracking error is reduced.

- (Not shown) There is a remarkable consistency in the D, E and C traces for repeated portions of the same inputs, showing a highly input-coherent and consistent operator response, as will be shown by the reduced data, later.

Frequency-Domain Data

Examination of the individual error scores and closed-loop describing functions showed that each of the subjects adopted similar behavior and so the results could be validly averaged, without loss of significant details in the average. Thus, approximately four runs each of four subjects were averaged for the data shown (a few runs were dropped due to data problems). The data shown here for the Full Motion Case with roll axis at 0 degrees (FC) is genuinely typical of all the cases investigated and was not selected as the best-examples available.

Spectra. — Figure 6 shows power spectra for the control stick, displayed error, and aircraft bank angle. The remnant shown (plotted at forcing function frequencies by the X symbols) is actually an average over neighboring (non-overlapping) estimates. The small standard deviations shown for all signal components indicate that all subjects had essentially the same, low variability, behavior. The signal-to-noise ratio is quite good at all but the very highest frequencies and implies a high coherency between the two inputs and responses. This permits the major part of the responses to be described by linearized describing functions. Notice that the spectrum of Φ_{plant} is large at low target frequencies (to follow the target) while its spectrum at low disturbance frequencies (◇) is lower, as desired.

Closed-Loop Describing Functions. — Figure 7 illustrates typical closed-loop describing function data (to which the model was fitted by the MFF procedure described earlier) for the control stick and task error responses to target and disturbance inputs. The frequencies used in the model fits are indicated by the arrows labeled "Fitted Freqs". Not all data points were used for computational economy. A preliminary analysis indicated that the selected frequency response points were the most sensitive indicators of pilot behavior.

Generally, the closed-loop data exhibit very low variability and the model fits capture every nuance of all the responses, using one set of model parameters and the various closed-loop relationships (e.g., in Fig. 2). The wiggles in the describing functions due to various low-damped modes, would greatly complicate simple interpolations between target frequencies to obtain vectors at disturbance frequencies, as done by earlier investigators (Refs. 4, 5).

Model Fits. — Table 5 summarizes the model parameters fit to the data for all dual-input cases. Only nine of the twelve parameters in Fig. 3 were

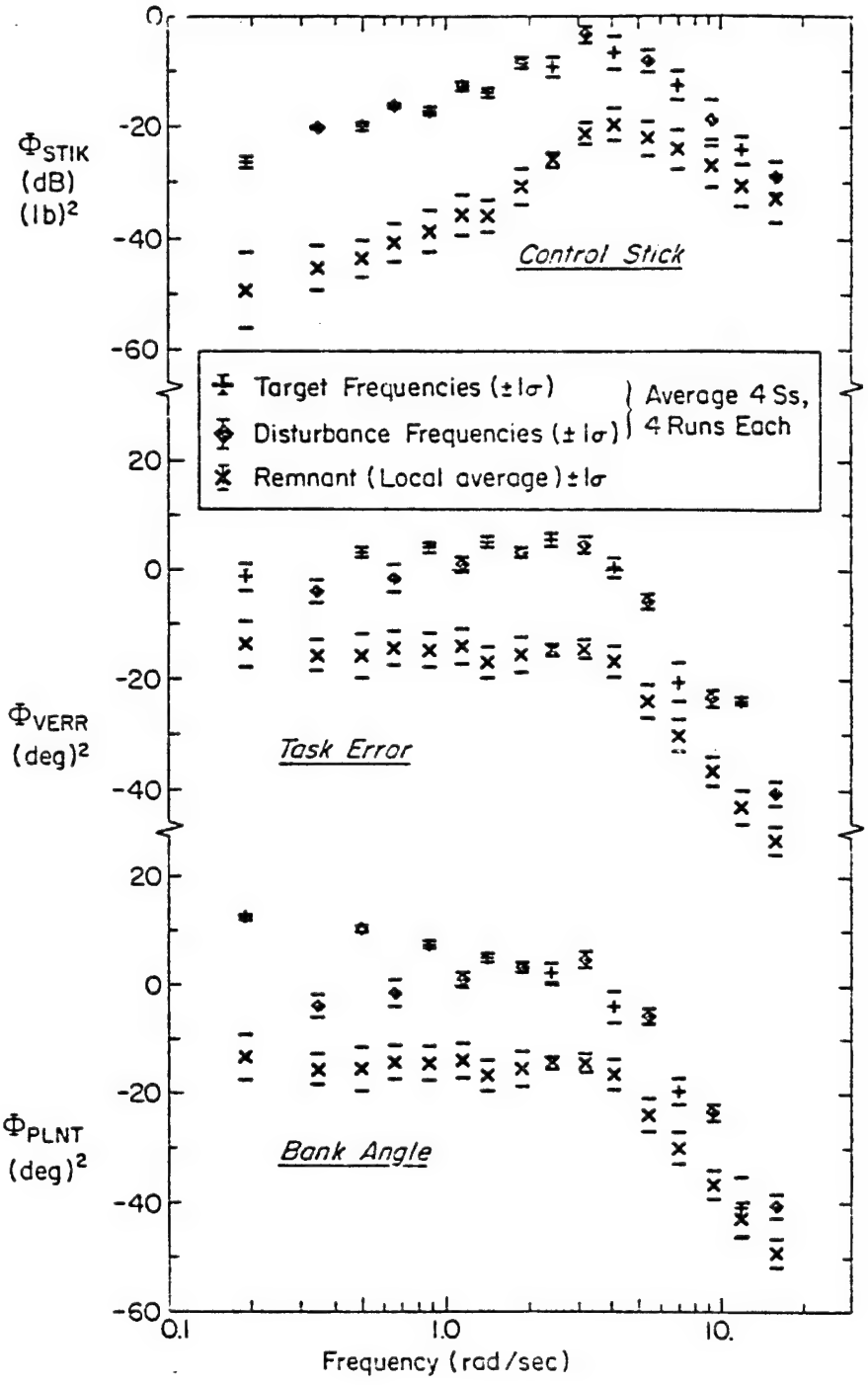

Figure 6. Typical Power Spectra for Full Motion, Erect (Case FO)

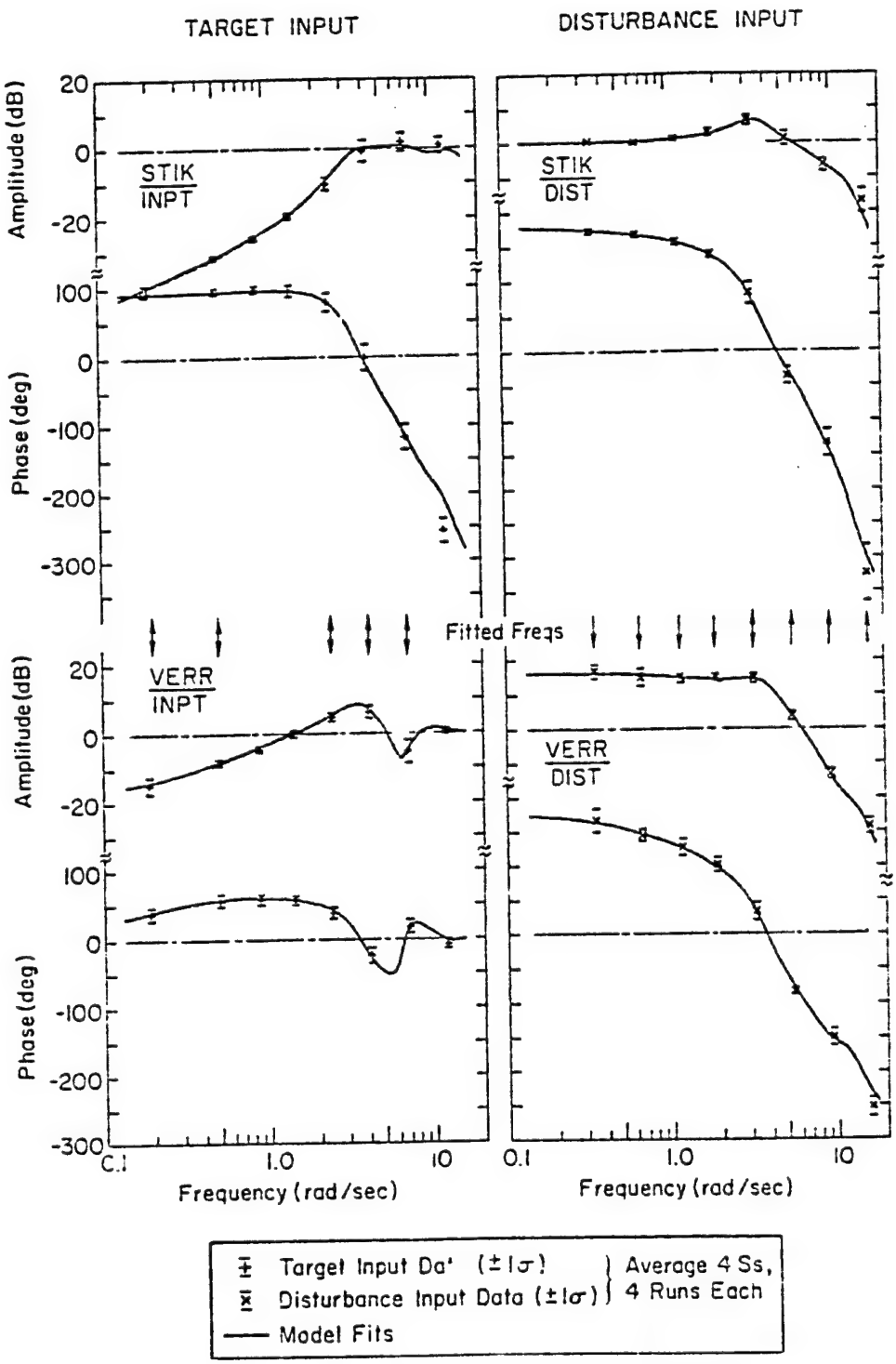

Figure 7. Typical Closed Loop Describing Function Data and Model Fits for Full Motion, Erect (Dual Input, Case FC)

TABLE 5. SUMMARY OF MODEL PARAMETERS FIT TO DATA

CASE Motion Condition	MODEL PARAMETERS												REMARKS
	Visual					Motion			Neuromuscular				
	K_D	K_R	τ_V	$\frac{K_R}{K_D}$	$\frac{K_R}{K_D} - \tau_V$	K_T	K_V	K_A	τ_M	ζ_N	ω_N	$\tau_M + A_1$	
	$\frac{lb}{deg}$	$\frac{lb}{deg/s}$	sec	sec	sec	$\frac{lb}{deg}$	$\frac{lb}{deg/s}$	$\frac{lb}{deg/s^2}$	sec	—	$\frac{rad}{sec}$	sec	
FgO Real World	0.149	0.068	0.16	0.46	0.30	-.0001	0.076	0.026	0.15	0.26	9.3	0.20	Theor. $K_T \approx 0$
FO Full Motion	0.156	0.074	0.15	0.54	0.3	0.022	0.076	0.026	0.15	0.29	10.4	0.30	$\tau_M + A_1$ = Effective Delay
W2 2nd Washout	0.134	0.090	0.12	0.67	0.55	0.023	0.048	0.019	0.11	0.39	7.6	0.22	
W1 1st Washout	0.150	0.079	0.12	0.61	0.49	0.034	0.060	0.023	0.11	0.38	7.6	0.21	
W', A 1st Wash + Atten.	0.119	0.070	0.08	0.59	0.51	0.046	0.081	0.031	0.17	0.38	9.0	0.25	
A Atten. Motion	0.122	0.065	0.06	0.53	0.47	0.092	0.151	0.058	0.15	0.15	8.2	0.19	K_T, $K_V \approx$ twice Values for FO
SO Static	0.072	0.064	—	0.89	—	—	—	—	0.18	0.18	7.0	0.25	

(K_1, F_1, A_2 set to 0)

needed, as preliminary fits showed that a second order fit was sufficient for the neuromuscular mode ($T_N = 0$) and there appeared to be no error integrating action ($K_I = P_I = 0$). Lack of K_I and P_I (the so called α-effect in the Extended Crossover Model) may have been due to presence of the tilt cue in the motion cases with roll axis at 4 deg, but its absence at F90 and Static conditions is unusual.

The additional columns in Table 5 detail the effective lead time constant in the visual path ($T_L = K_R/K_D$) and the effective time delay in the neuromuscular path ($\tau_e \doteq \tau_M + A_1$). Note that the visual displacement gain, K_D, nearly doubles when going from Static to any Motion condition, and the tilt sensitivity, K_T, is negligible for the F90 case, as it should be, since no tilt cue is available.

Opened-Loop Describing Functions. — A number of other trends and covariations among parameters are evident; however, these effects can best be illustrated by using the "opened-loop" responses calculated using the measured closed-loop data along with the loop structure of Fig. 2 or the parameters in Table 5 with the model of Figs. 2 and 3. Figure 8 shows the resulting "opened loop" data and computed model curve for the Full Motion, F90 Case. As with the closed loop responses the model curve fits the actual "opened-loop" data very well — it truly represents the data. These data and fits for this example are typical; i.e., the other cases show effects similar in kind, differing only in degree. Thus, comparisons among cases can be made using the curve fits, as we will do in the remainder of this paper.

These multiple "opened-loop" describing functions have all of the appearance and significance of single open-loop transfer functions, and similar descriptive parameters apply. Some of these have been labeled in Fig. 7, as defined below:

ω_u = "unstable frequency" (180 deg phase crossover). This sets the maximum bandwidth of the loop, and is the frequency at which oscillations set in if the gain were further increased by K_M dB.

ω_c = "crossover frequency" (0 dB gain crossover). This sets the effective bandwidth of the loop, and determines the resulting stability margins.

K_M = "gain margin" — allowable gain increase for incipient loop instability.

γ_M = "phase margin" — allowable phase lag for incipient loop instability.

In Fig. 8, it is apparent that the disturbance loop (dominated by the motion pathway) has a higher bandwidth and lower phase margin than the target loop (dominated by the visual pathway). This implies lower tracking errors, as will be shown later.

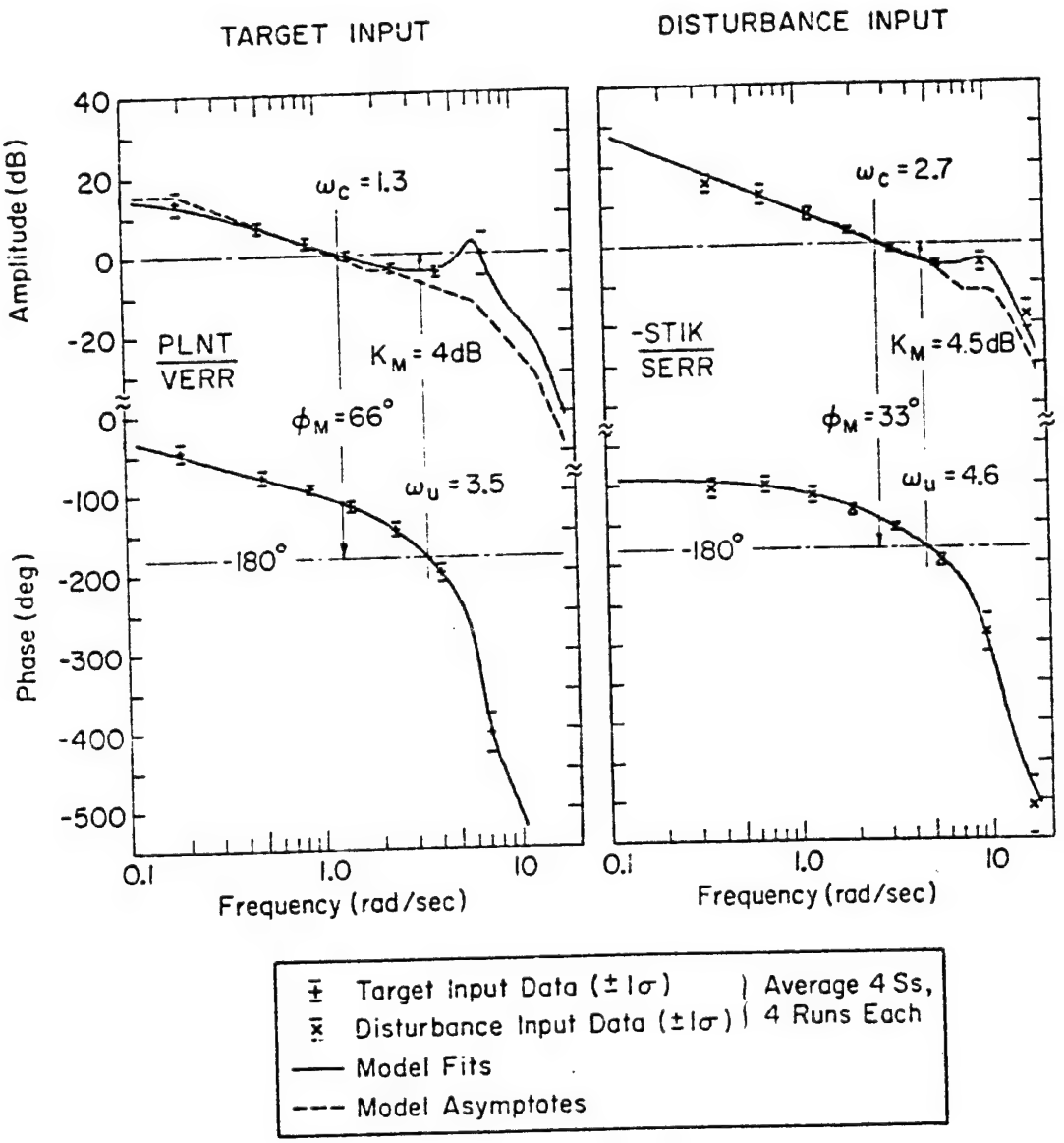

Figure 8. Typical Effective "Opened Loop" Data and Model Curve for Full Motion, Erect (Dual Input, Case F0)

The kinks in the dashed "asymptotes" in Fig. 8 show the poles (break downwards) and zeroes (break upward) of the model. The need for the relatively high order pilot-vehicle model used here is clearly shown by the spread between the asymptote breaks and the model fits as well as the different asymptotes in each "opened-loop."

Effects of Full Motion vs. Static Conditions

Figure 9 compares various performance measures for Full Motion and Static cases. Variances are used because they can be partitioned into summable vector components due to: Target, Disturbance and Remnant. Concentrating on task error, Fig. 9b, for the STATIC Case, the error components from Disturbance (D) and Target (T) inputs are essentially the same, reflecting the dual input spectrum design objective mentioned earlier. For the Full Motion at 90 deg (F90) case the target errors (T) are the same as for a Static cab, while the disturbance errors (D) are much smaller. Going from Full Motion, at 90 deg to the 0 deg (F0) case shows that the target following errors (T) are reduced slightly while the disturbance errors are unchanged.

These basic trends in the tracking performance are explained by the changes in the opened-loop describing functions (DF) shown in Fig. 10. For the Target Input DFs the Supine and Static cases having no tilt cues show essentially the same DF (which results in the same target following errors) whereas the Erect case (with the maximum tilt cue) has a smaller target error. For the Disturbance Input DF both motion cases (F0, F90) have the same DF, which explains why their "D" components were the same in Figs. 9a,b,c,d. Furthermore, the "Rate Cue Effect" (lower loop lags leading to higher crossover frequencies with motion) leads to the motion/static performance effects denoted by the arrows. Thus Figs. 9 and 10 show that the subjects used motion cues to improve performance in two main ways.

- The lower lags (and higher ω_u) permitted by the vestibular sensory-motor loop enables, in effect, a "roll-rate damper loop" to be closed by the pilot, thereby allowing a tighter disturbance regulation loop to be used by him (a loop gain increase of about 2.7/1.7 = 1.6). Consequently, the disturbance variance is reduced significantly.

- The tilt-cue was used at low frequencies to provide a sense of zero reference and, thereby, to avoid drifts and overshoots, the effects showing up as a low frequency phase reduction on the target "opened-loop."

Components of the Multiloop Describing Function Under Motion

Further insight may be gained into the complexity of the multiloop interactions and motion effects via Fig. 11, in which the fitted model has been used, via the loop structure and equations of Fig. 2, to examine: each

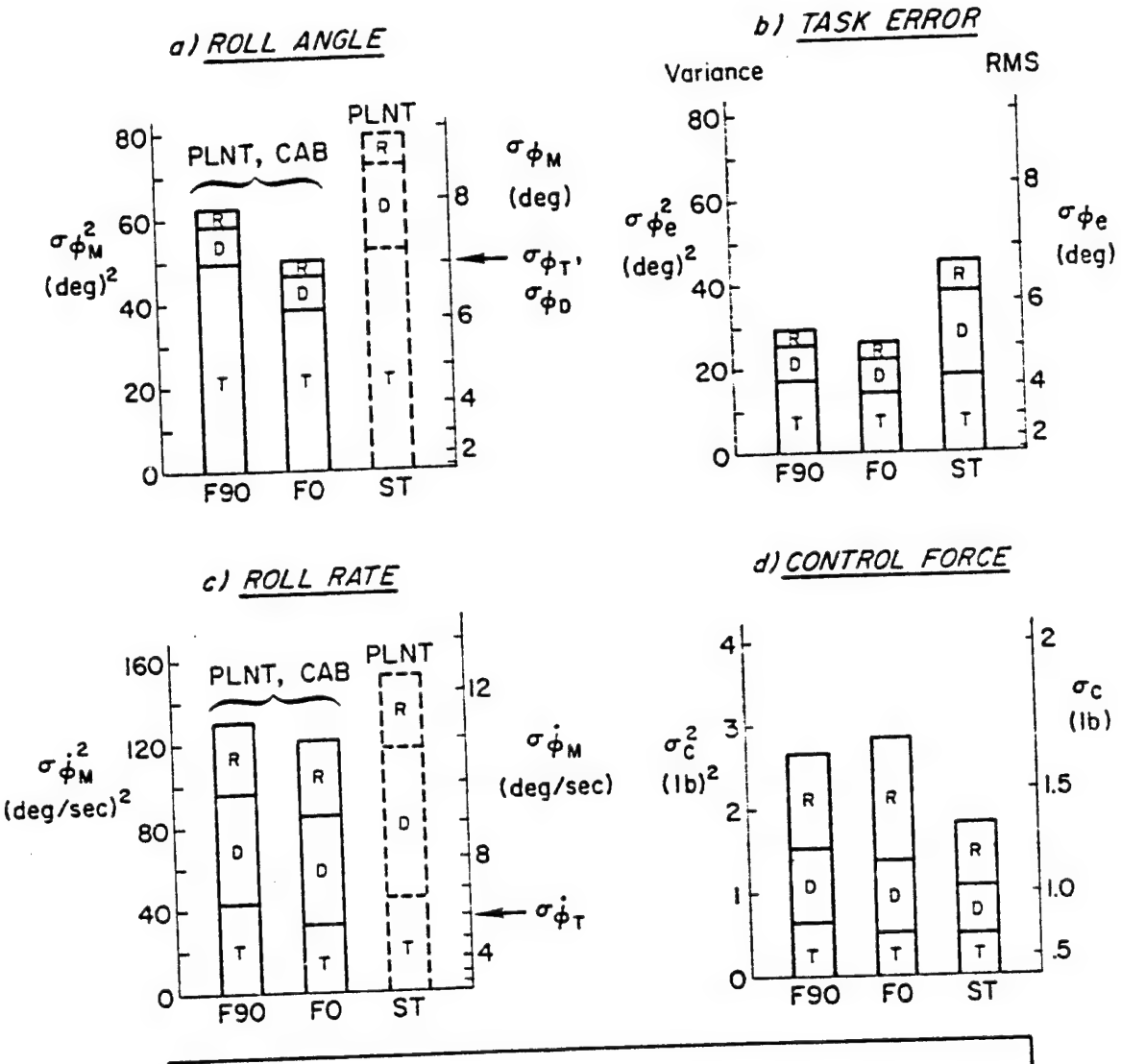

Figure 9. Effects of Full Motion (Supine, Erect) and Static Cases on Performance

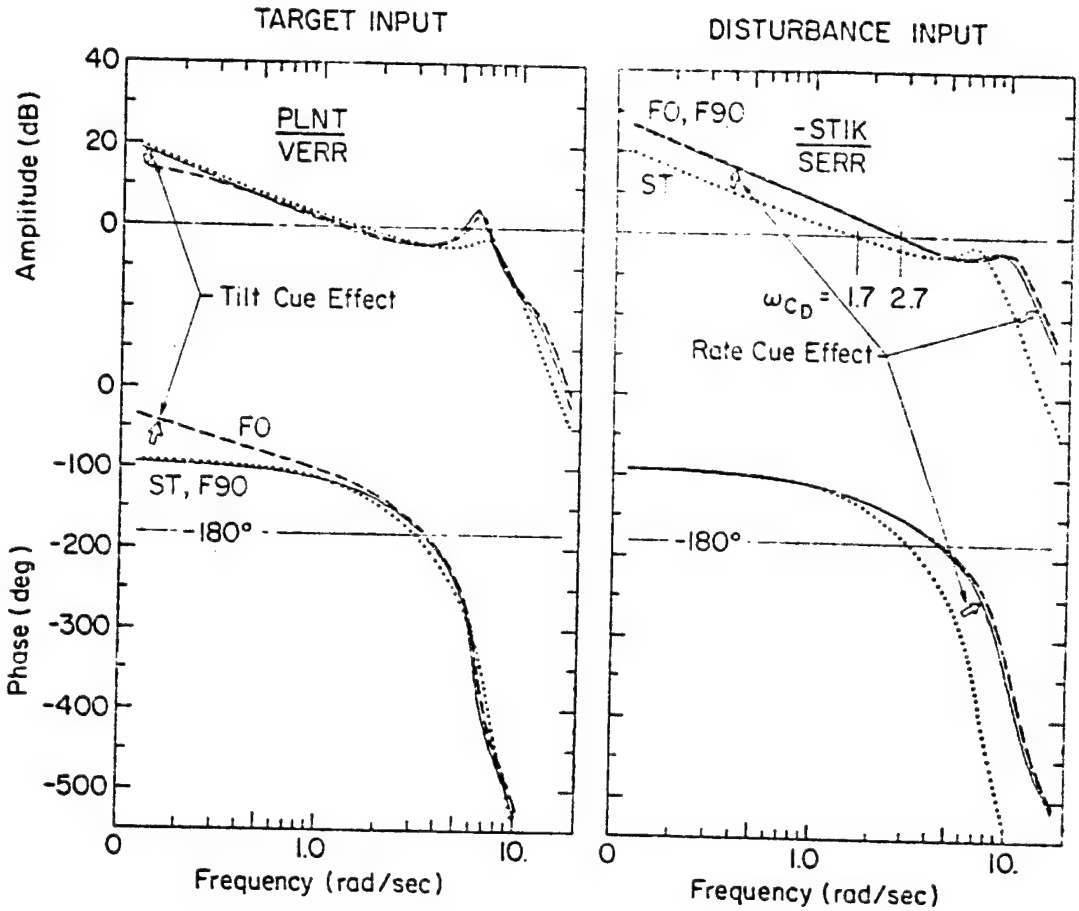

Model Fit	Case	
———	F90	Full Motion, Supine
— — —	FO	Full Motion, Erect
·····	ST	Static

Figure 10. Effect of Motion Cues on "Opened Loop" Describing Functions (Dual Input Cases)

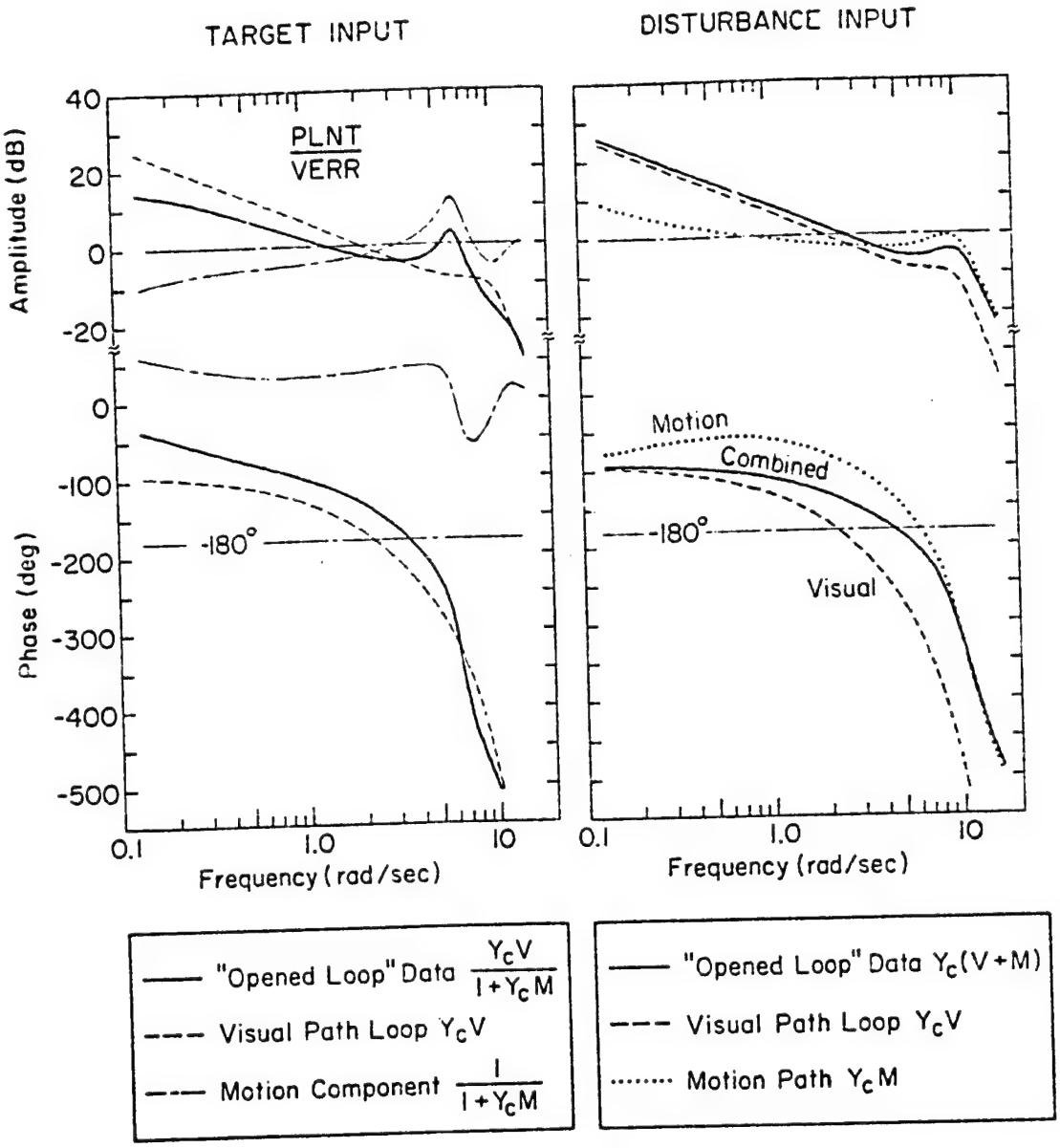

Figure 11. Behavioral Components of "Opened Loop" Data
(Dual Input, Full Motion Erect Case F0)

sensory loop individually (visual = dashed, motion = dotted) with the other simply turned off, and then the combined "opened-loop" (solid line) as discussed earlier in Section II-C. Remember that the "opened-loop" DF is a complex vector function of V and M, as noted in the legend.

Without going into details, the key points revealed by Fig. 11 are as follows:

- The Disturbance Input loop (on right) is a simple vector sum of VY_c and MY_c. The flat amplitude of the motion loop (dotted) shows that MY_c acts like a roll-rate feedback loop with an effective time delay, τ_e, appreciably less than the visual loop (for MY_c; $\tau_e \doteq .20$ sec, for VY_c; $\tau_e \doteq .20 + .15 = .35$s). Over the important crossover frequency region of 0.5-5.0 r/s, their vector sum (solid) has an apparent τ_e even <u>less</u> than MY_c alone! This is consistent with and "explains" the results of Stapleford (Ref. 1) and Shirley (Ref. 2).

- At low frequencies the Disturbance regulation (solid) is dominated by (closest to) the visual loop at low frequencies and motion loop at high frequencies.

- The Target following loop (on the left) is a more complex function of VY_c and MY_c as seen in the equations in the box. (The motion component $(1 + Y_cM)^{-1}$ is shown dash-dotted to distinguish it from Y_cM alone. Here, the solid curve is the vector <u>product</u> of the two components). In both amplitude and phase, the Target following loop dynamics are dominated by the visual loop (dashed) at all frequencies.

- A comparison (not shown here) of the purely visual static case <u>per se</u> (dotted curve of previous Fig. 10) and the isolated VY_c (dashed curve of Fig. 11) shows that they are <u>not</u> the same. When <u>motion is present</u>, the visual loop can be (and is) operated at higher gains, albeit with a slightly larger lead equalization (T_L) and consequently larger τ_e. (Per Table 5, $T_L \doteq 0.89$ sec and $\tau_e \doteq 0.23$ sec for the ST case; while $T_L = 0.54$ sec and $\tau_e = 0.20 + 0.15 = 0.35$ sec for the FC Case).

This analysis of Fig. 11, and others like it, clearly shows that one cannot simply add a motion feedback loop to the static case dynamics to get the combined result. Instead the operator optimizes his combined loop properties for the case at hand.

Effects of Single vs. Dual Forcing Functions

For some Full Motion cases (F90, F0), data were taken for Target input alone; and for Case F90, Disturbance input alone, to compare with the dual input case. When either input was used alone, it was increased by the square-root-of-two to keep the rms input the same as in the dual input case.

In general one might expect that if the disturbance alone were present, the pilot would adopt a different optimum behavior, because all he would have to do is to suppress both the felt and seen motions. Conversely, for the target alone, the pilot might more agressively track the error, because the unseen disturbances were absent.

The results, shown in the opened-loop describing functions in Fig. 12, did not follow these expectations! For simplicity, the curve in Fig. 12 is that fitted to the corresponding dual input case, for which it passed precisely thru every data point on both sets of DF (e.g., see Fig. 8). The single-input data are shown relative to this dual-input curve in Fig. 12, remembering that each of the data plots represents a different set of runs. Somewhat to our surprise, the single input data are not significantly different from the dual input case, for the points generally lie within one symbol width of the curve and almost all lie well within ± 1 standard deviation of the dual-input curve.

How can this be, in the light of the theoretical expectations discussed above, considering that all pilots were given plenty of practice on every case, and noting that all behaved similarly (evidenced by the low scatter)?

Some hypotheses are:

- The "optimum" behavior was, perhaps fortuitously, nearly identical for the single and dual input cases. The combination of lightly damped modes in the controlled element near the neuromuscular modes plus stick lags has been identified as the so-called "Pilot Induced Oscillation Syndrome" of Ref. 9. These restrict the degree of equalization which can be used by the pilot to improve performance. Consequently, he may be operating near this constrained limit in all cases.

- The pilots were so overtrained in the dual case that they did not adapt "optimum" behavior in the single input cases despite plenty of practice with it. If so, this raises questions with respect to the assumption that pilots adopt an "optimum" behavior.

- There was some error in the experiment, such that dual inputs were really present. We checked this and verified that only the specified single input spectra and rms signals were present.

Here is an ideal, simple test case against which to validate the optimal adaptation models (e.g., Ref. 4). The inputs are analytically tractable, the good model fits show that the data are representable by linear, modest-order state equations, and the data are precise, have high signal-to-noise, and are internally self consistent. Such a validation remains as a future task.

Meanwhile, this result tentatively implies that the dual-input results should apply to the single input situations, if the inputs and controlled elements are similar to those used herein.

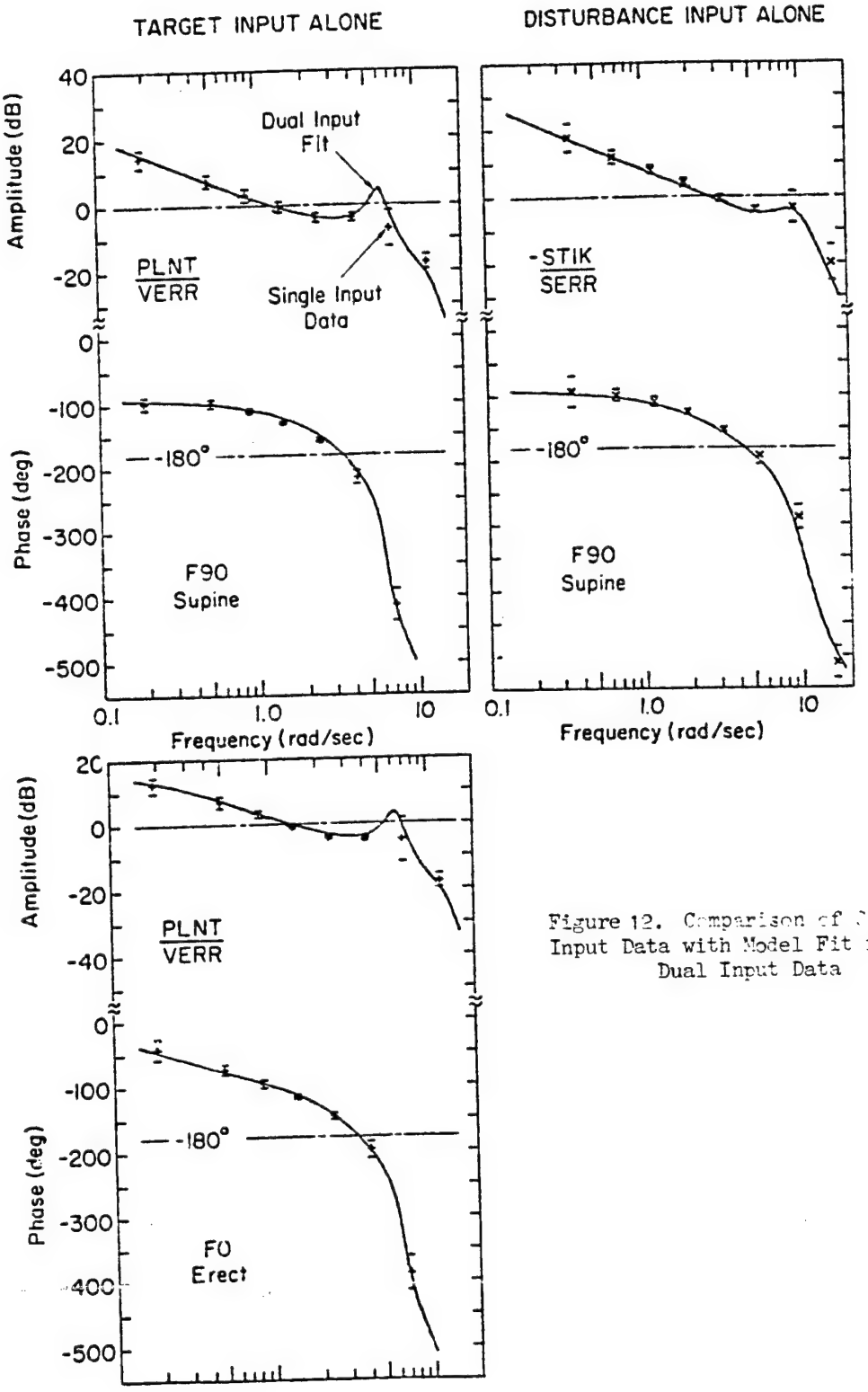

Figure 12. Comparison of Single Input Data with Model Fit from Dual Input Data

Effects of Motion Shaping (Washouts)

Having presented the results on our first question — that of basic motion effects vs. no motion, we turn now to the second question: What are the effects of various motion "shaping" (attenuations and/or washouts)? For this purpose, the data will be restricted to the dual-input cases, all with roll axis horizontal, i.e., FO, W2, W1, W1A, ATT, in the order of decreasing recovered roll angle.

Figure 13 shows various performance measures for these cases. Consider first the variance of recovered (measured physical) roll angle, $\sigma^2_{\phi_M}$, shown at the upper left, each case broken down in terms of the components due to target, disturbance and remnant. Noted on the margin are the variances for the target (or disturbance) alone, and their sum. Ideally, the recovered variance would consist of only the target component (equal to $\sigma^2_{\phi_T}$, attenuated by the motion shaping washout) and no disturbance or remnant portions. It may be recalled from Fig. 9 that in the (real-world) "F-90" case this ideal is approached, in that the target component nearly equals the commands, while the disturbance and remnant portions were small fractions of that.

With these standards in mind, let us consider the effects of various washouts. As described in Section II on Experimental Design, the overall scheme was to select different forms of motion washout, each selected (albeit crudely) to give the same attenuation of roll angle to about 50 percent of the basic, FO, case (i.e., the target roll variance of 1/4 of the basic level). As seen in Fig. 13a, this was achieved closely only for the pure attenuation case ($\sigma_{\phi_M} \doteq 3.6$ deg vs. $\sigma_{\phi_T} \doteq 7.0$ deg). The ATT computed roll motions (shown dashed) were nearly equal to the FO case, as were the other task performance measures in Fig. 13 (e.g., tracking error and control force) implying a close matching of the visual and motion-loop behavior in the basic and ATT cases, despite the lower magnitude of motion cues in the latter. (More on this later).

The Second Order Washout (W2) (which greatly attenuates the lowest frequencies) distorted the perceived motion cues (per the subjective questionnaire) and failed to reduce the motions as intended. Analysis of these results showed that this was due to the following reasons:

a. The washout was a compromise design* such that the high-frequency asymptote magnified the roll angles (and rates) above the break frequency of .85 r/s by a factor of about 1.2, causing the roll rate variance (Fig. 13-c), and high frequency portions of the roll angle variance, to be increased by $(1.2)^2 = 1.4$ relative to the intended case.

* The DES is a velocity system and as such would drift whenever a cascade washout was used. Consequently, a feedback scheme was devised that approximated the desired cascade washout but a perfect match at both high and low frequencies was not possible.

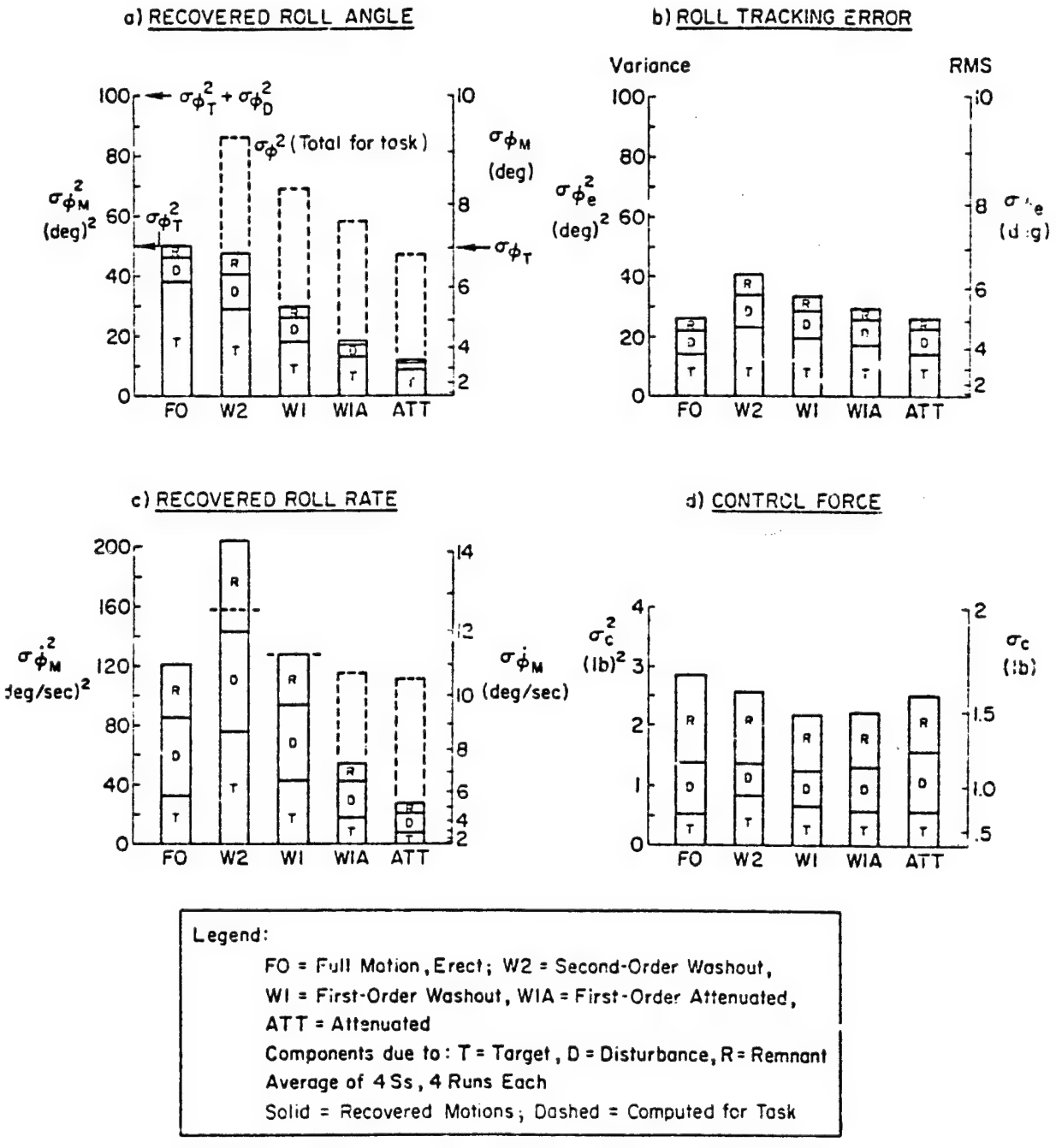

Figure 13. Effects of Motion Shaping on Performance

b. The distortion of the felt motions relative to the visual motions caused the pilots to perform even worse than in the static case.

The other washouts were intermediate in recovered motion and plant motion between the Full and Attenuated cases.

Attenuation reduces both the recovered roll angles and roll rates in the same proportion, but washout reduces mainly the low frequency components and, thereby, reduces the roll rates less than the roll angles. This can be seen by comparing Figs. 13a vs. 13c for the W2 and W1 cases, especially.

Except for the anomalous W2 case, discussed above, the performance measures of tracking error and control force were not significantly different among any of the first order or attenuated wash out cases (See Figs. 13b and 13d. Even the proportions of each variance due to: target inputs, disturbances, and remnant were about the same as for the full motion case (FC).

Further insight into the pilot's tracking behavior under these washouts is given by the opened-loop describing functions in Fig. 14. It is immediately apparent that the disturbance-loop describing functions are nearly identical, implying the following:

- Despite attenuated, reduced-low-frequency motions, and phase distortions, the pilot compensated to give the same opened-loop DF.

- In the ATT case, the rms roll angle was reduced from 7 deg to 3.6 deg, the pilot had double his tilt and roll rate gains, (K_T, K_V) as verified by the fitted coefficients in Table 5, and summarized below:

Case:	σ_ϕ	K_T	K_V	K_A
FO	7°	.022	.070	.022
ATT	3.6°	.056	.131	.028
Ratio: (ATT/FO)	.51	2.55	1.87	1.27

Despite the fact that the rms tilt angle in the ATT case represents a lateral-specific-force cue of less than $3.6/57.3 = .063\ g_y$, the roll rates were apparently sufficiently high to be readily sensed and used to compensate for the reduced motion cue over the FO case.

On the left of Fig. 14 is the target-loop DF, where the following effects of washout are clearly apparent:

- the FO and ATT cases are nearly identical for the same reasons given above for the invariant disturbance loop DF.

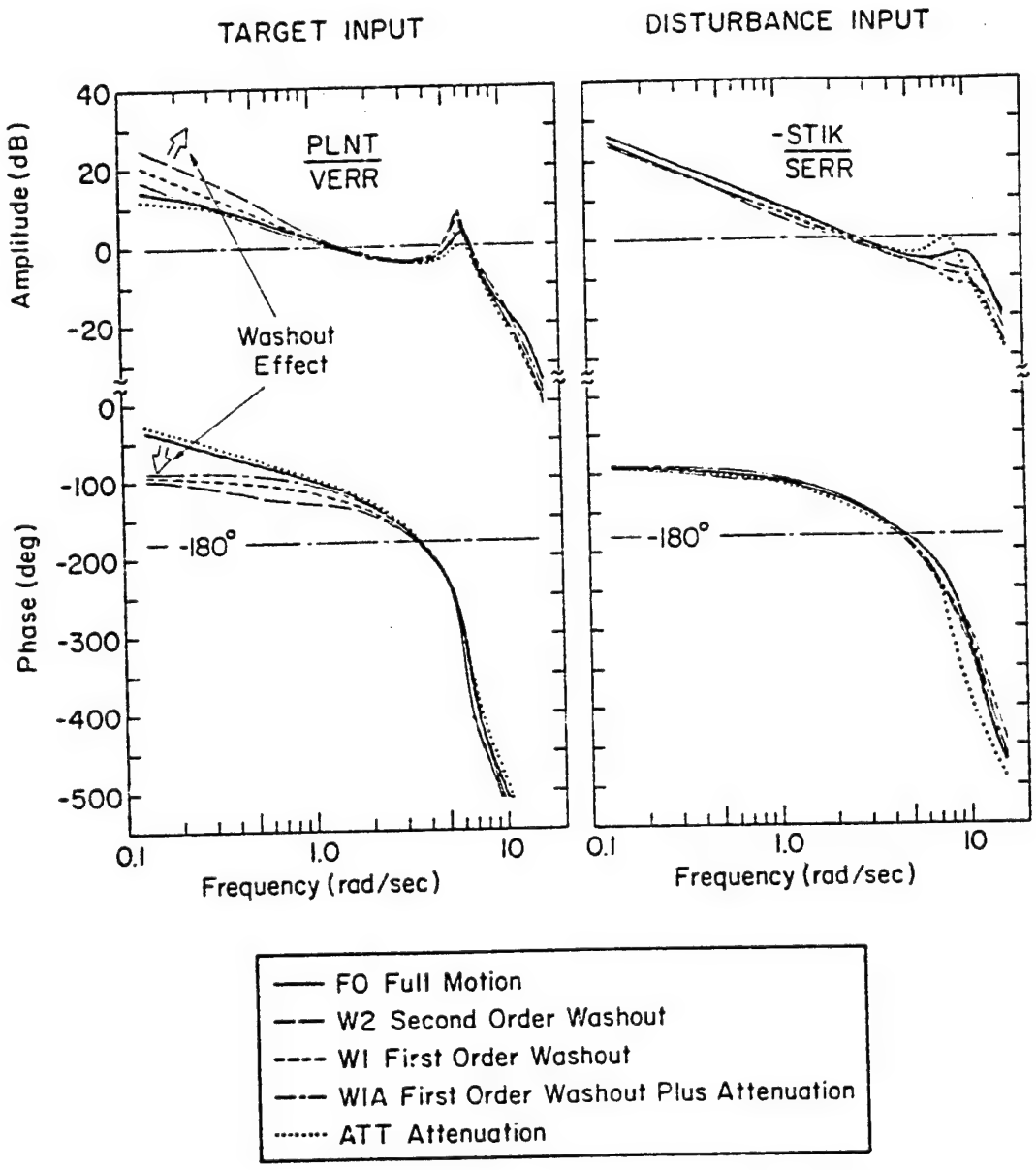

Figure 14. Effects of Motion Shaping for "Opened Loop" Describing Function (Dual Input Cases, Roll Axis Horizontal)

- the other washouts induce (at low frequencies) higher amplitude ratio and more phase lag as the washout degree is increased from ATT, to W2. An analysis indicates that these trends reflect fairly complex interactions similar to that of Fig. 11 (Left side). Note that inserting a low frequency washout to the motion path (M in Fig. 11) causes the resulting curve to start (at low frequencies) on the dashed curve and transition to the solid curve with increasing frequency. These amplitude and phase trends explain the "Washout Effect" in Fig. 14.

Optimum Washout

One of the objectives of this experiment was to find the optimum washout for AMRL's roll-only simulators. The desirable criteria are relative to the "real-world" case: a) significant reduction in roll amplitude and rates, and b) similar pilot behavior and performance.

Inspection of the foregoing results reveals that the clear choice is the first-order attenuated washout (W1A). Figure 15 justifies this selection based on the following comparisons with the F90 ("real-world" baseline) case:

- Large reduction is recovered roll-angle and rate — as shown in Fig. 15a — with similar plant roll angles and rates.
- Very similar tracking error performance and control activity, as shown in Fig. 15b and 15c. Even the distributions of mean variance from target, disturbance, and remnant inputs is closely matched.
- The opened-loop describing functions, shown in Fig. 15d, are practically identical. This is because the effect of tilt cue usage previously described in connection with Fig. 10, is almost exactly cancelled by the washout-break effect noted in Fig. 14.
- (Not shown) The subjective comments were more favorable for this washout than any other except pure attenuation.

Thus, we recommend first-order attenuated washout for use on all AMRL roll-only type simulators. The degree to which this form can be extended has not been determined, but the data suggest the following as likely to be both useful and satisfactory to pilots:

- Attenuation factor of 0.5 to 0.7
- Break frequency of 0.3+ to 0.5 rad/sec (Washout time-constant of 2-3 sec).

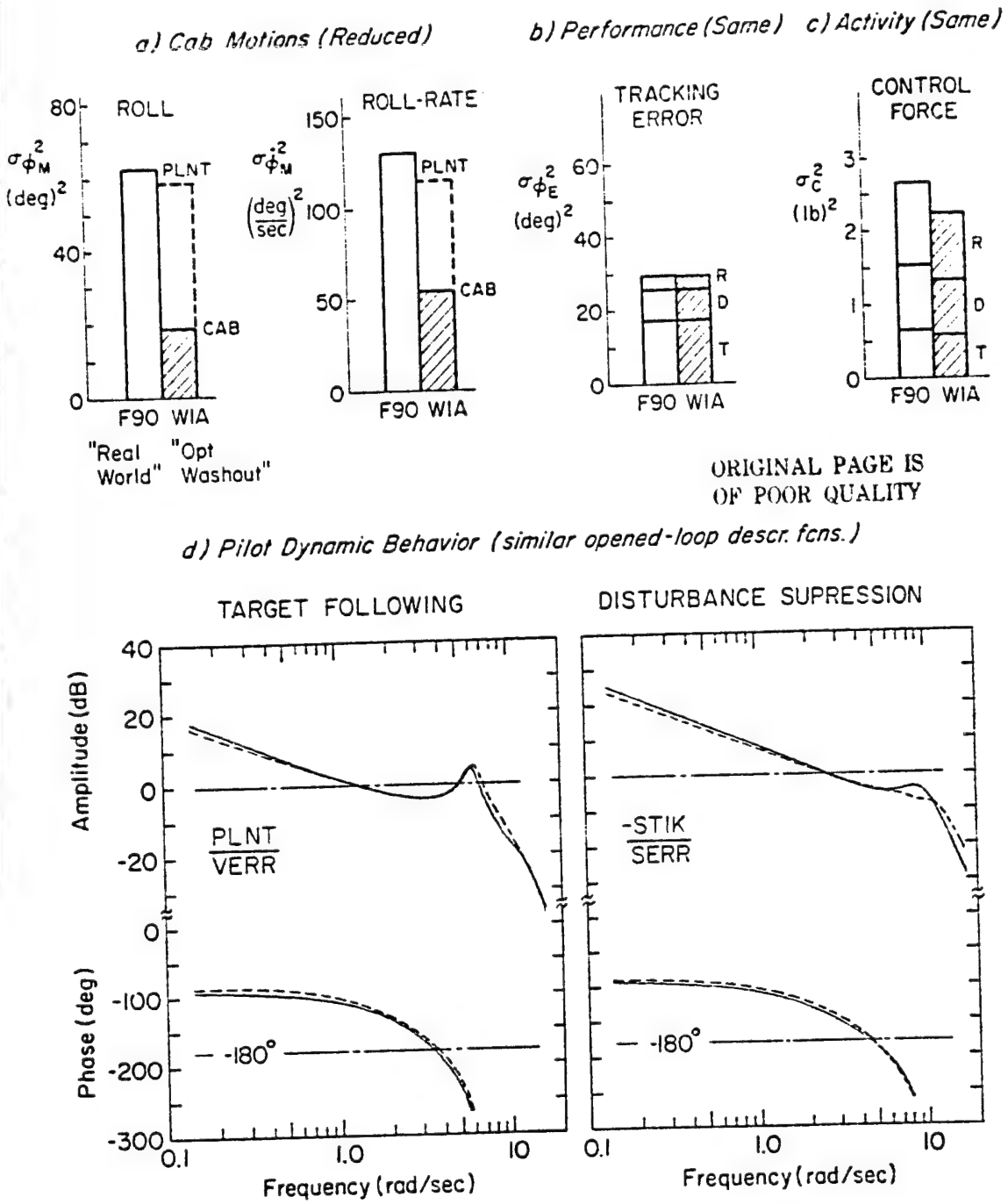

Motion Fit	Case	
———	F90	"Real World", Full Motion, Supine
- - - - -	WIA	Optimum Washout (first order washout plus attenuation)
		1/T = 0.4 rad/sec, Attenuation = 0.7

Figure 15. Comparison of Optimum Washout with "Real World" Case

CONCLUSIONS

This research has covered several very well trained subject's responses to a variety of motion cases in a roll-only motion simulator, with simultaneous target and disturbance inputs. The results presented here support the following conclusions:

1. Across all seven conditions the four subjects were very consistent in their tracking behavior and scores, providing an exceptionally, reliable, and definitive data base worthy of detailed analysis, even beyond that performed herein (e.g., on remnant effects).

2. The multiloop model structure presented in Fig. 1, which has both visual, motion and (a common) neuromuscular dynamic elements, proved capable of accurately fitting the closed- and "opened"-loop describing functions at all measurable signal points within the loop. In combination with the interleaved sum-of-sinusoids target and disturbance inputs the new STI Multiloop Fitting Program (MFP) provided efficient fits of 10 parameters in a multiloop situation which had heretofore been very difficult to fit because of the complex interactions involved between the visual and motion feedback paths.

3. Untangling the closed-multiple loop describing function data in the "opened-loop" manner shown here provides a ready comparison with traditional single open-loop data. Similar effects (e.g., the Crossover-law adaptive behavior) are shown for the dual input case, with the disturbance loop having the higher bandwidth (limited mainly by the controlled element and vestibular rate-sensing dynamics).

4. After lots of analysis and digesting of complex trends in the various cases, the key to understanding it all seems to be the following:

   - Given reasonable rate motion cues at frequencies above about 0.5-1.0 rad/sec, the pilot's motion feedback system acts like an adaptive roll-rate damper with a bandwidth of nearly 3 rad/sec. This tends to suppress disturbances but opposes target following motions, while stabilizing both loops.

   - The pilot then uses sufficient extra visual compensatory (error correcting) gain to follow target commands as well under motion as in the static case, and with less remnant and disturbance components.

5. The affects of motion are consistent with the prior work of Stapleford (Ref. 1), Shirley (Ref. 2) and Levison et al (Ref. 4), while extending this work to the new case of equally strong target and disturbance inputs each having comparable apparent spectra at the display.

6. The describing functions and fitted tilt-cue parameter clearly showed that the spurious tilt cues from rolling with roll-axis horizontal are used, even though the rms lateral specific force was in some cases much less than 0.1 g. A very simple model for the use of this cue is given. Nevertheless, use of this cue resulted in only small improvements in tracking performance in this random-input tracking task.

7. The four types of motion washout investigated (second-order, first-order, first-order-attenuated, and purely-attenuated) showed distinct effects compared to the "real-world" reference case of full motion about a vertical roll axis; the second-order case was the least desirable because of large differences in performance, behavior, (describing functions) and subjective ratings. The other cases provided roughly similar performance measures with some small differences in relative remnant, describing functions, and ratings.

8. The pilots clearly adapted differently to the various washouts, thus complicating the job of predicting the net effects for a given washout.

9. The optimum washout for roll-only-simulators (from the standpoint of performance, behavior and ratings similar to the "real-world" reference case) was clearly the first-order, attenuated washout. Recommended parameters (for this type of task) would be: attenuation factor 0.5-0.7, and washout time-constant of 2-3 seconds (break at 0.5-0.5 rad/sec).

The data base for this paper is being prepared for permanent filing and general access at the U.S. Defense Documentation Center (DDC); and may be requested through the third author, at AMRL.

It would be interesting and fruitful to analyze and model the remnant portion of these data, using the closed-loop spectral data available (e.g., as in Fig. 6). Because the inputs were carefully selected and shaped to be representable by filtered white noise, various optimal-control-theories could be tested against this very consistent, accurate, and definitive data base. Finally, using these model and parameters (which precisely fit almost every data point,) various analytical manipulations of the data can be performed to gain further insight about pilot adaptation to motion cues and washouts.

REFERENCES

1. Stapleford, Robert L., Richard A. Peters, and Fred R. Alex, Experiments and a Model for Pilot Dynamics with Visual and Motion Inputs, NASA CR-1325, May 1969.

2. Shirley, R. S., "Motion Cues in Man-Vehicle Control," M.I.T., Cambridge, MA, Sc.D. Thesis, Jan. 1968.

3. Levison, W. H., S. Baron, and A. M. Junker, Modeling the Effects of Environmental Factors on Human Control and Information Processing, AMRL-TR-75-74, Aerospace Medical Research Laboratory, Wright-Patterson AFB, Ohio, Aug. 1976.

4. Levison, W. H. and A. M. Junker, A Model for the Pilot's Use of Motion Cues in Roll-Axis Tracking Tasks, Bolt Beranek and Newman, Inc., Cambridge, MA, Report No. 3528, Apr. 1977.

5. McRuer, Duane T., and E. S. Krendel, Mathematical Models of Human Pilot Behavior, AGARDograph No. 188, Jan. 1974.

6. Zacharias, G. L., and L. R. Young, Manual Control of Yaw Motion with Combined Visual and Vestibular Cues, presented at 13th Annual Conf. on Manual Control, M.I.T., Cambridge, MA, 15-17 June 1977.

7. Magdaleno, Raymond E., and R. Wade Allen, Modeling Biodynamic Effects of Vibration, AFOSR 75-1256 TR, July 1975.

8. Ashkenas, I. L., H. R. Jex, and D. T. McRuer, Pilot-Induced Oscillations: Their Cause and Analysis, Northrop Corp., Norair Div., Rept. NOR 64-143, June 1964 (AD 481994).

N79-15623

A METHOD OF MOTION SIMULATOR DESIGN BASED ON MODELING CHARACTERISTICS OF THE HUMAN OPERATOR

D. W. Repperger A. M. Junker

Aerospace Medical Research Laboratory
Wright-Patterson Air Force Base, Ohio 45433

Introduction

A problem of interest in the design of simulators is the development of a design criteria such that the simulators can be adjusted until they emulate real world situations. In this paper such a design criteria is obtained to compare two simulators and evaluate their equivalence or credibility. In the subsequent analysis the comparison of two simulators can be considered as the same problem as the comparison of a real world situation and a simulation's representation of this real world situation.

The design criteria developed here involves modeling of the human operator and defining simple parameters to describe his behavior in the simulator and in the real world situation. In the process of obtaining human operator parameters to define characteristics to evaluate simulators, measures are also obtained on these human operator characteristics which can be used to describe the human as an information processor and controller. Such modeling is motivated by the work of Fitts [1], Senders [2], Verplank [3], and others. First a study is conducted on the simulator design problem in such a manner that this modeling approach can be used to develop a criteria for the comparison of two simulators.

Symbols

$ST(t)$	Stick response of the human operator.
$\hat{x}(t)$	The Kalman filter's best estimate of $ST(t)$.
$\gamma(t)$	The residuals, innovations, or modeling error.
S	An approximation to signal power generated by the human.
N	An approximation to noise power generated by the human.

Symbols

$e(t)$, $E(s)$	The closed loop error signal and its Laplace transform.
ϕ	The discrete state transition matrix.
1σ	One standard deviation of a parameter estimate.
K_o	The Kalman Gain matrix.
A,B,H	The system gain matrices.
$x_1(t), x_2(t)$	State variables which describe ST(t) and $\frac{d}{dt}$ ST(t).
P,R,Q	Unknown covariance matrices.
$\hat{C}_k$	Sample covariance function (from the data).
$\hat{\rho}_k$	Sample, normalized autocorrelation function.
BW	An approximation to bandwidth of the human operator.

THE SIMULATOR DESIGN PROBLEM

In the comparison of two simulators or in the comparison of a simulator with a real world situation, an assumption is made as follows:

Assumption (1):
Simulator A = Simulator B if the human operator in Simulator A has the same "model characteristics" as the human operator in Simulator B.

The key term, "model characteristics" will be more explicitly defined via the modeling procedure. An alternative problem that can be solved via this procedure is the validation of a simulator in comparison to a real world situation. In this case the definition of simulator credibility is best described by assumption (2)

Assumption (2):
Simulator A = the real world if the human operator in Simulator A has the same "model characteristics" as the human operator in the real world situation.

In practice, the usefulness of assumption (2) has application if it is possible to take data in the real world situation as well as in the simulator. If the simulator can be adjusted so that the human operator parameters in the real world situation are close to the human operator parameters in the simulator, then the simulator has replicated the real world situation. This agrees intuitively with the definition of a replication of an experiment. A replication of an experiment is simply two empirical runs of data in which some variable shows consistency in both of the two empirical runs. In this case the variables that are to show consistency are the human operator model parameters. If these parameters show consistency between the real world situation and the simulator, then the simulator has replicated the real world situation. If the human operator appears the same in both the simulator and in the real world situation, and he rates the two to be the same subjectively, then the simulator has reproduced the desired environment from the point of view of the human.

The data base used to study the measures of simulator credibility involves a washout experiment as discussed in [4]. This experiment provides a unique opportunity to study how well the simulator replicates the real world situation.

THE G-VECTOR TILT WASHOUT EXPERIMENT

The G-Vector tilt washout experiment conducted at the Aerospace Medical Research Laboratory provides a data base to investigate the simulator credibility question. The data base used here involved a large centrifuge which has the capability of positioning the roll axis normal to the earth's gravity (called 0°) or parallel with the earth's gravity vector in which the subject is on his back or supine (called 90°). Six experimental conditions were considered in this study.

0° Conditions (Upright Position)	90° Condition (Subject on his back)
0° Motion	90° Motion
0° Washout - Attenuation only	
0° Washout - 1st. order washout	
0° Washout - 1st. order + attenuation	
0° Washout - 2nd. order	

As the subject makes a command stick response, the simulator rolls to simulate an aircraft in a banking maneuver. It is obvious that in the 0° (upright) motion case the human has both tilt cue information as well as angular acceleration cue information. In the 90° (subject on his back) motion case, the human does not have the tilt cue information. The four washout conditions were conducted at 0° (upright position) and a washout circuit was installed between the stick response and the plant's roll characteristics (Fig. (1a-b)). The effect of the washout circuit is to distort the motion cues to the human.

The manner in which this data base is equivalent to the simulator credibility problem is that the "real world" is defined as the 90° motion case.

The question is then asked, which washout scheme at 0^o is closest to the real world 90^o motion case? The 0^o washout conditions contain reduced tilt cue information and also contain some distorted motion cues from the washout circuits. The modeling procedure which enables the determination of an equivalence definition between two simulators is presented next.

THE MODELING APPROACH

Figure (2) illustrates how the modeling approach was conducted here. After the data was collected from the various experimental conditions a post experimental analysis was conducted with a model developed in such a manner that the human operator can be modeled as an information processor and controller. With reference to figure (2), the input to the model is the time series e(t) (the displayed error signal). The purpose of this modeling approach is to choose model parameters such that the model's output $\hat{x}(t)$ is an accurate representation of the measured stick response of the human. The measure of modeling accuracy is expressed in the residuals or output modeling error $v(t)$ which satisfies:

$$v(t) = ST(t) - \hat{x}(t) \tag{1}$$

If the model is appropriately fitted to the data, then $v(t)$ should be a random white process which satisfies:

$$\text{mean } [\ v(t)\ ] = E[v(t)] = 0 \tag{2}$$

$$\text{var } [v(t)] = E[v(\ )v^T(\tau)] = R\ \delta(t-\tau) \tag{3}$$

It will be necessary in the subsequent analysis to test $v(t)$ for whiteness and determine R of equation (3). If $v(t)$ is a random white process, then the expected value of the model is equal to the expected value of the human's output. This is one method to validate such a model. A simple model structure is discussed next to describe the human's characteristics of interest.

A SIMPLE MODEL TO DESCRIBE HUMAN OPERATOR CHARACTERISTICS

It is desired to develop a model to characterize the human operator parameters of interest for this study. From previous studies [5,6], other simple representations of the human which have application in specific situations have been developed. In this paper a modeling approach will be used that will give rise to simple methods to characterize human operator parameters across several experimental conditions (or simulator designs). These modeling characteristics turn out to be analogous to an information theory representation of the human. Using the definition of channel capacity:

$$\text{channel capacity} = \text{Bandwidth} * \log_{10}\left(\frac{S+N}{N}\right) \tag{4}$$

The Bandwidth term is analogous to speed and the term $\log_{10}(\frac{S+N}{N})$ is analogous to accuracy. If the human operator has characteristics similar to an information channel, one would expect a product of the form of equation (4) to be invariant over several experimental conditions. It is then necessary to determine only two characteristics of the human operator in this representation of responses. To determine bandwidth, use is made of the human describing function plots. In the determination of the accuracy measure, a Kalman filter must be used.

From figure (3), it is desired to have a method by which an approximate measure of human operator signal/noise ratio can be determined. In this modeling procedure, the Kalman filter is initially specified to have input-output characteristics similar to those obtained from the describing function with the addition of some phase lag to account for the time delay of the human. The unknown Kalman gain coefficients (which represent the uncertainty terms or covariance matrices) are updated [7] in such a manner that the residuals $\nu(t)$ are white. The signal to noise ratio can then be approximated by:

$$\frac{S+N}{N} \approx \frac{\sum_{i=1}^{N} [ST(t_i)]^2}{\sum_{i=1}^{N} [\nu(t_i)]^2} \qquad (5)$$

It is noted that the variance of the residuals $\nu(t)$ are a measure of human uncertainty with respect to the error signal. This is true because the Kalman filter output $\hat{x}(t)$ is that portion of the stick response correlated with the error signal. The residuals $\nu(t)$ are that portion of the stick output not correlated with the error signal. This definition of human uncertainty differs from the classical definition of remnant [8,9] which is defined as that portion of human response not correlated with the input forcing function. This definition of human uncertainty is concerned with that part of the human response which is totally non-productive in reducing the error signal. This is easily seen to be true by noting that $\nu(t)$ when passed through the plant and around the loop still is uncorrelated with the error signal. Hence it cannot constructively be used to reduce the error signal because of its orthogonality to it. This measure of human uncertainty is a true measure of human output not useful in the tracking task. Next, a description of the measures of bandwidth and accuracy obtained from this modeling procedure are presented.

CALCULATION OF BANDWIDTH

In the computation of a measure of the bandwidth of the human operator, several difficulities exist in attempting to treat the human as an information channel [10]. This is due to difficulities in determining the true describing function from measured data variables and the effects of correlation between the human's remnant response and portions of the measured error signal. In this paper several approximations will be made. Figure (4) illustrates the

describing function of the human for the 0^{o} motion case. Across the six experimental conditions considered here, the shape of the human operator describing function remained essentially the same; the major change between experimental conditions was only due to the d.c. gain values where the describing function was at a maximum. The ensuing analysis was conducted on the spectrum generated by the target frequencies. The reason it is necessary to work with the target frequencies is that if the target forcing function were zero, the describing function of the human operator obtained from only the human operator response (or for small values of disturbance input) is just equal to -1/plant. This result is well known [10,11].

From the target spectrums all experimental conditions are rated in order of their maximum gain value (table I). From table I it is seen that 0^{o} static has the lowest gain value. The largest frequency the human will pass for this value of gain is now determined for each experimental condition.

This definition of the human operator bandwidth is the highest frequency at which the human will respond with gain of 0.5 db. In other words across all experimental conditions, the range of frequencies (from 0.0 radians and upward) is obtained that the human will pass with gain greater than 0.5db. In this manner a normalization is conducted on one experimental condition versus the remaining experimental conditions. This is a logical definition of human bandwidth and is one of many possible methods to approximate the bandwidth of a control system [12]. Measures of human uncertainty in tracking are determined next.

Table I - Bandwidth Computation - Subject - Eric

Experimental Condition	Maximum Gain in db	Bandwidth $\triangleq$ Higest Frequency where gain $\geq$ 0.5 db	1σ
0° Motion	6.5db	10.8 Rad/Sec	2.0
Washout Attenuation only	4.8db	9.8 Rad/Sec	0.3
90° Motion	4.5db	9.5 Rad/Sec	0.7
Washout 1st Order + Attenuation	3.5db	9.2 Rad/Sec	1.1
Washout 1st Order	2.9db	8.3 Rad/Sec	0.8
Washout 2nd Order	3.3db	8.2 Rad/Sec	1.1
0° Static	0.5db	7.3 Rad/Sec	1.0

MEASUREMENT OF ACCURACY OR SUBJECT UNCERTAINTY

With reference to figure (5) it is desired to update the model parameters in such a way that the innovations sequence $\nu(t)$ is a white, random process. The method of updating the parameters is based on an algorithm [7] which is actually a maximum liklihood procedure. In this manner a unique value of the optimal gain can be determined which maximizes the probability density function of the structure of the assumed model based on all the available data points. The optimal gain is the principal part of the discrete Kalman filter model which is described by:

$$\hat{x}_{i+1/i} = \phi\, \hat{x}_{i/i} + \int_0^{\Delta t} e^{A\tau} d\tau B \,\mathrm{col}[e(t), \dot{e}(t)] \quad (6)$$

$$\hat{x}_{i/i} = \hat{x}_{i/i-1} + K_o [\, z_i - H\, \hat{x}_{i/i-1}\,] \quad (7)$$

where $\hat{x}_{i/i}$ is the minimum variance estimate of the human's stick response. The matrix ϕ is the discrete transition matrix associated with the human's transfer function determined as follows:

$$\text{Let} \qquad \frac{ST[s]}{E[s]} = \frac{d(s+a)}{(s+b)(s+c)} \quad (8)$$

i.e. a fit of one zero and two poles is conducted on the human's transfer function to the describing function data (Bode plot). The coefficients a,b,c, and d are adjusted to try to match the phase data as well as the magnitude data. Implicitly the human's time delay has been included in the representation (8) through the adjustment of the parameters b and c. Future work will be done to study more exact fits. The matrix ϕ is then determined via $\phi = e^{A\Delta t}$ where $\Delta t = .04$ seconds (the sampling rate) and the matrix A is determined via:

$$\begin{bmatrix} \dot{x}_1 \\ \dot{x}_2 \end{bmatrix} = A \begin{bmatrix} x_1 \\ x_2 \end{bmatrix} + B \begin{bmatrix} e(t) \\ \dot{e}(t) \end{bmatrix} \quad (9)$$

where

$$x_1(t) = ST(t)$$

$$x_2(t) = \frac{d}{dt} ST(t)$$

and equation (9) is the time domain representation of equation (8). The matrix H in equation (7) is specified by $H = [1,0]$. The Kalman gain K_o satisfies:

$$K_o = P\, H^T (HPH^T + R)^{-1}$$

$$P = \phi\, [P - PH^T (HPH^T + R)^{-1} HP] \phi^T + Q$$

where the covariance matrices Q and R describe the human's uncertainty in the tracking task. The manner of obtaining the Q and R matrices is based on the algorithm in [7]. Initial matrix values denoted as Q_o and P_o are chosen. In order to establish the updating rule, it is necessary to define the sample covariance function.

Let:
$$\hat{C}_k = \frac{1}{N} \sum_{i=k}^{N} \nu_i \nu_{i-k}^T$$

is a sample covariance function. The matrices R and Q are now updated [7] via:

$$R_k = \hat{C}_o - H(P_k H^T)$$

where
$$P_k H^T = K_o \hat{C}_o + A^* \begin{bmatrix} \hat{C}_1 \\ \hat{C}_2 \end{bmatrix}$$

where
$$A^* = (\bar{A}^T \bar{A})^{-1} \bar{A}^T$$

and
$$\bar{A} = \begin{bmatrix} H\phi \\ H\phi(I-K_o H)\phi \end{bmatrix}$$

and finally Q is determined via:

$$Q_k = P - \phi K R_k K^T \phi^T - \phi(I-KH)P(I-KH)^T \phi^T$$

This algorithm has been shown to converge [7] and is equivalent to maximizing the log-likelihood function of the model structure conditioned on the data.

The final validation of this modeling effort is the need to test the residuals for whiteness. To accomplish this goal the normalized auto correlation function $\hat{\rho}_k$ is computed as follows:

$$\hat{\rho}_k = \frac{\hat{C}_k}{\hat{C}_o}$$

The test of whiteness of the residuals is a 95% whiteness test on $\hat{\rho}_k$. The 95% confidence limits for $\hat{\rho}_k$ are $1.96/\sqrt{N}$ where N is the number of samples. The band $\pm 1.96/\sqrt{N}$ is constructed about zero. If less than 5% of the sample points lie outside the band, the sequence is white. If more than 5% of the sample points lie outside the band, then a significant correlation exists in the residuals and the sequence is not white. Figure (6) illustrates the sample auto-correlation function obtained here from the data after the residuals have been whitened via this algorithm.

RESULTS FROM THIS ANALYSIS

Figure (7) represents the type of diagram obtainable from this type of

analysis procedure. The vertical axis is a plot of the measure of bandwidth as shown in Table I. The horizontal axis indicates numerical values of the accuracy measure or S/N ratio obtained here. Also plotted is the curve of constant capacity based on this analysis procedure. The numerical values resulting from this investigation of the data are given in Table II:

Table II - Speed - Accuracy Results

Exp Condition	Mean BW	1σ of BW	N=Mean $\log_{10}$S/N	1σ $\log_{10}$S/N	Mean Capacity BW*$\log_{10}$(1+S/N)
0° motion	10.8	2.0	3.265	.191	34.346
Washout Attenuation only	9.8	0.3	3.278	.088	31.719
90° motion	9.5	0.7	3.358	.089	31.5025
Washout 1st order + Attenuation	9.2	1.1	3.378	.064	30.79
Washout 1st Order	8.3	0.8	3.373	.043	27.813
Washout 2nd Order	8.2	1.1	3.412	.082	27.634

Also plotted in figure (7) is the invariant rule:

$$BW * \log_{10}(1+S/N) = \text{Constant} = 30.6 \qquad (11)$$

The constant 30.6 is the mean of the values of capacities obtained in the right most column in Table II. From figure (7) it is noted that most of the experimental conditions fall near this line.

Figure (7), by itself, is the diagram which can be used to assess the fidelity of a simulator in comparison to the real world data. If 90° motion is considered the real world situation, the washout scheme closest (distance wise) to this situation is 1st. order + attenuation. The other washout schemes are sucessively further away in this diagram and therefore, further from reality. The reason why it is said that the two experimental conditions best replicate each other is that the human exhibits almost the same bandwidth (or speed characteristics in tracking) and almost the same uncertainty characteristics (as measured by the S/N ratio).

Another interpretation of figure (7) is to consider the inverse problem associated with modeling; i.e. given the model parameters, can an analog simulation be built which will recreate the original empirical data. If the human in the loop were replaced by a quantitative description (e.g.

bandwidth and S/N ratio), the analog simulations of the 90^{o} motion case and washout 1st order + attenuation would most closely replicate one another. This is true because the only difference between the two simulations would be the parameters which describe the human operator. If these parameters are close to one another in some sense, then these simulations would best match. This is the motivation for using figure (7) to study simulator fidelity.

One additional comment needs to be made about why the washout scheme of 1st. order + attenuation best matched the 90^{o} motion case. The 0^{o} washout condition provided tilt cue information but the 1st. order + attenuation washout filter phase lag had the effect of distorting these tilt cues sufficiently to replicate the 90^{o} motion case. For the case of attenuation only, the tilt cue had an effect closer to 0^{o} motion (as expected). Also, as the washout scheme added more phase lag (2nd order case), the deviation from reality became more pronounced and the human operator dropped his bandwidth accordingly.

Future Research

The primary approximation used here was in the evaluation of human operator bandwidth. This approximation also effected the S/N ratio because the A matrix in the Kalman filter depends on this approximation. Future research will consider more accurate methods of evaluating bandwidth and including human time delay. In addition, a comparison will be made in the information rate obtained here to results from discrete tasks (approximately 3.0 bits/sec [13]) and to other information measures obtained from vision [14], reading [15], and control systems in general [16]. Another approximation utilized here was that the S/N ratio of the human was assumed to be constant over the entire frequency spectrum. In [3] the analysis procedure was able to study the capacity measure across the entire frequency spectrum. The procedure considered here can be extended in this respect. Also, since the analysis conducted here only involved one subject, future work will consider this analysis across different subjects, and use will be made of these measures of human invariance and subjective uncertainty in various task situations.

SUMMARY AND CONCLUSIONS

A study of design rules for the evaluation of a simulator's fidelity to the real world situation was conducted. The measures of model parameters obtained here give rise to information-theoretic models of the human operator. It appears that an invariant rule may exist on the human's ability to do information processing over a variety of different experimental conditions.

REFERENCES

1. Fitts, P.M.,"The Information Capacity of The Human Motor System in Controlling the Amplitude of Movement", Journal of Experimental Psychology, 1954, 47, pp. 381-391.

2. Senders, J.W. and J.J.M. Posner,"A Queueing Model of Monitoring and Supervisory Behavior", in Monitoring Behavior and Supervisory Control, by T.B. Sheridan and G. Johannsen, Plenum Press, 1976.

3. Verplank, W.L.,"The Facilitating Effects of Uncertainty in Long-Term Manual Control", Proceedings of the 1977 International Conference on Cybernetics and Society, September, 1977, Washington, D.C.

4. Jex, H.R. and A.M. Junker, "Roll Tracking Effects of G-Vector Tilt and Various Types of Motion Washout", The Fourteenth Annual NASA - University Conference on Manual Control, April 25-27, 1978, Los Angeles, California.

5. Repperger, D.W. and A.M. Junker, "Using Model Order Tests to Determine Sensory Inputs in a Motion Study", The Thirteenth Annual Conference on Manual Control, MIT, Cambridge, MA., 1977

6. Repperger, D.W. and A.M. Junker, "Performance Evaluation of Tracking Based on a Low Pass Filter Model", Eleventh Annual Conference on Manual Control, NASA TM X-62,464, pp. 599-624.

7. Mehra, R.K.,"On The Identification of Variances and Adaptive Kalman Filtering", IEEE Transactions on Automatic Control, Vol. AC-15, No. 2, April, 1970, pp. 175-184.

8. Jex, H.R.,R.W. Allen, and R.E. Magdaleno, "Display Format Effects on Precision Tracking Performance, Describing Functions, and Remnant", AMRL-TR-71-63, August, 1971.

9. Levison, W.H., S. Baron, and D.L. Kleinman,"A Model for Human Controller Remnant", IEEE Transactions on Man-Machine Systems, Vol. MMS-10, No. 4, pp. 101-108, December, 1969.

10. Wingrove, R.C., "Comparison of Methods for Identification of Pilot Describing Functions From Closed Loop Operating Records", NASA TN D-6235, 1971.

11. McRuer, D.,D. Graham, E. Krendel, and W. Reisener, "Human Pilot Dynamics in Compensatory Systems - Theory, Models, and Experiments with Controlled Element and Forcing Function Variations", AFFDL-TR-65-15, July, 1965.

12. Lynch, W.A., and J. G. Truxal, "Introductory System Analysis", McGraw-Hill, 1961.

REFERENCES

13. Miller, G.A.,"The Magical Number Seven, Plus or Minus Two: Some Limits on Our Capacity for Processing Information", The Psychological Review, vol. 63, No. 2, March, 1956, pp 81-97.

14. Kelly, D.H.,"Information Capacity of a Signal Retinal Channel", IRE Transactions on Information Theory, April, 1962, pp 221-226.

15. Pierce, J.R. and J.E. Karlin, "Reading Rates and The Information Rate of a Human Channel", The Bell System Technical Journal, March, 1957, pp 497-516.

16. Rink, R.E., "Optimal Utilization of Fixed-Capacity Channels in Feedback Control", Automatica , Vol. 9, pp 251-255, 1973.

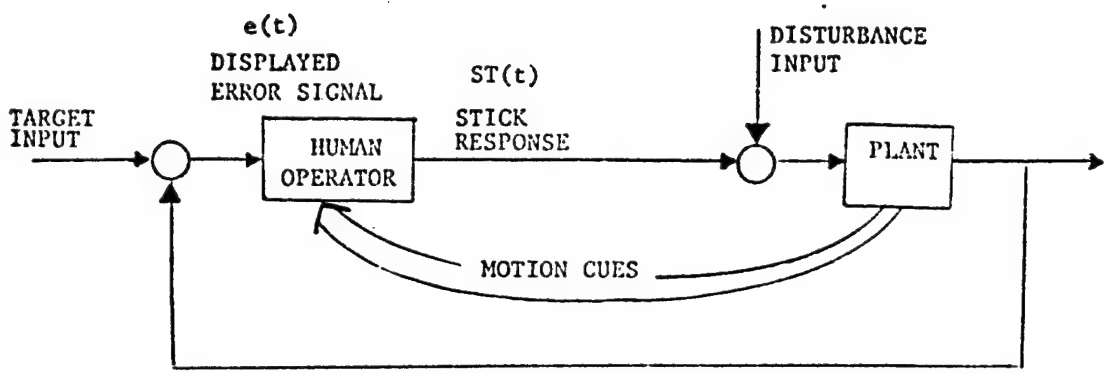

FIGURE (1a) -90° Motion Tracking

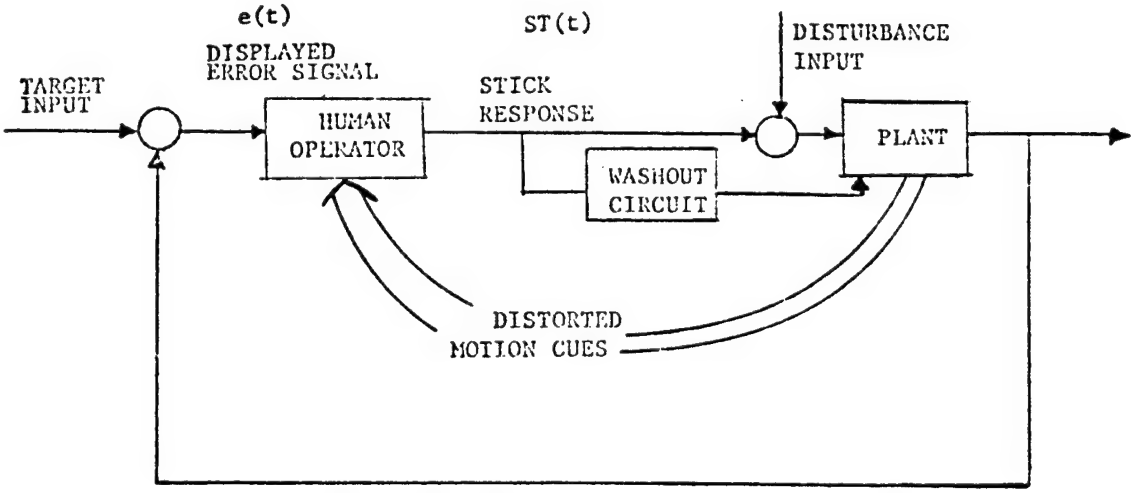

FIGURE (1b) -0° Washout Circuit

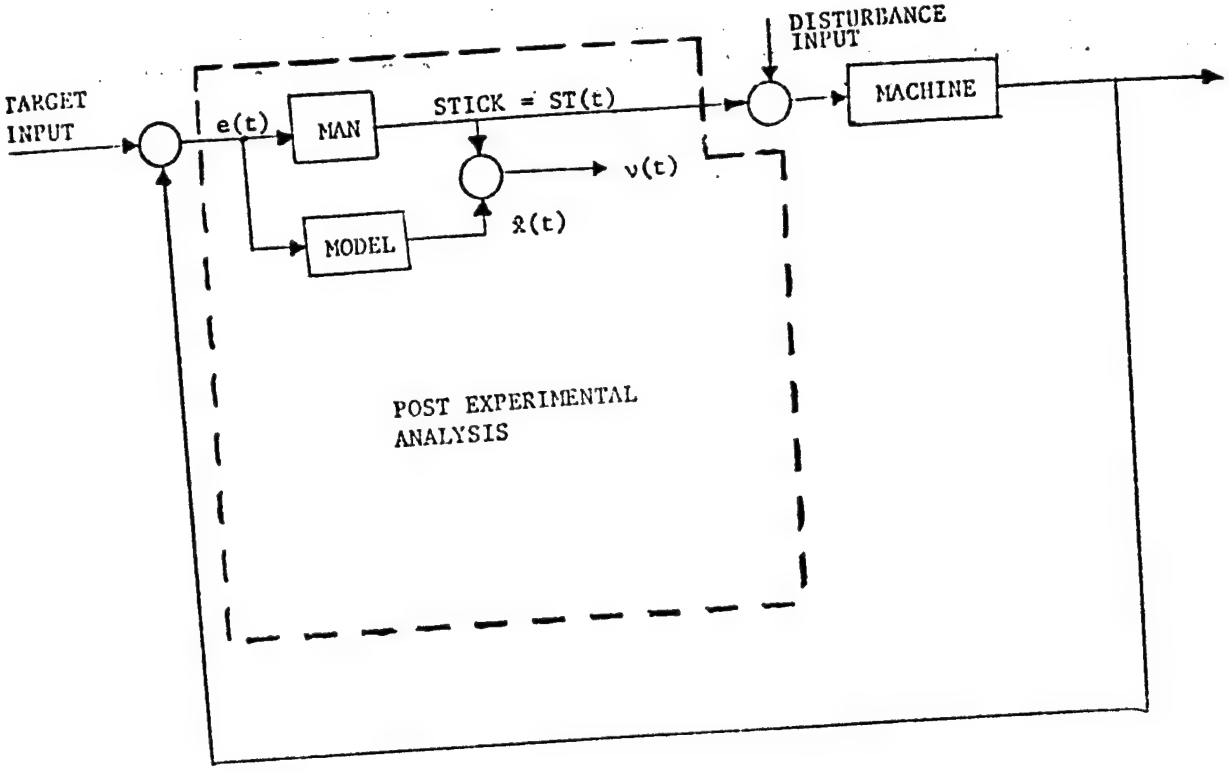

FIGURE (2)

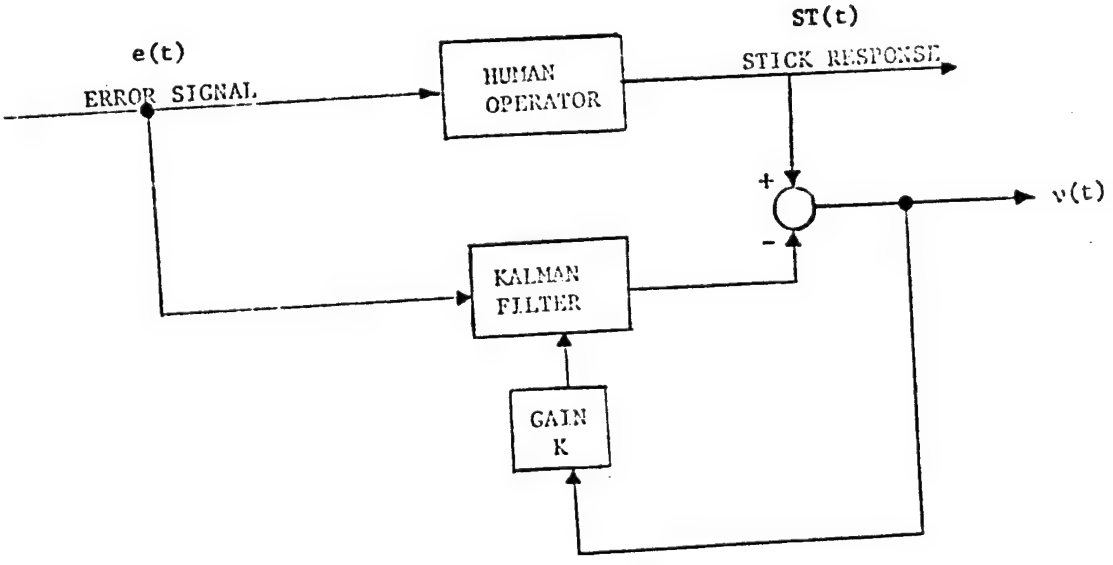

FIGURE (3)

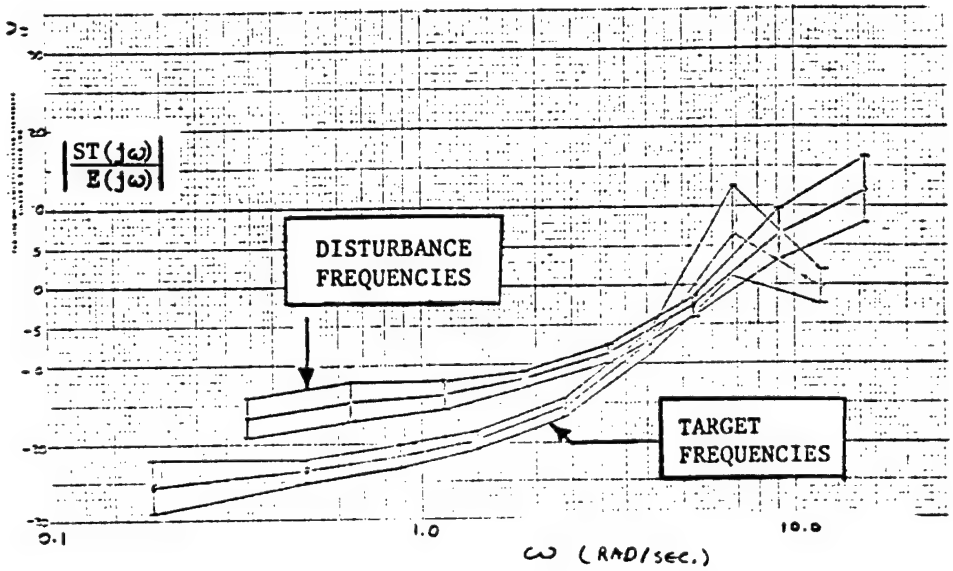

FIGURE (4) - The Human Operator Describing Function
0° Motion Case

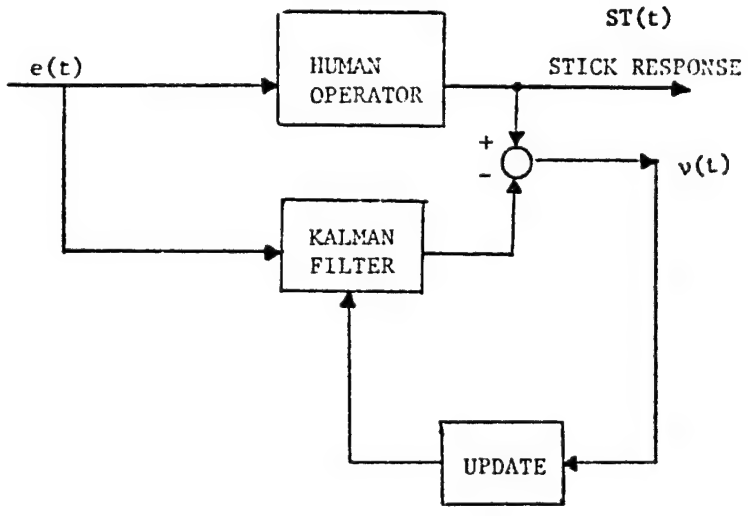

FIGURE (5) - Calculation of Subject Uncertainty

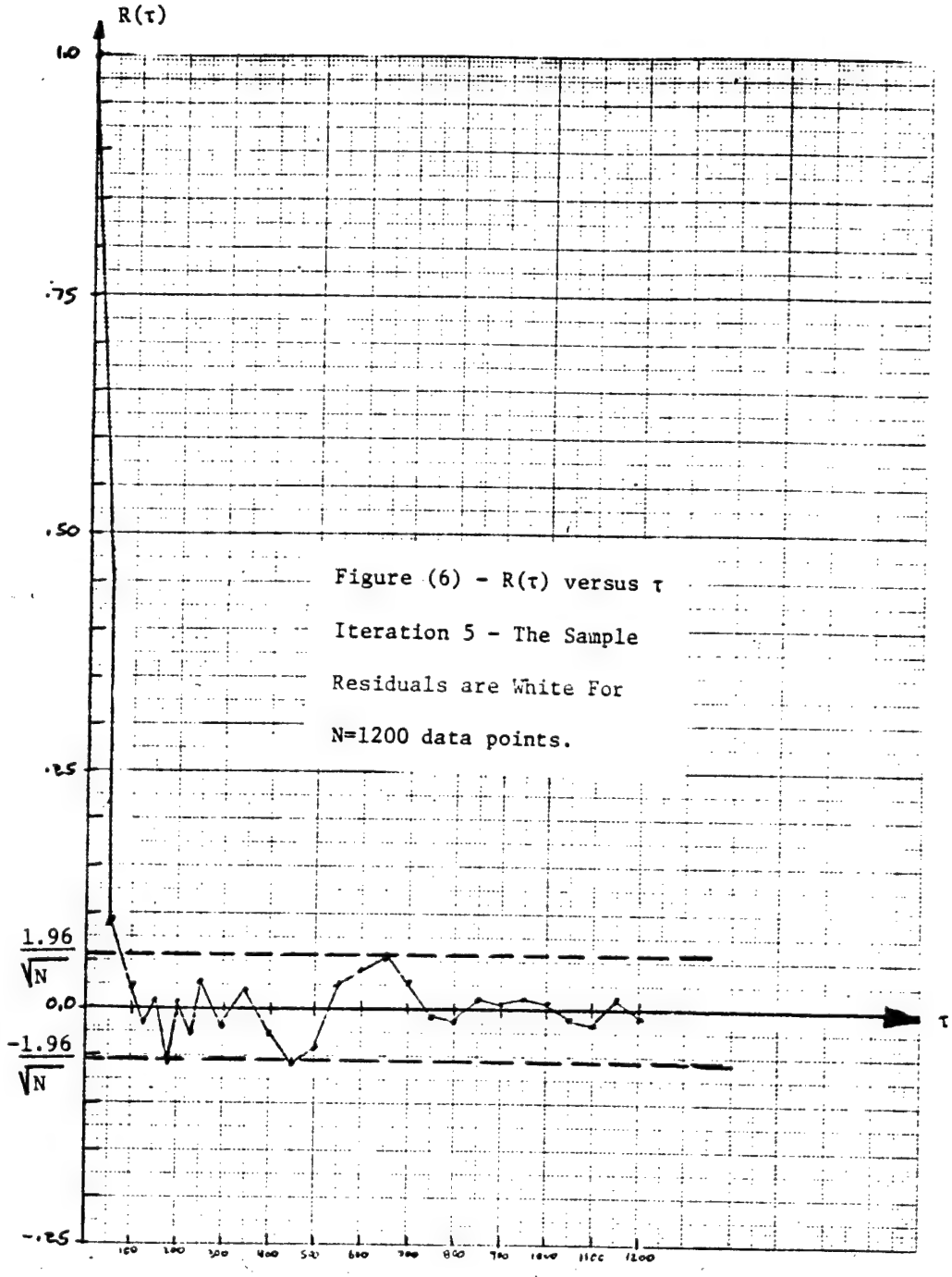

Figure (6) - $R(\tau)$ versus τ Iteration 5 - The Sample Residuals are White For N=1200 data points.

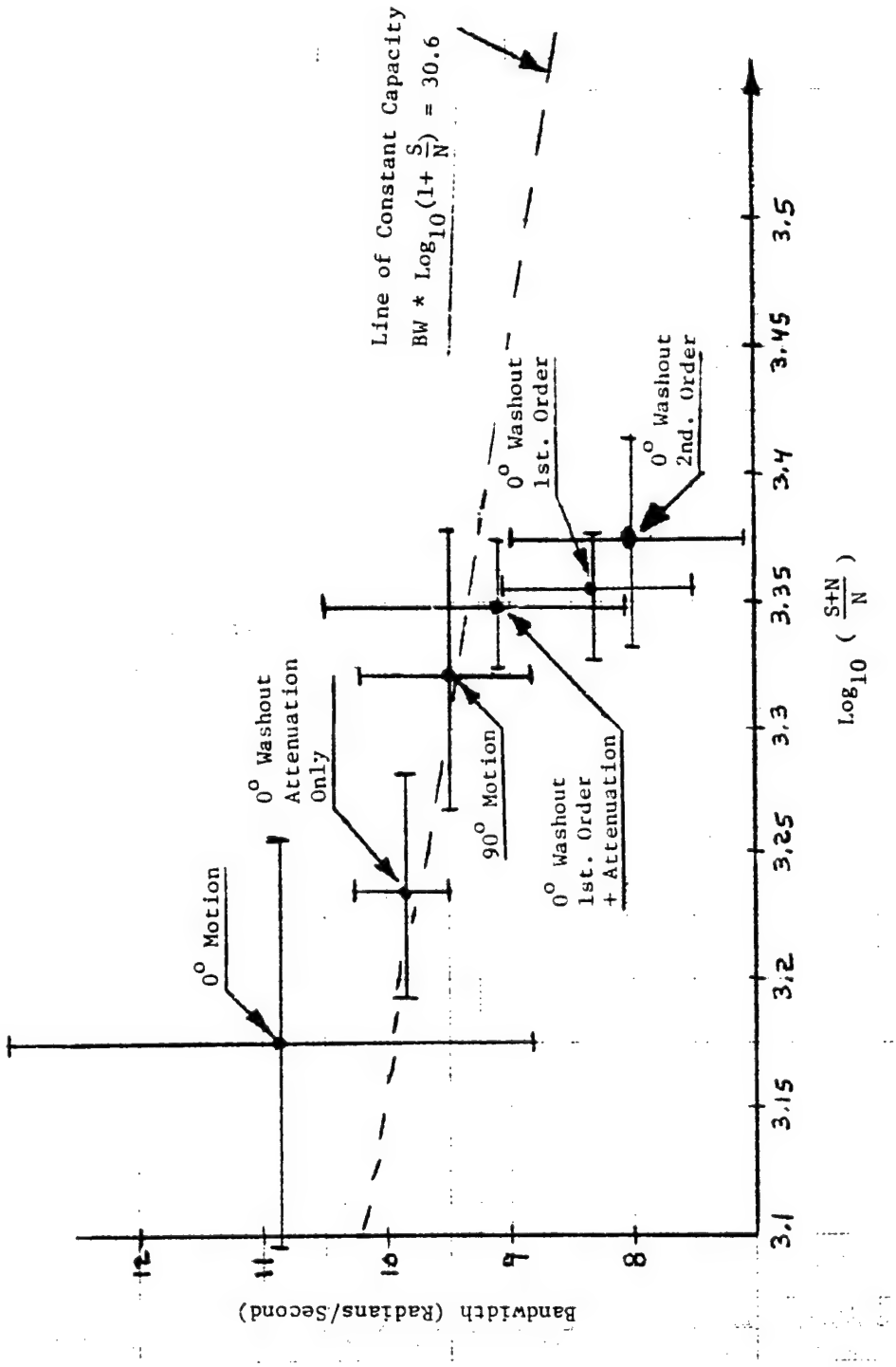

Figure (7) - A Diagram Which Allows Comparisons Between Simulators

N79-15624

INVESTIGATION OF NONLINEAR MOTION SIMULATOR WASHOUT SCHEMES

By Susan A. Riedel and L. G. Hofmann

Systems Technology, Inc.

Hawthorne, California

INTRODUCTION

Research interest in washout filters for motion simulator drives arises out of a desire to maximize the fidelity of motion cues presented to simulator pilots. Washout filters must satisfy two important, usually conflicting, requirements:

1. The filter (along with the limiters) must prevent the simulator from reaching the mechanical limits imposed on displacement, velocity and acceleration in each axis.

2. The filter must reproduce actual motion cues without perceptible distortion. That is, motions contributed because of the washout must be imperceptible to the pilot.

The first requirement basically dictates integrated consideration of known motion base limits, existing limiter circuitry and the proposed washout design. The result should be a design which is not at crossed purposes with the limiters. The second requirement, however, demands knowledge of the physiology of motion perception. Research in engineering, physiology and psychology has lead to models of certain mechanisms for motion perception, and has greatly sharpened our knowledge of human motion perception capability. These capabilities (or lack thereof) can then be exploited by the washout designer in fulfilling the second requirement.

The first section of this paper presents an overview of some of the promising washout schemes which have recently been devised. The four schemes presented fall into two basic configurations; crossfeed and crossproduct. Various nonlinear modifications further differentiate the four schemes.

The second section of this paper discusses one nonlinear scheme in detail. This washout scheme takes advantage of subliminal motions to speed up simulator cab centering. It exploits so-called perceptual indifference thresholds to center the simulator cab at a faster rate whenever the input to the simulator is below the perceptual indifference level. The effect is to reduce the angular and translational simulator motion by comparison with that for the linear washout case.

520

The final section of this paper presents the conclusions and implications for further research in the area of nonlinear washout filters.

An Overview of Nonlinear Washout Techniques

All nonlinear washout schemes presented here are modifications to one of the two basic linear designs shown in figure 1. For simplicity, a single set of coupled axes for each design is depicted. The crossproduct scheme, attributed to Schmidt and Conrad (reference 5), is currently implemented on the Large Amplitude Multimode Aerospace Research Simulator (LAMARS) (reference 7). The crossfeed scheme (reference 6) attributed to Bray is implemented on the Flight Simulator for Advanced Aircraft (FSAA) (reference 8).

An interesting aspect of the crossproduct scheme is that the recovered specific force always equals the input specific force in the absence of any additional filtering of translational acceleration. In the figure, this implies $\dot{V}_{po} = \dot{V}_{poF}$. This result is due to the configuration of the residual tilt and coordinating crossfeed paths. Notice that because of the different arrangements for the coordinating crossfeed and residual tilt paths in the crossfeed scheme, $\dot{V}_{po}$ and $\dot{V}_{poF}$ are not necessarily equal.

Table 1 compares four nonlinear washout schemes which are in various stages of development. Because of the nonlinear nature of these schemes it is not possible to predict the outcome of a given experiment based on the results of previous experiments. Thus, conclusions drawn from test results for these nonlinear schemes are, at best, tentative.

Figure 2 presents a roll axis example of the adaptive gain (Parrish, references 2 and 3) scheme. The gain K_p is computed on-line based upon a cost function. This cost function is a function of roll rate, roll angle and initial K_p. It includes several constants which can be varied to "tune" the filter. The cost function is integrated and limits are imposed to obtain the filter gain. This gain varies with time. When the filter is tuned for a particular application, Parrish and Martin found it helpful for reducing the so-called "false cue" observed in pulse-type maneuvers.

Figure 3 illustrates a sway-axis example of the varying break frequency (Jewell, reference 1) scheme. In this case a cost function is used to compute the time-varying break frequency of the second-order translational washout. The cost function is a function of the translational acceleration, velocity and position as well as break frequency itself. Constants are available to tune the filter. The cost function is then integrated and a limit is imposed to obtain the break frequency. Jewell has demonstrated in a computer simulation that a two-fold reduction in translational motion can be achieved for a quasi-random input.

Figure 4 presents a portion of the surge axis as it appears in a signal compression scheme which incorporates parabolic limiting. While both the Parrish and the Jewell schemes addressed the problem of increased simulation fidelity and decreased motion base requirements, this scheme proposes a solution for the problem of the hardware motion base limits. The essence of this

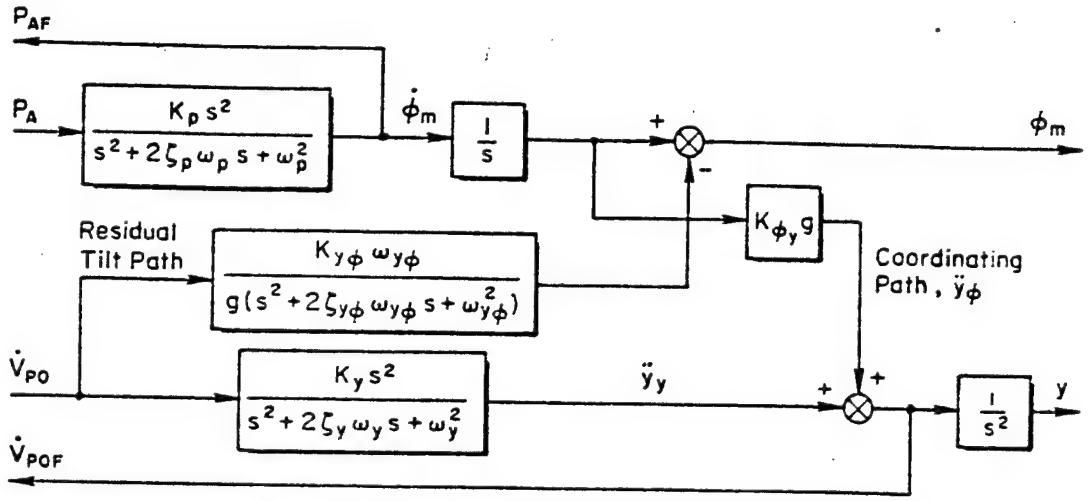

Crossfeed Scheme - Bray - FSAA

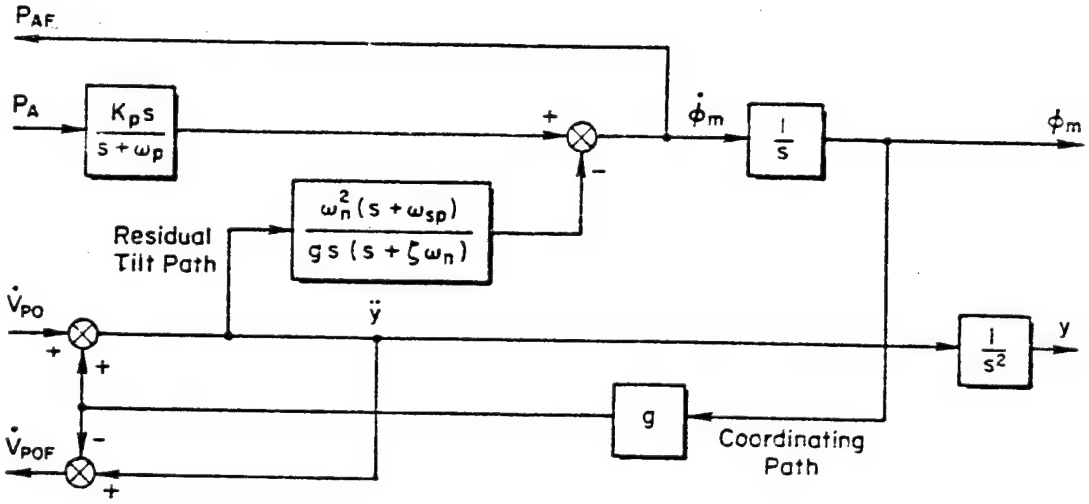

Crossproduct Scheme - Schmidt and Conrad - LAMARS

Figure 1. Basic Single-Axis Linear Washout Circuit Framework

TABLE 1. COMPARISON OF FOUR NONLINEAR WASHOUT SCHEMES

	Adaptive Gain	Variable Break Frequency	Parabolic Limiting	Subliminal
Description	Varies washout gain K using a cost function	Varies washout break frequency ω_b using a Parrish-type cost function	Incorporated in electrical drive to command maximum deceleration to stop simulator at limits	Increases washout rate when input is subthreshold to force cab back to zero position faster
Purpose	Eliminate "false cue"	Reduce motion base displacement requirements	Back-up system for hardware and software units	Reduce motion base displacement requirements
Principal Investigators	NASA-Langley Parrish Martin	STI Jewell Jex	NASA-Ames Bray Sinacori	STI Hofmann Riedel
Level of Investigation	Implemented on Langley Visual Motion Simulator	Computer model roll-sway axes	Implemented on FSAA	Computer model roll-sway axes
Underlying Linear Basis	Crossproduct	Crossproduct	Crossfeed	Crossproduct
Inputs for Which Scheme Is Most Effective	Pulse-type inputs	All inputs	Large inputs which could cause limiting	Small, subthreshold inputs
Level of Success	May eliminate "false cues"	Twofold reduction in lateral displacement requirement	Avoids hitting hardware limits	Twofold reduction in lateral displacement requirement
Side Effects	Increased nonlinearity with increased motion	Increase in lateral specific force miscoordination		Increase in lateral specific force miscoordination
References	2, 3	1	6	4

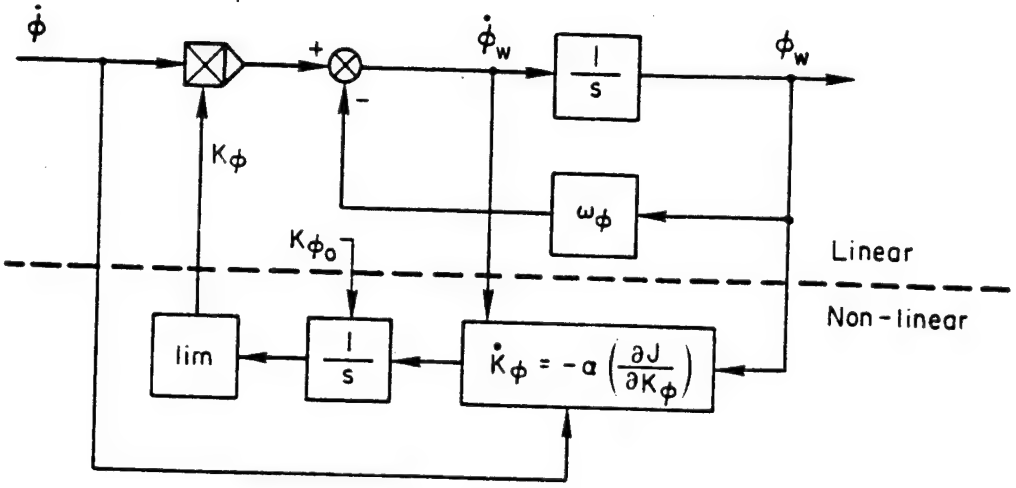

$$\dot{\phi}_\omega = K_\phi \dot{\phi} - \omega_\phi \phi_\omega$$

$$\dot{K}_\phi = -\alpha (\partial J / \partial K_\phi)$$

$$J = 1/2 \left[(\dot{\phi} - \dot{\phi}_\omega)^2 + b_\phi \phi_\omega^2 + b_{K_\phi}(K_\phi - K_{\phi_o})^2\right]$$

Figure 2. Adaptive Gain Scheme

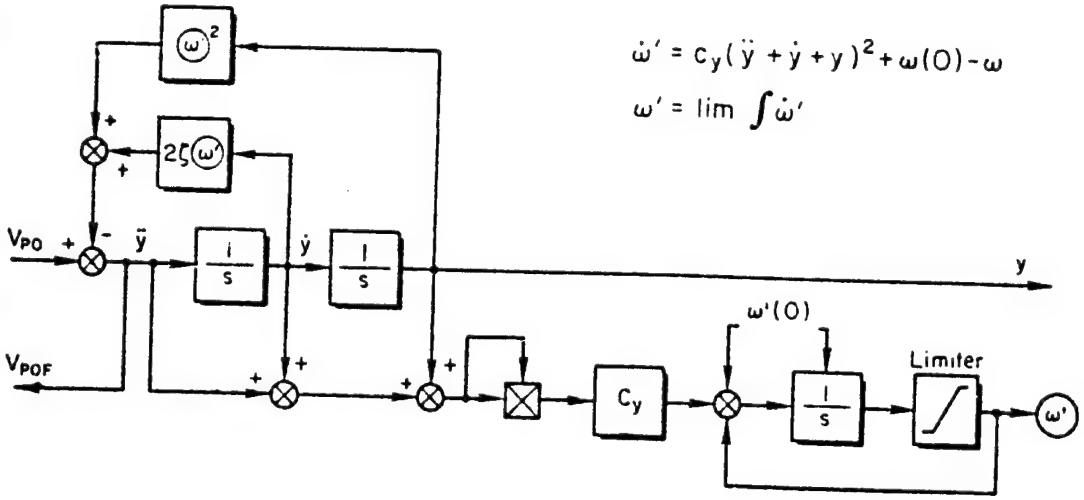

$$\dot{\omega}' = c_y(\ddot{y} + \dot{y} + y)^2 + \omega(0) - \omega$$

$$\omega' = \lim \int \dot{\omega}'$$

Figure 3. Varying Break Frequency Scheme

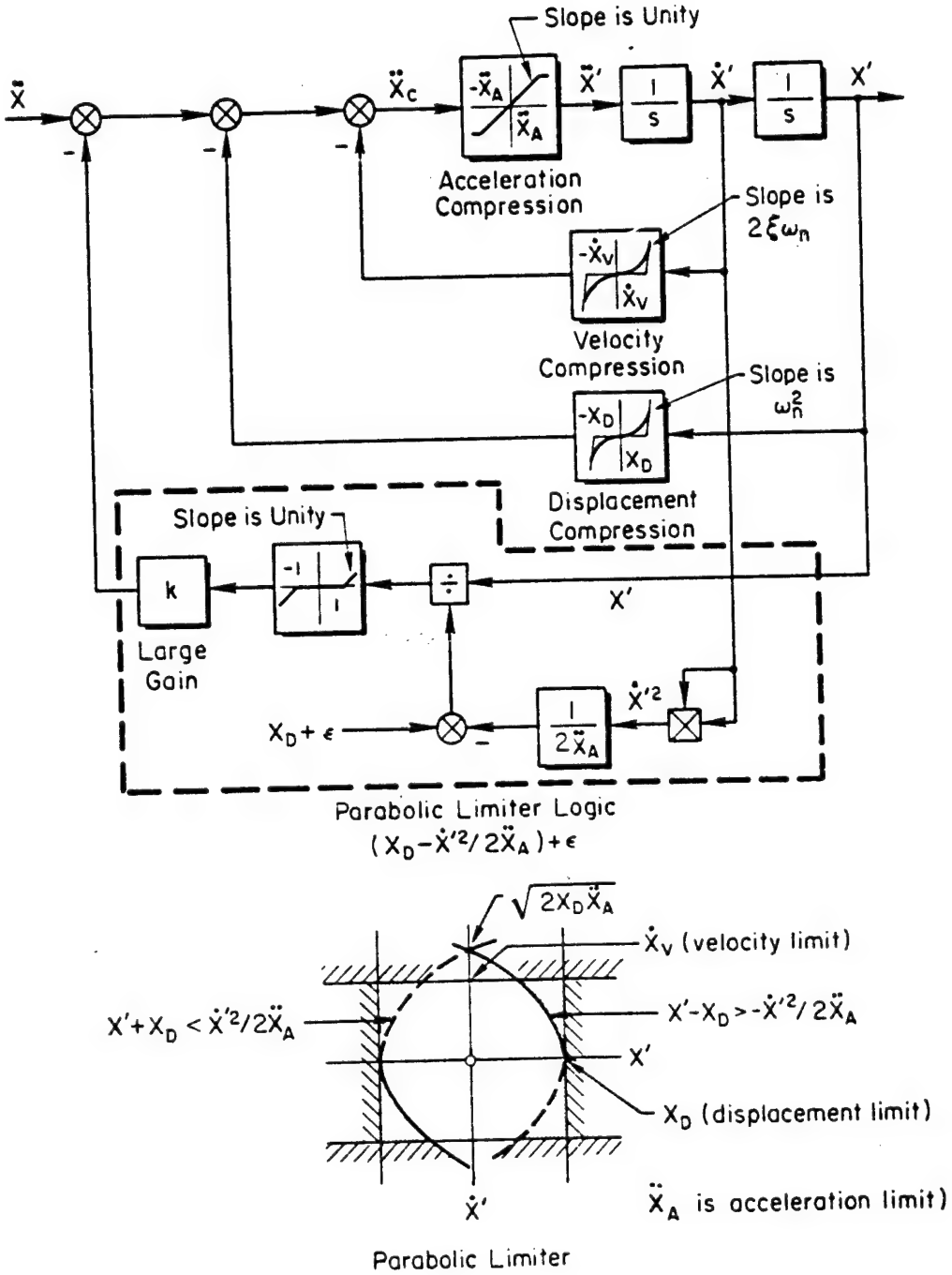

Figure 4. Parabolic Limiting Scheme Incorporating Signal Compression

scheme is a continuous calculation to assure that the cab can be brought to zero velocity before displacement limits are reached. The commanded motion is reproduced to the extent that a margin between the calculated stopping point and the displacement limits exists. In this way, maximum use may be made of the available motion capability.

The fourth washout, the subliminal scheme, is the subject of the next section of this paper.

THE SUBLIMINAL WASHOUT SCHEME

Figure 5 presents an application of the subliminal washout scheme to a first-order roll axis washout. This concept came about as the result of an attempt to utilize so-called "indifference" thresholds which pilots exhibit under normal workload. These thresholds may be operative for both angular velocity and specific force perception under normal workload. The hypothesis is that pilots do not perceive angular velocities and specific forces which are below the respective indifference thresholds. The washout design objective is to exploit this particular phenomenon to obtain reduced simulator motion requirements or increased motion fidelity.

The overall design goal is to drive the cab back to its zero position more rapidly than would the underlying linear washout whenever the motion stimulus is below the indifference threshold level. This is accomplished with the use of the two nonlinear functions in boxes A and B in figure 5. The input to the function in Block A is the scaled angular velocity. This function produces a weighting factor which serves as a variable feedback gain in the washout circuit. If the input magnitude is larger than the indifference threshold p_T, the weighting factor is zero. If the input is zero, the weighting factor is 1.0. Otherwise, the weighting factor is some fraction of 1.0 which is a sinusoid-like function of the input for the form of the weighting function used here.

The input to Block B, a soft saturation nonlinear function, is cab roll angle, Φ. If Φ is large, the value of the function output is the value of the indifference threshold level, $\pm p_T$. If Φ is small the value of the function output is proportional to Φ.

The outputs from Blocks A and B are then multiplied to arrive at an incremental washout rate command signal. The particular choice of functions in Blocks A and B assures that this signal's magnitude never exceeds the indifference threshold level. The smoothness of the functions in Blocks A and B tends to prevent discontinuous commanded changes in the washout rate. The value of this incremental washout rate command signal will be non-zero whenever the cab roll angle is non-zero and the input angular velocity is below the indifference threshold level. The signal is then subtracted from

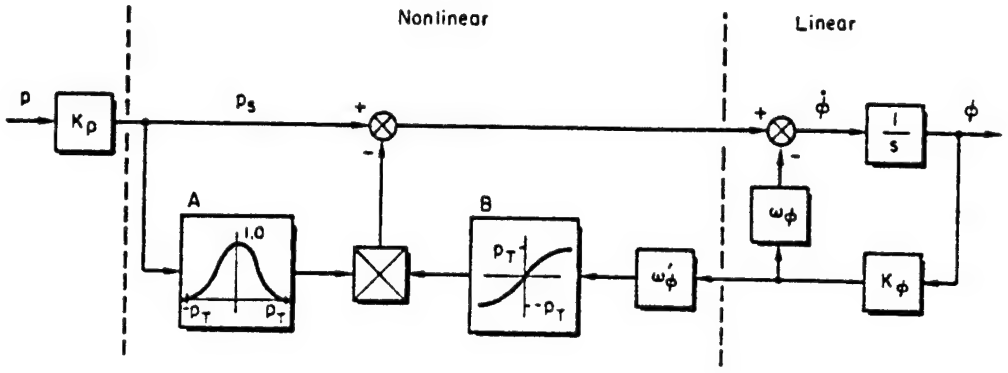

p = Input Angular Velocity

p_S = Scaled Angular Velocity

p_T = Indifference Threshold Level

$\dot{\phi}$ = Commanded Cab Roll Rate

ϕ = Commanded Cab Roll Angle

Figure 5. Nonlinear Washout Scheme (First-order Washout)

the scaled input angular velocity. The result is a smaller away-from-center angular velocity input to the integrator than would result for the underlying linear scheme. Thus, the cab is driven back to its zero position more quickly than it would be for the linear scheme, during intervals of sub-threshold inputs in angular velocity.

Preliminary tests of this subliminal washout concept for the roll axis showed it to be ineffective. There was some reduction in simulator motion requirements, but not really enough to warrant further investigation.

Figure 6 shows an application of this same washout concept to the lateral specific force channel of a crossproduct washout configuration for roll-sway axes.

It was pointed out in the discussion of the crossproduct scheme that the input specific force, $\dot{V}_{po}$, and the recovered specific force, $\dot{V}_{poF}$, are always equal for the crossproduct washout configuration. In this case the subliminal washout introduces intentional miscoordination of specific force. The indifference phenomenon allows this deliberate introduction of specific force miscoordination, and as long as this miscoordination does not exceed the specific force indifference threshold level, the pilot under normal workload will not detect the miscoordination.

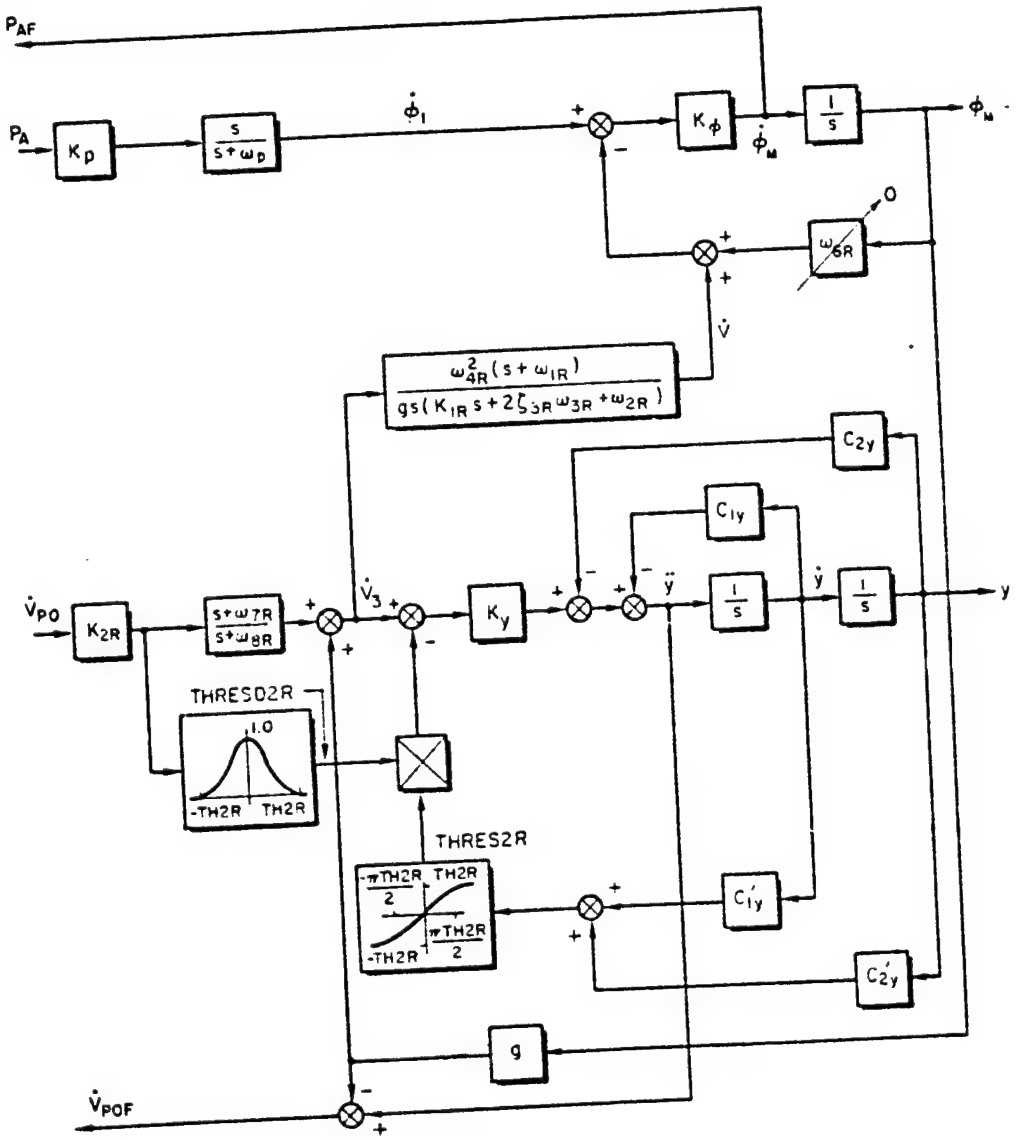

Figure 6. LAMARS Drive Logic Washout with Nonlinear Feedback Added to Specific Force Path Only

Computer simulation results for the washout in figure 6 are presented in figure 7. The input to the simulation corresponds to a roll-in to a constant 4 g turn. The inputs are roll rate, P_A, and lateral specific force, $\dot{V}_{po}$. There is no reduction in acceleration, $\ddot{y}$, slight reduction in velocity, $\dot{y}$, and significant reduction in lateral translation, y. These results show clearly that the subliminal washout substantially reduces simulator displacement motion requirements. Lateral translation reduction is 70 percent, i.e., from a maximum linear displacement of 4.05 m (13.5 ft) to a maximum displacement of 1.2 m (4 ft).

In order to accomplish this substantial reduction in lateral translational requirements, however, a substantial change in recovered specific force is generated because of miscoordination. This is due to the increased washout rate for the subliminal washout scheme. Since the increase in washout rate is constrained to at or below an indifference threshold level of 0.1 g, the change in recovered specific force is also constrained to that level. Thus, under normal workload the pilot should not be able to detect this level of miscoordination.

The computer simulation of the subliminal washout has been exercised for a variety of inputs. Significant reductions in motion base requirements have been observed. On the basis of these results the following conclusions can be drawn:

1. The subliminal washout concepts, as implemented in the translational axes of the crossproduct scheme, are effective in reducing the velocity and displacement requirements of the motion base.

2. The subliminal washout scheme is most effective for sub-indifference threshold specific force inputs. The washout reduces to the underlying linear scheme when inputs exceed this threshold.

3. The use of the subliminal threshold scheme results in an increase in recovered specific force which is spurious. This spurious motion is due to additional miscoordination. The nonlinear implementation insures that this miscoordination component is never greater than the assumed indifference threshold level. Thus under normal workload, the pilot should be unable to detect this false cue.

Much work remains to be performed in the investigation of this subliminal washout scheme. The initial results of the computer simulation have shed light on the scheme's major uses, and encourage further research and eventual simulator implementation.

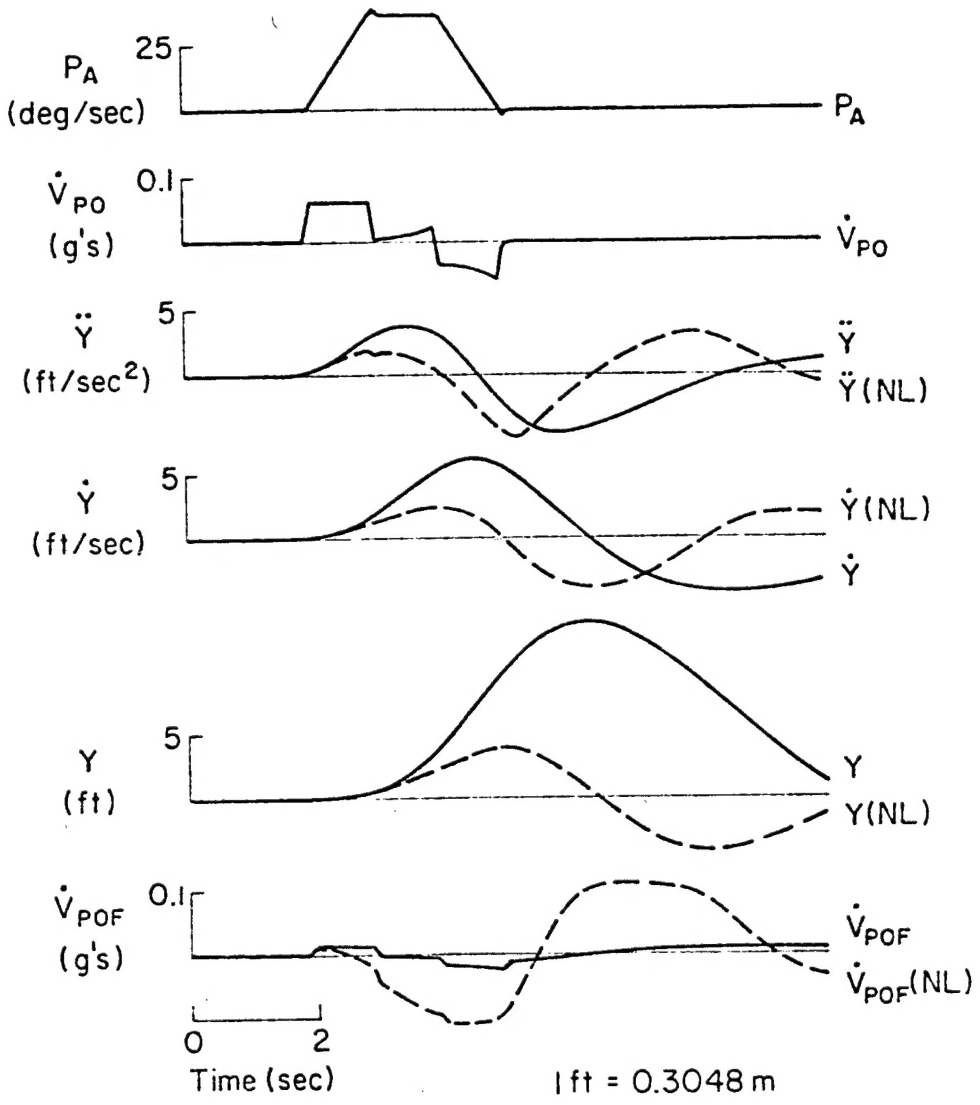

Figure 7. Comparison of Linear and Nonlinear Outputs

CONCLUSIONS

A sample of some new concepts in nonlinear washout filters has been presented here. Since each scheme addresses a different aspect of the washout problem, it may be desirable to combine several nonlinear concepts in a single, grand scheme. In this way, several problems in a particular simulation could be handled by a single washout circuit. Further research along these lines might lead to a well-defined method for designing a washout circuit to suit particular simulation needs, taking into account the peculiarities of the motion base as well as a description of the flying task to be simulated.

The research reported herein was sponsored by the Air Force Flight Dynamics Laboratory under Contract F33615-77-C-2065. (W. Klotzback, AFFDL/FGD and J. Bankovskis, AFFDL/FGD)

REFERENCES

1. Jewell, Wayne F., and Henry R. Jex, "A Second Order Washout Filter With a Time-Varying Break Frequency," STI WP-1094-3, Feb. 1978.

2. Parrish, R. V., and D. J. Martin, Jr., Comparison of a Linear and a Nonlinear Washout for Motion Simulators Utilizing Objective and Subjective Data from CTOL Transport Landing Approaches, NASA TN D-8157, 1976.

3. Parrish, R. V., J. E. Dieudonne, R. L. Bowles, and D. J. Martin, "Coordinated Adaptive Washout for Motion Simulators," AIAA Paper No. 73-930, Sept. 1973.

4. Riedel, Susan A., and L. G. Hofmann, "Preliminary Investigation of a New Nonlinear Washout Scheme," STI WP-1110-1, Dec. 1977.

5. Schmidt, S. F., and B. Conrad, Motion Drive Signals for Piloted Flight Simulation, NASA CR-1601, 1970.

6. Sinacori, J. B., "A Brief Survey of Motion Simulators' Drive Logic with Emphasis on the Roll Axis," STI WP-1094-2, May 1977.

7. Sinacori, J. B., "A Practical Approach to Motion Simulation," AIAA Paper No. 73-931, Sept. 1973.

8. Sinacori, J. B., Robert L. Stapleford, Wayne F. Jewell and John M. Lehman, Researchers Guide to the NASA Ames Flight Simulator for Advanced Aircraft (FSAA), STI-TR-1074-1, May 1977.

SESSION J: PERCEPTION AND ATTENTION ALLOCATION

Chairman: W. Rouse